NACA

RESEARCH MEMORANDUM

for the

Air Materiel Command, U. S. Air Force

AN INVESTIGATION OF THE MCDONNELL XP-85 AIRPLANE IN THE AMES 40- BY 80-FOOT WIND TUNNEL.- FORCE AND MOMENT TESTS

By Lynn W. Hunton and Harry A. James

Ames Aeronautical Laboratory
Moffett Field, Calif.

NATIONAL ADVISORY COMMITTEE FOR AERONAUTICS

WASHINGTON

Sept. 27, 1948

CONFIDENTIAL

NATIONAL ADVISORY COMMITTEE FOR AERONAUTICS

RESEARCH MEMORANDUM

for the

Air Materiel Command, U. S. Air Force

AN INVESTIGATION OF THE MCDONNELL XP-85 AIRPLANE IN THE AMES 40- BY 80-FOOT WIND TUNNEL.- FORCE AND MOMENT TESTS

By Lynn W. Hunton and Harry A. James

SUMMARY

Wind-tunnel tests of the McDonnell XP-85 airplane were conducted to determine its longitudinal, lateral, and directional stability and the characteristics of the aileron, the ruddervator, the leading-edge droop nose flap, and the stall control vanes. The directional stability of the airplane with numerous skyhook modifications and with a ventral fin was also investigated.

The results of the tests showed that the effectiveness of the droop nose flaps and the stall control vanes was negligible with regard to either the maximum lift or longitudinal stability of the airplane. Contrary to any previous small-scale results, extension of the skyhook caused a 75-percent reduction in the directional stability of the airplane for both low and high values of lift coefficient. The simplest solution to the problem short of a major redesign of the skyhook appears to be the adoption of a ventral fin.

INTRODUCTION

The McDonnell XP-85 airplane is a jet-propelled parasite fighter designed to operate from a mother ship for air-to-air take-off and landing. Due to the rather unique problems involved in such a design, the Air Materiel Command requested an investigation of the aerodynamic characteristics of the XP-85 airplane in the Ames 40- by 80-foot wind tunnel to facilitate the final phases of the airplane design and to insure the success of the initial air-to-air test flight.

This full-scale investigation included both force and pressure-distribution measurements. Reported herein are the results of only the force tests. These include the longitudinal, lateral, and directional stability characteristics of the airplane and in addition control-effectiveness data for the aileron and the unorthodox Vee-type tail. Also summarized herein are the results of a rather extensive investigation of the large destabilizing effect of the extended skyhook on the directional stability of the airplane. With the exception of this skyhook stability problem, no analysis or discussion of the data is presented in this report.

COEFFICIENTS AND SYMBOLS

The results of the tests are presented as standard NACA coefficients of forces referred to the wind axes and of moments referred to the stability axes as shown in figure 1. The axes originate at a center of gravity located at the 25 percent mean aerodynamic chord and 1.5 inches above the fuselage thrust axis. All angle-of-attack measurements refer to the fuselage thrust axis. The coefficients and symbols are defined as follows:

C_L lift coefficient $\left(\frac{\text{lift}}{qS}\right)$

C_D drag coefficient $\left(\frac{\text{drag}}{qS}\right)$

C_Y side-force coefficient $\left(\frac{\text{side force}}{qS}\right)$

C_m pitching-moment coefficient $\left(\frac{\text{pitching moment}}{qS\bar{c}}\right)$

C_n yawing-moment coefficient $\left(\frac{\text{yawing moment}}{qSb}\right)$

C_l rolling-moment coefficient $\left(\frac{\text{rolling moment}}{qSb}\right)$

C_h control-surface hinge-moment coefficient $\left(\frac{\text{hinge moment}}{2qM}\right)$

C_{n_ψ} directional stability parameter; rate of change of yawing-moment coefficient with angle of yaw $\left(\frac{\partial C_n}{\partial \psi}\right)$

α_u geometric angle of attack in the wind tunnel of fuselage thrust axis, degrees

α angle of attack, corrected for wind-tunnel-wall effects, of fuselage thrust axis, degrees

δ control-surface deflection, degrees

ψ angle of yaw, degrees

b wing span measured perpendicular to plane of symmetry, 21.13 feet

$\bar{c}$ wing mean aerodynamic chord $\left(\frac{\int_0^{b/2} c^2 dy}{\int_0^{b/2} c\, dy}\right)$, 5.15 feet

M first moment of area aft of control-surface hinge line about hinge line (M_a=0.928 ft^3, M_{r_u}=1.010 ft^3, M_{r_l}=0.218 ft^3)

q free-stream dynamic pressure, pounds per square foot

R Reynolds number

S wing area (100 sq ft)

V free-stream velocity, feet per second

Subscripts:

a aileron

r ruddervator

u upper

l lower

AIRPLANE AND EQUIPMENT

A three-view drawing of the XP-85 airplane giving pertinent dimensions is presented in figure 2. The rather unconventional proportions of this parasite fighter design were dictated by space limitations of the forward bomb bay of a B-36 airplane from which this fighter is designed to operate. Except for the installation of strut-support mounting pads on the wing, the only modification to the

airplane made for these tunnel tests was the removal of the turbojet engine and the installation of a straight circular duct of constant cross section through the fuselage.

The wing had a modified NACA 65_1-010 airfoil section parallel to the plane of symmetry, an angle of sweepback of 34° at the quarter-chord line, an aspect ratio of 4.5, and a tip to-root-chord ratio of 0.33. In addition, the wing was characterized by 4° of cathedral and a uniform twist giving 5° of washout at the tips. The incidence of the root chord of the wing with reference to the thrust line was 2°.

The wing was equipped with a 0.15-chord nose flap and stall control vanes but had no form of trailing-edge flaps. The nose flap shown in figure 2 had a maximum down-travel of 30° and extended over the outboard 42 percent of the wing span. The stall control vanes were not an integral part of the airplane but were installed during a portion of this tunnel investigation. They extended aft from the leading edge of the wing at the 55-percent, 65-percent, or 75-percent semispan stations. Details of the vanes are given in figure 3 and in the figures presenting data from this phase of the investigation.

The internal-sealed balance-type ailerons on the airplane were hinged about the 0.80 chord line. The balance area, accounting for one-half the seal area and for cutouts, was 37.5 percent of the aileron area aft of the hinge line. The right aileron only was tested and had a maximum travel of about ±12°.

Due to space limitations of the B-36 airplane bomb bay, an unorthodox five-unit tail design was resorted to for this airplane rather than a more conventional type which would have entailed a folding operation. As shown in figure 2, the design incorporates four movable control surfaces which operate on a Vee-tail principle. The ruddervator surfaces diametrically opposite were linked together. Thus there resulted two independent sets of surfaces which in turn were rigged in the standard Vee-tail-type fashion for longitudinal and directional control. For the majority of these tests, only one set of surfaces (upper right[1] and lower left looking forward) was used. All ruddervator surfaces were 30-percent-chord unsealed plain-type flaps with a shielded-horn balance.

Deflection of the movable surfaces was controlled remotely with a linear actuator drive installed in the cockpit and linked to the

[1]Henceforth in this report the upper-right and lower-left ruddervator combination will be referred to simply as the right ruddervator, while the upper-left and lower-right surface combination will be referred to as the left ruddervator.

control stick for either aileron action or combined rudder and elevator action (single set of ruddervators moved) and pure elevator action (both sets of ruddervators moved). For pure rudder action (both sets of ruddervators moved) the actuator was linked to the rudder pedal. Remote indication of the deflection angle of the surfaces was provided by autosyn transmitters installed in the linkage system near each of the three control surfaces. Surface hinge moments were determined using electrical resistance-type strain gages. The aileron was equipped with a bending-type gage, while the upper and lower ruddervators were each equipped with torsion-type gages. All control surfaces when not undergoing test were clamped in a neutral position.

Other apparatus on the airplane included a retractable trapeze hook (fig. 4), which throughout this report will be referred to as the skyhook in accordance with the nomenclature established by the manufacturer, and a dive brake (fig. 5(b)) located on the underside of the fuselage.

The installation of the airplane in the tunnel test section is shown in the photographs of figure 5. The support system used for the tests consisted of the regular two main support struts and pitch links which attached to the wing forward of the main strut attachment points.

TESTS

Force tests were made with the airplane in pitch and in yaw to determine the longitudinal, lateral, and directional stability characteristics of the airplane in the clean condition, and with various combinations of the stall control vanes, the droop nose flap, the skyhook, and the dive brake. Tests were also made with the center vertical tail fin removed. Tests to determine the effectiveness and hinge-moment characteristics of the right aileron and the right ruddervator were conducted with the airplane at several angles of attack and angles of yaw. The investigation of the ruddervator also included tests wherein both sets of ruddervators were moved simultaneously, first to give pure elevator action, then to give pure rudder action in order to determine the extent of effects of interaction of this Vee-type tail arrangement. The effects on the airplane directional stability of the skyhook and modifications thereto and of a ventral fin were determined. Throughout the entire investigation of the airplane the fuselage duct was left open.

All tests, except where noted otherwise, were made at a dynamic

pressure of 60 pounds per square foot which corresponds to an airspeed of about 155 miles per hour at standard sea-level conditions and to a Reynolds number of 7.4×10^6 based on the mean aerodynamic chord of 5.15 feet.

CORRECTIONS

No support-strut tares have been applied to the data, since no tare measurements existed for the support-strut configuration used in these tests. As an approximate indication of the order of magnitude of the tares a test was made at the test dynamic pressure of 60 pounds per square foot with the airplane removed from the tunnel and with the main struts, pitch links, and strands of control wires and pressure tubing supported in position by small rectangular flat plates set at zero incidence to the air stream to simulate the support attachment configuration as existed on the lower surface of the wing. This method obviously neglects all the mutual interference effects between the support strut and wing. Results of this test indicated tares based on the dimensions of this relatively small airplane of the order of 0.011, 0.031, and -0.024, all at zero lift, for $\Delta C_{L_{tare}}$, $\Delta C_{D_{tare}}$, and $\Delta C_{m_{tare}}$, respectively. All these tares, if applied to the data presented herein, would be subtracted algebraically.

Corrections for air-stream inclination and tunnel-wall effects have been applied to the data. Since investigations of tunnel-wall corrections for swept wings have indicated that boundary corrections are determined primarily by spans and areas of models and are not greatly affected by sweep, the following standard corrections for unswept wings have been applied to the angle of attack, drag coefficient, and pitching-moment coefficient data:

$$\Delta\alpha = 0.242\ C_L$$

$$\Delta C_D = 0.004\ C_L^2$$

$$\Delta C_m = 0.0065\ C_L$$

Corrections have also been applied to the ruddervator (both upper and lower) deflection angles. Since the autosyn indicator transmitters were installed on bell cranks near each of the ruddervator control surfaces, a correction was necessary to account for strain in the linkage system between the surface and the transmitter. For the aileron the transmitter was connected directly to an extension

of the hinge pin, thus necessitating no deflection correction.

PRECISION OF THE DATA

Due to the relatively small size of this airplane, some difficulty was encountered in attaining the normal accuracy of results expected in an investigation of this kind. A major portion of the scatter and minor inconsistencies in the data, especially pitching moments, as may be found by cross-checks of the data is believed to be the result of the relatively small forces involved. For purposes of an approximate indication of the accuracy with which the various aerodynamic coefficients could be measured based on the least count of the force scales, on the dimensions of the airplane, and on a test dynamic pressure of 60 pounds per square foot, the following coefficients were computed:

$$C_L = 0.002$$

$$C_D = 0.0003$$

$$C_Y = 0.0003$$

$$C_m = 0.01$$

$$C_n = 0.0003$$

$$C_l = 0.001$$

RESULTS AND DISCUSSION

General Characteristics

The results of this investigation of the XP-85 airplane are presented in figures 6 through 65 as outlined in table I. Included in these results of tests with the airplane in various configurations are the general longitudinal characteristics in figures 6 to 8, the longitudinal, lateral, and directional stability characteristics in figures 9 to 24, the characteristics of the aileron and tab in figures 25 to 33, and the characteristics of the ruddervators and tab in figures 34 to 65. It should be noted throughout these results that the configuration as noted in each figure title is complete (i.e., the various changes indicated are in each case based on the clean airplane), and that for the ruddervator-effectiveness data, except the lower ruddervator hinge-moment coefficient data, all

deflection angles refer to the angle of the upper ruddervator surface. The deflection angle of the lower ruddervator, which deviated slightly from that of the upper surface due to strain in the control rigging, is indicated by the data of lower ruddervator hinge-moment coefficient versus surface deflection. In this data the hinge-moment coefficient for the lower ruddervator is plotted against the true deflection of the lower ruddervator. The amount of deviation in deflection between the upper and lower surface may be seen by a comparison of the corresponding hinge-moment-coefficient test points for the upper and lower surface.

Throughout the results of both the yaw tests of the airplane and the aileron and ruddervator control-effectiveness tests made at various fixed angles of attack, it may be noted that the data shown for an angle of attack of 12° are somewhat erratic and irregular. Such results are attributed to an asymmetric stall of the wing which is clearly shown in figure 9 by the rolling-moment-coefficient versus lift-coefficient data obtained over the stall. For the airplane at zero angle of yaw these rolling-moment data indicate a definite roll-off on the left wing at a lift coefficient corresponding to 11° angle of attack as compared with approximately 15° angle of attack for maximum lift. Therefore, it is probable that all the data presented herein for the airplane at a fixed angle of attack of 12° were obtained with the left wing partially stalled.

Nose Flaps

In the course of the investigation of the maximum lift characteristics of the airplane, it was found that the droop nose flap deflected 30° was relatively ineffective as an auxiliary lift device (fig. 7). Therefore, in an attempt to uncover the cause of the ineffectiveness of this device, brief additional tests were made with the gap at the outboard ends of the flap sealed and with the deflection angle reduced from 30° to 15°. These results are also shown in figure 7. Although a reduction of the nose flap angle of deflection to 15° did show a slight improvement in the maximum lift coefficient, the increment in $C_{L_{max}}$ of only 0.05 for this nose flap would not seem to warrant its use as an auxiliary lift device on this wing.

Stall Control Vanes

Results of preliminary small-scale tests of the airplane (reference 1) indicated that the use of stall control vanes significantly

improved the longitudinal stability characteristics. Therefore, one of the purposes of this full-scale investigation of the airplane was to verify the small-scale results and to establish the optimum stall control vane configuration. In figures 8(a) and (b), data are presented for the airplane with various stall control vanes with the droop nose flap both retracted and extended to its normal down-position of 30°. From the results it may be seen that the effect of the vanes on the maximum lift or longitudinal stability characteristics of the clean airplane is negligible. With the droop nose extended, the vanes reduced the tendency toward neutral stability in pitch caused by the droop nose near stall. Since no one vane configuration appeared particularly advantageous by comparison with the others, the midposition vane P_2 of medium height (1-1/2 in.) was chosen to represent an average vane to be used for the portions of the tunnel investigation involving a stall vane.

Ruddervators

For the investigation of the effectiveness of the ruddervator only the right set of surfaces was employed, since only by this procedure could basic control-effectiveness data be obtained which would be useful in the analysis of virtually any control problem involving permutations of the rudder and elevator deflections. To test the complete ruddervator system would have restricted the test program to tests of specific conditions of control in order to avoid unlimited combinations of rudder and elevator deflections. However, the above procedure does involve some uncertainty regarding the effects of interaction. For this reason a few tests of the complete ruddervator system operated for pure elevator action and for pure rudder action were made for purposes of comparison with predicted results from tests of the single ruddervator set. These comparisons can be made from the data given in figures 37 to 43 and in 61 to 65 for the single set and complete ruddervator systems, respectively. For example, for the clean airplane at $\alpha=0°$ and $\psi=0°$ the yawing-moment coefficient C_n for $\delta_r=8°$ given in figure 37 is 0.004 for the single right ruddervator set (which value when doubled would be the predicted C_n for the complete ruddervator), while for the complete ruddervator system a value for C_n of 0.008 from figure 62 was measured. Since other similar comparisons indicated equally good agreement of control-effectiveness results, it was concluded that no measurable effect of interaction existed for this Vee-type tail arrangement.

Skyhook

The present full-scale investigation of the airplane revealed, contrary to any previous preliminary small-scale results, that the skyhook when extended caused a 75-percent reduction in directional stability C_{n_ψ}. As may be noted by a comparison of the slopes of the curves of C_n versus ψ at an angle of attack of 0° shown in figures 17 and 21 for the airplane clean and with the skyhook extended, respectively, C_{n_ψ} is -0.0016 for the clean airplane, while with the skyhook extended the value of C_{n_ψ} drops to -0.0004. Even at the higher angles of attack the destabilizing effect of the skyhook not only continued but increased slightly. Consequently, the general stability and control test program was rearranged in order to provide test data of numerous skyhook modifications. The results of the investigation which are summarized in figures 66(a) through (e) include only the directional stability characteristics in the form of yawing-moment coefficient plotted as a function of angle of yaw. These tests were designed to provide the manufacturer with not only the stability characteristics of a number of possible modifications or alternate hook designs but also with basic data which would be useful in an analysis of the problems involved with the present skyhook design. Included in the investigation were such modifications as fairings, venting of the hook, simulated doors, spoilers, ventral fin, and various simulated skyhooks of alternate design. Although the relative merits of these various modifications will not be discussed, these results indicate that the reduction in directional stability due to the skyhook is not associated with either a wake or a sidewash at the tail caused by the hook, but instead is probably the result of flow separation over both the canopy and aft portion of the fuselage due to the spoiler action of the operating mechanism at the base of the hook. This may be inferred from the fact that the effectiveness of the center vertical fin remained essentially intact with the skyhook either extended or retracted. As for the Vee tails, it seems unlikely that a wake from the skyhook could affect them without affecting the center fin since the majority of the Vee-tail area lies outboard of the fin. From the test results it would appear that the simplest solution to the problem short of a major redesign of the skyhook would be to increase the basic directional stability of the airplane by the adoption of a ventral fin similar to the one investigated.

Ames Aeronautical Laboratory,
National Advisory Committee for Aeronautics,
Moffett Field, Calif.

REFERENCE

1. Paulson, John W., and Johnson, Joseph L.: Preliminary Evaluation of the Low-Speed Stability and Control Characteristics of the McDonnell XP-85 Airplane From Tests of an Unballasted 1/5-Scale Model in the Langley Free-Flight Tunnel. NACA RM No. L7C27, 1947.

TABLE I.- INDEX TO THE BASIC DATA FIGURES

General Configuration	ψ (deg)	α_u (deg)	Fig. No.
Longitudinal characteristics			
Clean condition (R effect)	0	Variable	6
Droop nose flaps	0	Do.	7
Stall control vanes	0	Do.	8(a)
Stall control vanes + droop nose flap	0	Do.	8(b)
Longitudinal, lateral, directional stability			
Clean condition	0,4,8	Variable	9
Do.	Variable	0,6,9,12	17
Droop nose flap	0,4,8	Variable	10
Do.	Variable	0,6,9,12	18
Stall control vane	0,4,8	Variable	11
Do.	Variable	0,6,9,12	19
Droop nose flap + stall vane	0,4,8	Variable	12
Do.	Variable	0,6,9,12	20
Skyhook	0,4,8	Variable	13
Do.	Variable	0,6,9,12	21
Dive brake	0,4,8	Variable	14
Do.	Variable	0,6,9,12	22
Stall vane - center vertical tail fin	0,4,8	Variable	15
Do.	Variable	0,6,9,12	23

TABLE I.- CONTINUED.

General Configuration	ψ (deg)	α_u (deg)	Fig. No.
Longitudinal, lateral, directional stability (cont.)			
Stall vane + skyhook – center fin	0,4,8	Variable	16
Do.	Variable	0,6,9,12	24
Aileron characteristics			
Clean condition (δ_a=0,±6,12)	0	Variable	25
Clean condition (δ_a var.)	0	0,6,12	26
Do.	4	0,6,12	27
Do.	8	0,6,12	28
Do.	–4	0,6,12	29
Do.	–8	0,6,12	30
Do.	–12	0,6,12	31
Clean condition (δ_a=0; δ_{tab}=0,5)	0	Variable	32
Clean condition (δ_a var; δ_{tab}=0,–10)	0	0	33
Ruddervator characteristics (single set)			
Clean condition (δ_r=0,±8,–16)	0	Variable	34
Skyhook (δ_r=0,±8,–16)	0	Variable	35
Divebrake (δ_r=0,±8,–16)	0	Do.	36

TABLE I.- CONTINUED.

General Configuration	Ψ (deg)	α_u (deg)	Fig. No.
Ruddervator characteristics (single set) (cont.)			
Clean condition (δ_r var.)	0	0,6,12	37
Do.	4	0,6,12	38
Do.	8	0,6,12	39
Do.	12	0,6,12	40
Do.	-4	0,6,12	41
Do.	-8	0,6,12	42
Do.	-12	0,6,12	43
Skyhook (δ_r var.)	0	0,6,12	44
Do.	4	0,6,12	45
Do.	8	0,6,12	46
Do.	-4	0,6,12	47
Dive brake (δ_r var.)	0	0,6,12	48
Do.	4	0,6,12	49
Do.	8	0,6,12	50
Do.	-4	0,6,12	51
Do.	-8	0,6,12	52
Clean condition (δ_r=0,±8,-12)	Variable	0	53
Do.	Do.	6	54

TABLE I.- CONCLUDED.

General Configuration	ψ (deg)	α_u (deg)	Fig. No.
Ruddervator characteristics (single set) (cont.)			
Skyhook (δ_r=0,±8,-12)	Variable	0	55
Do.	Do.	6	56
Dive brake (δ_r=0,±8,-12)	Do.	0	57
Do.	Do.	6	58
Clean condition (δ_r=0;δ_{tab}=0,10,15)	0	Variable	59(a)
Clean condition (δ_r=-16;δ_{tab}=0,10,15)	0	Do.	59(b)
Clean condition (δ_r=8;δ_{tab}=0,-10)	0	Do.	59(c)
Clean condition (δ_r var.; δ_{tab}=0,10)	0	0	60
Elevator characteristics (complete ruddervator system)			
Clean condition (δ_r var.)	0	0,6,12	61
Rudder characteristics (complete ruddervator system)			
Clean condition (δ_r var.)	0	0,6,12	62
Do.	4	0,6,12	63
Do.	8	0,6,12	64
Do.	12	0,6,12	65
Directional stability			
Modifications to skyhook	Variable	0,9	66

FIGURE LEGENDS

Figure 1.- Sign convention for the standard NACA coefficients. All forces, moments, angles, and control-surface deflections are shown as positive.

Figure 2.- Three-view drawing of the McDonnell XP-85 airplane.

Figure 3.- Details of the stall control vane test installations.

Figure 4.- Detail of the skyhook in the extended position on the McDonnell XP-85 airplane.

Figure 5.- View of the installation of the McDonnell XP-85 airplane in the Ames 40- by 80-foot wind tunnel. (a) Airplane with stall control vanes P_2.

Figure 5.- Concluded. (b) Airplane with stall control vanes P_2 and the dive brake extended.

Figure 6.- Effect of a variation in Reynolds number on the aerodynamic characteristics of the airplane. Clean condition; ψ, 0°.

Figure 7.- Aerodynamic characteristics of the airplane with various droop nose modifications. ψ, 0°.

Figure 8.- Effect of stall control vane location and height on the aerodynamic characteristics of the airplane. ψ, 0°. (a) Droop nose flap retracted.

Figure 8.- Concluded. (b) Droop nose flap extended.

Figure 9.- Aerodynamic characteristics in pitch of the airplane at various angles of yaw. Clean condition. (a) C_D, α, C_m vs C_L.

Figure 9.- Concluded. (b) C_Y, C_n, C_l vs C_L.

Figure 10.- Aerodynamic characteristics ir pitch of the airplane at various angles of yaw. Droop nose flap extended. (a) C_D, α, C_m vs C_L.

Figure 10.- Concluded. (b) C_Y, C_n, C_l vs C_L.

Figure 11.– Aerodynamic characteristics in pitch of the airplane at various angles of yaw. Stall control vanes P_2 installed. (a) C_D, α, C_m vs C_L.

Figure 11.– Concluded. (b) C_Y, C_n, C_l vs C_L.

Figure 12.– Aerodynamic characteristics in pitch of the airplane at various angles of yaw. Droop nose flap extended; stall control vanes P_2 installed. (a) C_D, α, C_m vs C_L.

Figure 12.– Concluded. (b) C_Y, C_n, C_l vs C_L.

Figure 13.– Aerodynamic characteristics in pitch of the airplane at various angles of yaw. Skyhook extended. (a) C_D, α, C_m vs C_L.

Figure 13.– Concluded. (b) C_Y, C_n, C_l vs C_L.

Figure 14.– Aerodynamic characteristics in pitch of the airplane at various angles of yaw. Dive brake extended. (a) C_D, α, C_m vs C_L.

Figure 14.– Concluded. (b) C_Y, C_n, C_l vs C_L.

Figure 15.– Aerodynamic characteristics in pitch of the airplane at varous angles of yaw. Center vertical fin removed; stall vane P_2 installed. (a) C_D, α, C_m vs C_L.

Figure 15.– Concluded. (b) C_Y, C_n, C_l vs C_L.

Figure 16.– Aerodynamic characteristics in pitch of the airplane at various angles of yaw. Center vertical fin removed; stall vane P_2 installed; skyhook extended. (a) C_D, α, C_m vs C_L.

Figure 16.– Concluded. (b) C_Y, C_n, C_l vs C_L.

Figure 17.– Aerodynamic characteristics in yaw of the airplane at various angles of attack. Clean condition. (a) C_Y, C_l, C_n vs ψ.

Figure 17.– Concluded. (b) C_L, C_m vs ψ.

Figure 18.– Aerodynamic characteristics in yaw of the airplane at various angles of attack. Droop nose flap extended. (a) C_Y, C_l, C_n vs ψ.

Figure 18.– Concluded. (b) C_L, C_m vs Ψ.

Figure 19.– Aerodynamic characteristics in yaw of the airplane at various angles of attack. Stall control vanes P_2 installed. (a) C_Y, C_L, C_n vs ψ.

Figure 19.– Concluded. (b) C_L, C_m vs Ψ.

Figure 20.– Aerodynamic characteristics in yaw of the airplane at various angles of attack. Droop nose flap extended; stall control vanes P_2 installed. (a) C_Y, C_l, C_n vs Ψ.

Figure 20.– Concluded. (b) C_L, C_m vs Ψ .

Figure 21.– Aerodynamic characteristics in yaw of the airplane at various angles of attack. Skyhook extended. (a) C_Y, C_l, C_n vs Ψ.

Figure 21.– Concluded. (b) C_L, C_m vs Ψ.

Figure 22.– Aerodynamic characteristics in yaw of the airplane at various angles of attack. Dive brake extended. (a) C_Y, C_l, C_n vs Ψ.

Figure 22.– Concluded. (b) C_L, C_m vs Ψ.

Figure 23.– Aerodynamic characteristics in yaw of the airplane at various angles of attack. Center vertical fin removed; stall control vanes P_2 installed. (a) C_Y, C_l, C_n vs Ψ.

Figure 23.– Concluded. (b) C_L, C_m vs Ψ.

Figure 24.– Aerodynamic characteristics in yaw of the airplane at various angles of attack. Center vertical fin removed; stall control vanes P_2 installed; skyhook extended. (a) C_Y, C_l, C_n vs Ψ.

Figure 24.– Concluded. (b) C_L, C_m vs Ψ.

Figure 25.– Effect of fixed deflections of the right aileron on the aerodynamic characteristics of the airplane in pitch. Clean condition; Ψ , 0°. (a) α, C_m, C_n vs C_L.

Figure 25.– Concluded. (b) C_l, C_{h_a} vs C_L.

Figure 26.- Variation with deflection of the right aileron of the aerodynamic characteristics of the airplane at several angles of attack. Clean condition; ψ, 0°. (a) C_l, C_{h_a} vs δ_a.

Figure 26.- Concluded. (b) C_n, C_m vs δ_a.

Figure 27.- Variation with deflection of the right aileron of the aerodynamic characteristics of the airplane at several angles of attack. Clean condition; ψ, 4°. (a) C_l, C_{h_a} vs δ_a.

Figure 27.- Concluded. (b) C_n, C_m vs δ_a.

Figure 28.- Variation with deflection of the right aileron of the aerodynamic characteristics of the airplane at several angles of attack. Clean condition; ψ, 8°. (a) C_l, C_{h_a} vs δ_a.

Figure 28.- Concluded. (b) C_n, C_m vs δ_a.

Figure 29.- Variation with deflection of the right aileron of the aerodynamic characteristics of the airplane at several angles of attack. Clean condition; ψ, -4°. (a) C_l, C_{h_a} vs δ_a.

Figure 29.- Concluded. (b) C_n, C_m vs δ_a.

Figure 30.- Variation with deflection of the right aileron of the aerodynamic characteristics of the airplane at several angles of attack. Clean condition; ψ, -8°. (a) C_l, C_{h_a} vs δ_a.

Figure 30.- Concluded. (b) C_n, C_m vs δ_a.

Figure 31.- Variation with deflection of the right aileron of the aerodynamic characteristics of the airplane at several angles of attack. Clean condition; ψ, -12°. (a) C_l, C_{h_a} vs δ_a.

Figure 31.- Concluded. (b) C_n, C_m vs δ_a.

Figure 32.- Effect of fixed deflections of the right aileron balance tab on the aerodynamic characteristics of the airplane in pitch. Clean condition; δ_a, 0°; ψ, 0°.

Figure 33.- Effect of fixed deflections of the balance tab on the effectiveness of the right aileron. Clean condition; α_u, 0°; ψ, 0°.

Figure 34.– Effect of fixed deflections of the upper right and lower left ruddervator on the aerodynamic characteristics of the airplane in pitch. Clean condition; ψ, 0°. (a) α, C_l, C_Y vs C_L.

Figure 34.– Concluded. (b) C_m, C_n, C_{h_r} vs C_L.

Figure 35.– Effect of fixed deflections of the upper right and lower left ruddervator on the aerodynamic characteristics of the airplane in pitch. Skyhook extended; ψ, 0°. (a) α, C_l, C_Y vs C_L.

Figure 35.– Concluded. (b) C_m, C_n, C_{h_r} vs C_L.

Figure 36.– Effect of fixed deflections of the upper right and lower left ruddervator on the aerodynamic characteristics of the airplane in pitch. Dive brake extended; ψ, 0°. (a) α, C_l, C_Y vs C_L.

Figure 36.– Concluded. (b) C_m, C_n, C_{h_r} vs C_L.

Figure 37.– Variation with deflection of the upper right and lower left ruddervator of the aerodynamic characteristics of the airplane at several angles of attack. Clean condition; ψ, 0°. (a) C_n, C_m, C_{h_r} vs δ_r.

Figure 37.– Concluded. (b) C_L, C_Y, C_l, vs δ_r.

Figure 38.– Variation with deflection of the upper right and lower left ruddervator of the aerodynamic characteristics of the airplane at several angles of attack. Clean condition; ψ, 4°. (a) C_n, C_m, C_{h_r} vs δ_r.

Figure 38.– Concluded. (b) C_Y, C_l, vs δ_r.

Figure 39.– Variation with deflection of the upper right and lower left ruddervator of the aerodynamic characteristics of the airplane at several angles of attack. Clean condition; ψ, 8°. (a) C_n, C_m, C_{h_r} vs δ_r.

Figure 39.– Concluded. (b) C_Y, C_l vs δ_r.

Figure 40.- Variation with deflection of the upper right and lower left ruddervator of the aerodynamic characteristics of the airplane at several angles of attack. Clean condition; ψ, 12°. (a) C_n, C_m, C_{h_r} vs δ_r.

Figure 40.- Concluded. (b) C_Y, C_l vs δ_r.

Figure 41.- Variation with deflection of the upper right and lower left ruddervator of the aerodynamic characteristics of the airplane at several angles of attack. Clean condition; ψ, -4°. (a) C_n, C_m, C_{h_r} vs δ_r.

Figure 41.- Concluded. (b) C_Y, C_l vs δ_r.

Figure 42.- Variation with deflection of the upper right and lower left ruddervator of the aerodynamic characteristics of the airplane at several angles of attack. Clean condition; ψ, -8°. (a) C_n, C_m, C_{h_r} vs δ_r.

Figure 42.- Concluded. (b) C_Y, C_l vs δ_r.

Figure 43.- Variation with deflection of the upper right and lower left ruddervator of the aerodynamic characteristics of the airplane at several angles of attack. Clean condition; ψ, -12°. (a) C_n, C_m, C_{h_r} vs δ_r.

Figure 43.- Concluded. (b) C_Y, C_l vs δ_r.

Figure 44.- Variation with deflection of the upper right and lower left ruddervator of the aerodynamic characteristics of the airplane at several angles of attack. Skyhook extended; ψ, 0°. (a) C_n, C_m, C_{h_r} vs δ_r.

Figure 44.- Concluded. (b) C_L, C_Y, C_l vs δ_r.

Figure 45.- Variation with deflection of the upper right and lower left ruddervator of the aerodynamic characteristics of the airplane at several angles of attack. Skyhook extended; ψ, 4°. (a) C_n, C_m, C_{h_r} vs δ_r.

Figure 45.- Concluded. (b) C_Y, C_l vs δ_r.

Figure 46.- Variation with deflection of the upper right and lower left ruddervator of the aerodynamic characteristics of the airplane at several angles of attack. Skyhook extended; ψ, 8°. (a) C_n, C_m, C_{h_r} vs δ_r.

Figure 46.- Concluded. (b) C_Y, C_l vs δ_r.

Figure 47.- Variation with deflection of the upper right and lower left ruddervator of the aerodynamic characteristics of the airplane at several angles of attack. Skyhook extended; ψ, -4°. (a) C_n, C_m, C_{h_r} vs δ_r.

Figure 47.- Concluded. (b) C_Y, C_l vs δ_r.

Figure 48.- Variation with deflection of the upper right and lower left ruddervator of the aerodynamic characteristics of the airplane at several angles of attack. Dive brake extended; ψ, 0°. (a) C_n, C_m, C_{h_r} vs δ_r.

Figure 48.- Concluded. (b) C_L, C_Y, C_l vs δ_r.

Figure 49.- Variation with deflection of the upper right and lower left ruddervator of the aerodynamic characteristics of the airplane at several angles of attack. Dive brake extended; ψ, 4°. (a) C_n, C_m, C_{h_r} vs δ_r.

Figure 49.- Concluded. (b) C_Y, C_l vs δ_r.

Figure 50.- Variation with deflection of the upper right and lower left ruddervator of the aerodynamic characteristics of the airplane at several angles of attack. Dive brake extended; ψ, 8°. (a) C_n, C_m, C_{h_r} vs δ_r.

Figure 50.- Concluded. (b) C_Y, C_l vs δ_r.

Figure 51.- Variation with deflection of the upper right and lower left ruddervator of the aerodynamic characteristics of the airplane at several angles of attack. Dive brake extended; ψ, -4°. (a) C_n, C_m, C_{h_r} vs δ_r.

Figure 51.- Concluded. (b) C_Y, C_l vs δ_r.

Figure 52.- Variation with deflection of the upper right and lower left ruddervator of the aerodynamic characteristics of the airplane at several angles of attack. Dive brake extended; ψ, -8°. (a) C_n, C_m, C_{h_r} vs δ_r.

Figure 52.- Concluded. (b) C_Y, C_l vs δ_r.

Figure 53.- Effect of fixed deflections of the upper right and lower left ruddervator on the aerodynamic characteristics of the airplane in yaw. Clean condition; α_u, 0°. (a) C_n, C_m, C_{h_r} vs ψ.

Figure 53.- Concluded. (b) C_Y, C_l vs ψ.

Figure 54.- Effect of fixed deflections of the upper right and lower left ruddervator on the aerodynamic characteristics of the airplane in yaw. Clean condition; α_u, 6°. (a) C_n, C_m, C_{h_r} vs ψ.

Figure 54.- Concluded. (b) C_Y, C_l vs ψ.

Figure 55.- Effect of fixed deflections of the upper right and lower left ruddervator on the aerodynamic characteristics of the airplane in yaw. Skyhook extended; α_u, 0°. (a)C_n, C_m, C_{h_r} vs ψ.

Figure 55.- Concluded. (b) C_Y, C_l vs ψ.

Figure 56.- Effect of fixed deflections of the upper right and lower left ruddervator on the aerodynamic characteristics of the airplane in yaw. Skyhook extended; α_u, 6°. (a) C_n, C_m, C_{h_r} vs ψ.

Figure 56.- Concluded. (b) C_Y, C_l vs ψ.

Figure 57.- Effect of fixed deflections of the upper right and lower left ruddervator on the aerodynamic characteristics of the airplane in yaw. Dive brake extended; α_u, 0°. (a) C_n, C_m, C_{h_r} vs ψ.

Figure 57.- Concluded. (b) C_Y, C_l vs ψ.

Figure 58.- Effect of fixed deflections of the upper right and lower left ruddervator on the aerodynamic characteristics of the airplane in yaw, Dive brake extended; α_u, 6°. (a) C_n, C_m, C_{h_r} vs ψ.

Figure 58.- Concluded. (b) C_Y, C_l vs ψ.

Figure 59.- Effect of fixed deflections of the upper right ruddervator balance tab on the aerodynamic characteristics of the airplane in pitch. Clean condition; ψ, 0°. (a) δ_r, 0°.

Figure 59.- Continued. (b) δ_r, -16°.

Figure 59.- Concluded. (c) δ_r, 8°.

Figure 60.- Variation with deflection of the upper right and lower left ruddervator of the aerodynamic characteristics of the airplane with various fixed deflections of the upper right ruddervator balance tab. Clean condition; α_u, 0°; ψ, 0°.

Figure 61.- Variation of the aerodynamic characteristics of the airplane at several angles of attack with deflection of the complete ruddervator system operated for pure elevator action. Clean configuration; ψ, 0°.

Figure 62.- Variation of the aerodynamic characteristics of the airplane at several angles of attack with deflection of the complete ruddervator system operated for pure rudder action. Clean configuration; ψ, 0°. (a) C_n, C_m, C_{h_r} vs δ_r.

Figure 62.- Concluded. (b) C_Y, C_l vs δ_r.

Figure 63.- Variation of the aerodynamic characteristics of the airplane at several angles of attack with deflection of the complete ruddervator system operated for pure rudder action. Clean configuration; ψ, 4°. (a) C_n, C_m, C_{h_r} vs δ_r.

Figure 63.- Concluded. (b) C_Y, C_l vs δ_r.

Figure 64.- Variation of the aerodynamic characteristics of the airplane at several angles of attack with deflection of the complete ruddervator system operated for pure rudder action. Clean configuration; ψ, 8°. (a) C_n, C_m, C_{h_r} vs δ_r.

Figure 64.- Concluded. (b) C_Y, C_l vs δ_r.

Figure 65.- Variation of the aerodynamic characteristics of the airplane at several angles of attack with deflection of the complete ruddervator system operated for pure rudder action. Clean configuration; ψ, 12°. (a) C_n, C_m, C_{h_r} vs δ_r.

Figure 65.- Concluded. (b) C_Y, C_l vs δ_r.

Figure 66.- Summary of the directional stability characteristics of the airplane from tests of 20 modifications made in the investigation of the skyhook directional stability problem.
(a) Modifications 1 to 4.

Figure 66.- Continued. (b) Modifications 5 to 8.

Figure 66.- Continued. (c) Modifications 9 to 12.

Figure 66.- Continued. (d) Modifications 13 to 16.

Figure 66.- Concluded. (e) Modifications 17 to 20.

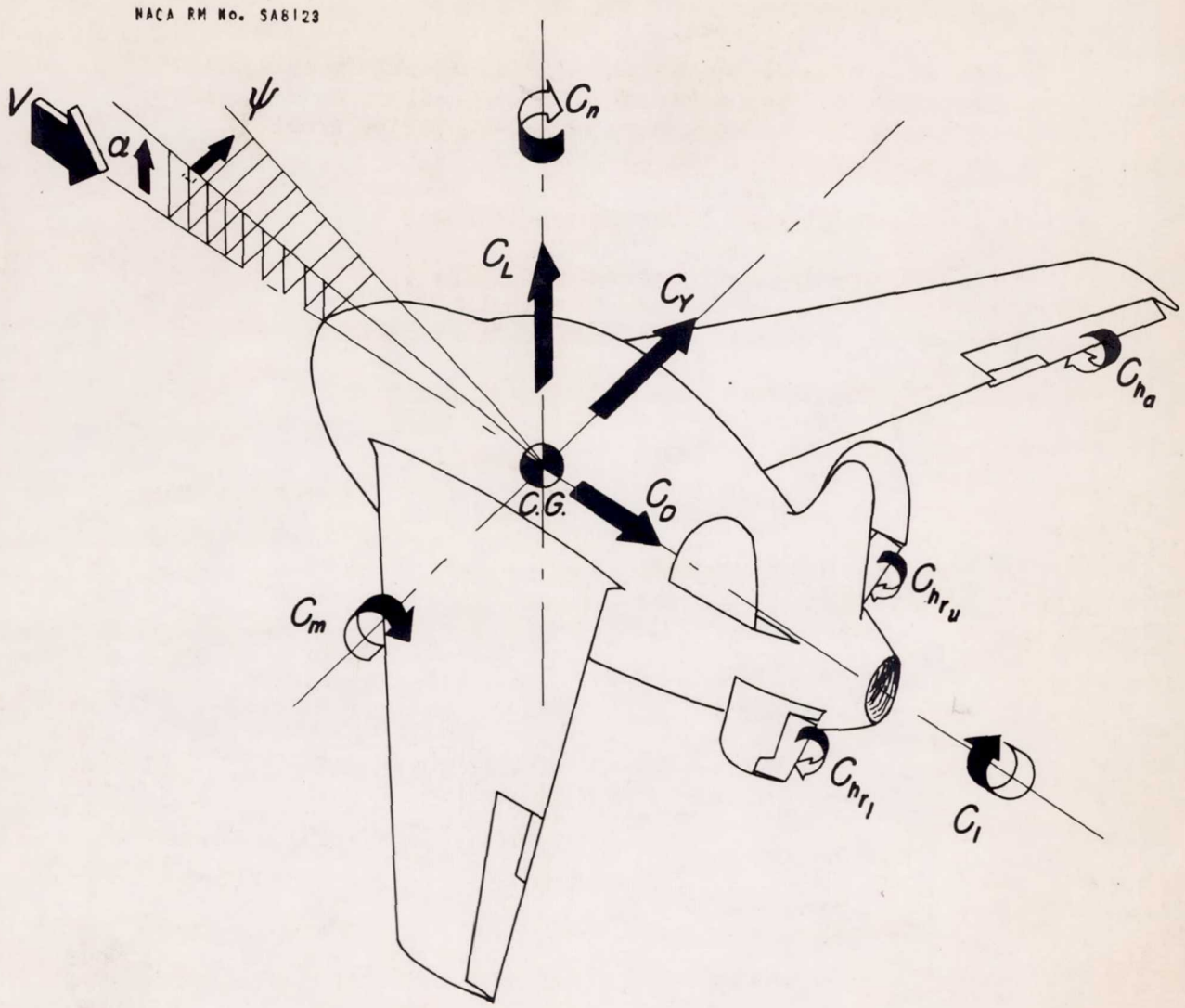

Figure 1.- Sign convention for the standard NACA coefficients. All forces, moments, angles, and control surface deflections are shown as positive.

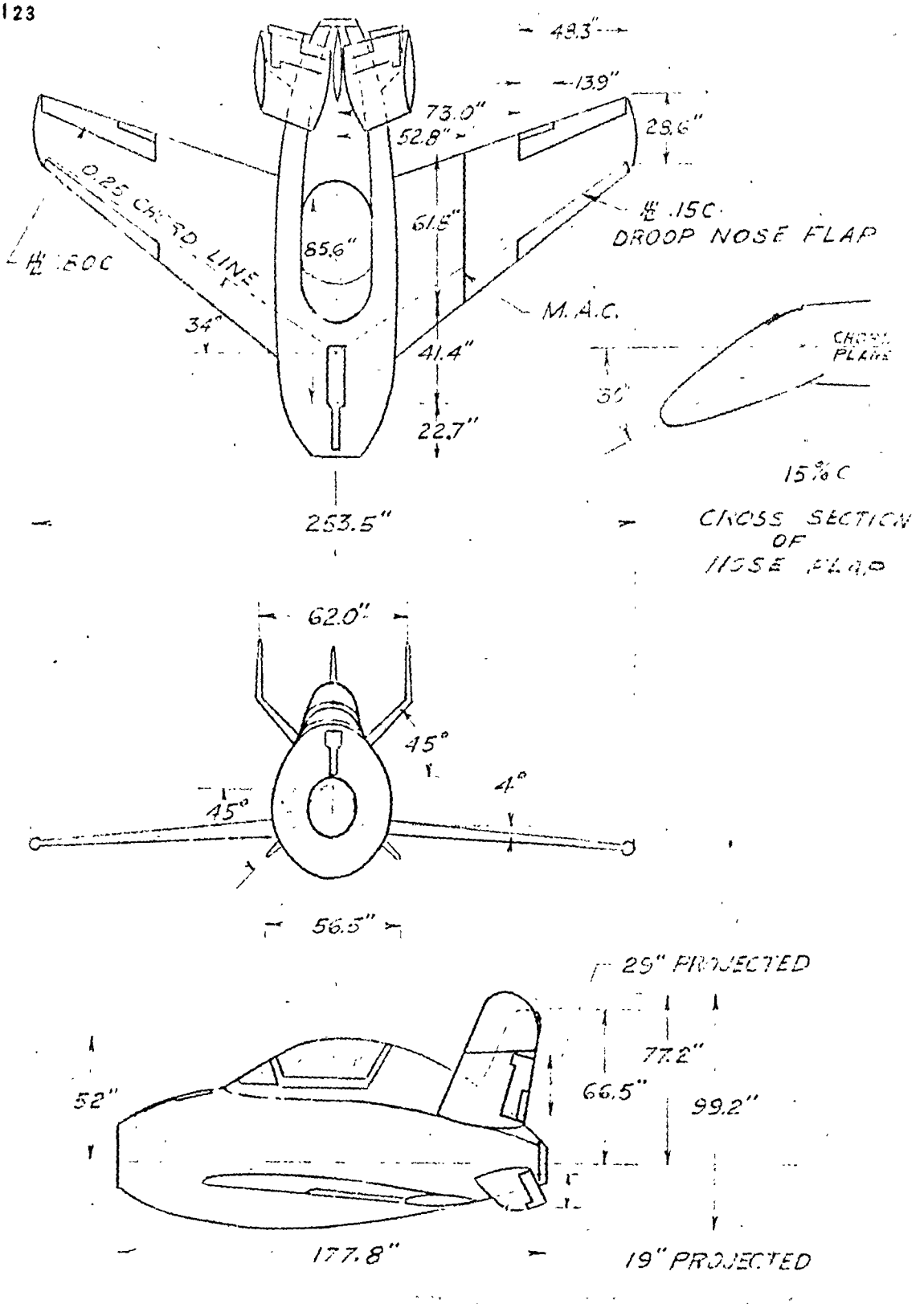

FIGURE 2.- THREE-VIEW DRAWING OF THE MCDONNELL XF-85 AIRPLANE.

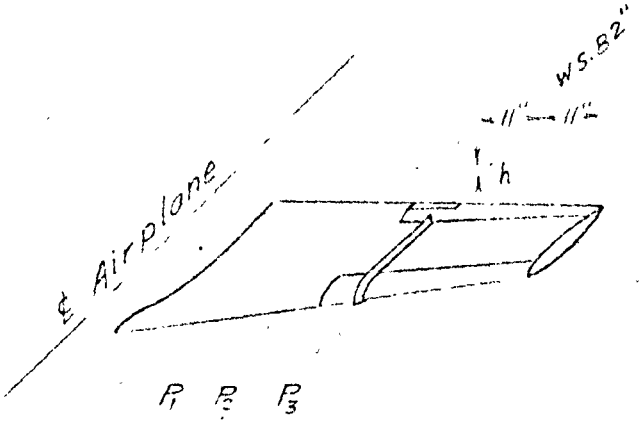

(a) DROOP NOSE FLAP RETRACTED.

STALL VANE	NOMINAL SPANWISE POSITION (% SPAN)	CHORDWISE LENGTH (% CHORD)	HEIGHT, h (IN.)
P_1	55	80	1-1/2
P_2	65	80	1-1/2, 1, 3
P_3	75	80	1-1/2

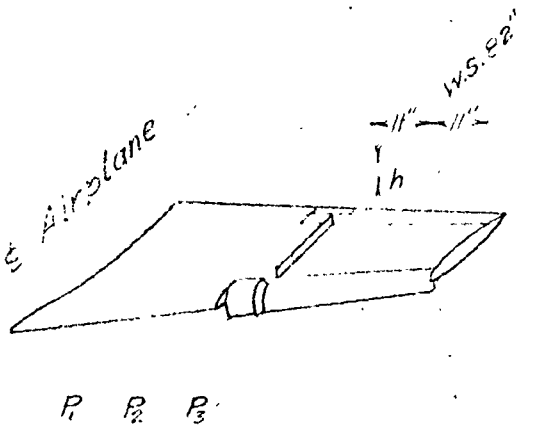

(b) DROOP NOSE FLAP EXTENDED.

CONFIDENTIAL

NATIONAL ADVISORY COMMITTEE FOR AERONAUTICS

FIGURE 3.- DETAILS OF THE STALL CONTROL VANE TEST INSTALLATIONS.

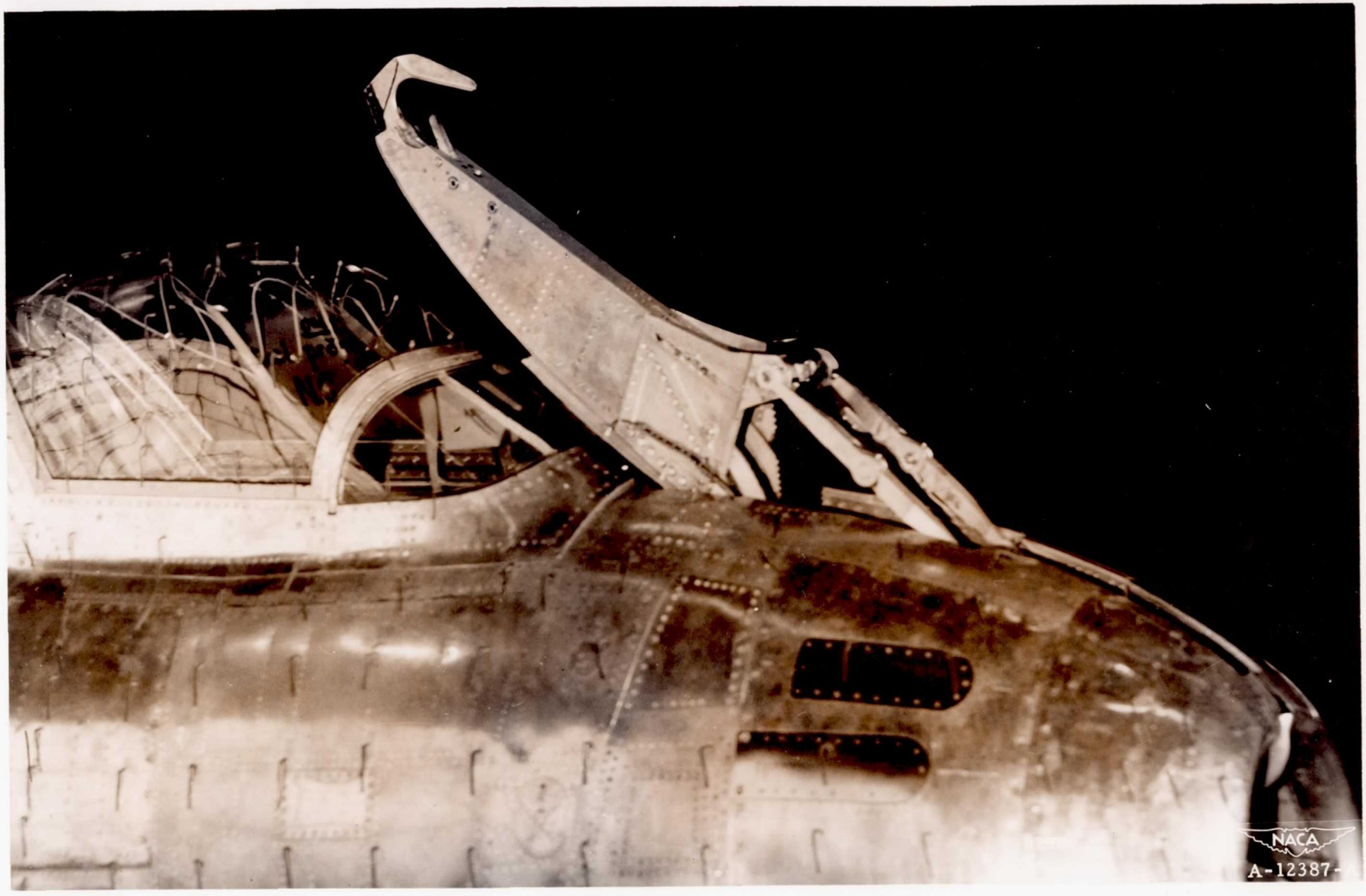

Figure 4.- Detail of the skyhook in the extended position on the McDonnell XP-85 airplane.

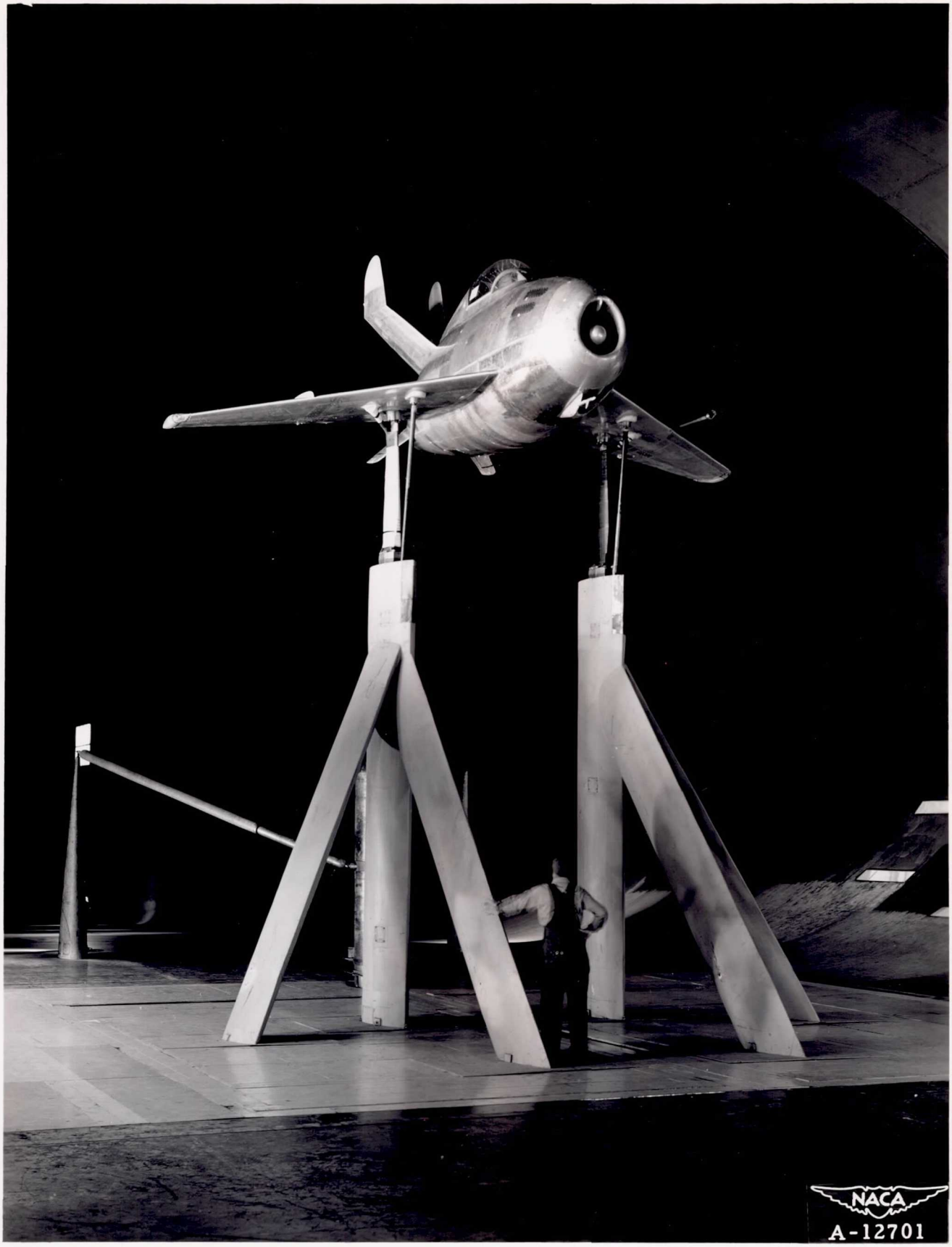

(a) Airplane with stall control vanes (P_2).

Figure 5.- View of the installation of the McDonnell XP-85 airplane in the Ames 40- by 80-foot wind tunnel.

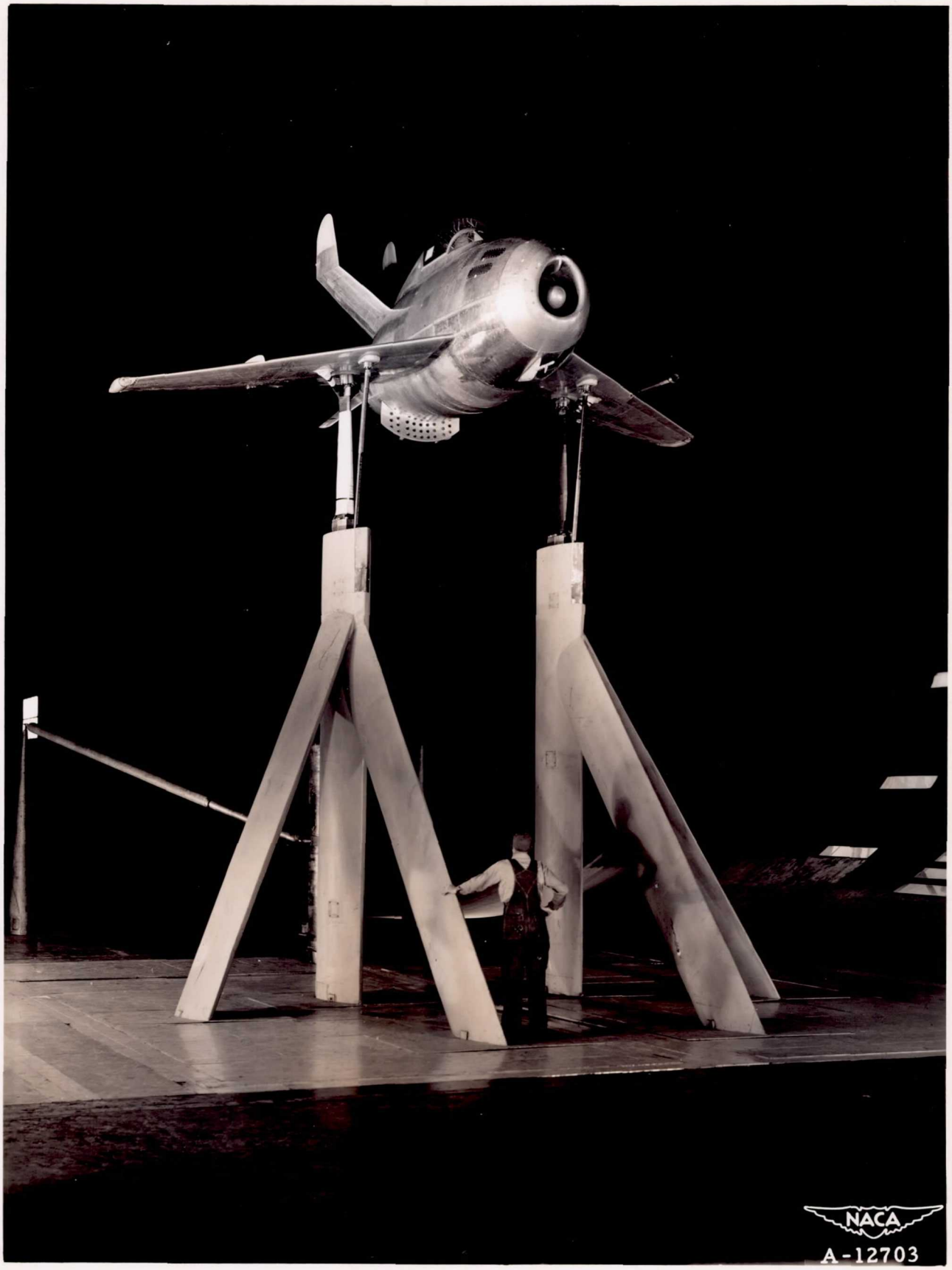

(b) Airplane with stall control vanes (P_2) and the dive brake extended.

Figure 5.- Concluded.

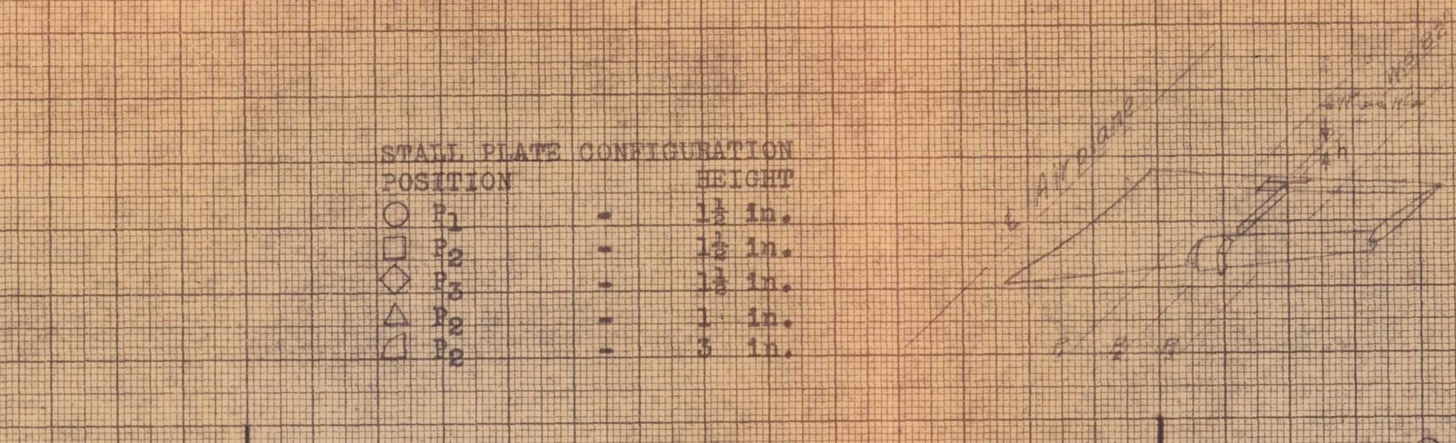

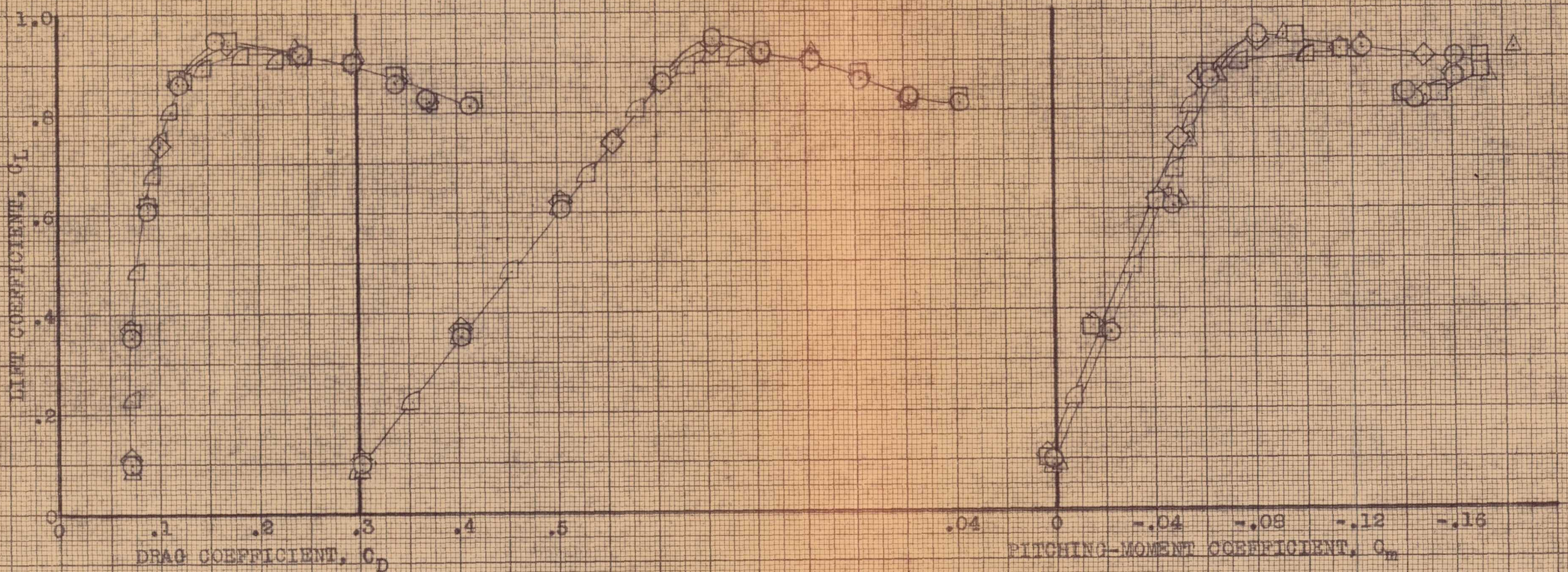

FIGURE 8.- CONCLUDED.
(b) DROOP NOSE FLAP EXTENDED.

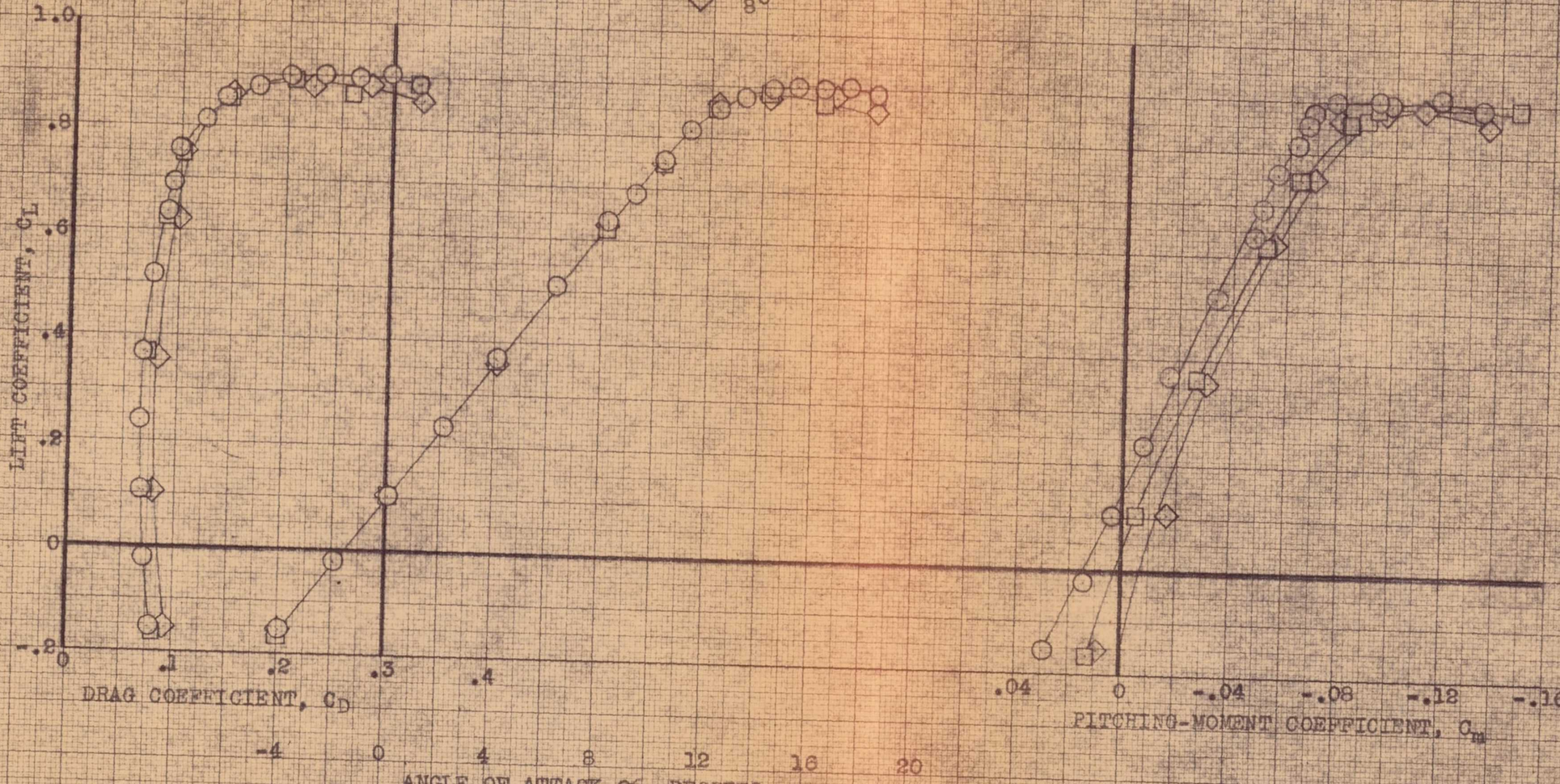

FIGURE 9.- AERODYNAMIC CHARACTERISTICS IN PITCH OF THE AIRPLANE AT VARIOUS ANGLES OF YAW. CLEAN CONDITION.

(a) C_D, α, C_m vs C_L.

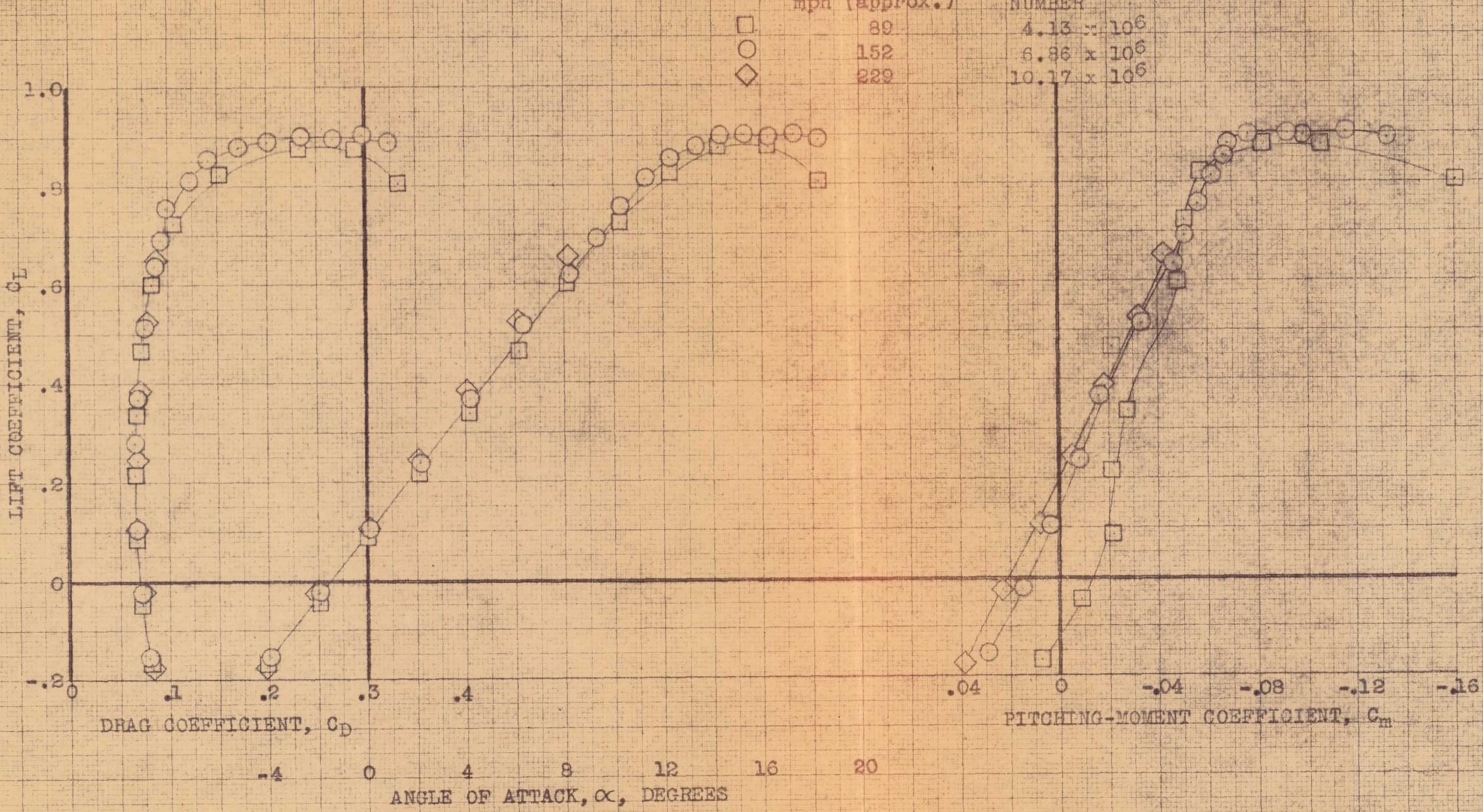

FIGURE 6.- EFFECT OF A VARIATION IN REYNOLDS NUMBER ON THE AERODYNAMIC CHARACTERISTICS OF THE AIRPLANE. CLEAN CONDITION; ψ, 0°.

CONFIGURATION

- ○ CLEAN
- □ DROOP NOSE DEFLECTED 30°
- ◇ DROOP NOSE DEFLECTED 30°, GAP AT OUTBOARD ENDS SEALED
- △ DROOP NOSE DEFLECTED 15°

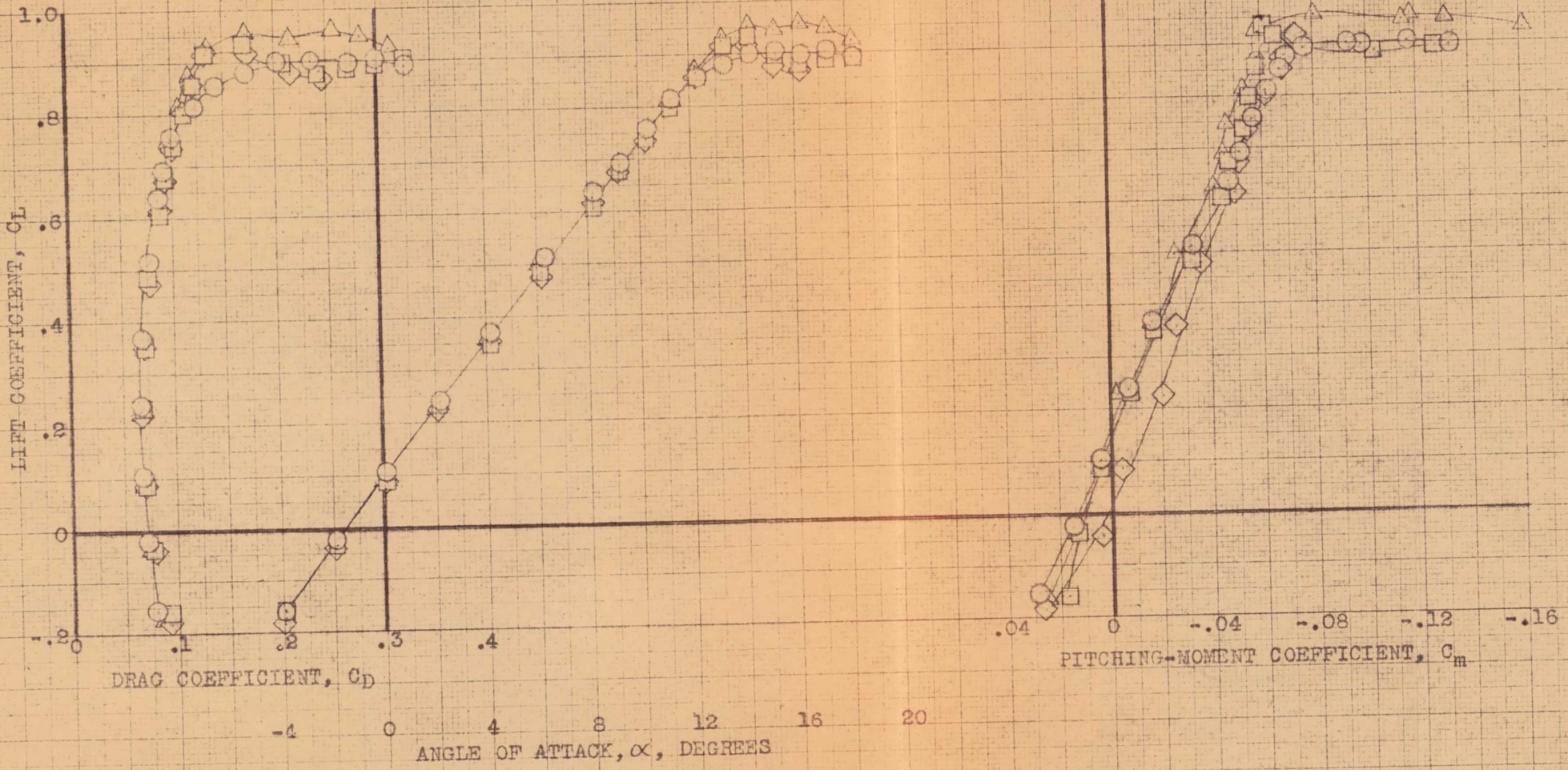

FIGURE 7.- AERODYNAMIC CHARACTERISTICS OF THE AIRPLANE WITH VARIOUS DROOP NOSE MODIFICATIONS. ψ, 0°.

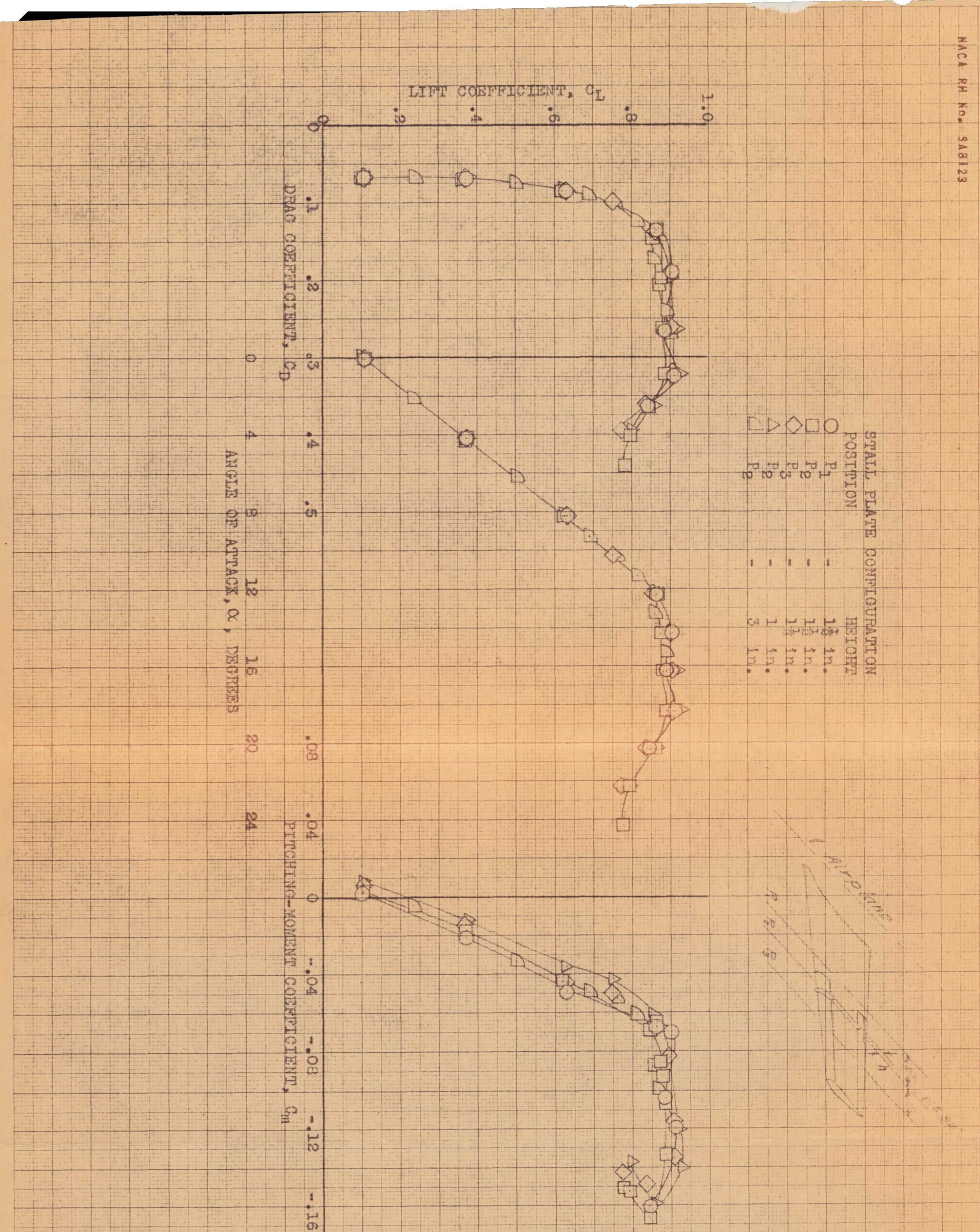

(a) DROOP NOSE FLAP RETRACTED.

FIGURE 8.- EFFECT OF STALL CONTROL VANE LOCATION AND HEIGHT ON THE AERODYNAMIC CHARACTERISTICS OF THE AIRPLANE. ψ, 0°.

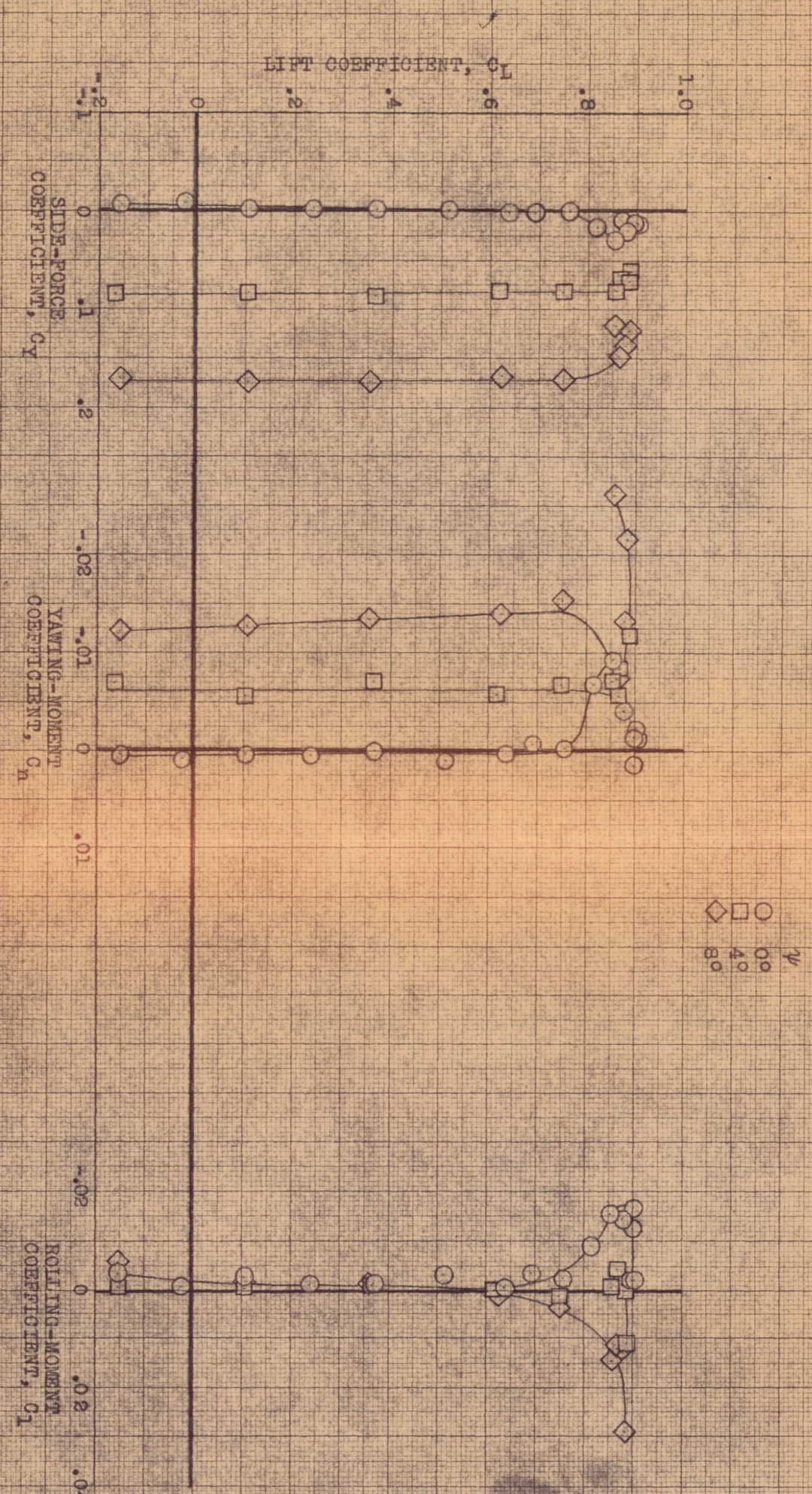

(b) C_Y, C_n, C_l, vs C_L.

FIGURE 9.- CONCLUDED.

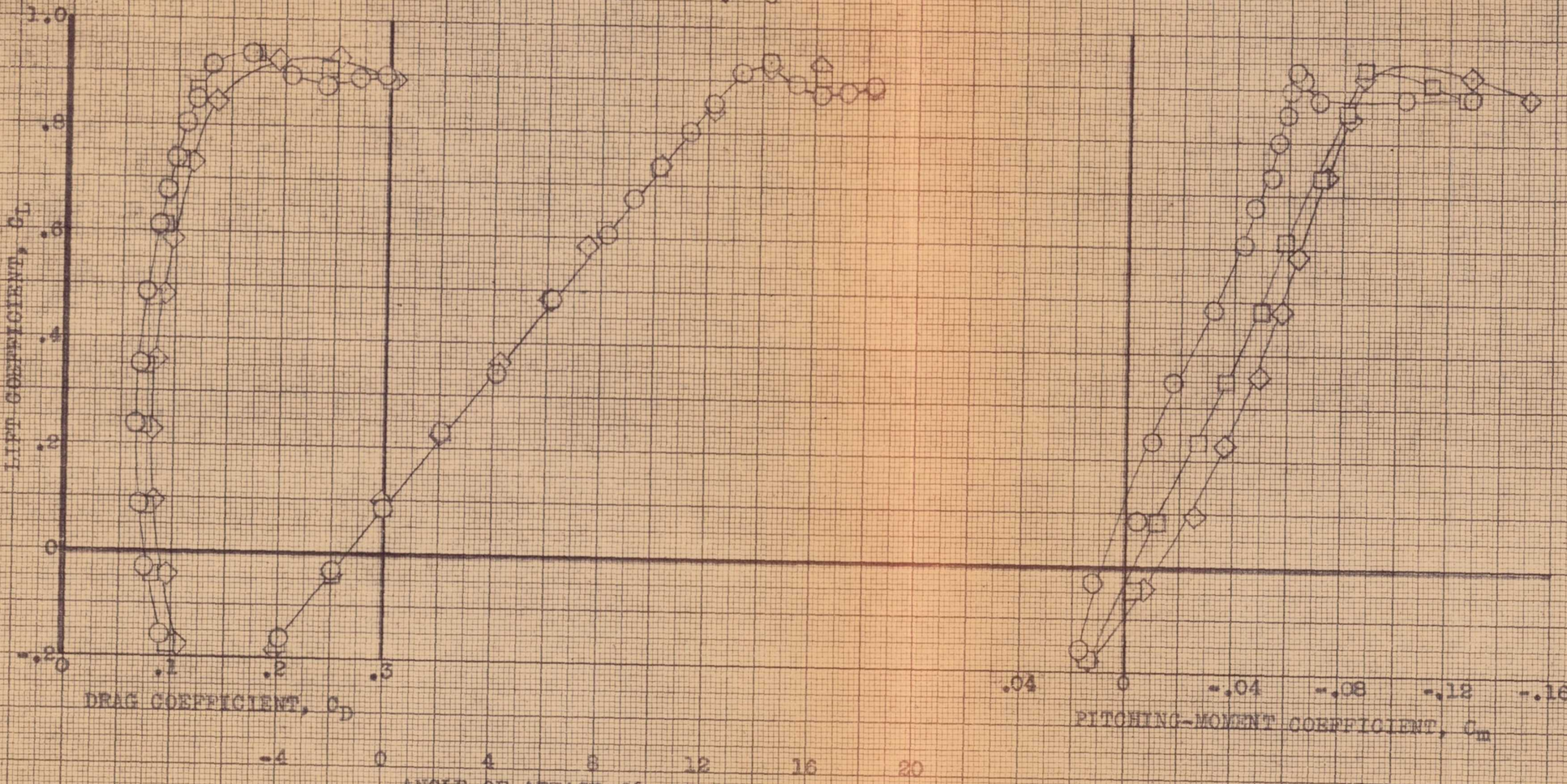

(d) C_D, α, C_m vs C_L.

FIGURE 10.- AERODYNAMIC CHARACTERISTICS IN PITCH OF THE AIRPLANE AT VARIOUS ANGLES OF YAW. DOUGLAS FLAP EXTENDED.

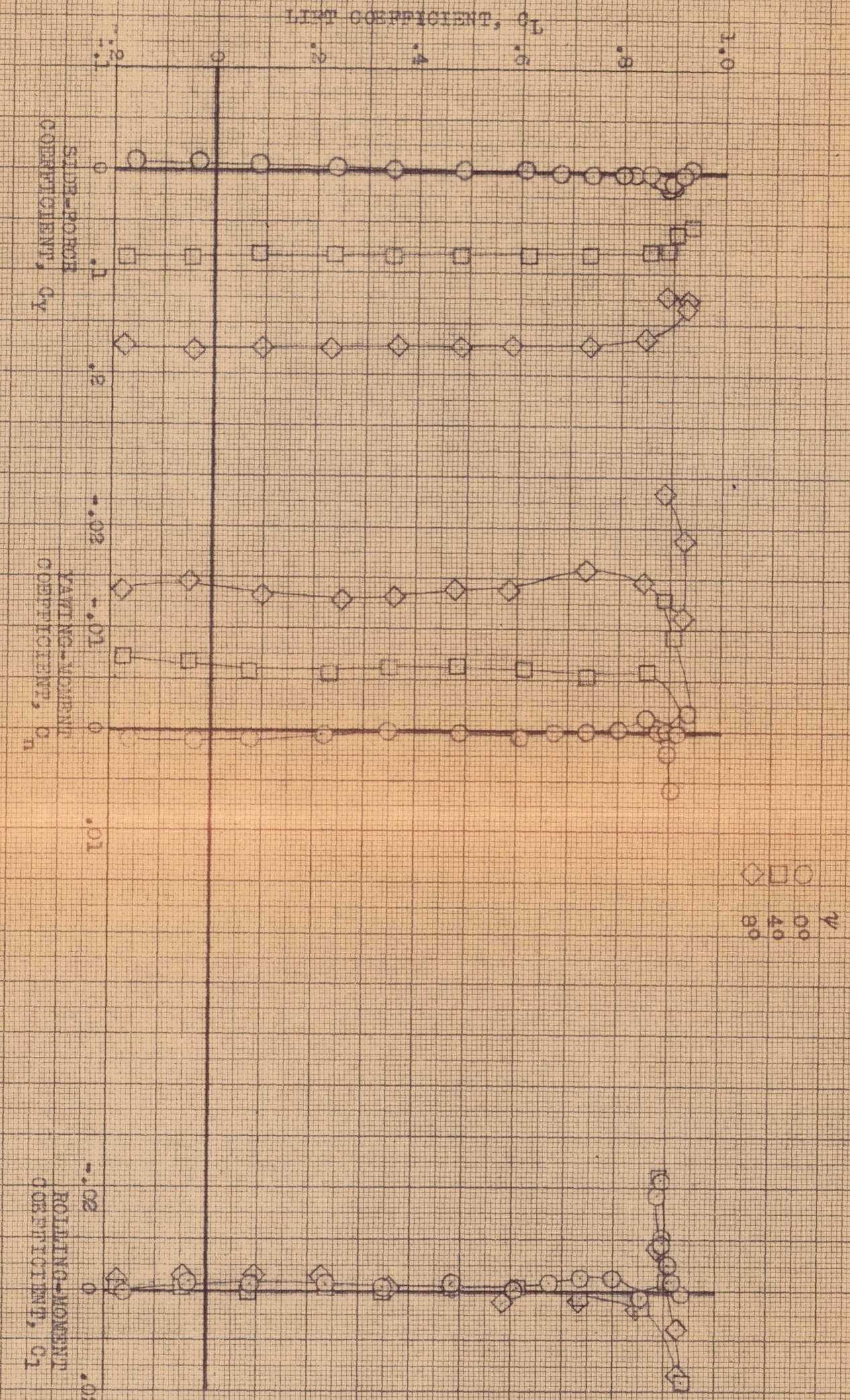

(b) C_Y, C_n, C_l vs C_L.

FIGURE 10.- CONCLUDED.

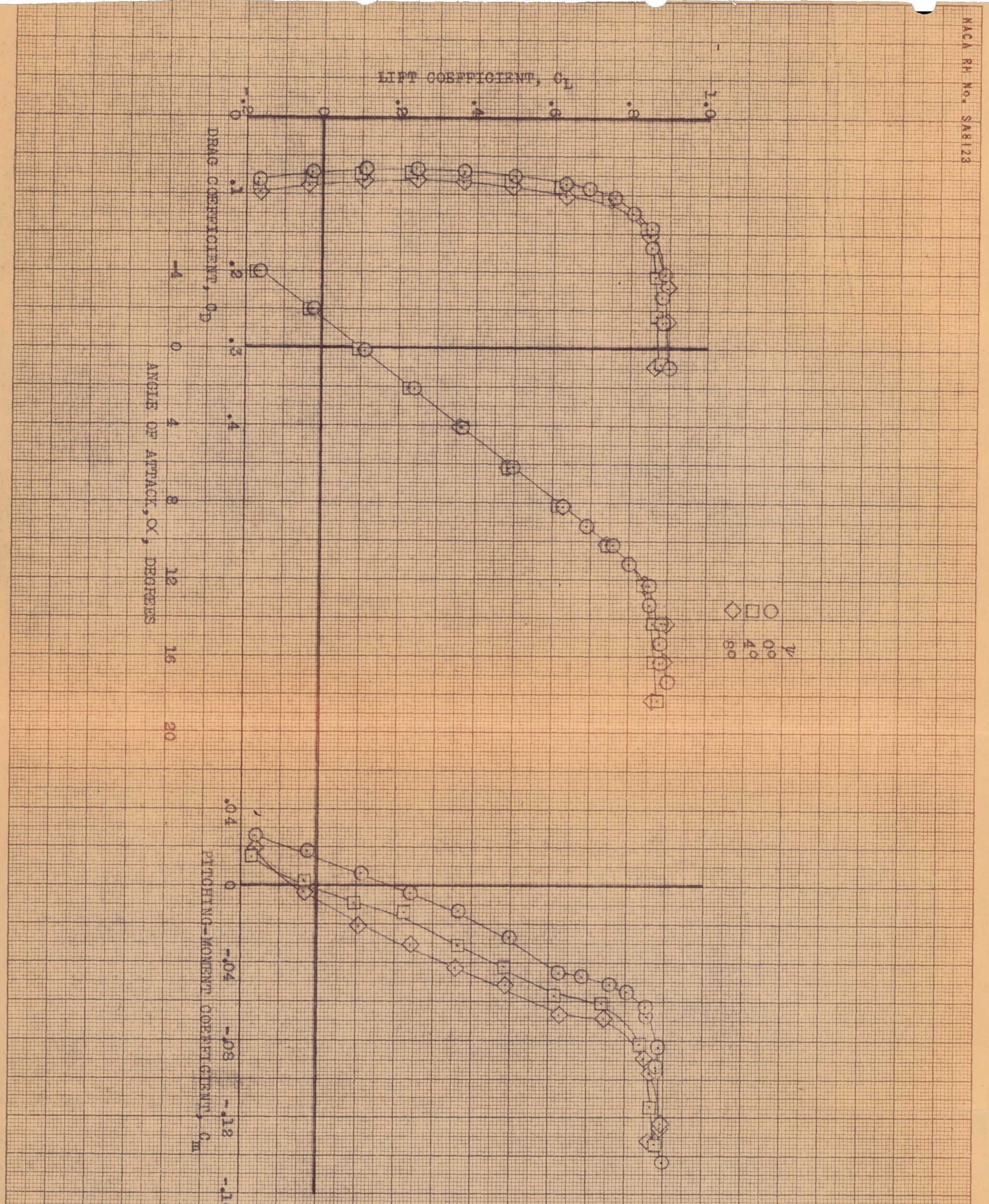

(a) C_D, α, C_m vs C_L.

FIGURE 11.- AERODYNAMIC CHARACTERISTICS IN PITCH OF THE AIRPLANE AT VARIOUS ANGLES OF YAW. STALL CONTROL VANES P_2 INSTALLED.

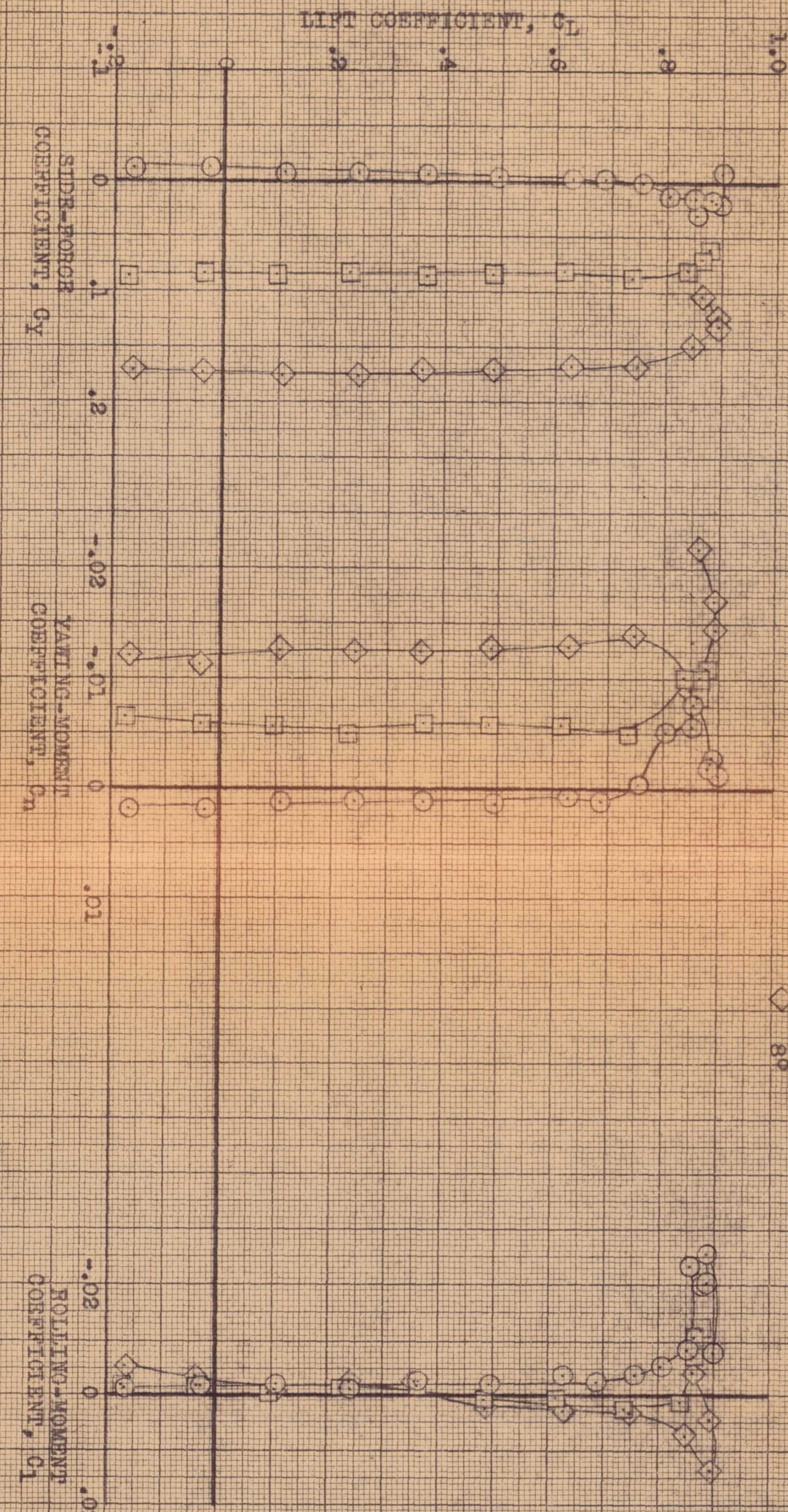

(b) C_Y, C_n, C_l vs C_L.

FIGURE 11.- CONCLUDED.

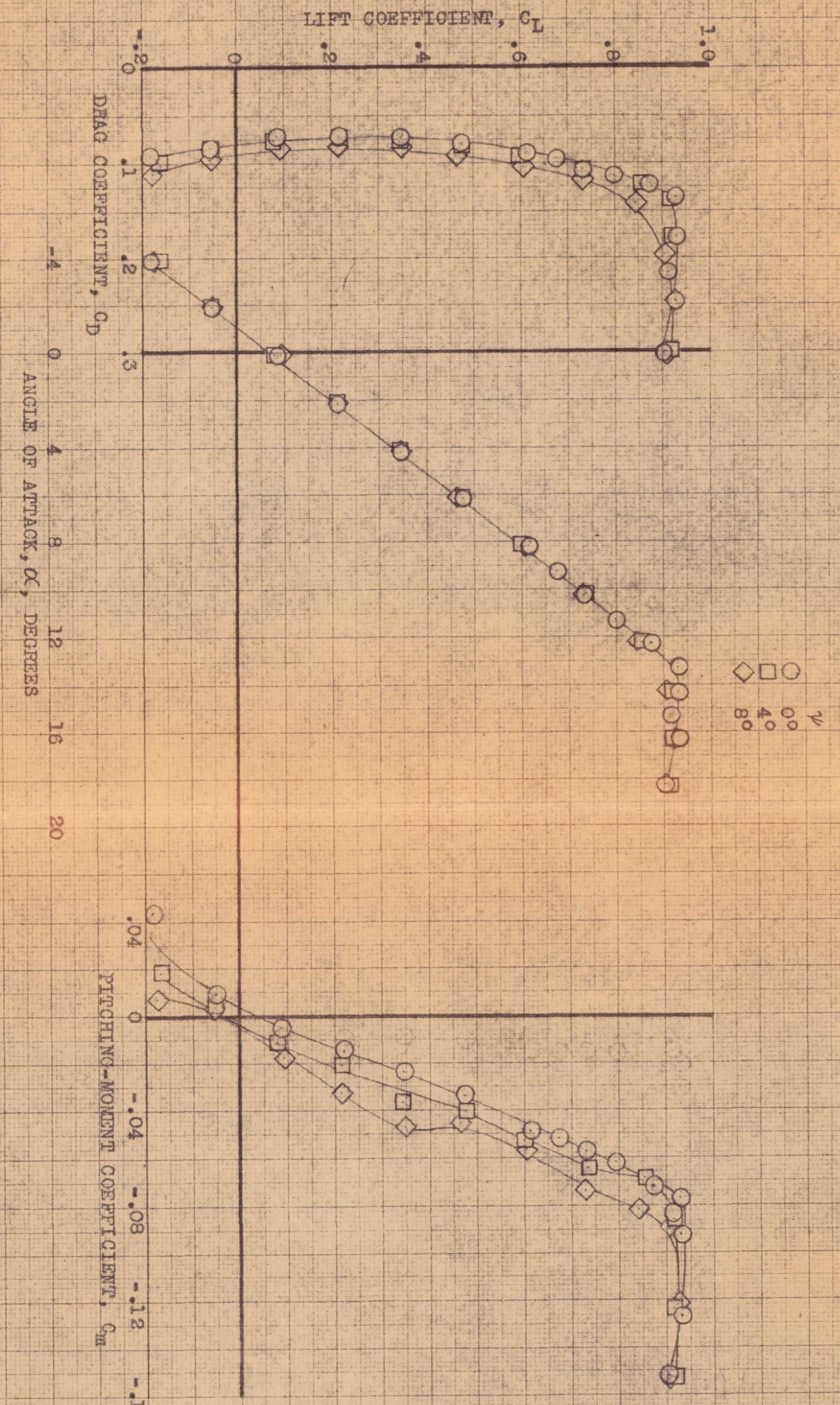

(a) C_D, α, C_m vs C_L.

FIGURE 12.- AERODYNAMIC CHARACTERISTICS IN PITCH OF THE AIRPLANE AT VARIOUS ANGLES OF YAW. DROOP NOSE FLAP EXTENDED; STALL CONTROL VANES P_2 INSTALLED.

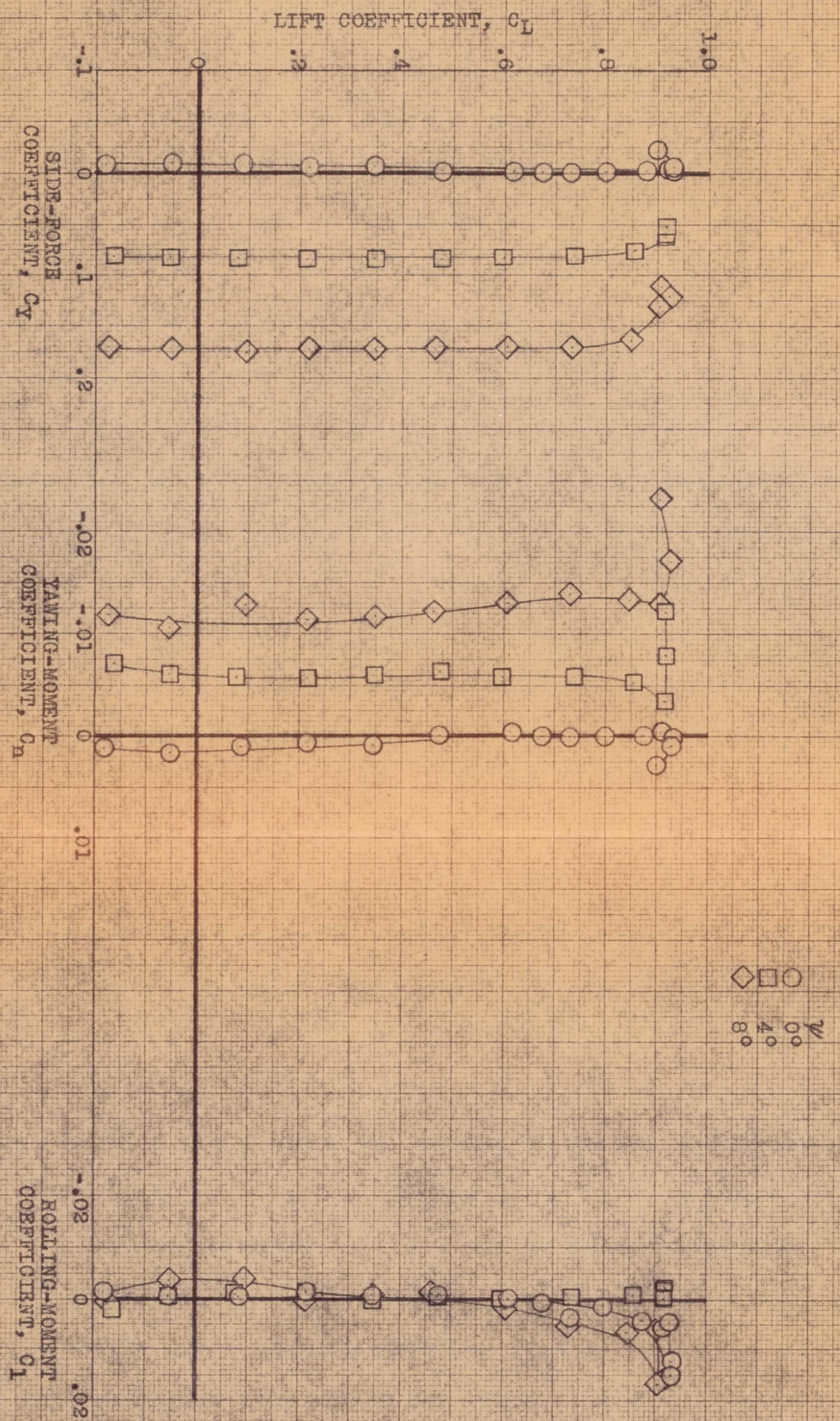

(b) C_Y, C_n, C_l vs C_L.

FIGURE 12.- CONCLUDED.

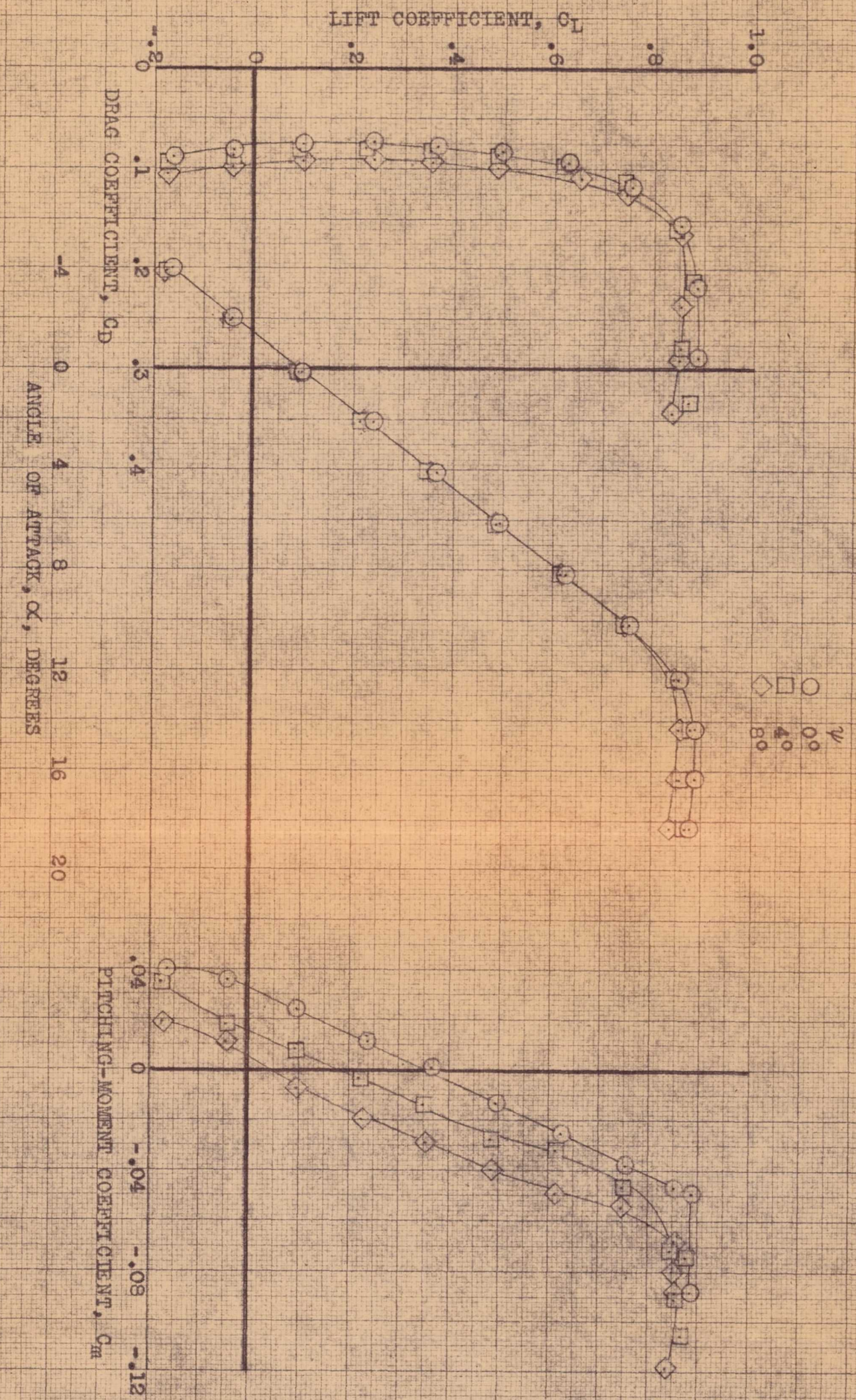

(a) C_D, α , C_m vs C_L.

FIGURE 13.- AERODYNAMIC CHARACTERISTICS IN PITCH OF THE AIRPLANE AT VARIOUS ANGLES OF YAW. SKYHOOK EXTENDED.

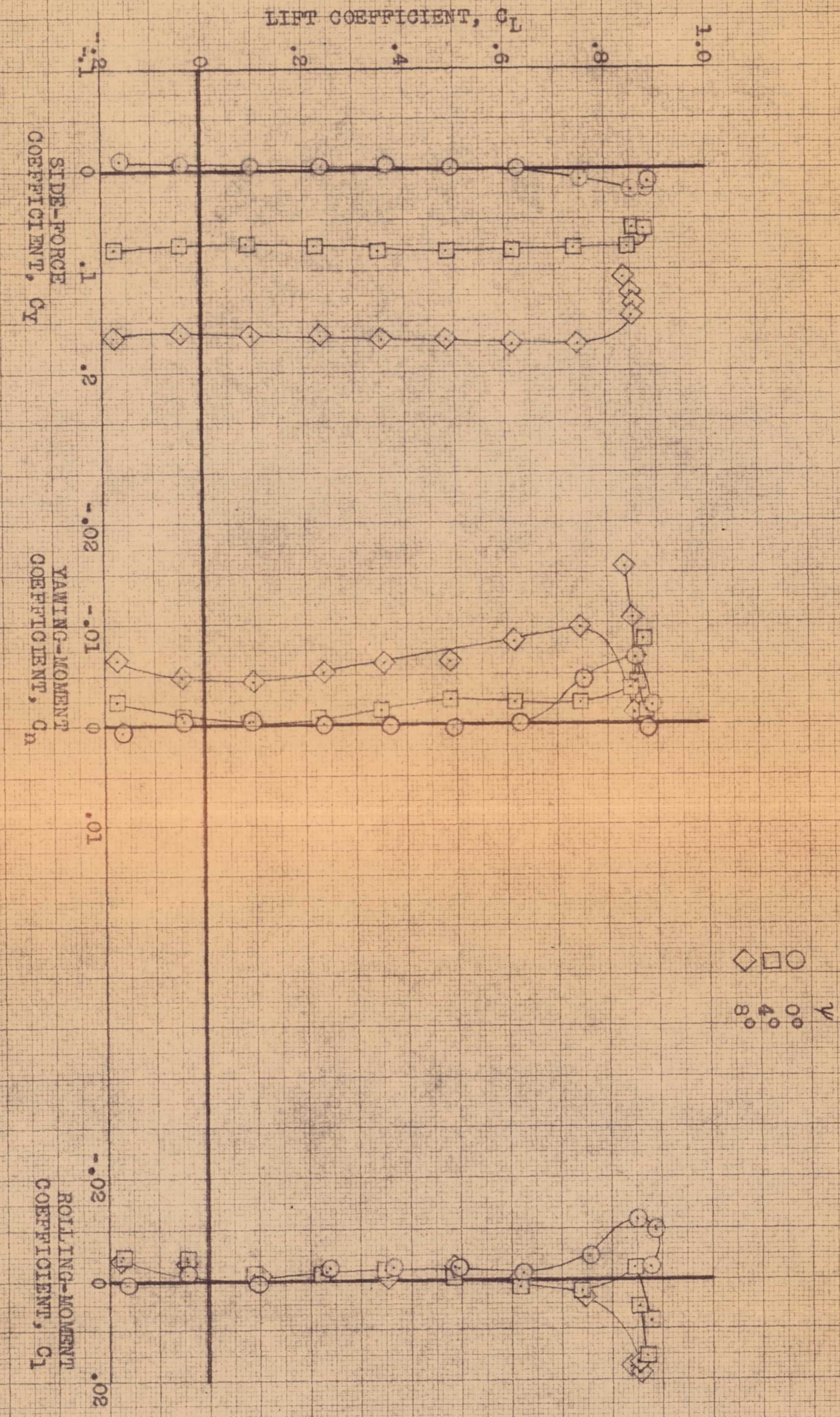

(b) C_Y, C_n, C_l vs C_L.

FIGURE 13.- CONCLUDED.

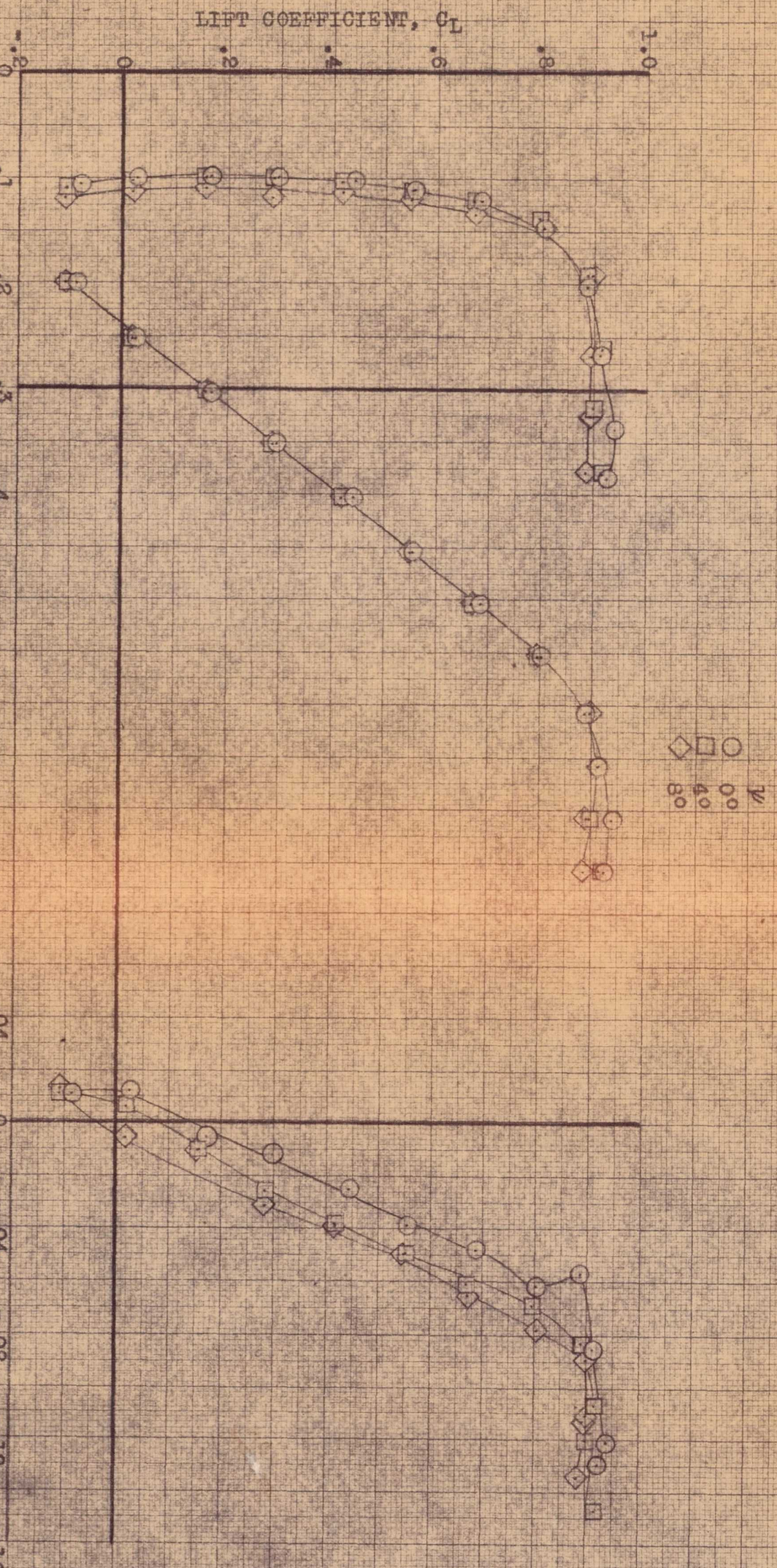

(a) C_D, α, C_m vs C_L.

FIGURE 14.- AERODYNAMIC CHARACTERISTICS IN PITCH OF THE AIRPLANE AT VARIOUS ANGLES OF YAW. DIVE BRAKE EXTENDED.

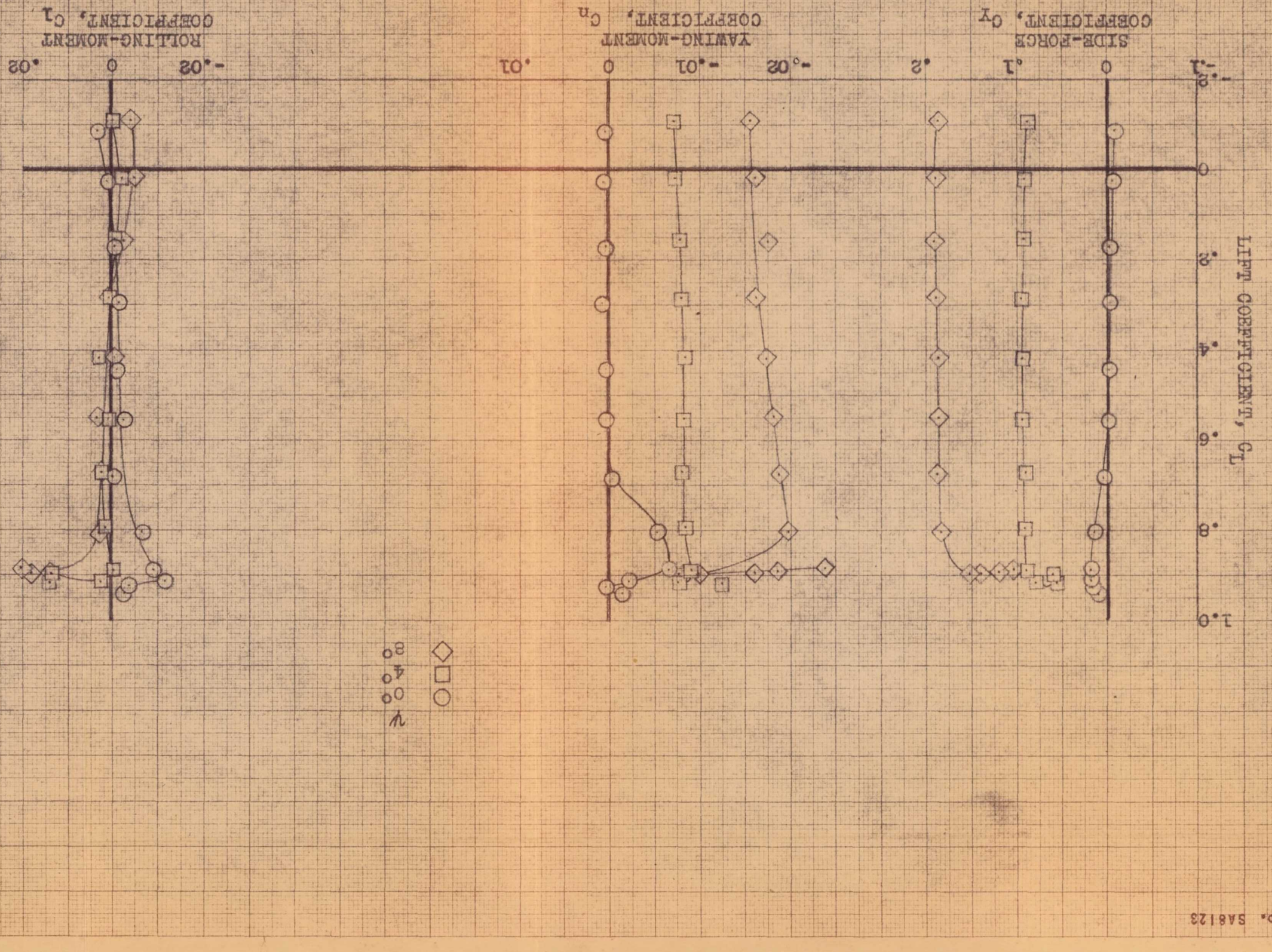

(b) C_Y, C_n, C_l vs C_L.

FIGURE 14.- CONCLUDED.

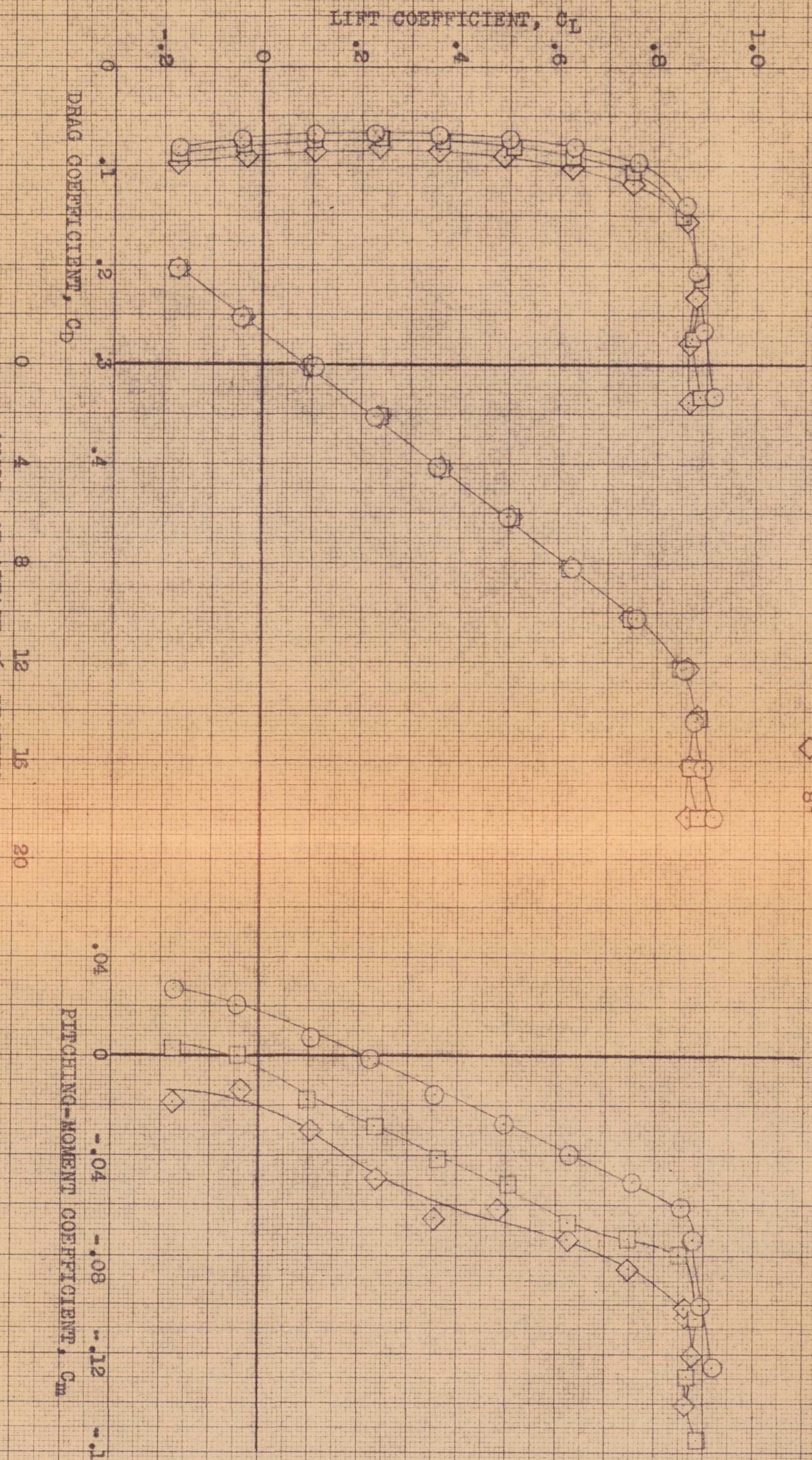

(a) C_D, α, C_m vs C_L.

FIGURE 15.- AERODYNAMIC CHARACTERISTICS IN PITCH OF THE AIRPLANE AT VARIOUS ANGLES OF YAW. CENTER VERTICAL FIN REMOVED; STALL VANE P_2 INSTALLED.

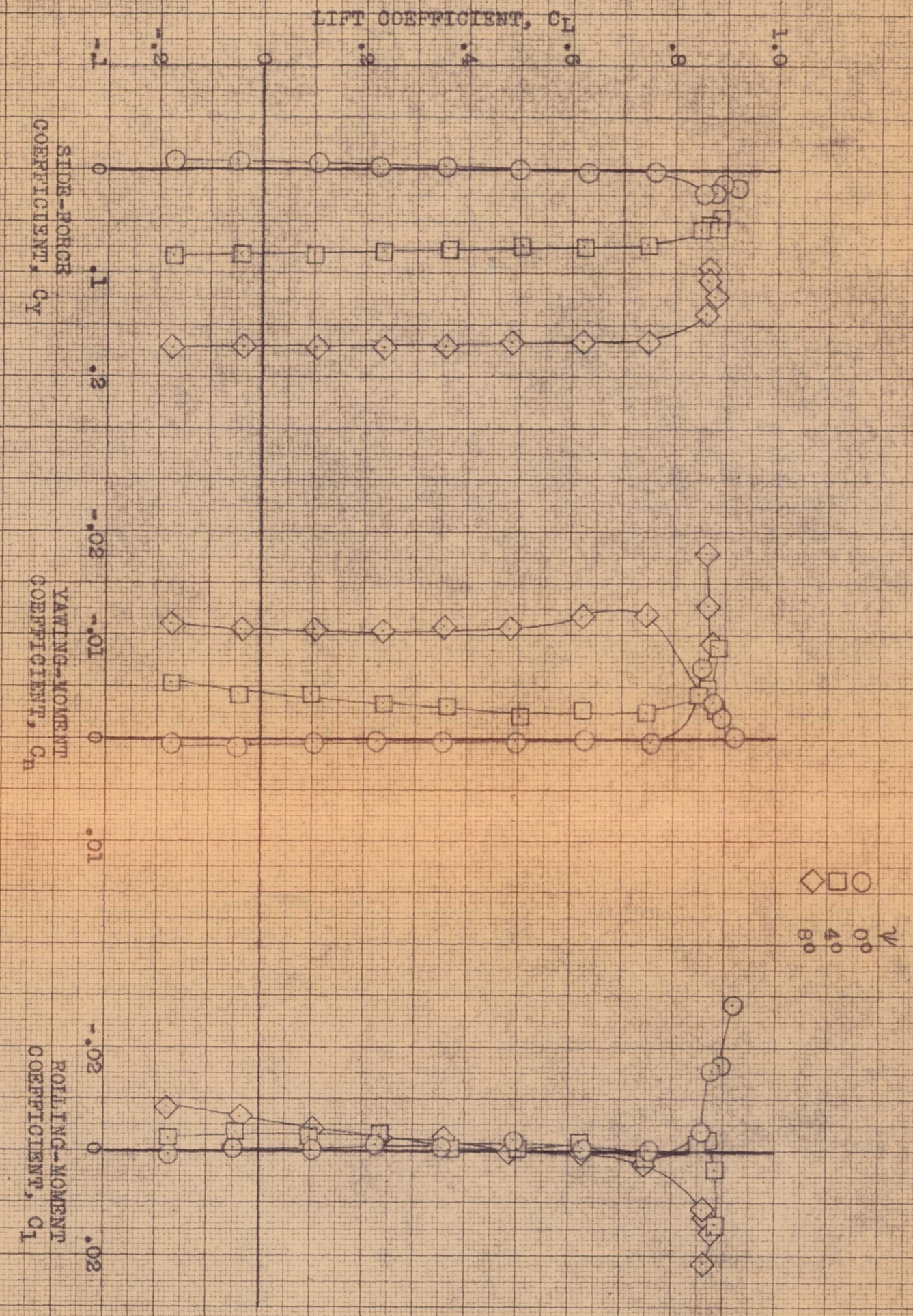

(b) C_Y, C_n, C_l vs C_L.

FIGURE 15.- CONCLUDED.

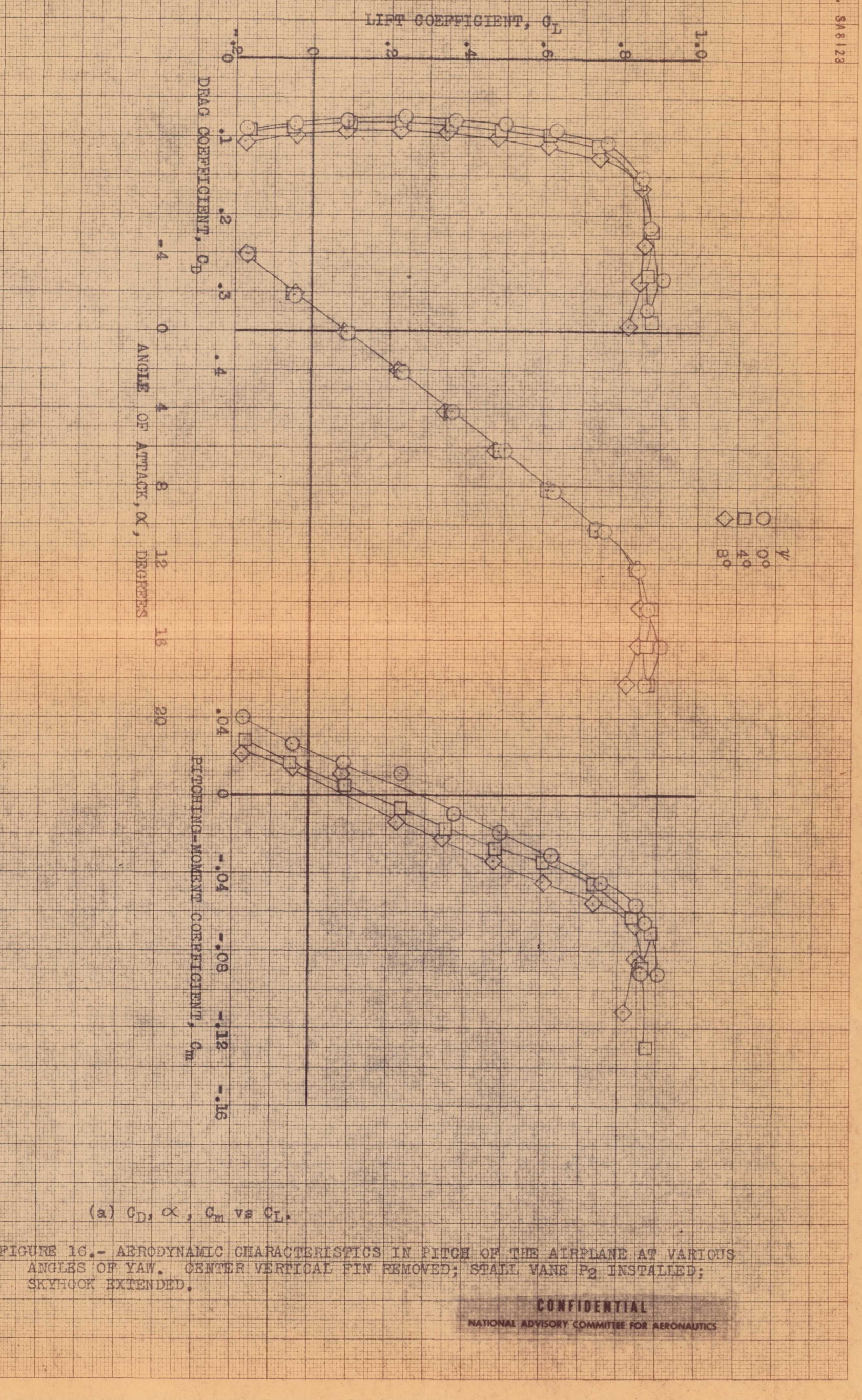

(a) C_D, α, C_m vs C_L.

FIGURE 16.- AERODYNAMIC CHARACTERISTICS IN PITCH OF THE AIRPLANE AT VARIOUS ANGLES OF YAW. CENTER VERTICAL FIN REMOVED; STALL VANE P_2 INSTALLED; SKYHOOK EXTENDED.

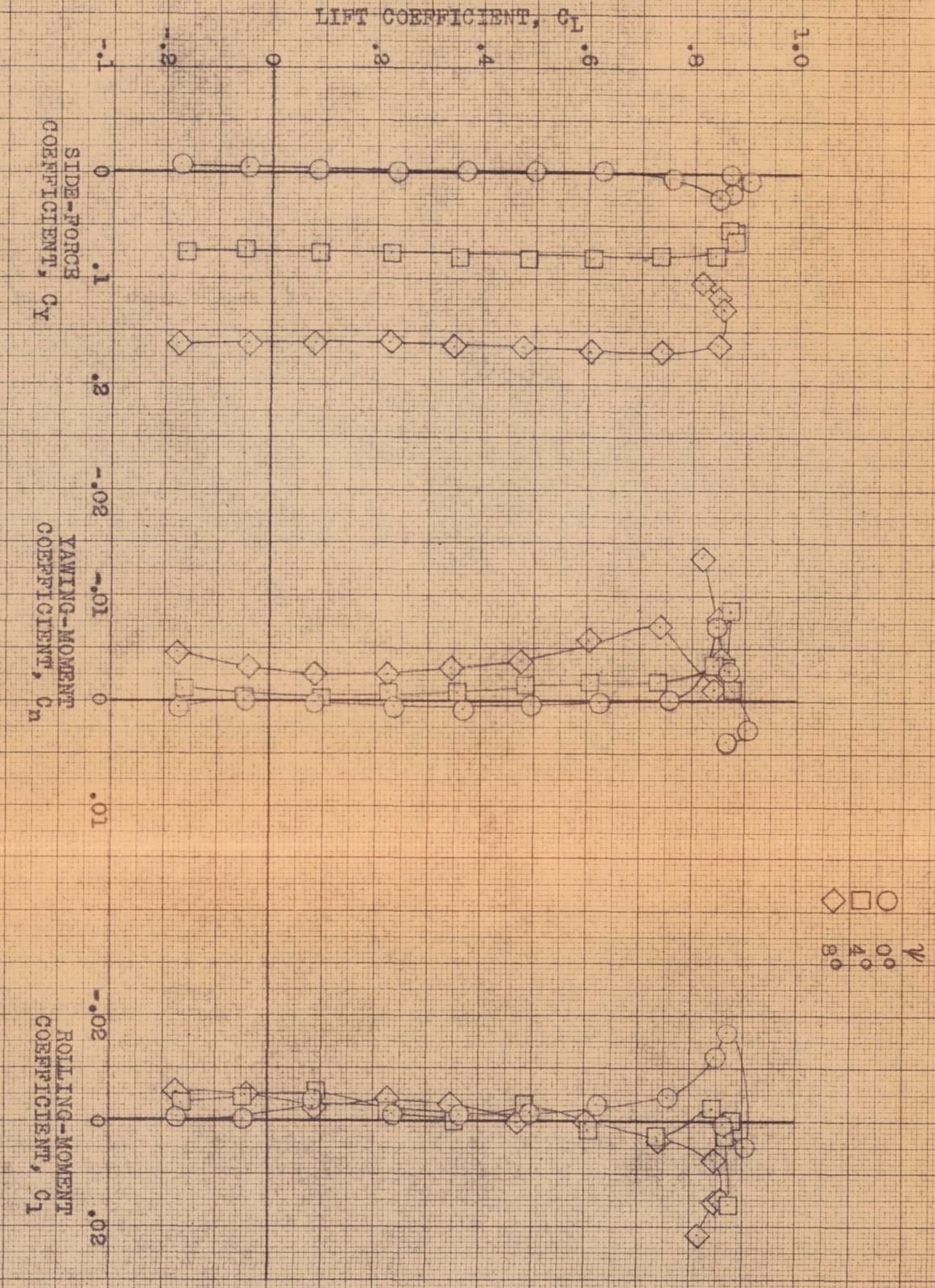

(b) C_Y, C_n, C_l vs C_L.

FIGURE 16.- CONCLUDED

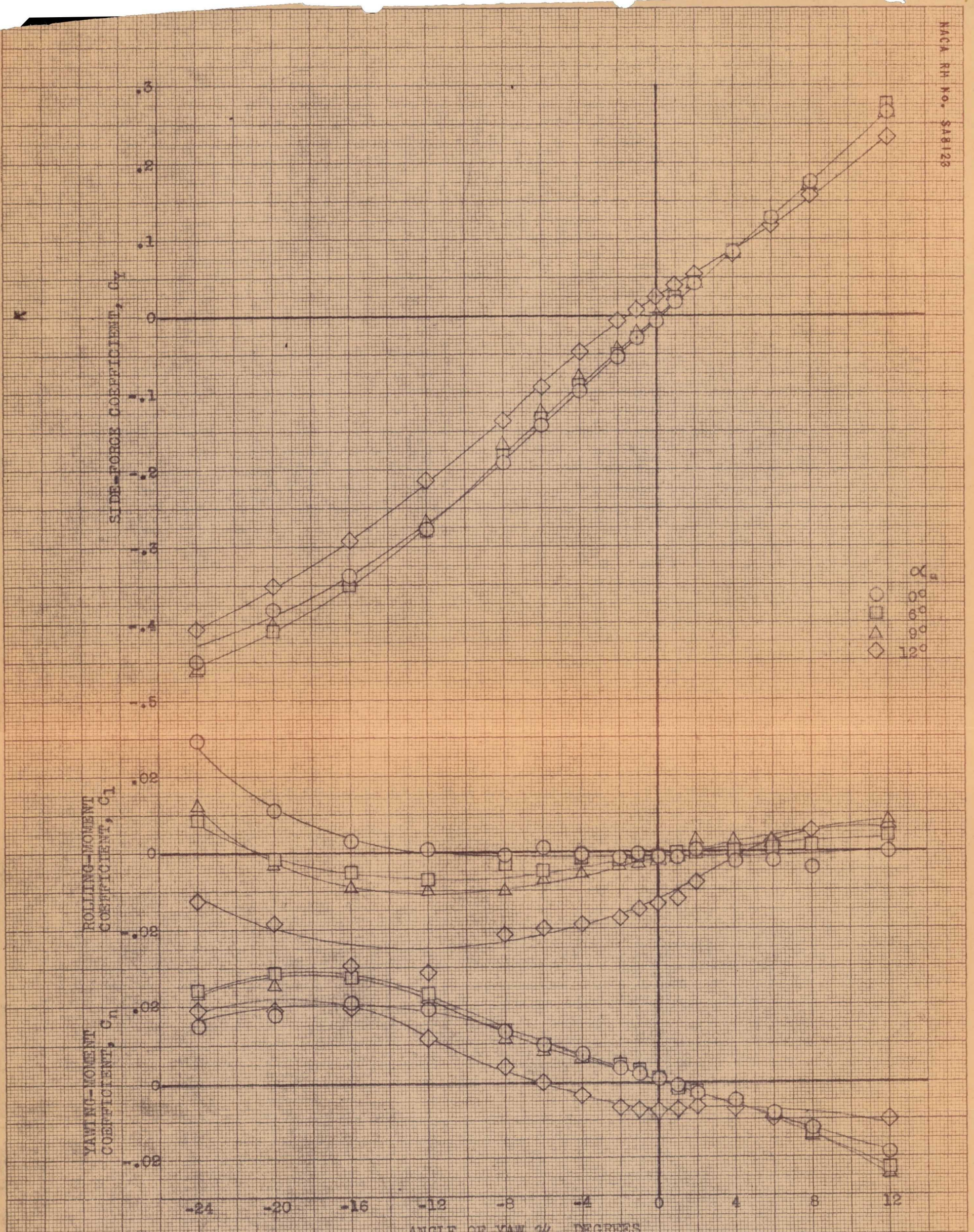

(a) C_Y, C_l, C_n vs ψ.

FIGURE 17.- AERODYNAMIC CHARACTERISTICS IN YAW OF THE AIRPLANE AT VARIOUS ANGLES OF ATTACK. CLEAN CONDITION.

FIGURE 17.- CONCLUDED.

(b) C_L, C_m vs ψ.

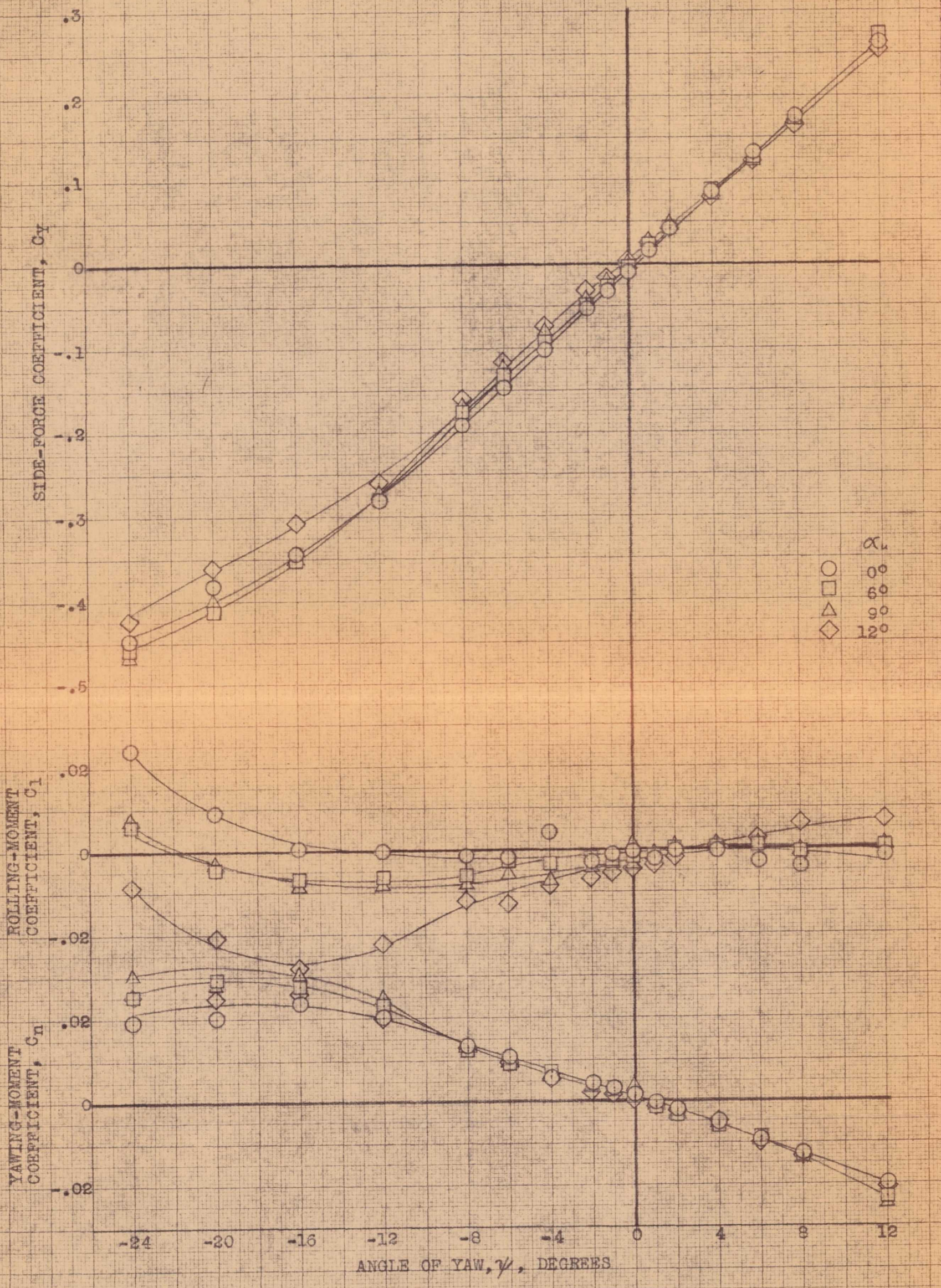

(a) C_Y, C_l, C_n vs ψ.

FIGURE 18.- AERODYNAMIC CHARACTERISTICS IN YAW OF THE AIRPLANE AT VARIOUS ANGLES OF ATTACK. DROOP NOSE FLAP EXTENDED.

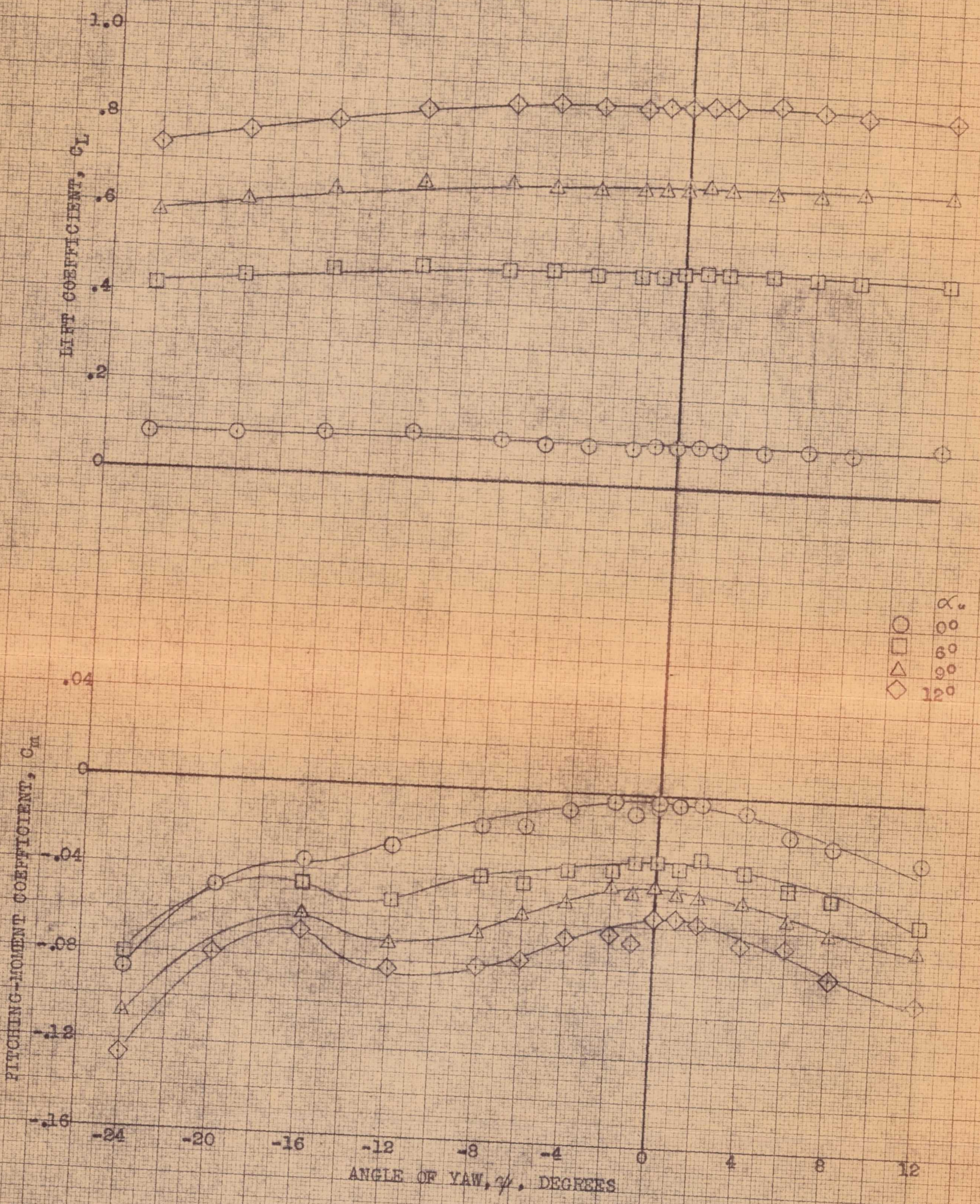

(b) C_L, C_m vs ψ.

FIGURE 18.- CONCLUDED.

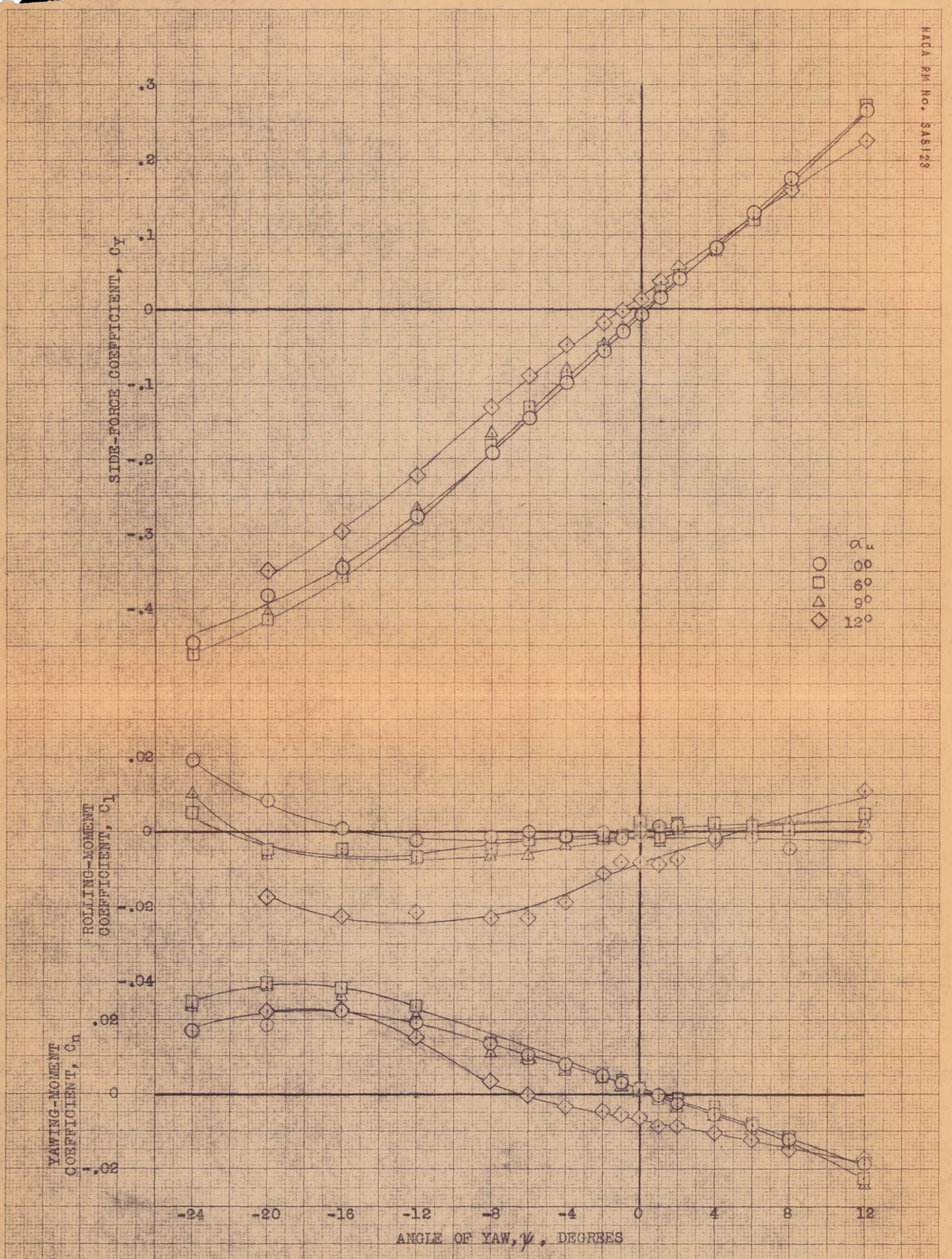

(a) C_Y, C_l, C_n vs ψ.

FIGURE 19.- AERODYNAMIC CHARACTERISTICS IN YAW OF THE AIRPLANE AT VARIOUS ANGLES OF ATTACK. STALL CONTROL VANES P_2 INSTALLED.

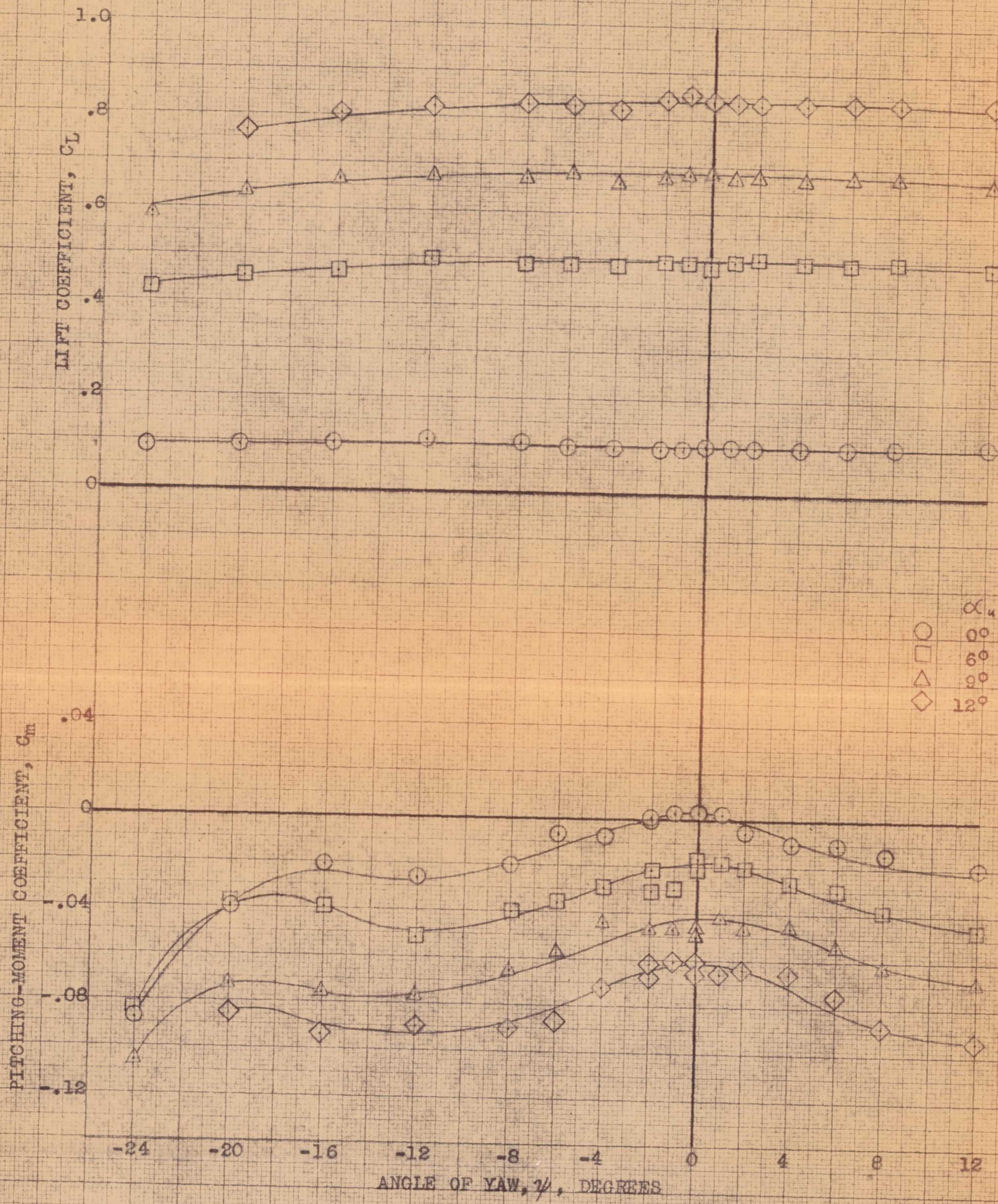

(b) C_L, C_m vs ψ.

FIGURE 19.- CONCLUDED.

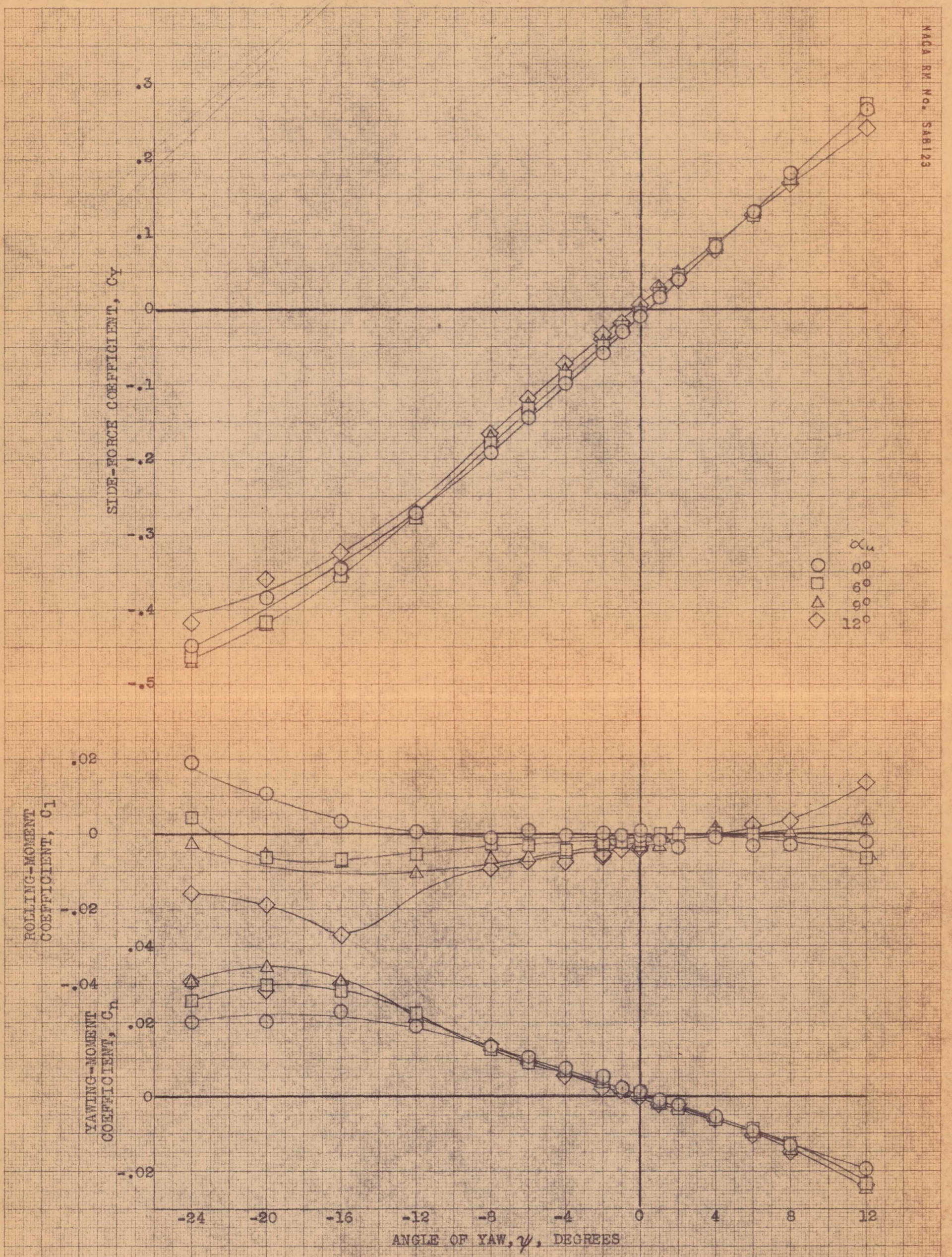

(a) C_Y, C_l, C_n vs ψ.

FIGURE 20.- AERODYNAMIC CHARACTERISTICS IN YAW OF THE AIRPLANE AT VARIOUS ANGLES OF ATTACK. DROOP NOSE FLAP EXTENDED; STALL CONTROL VANES P_2 INSTALLED.

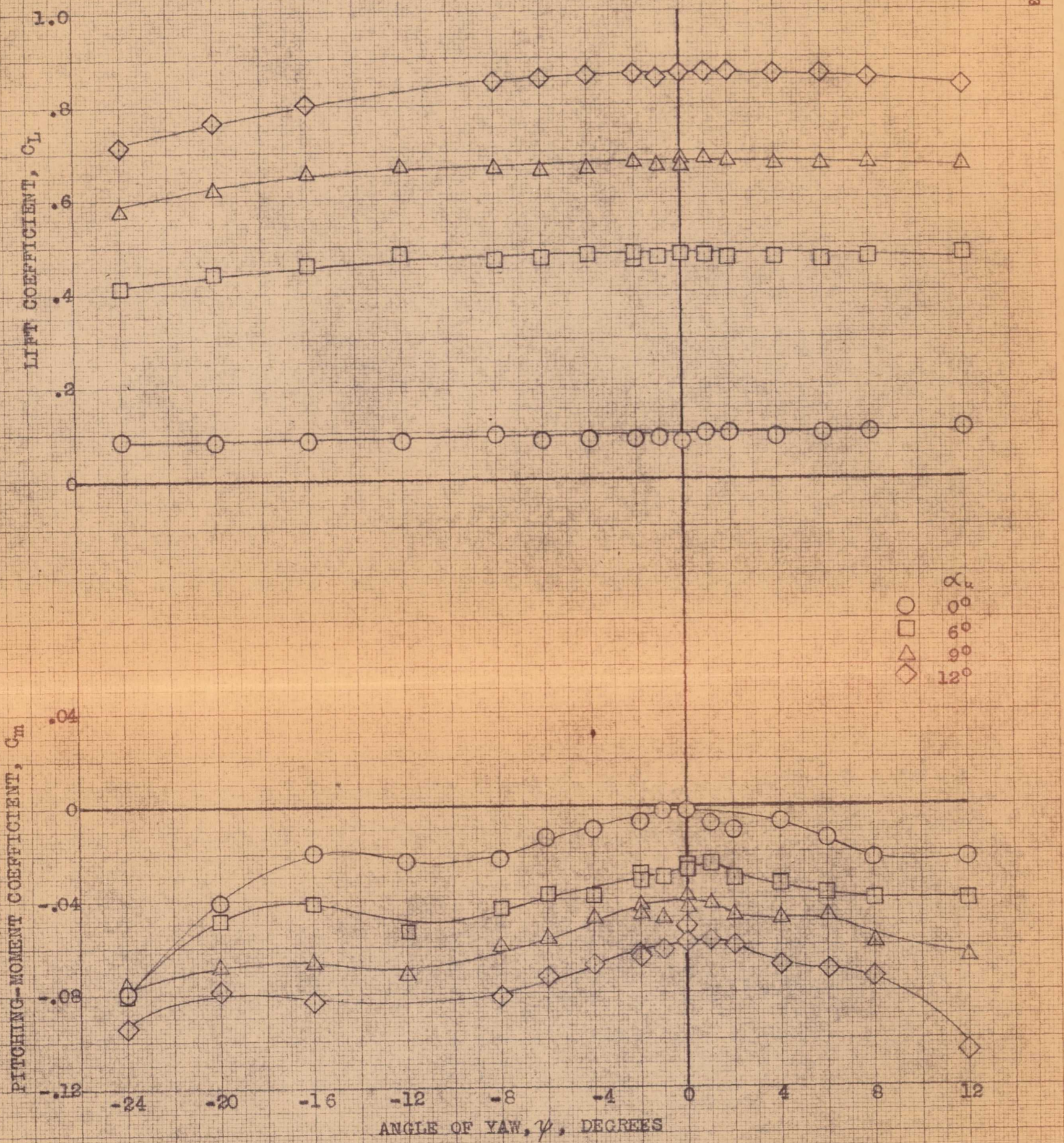

(b) C_L, C_m vs ψ.

FIGURE 20.- CONCLUDED.

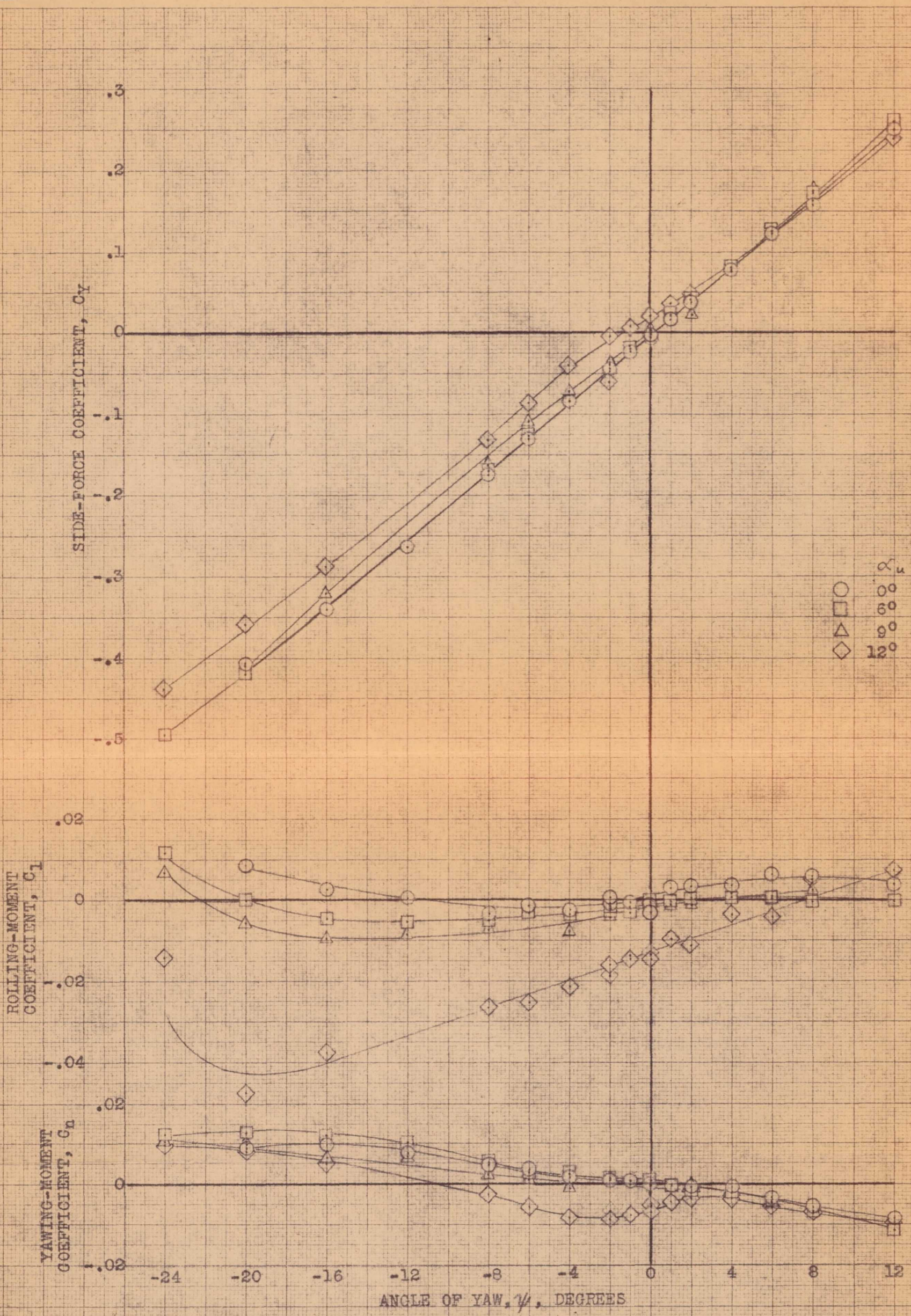

(a) C_Y, C_l, C_n vs ψ.

FIGURE 21.- AERODYNAMIC CHARACTERISTICS IN YAW OF THE AIRPLANE AT VARIOUS ANGLES OF ATTACK. SKYHOOK EXTENDED.

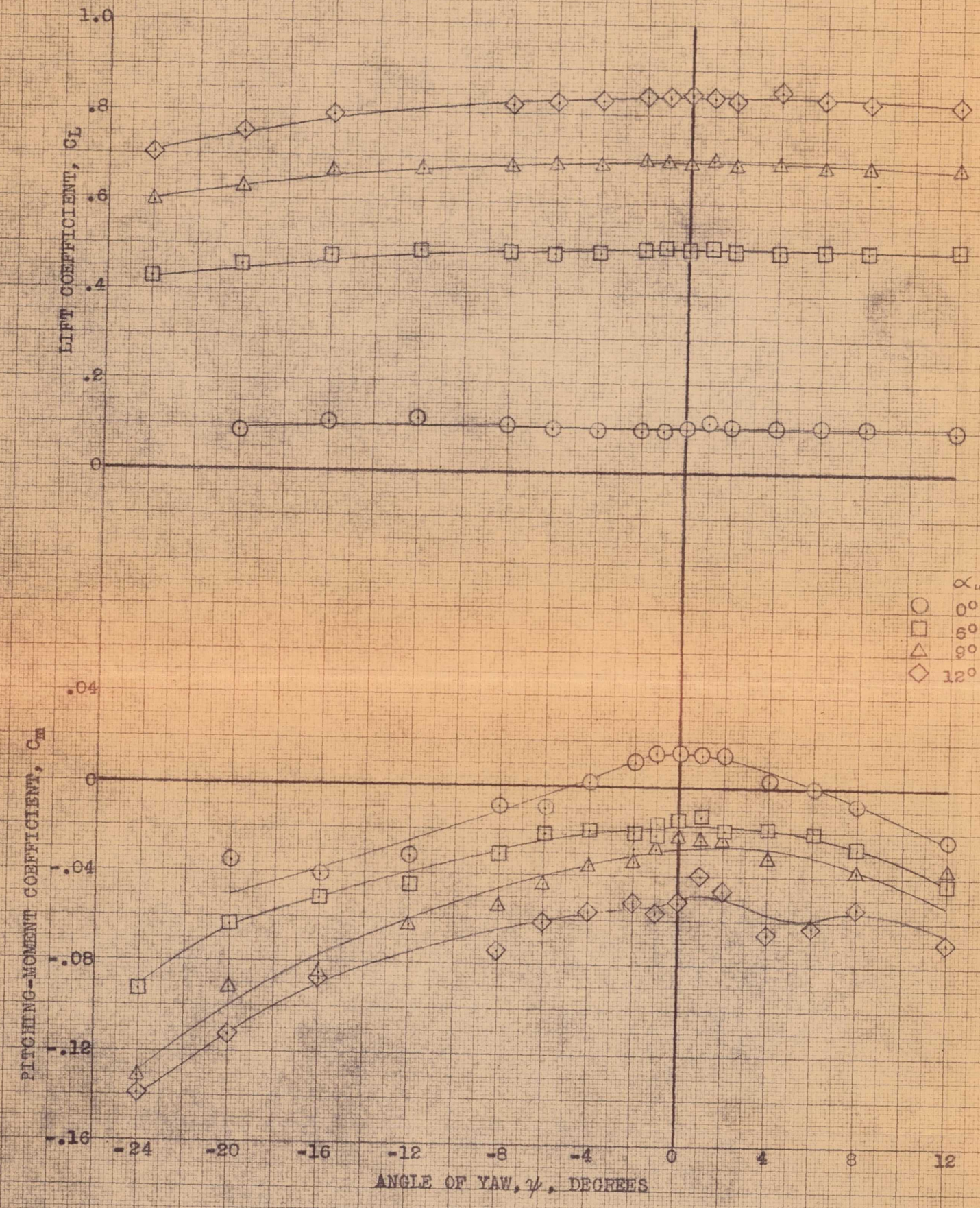

(b) C_L, C_m vs ψ.

FIGURE 21.- CONCLUDED.

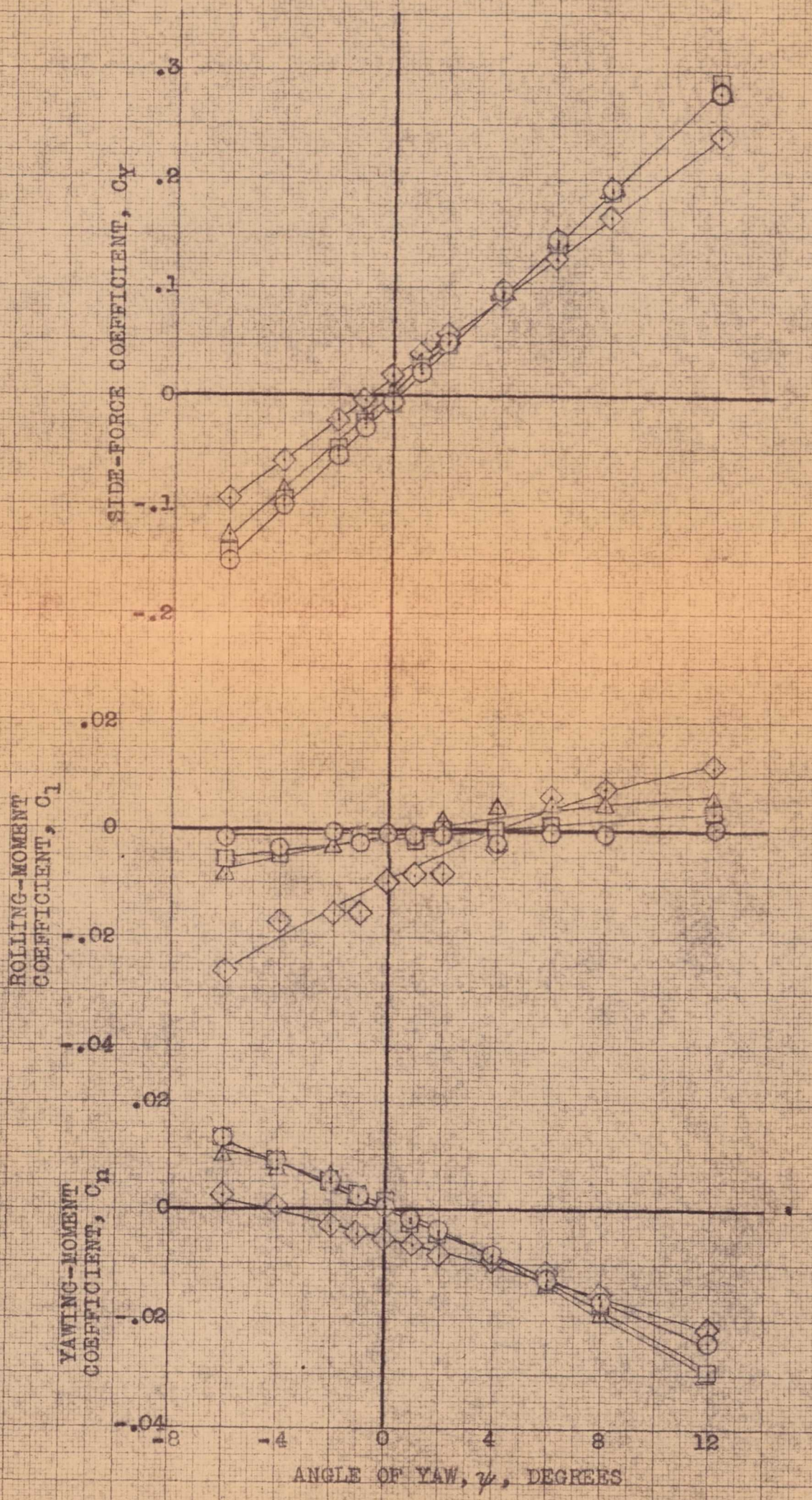

(a) C_Y, C_l, C_n vs ψ.

FIGURE 22.- AERODYNAMIC CHARACTERISTICS IN YAW OF THE AIRPLANE AT VARIOUS ANGLES OF ATTACK. DIVE BRAKE EXTENDED.

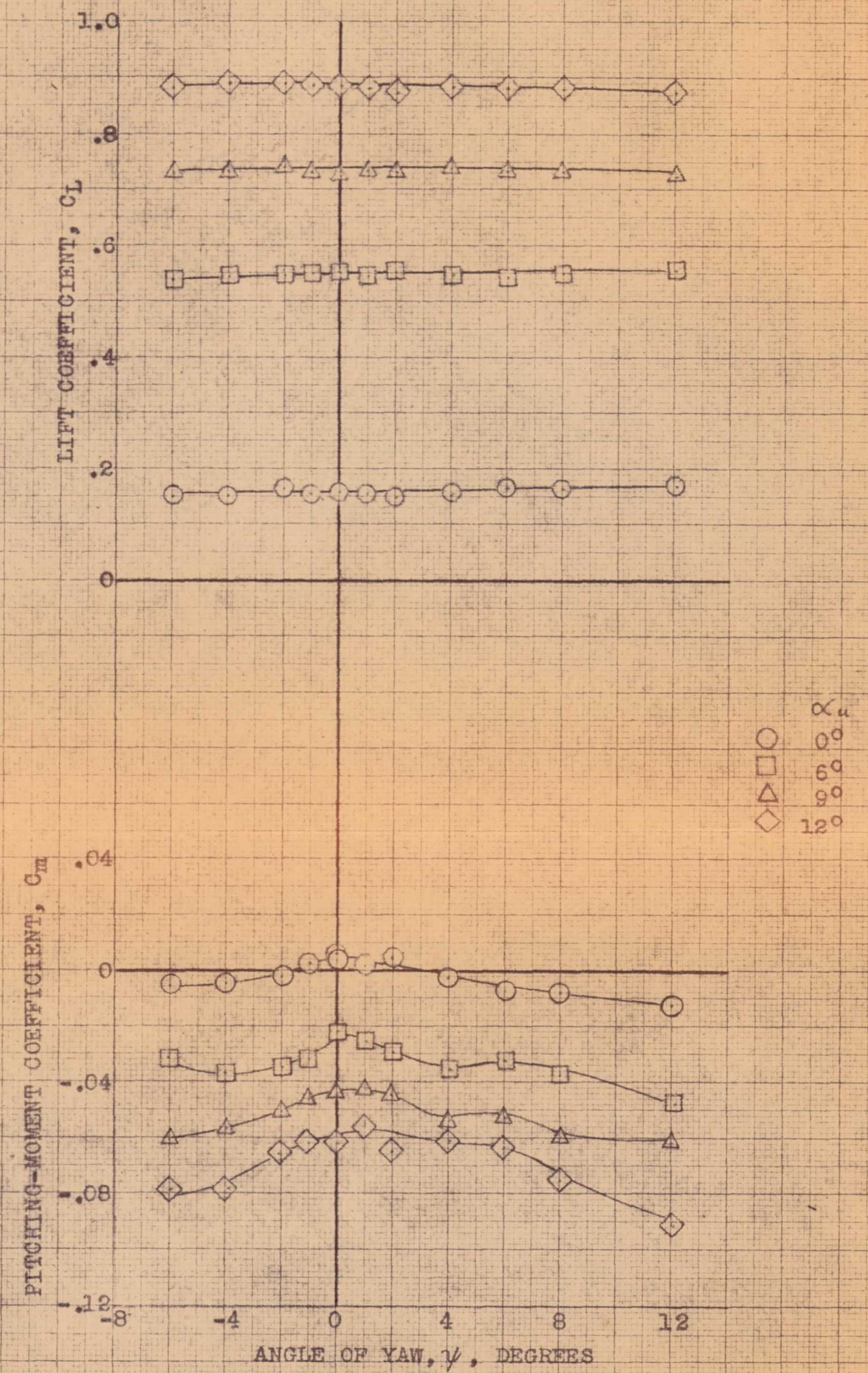

(b) C_L, C_m vs ψ.

FIGURE 22.- CONCLUDED.

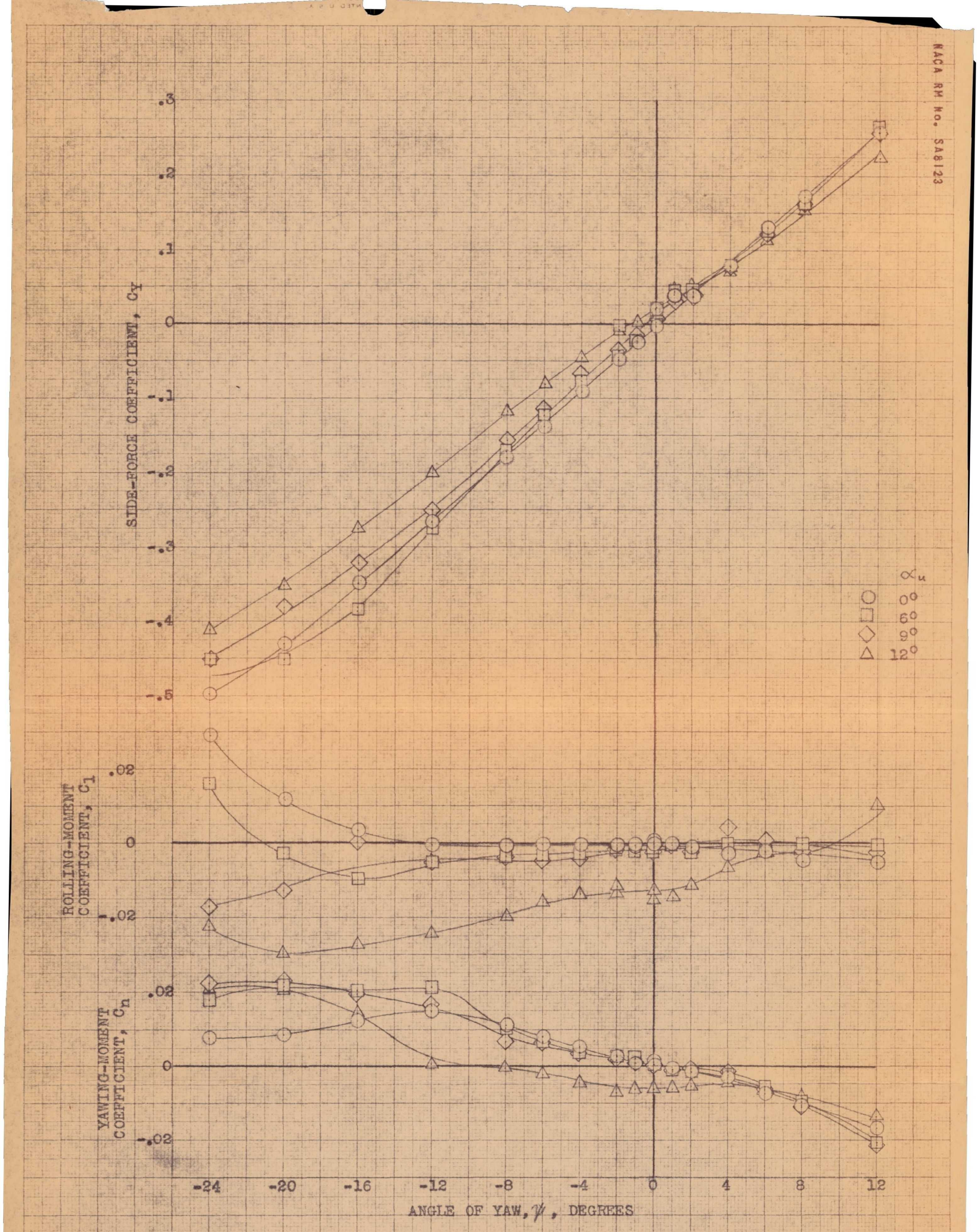

(a) C_Y, C_l, C_n vs ψ.

FIGURE 23.- AERODYNAMIC CHARACTERISTICS IN YAW OF THE AIRPLANE AT VARIOUS ANGLES OF ATTACK. CENTER VERTICAL FIN REMOVED; STALL CONTROL VANES P_2 INSTALLED.

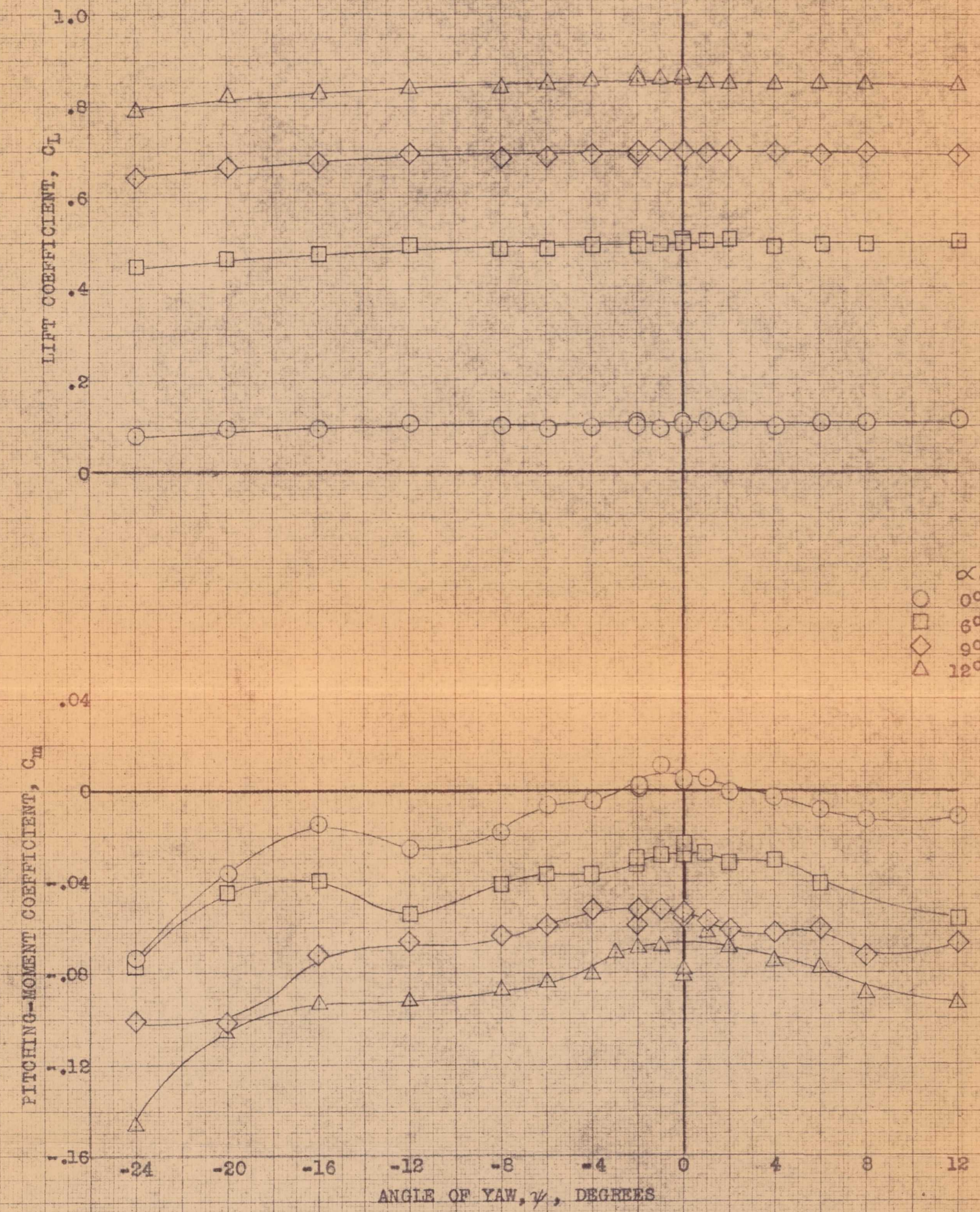

(b) C_L, C_m vs ψ.

FIGURE 23.- CONCLUDED.

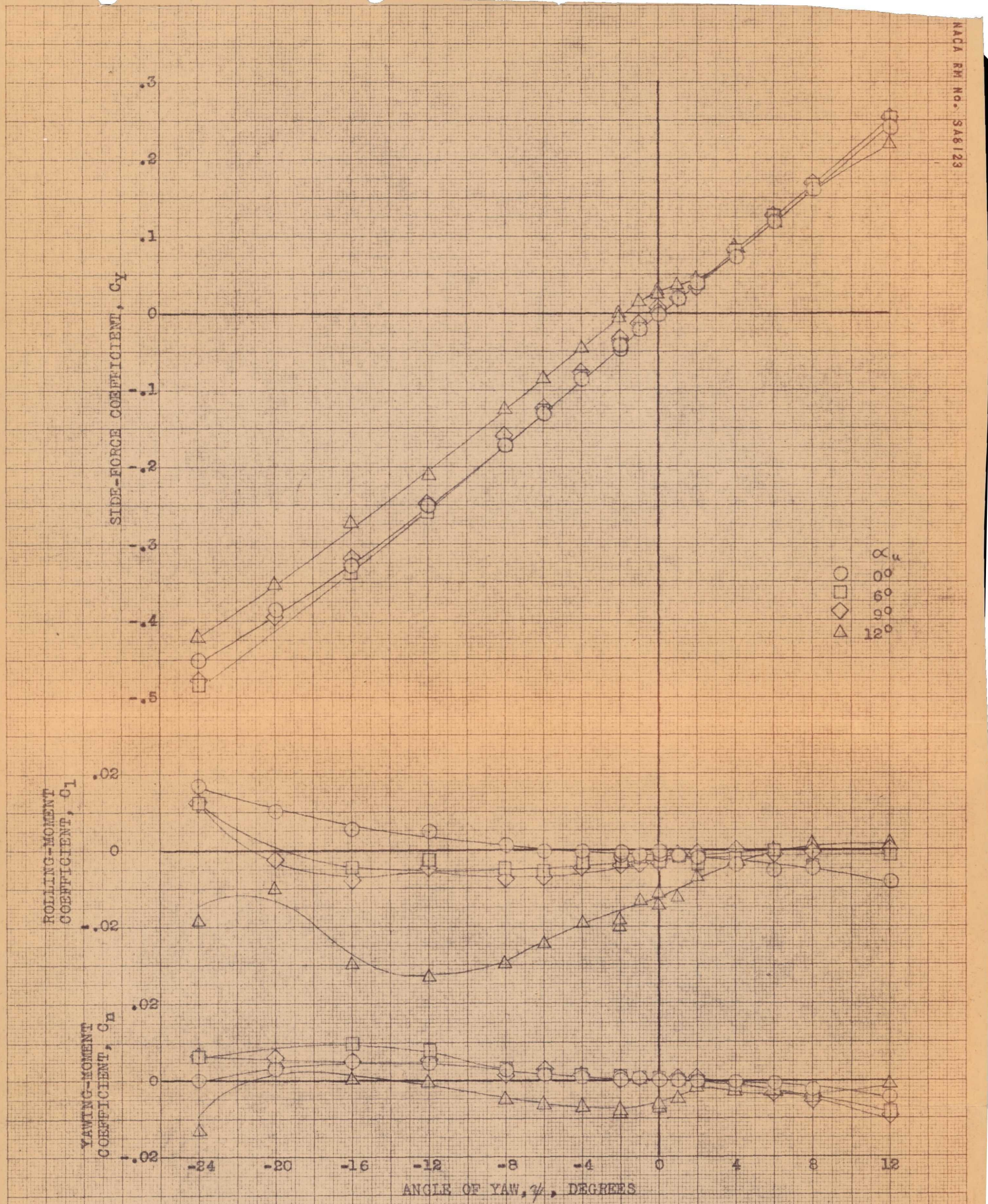

(a) C_Y, C_l, C_n vs ψ.

FIGURE 24.- AERODYNAMIC CHARACTERISTICS IN YAW OF THE AIRPLANE AT VARIOUS ANGLES OF ATTACK. CENTER VERTICAL FIN REMOVED; STALL CONTROL VANES P_2 INSTALLED; SKYHOOK EXTENDED.

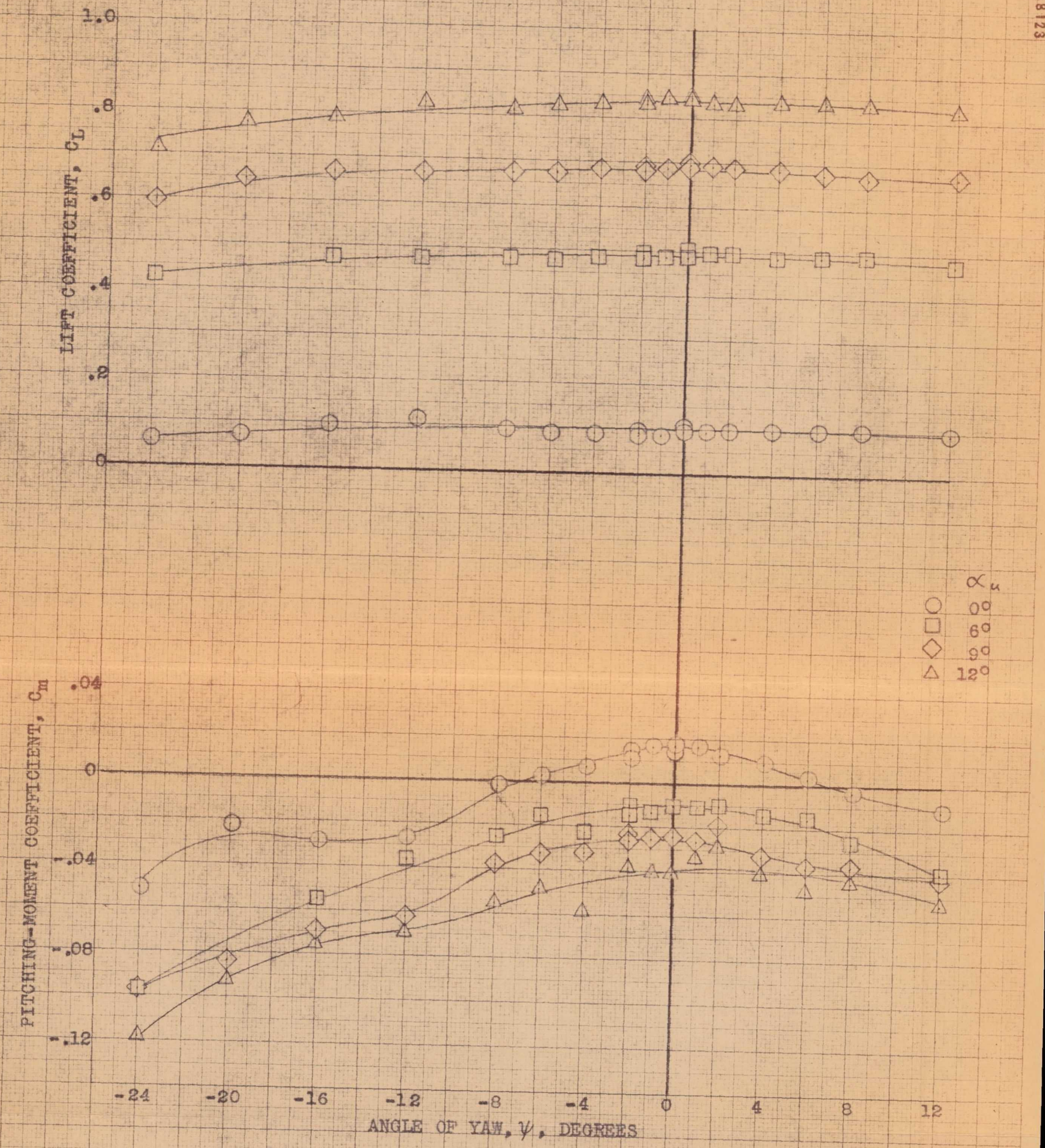

(b) C_L, C_m vs ψ.

FIGURE 24.- CONCLUDED

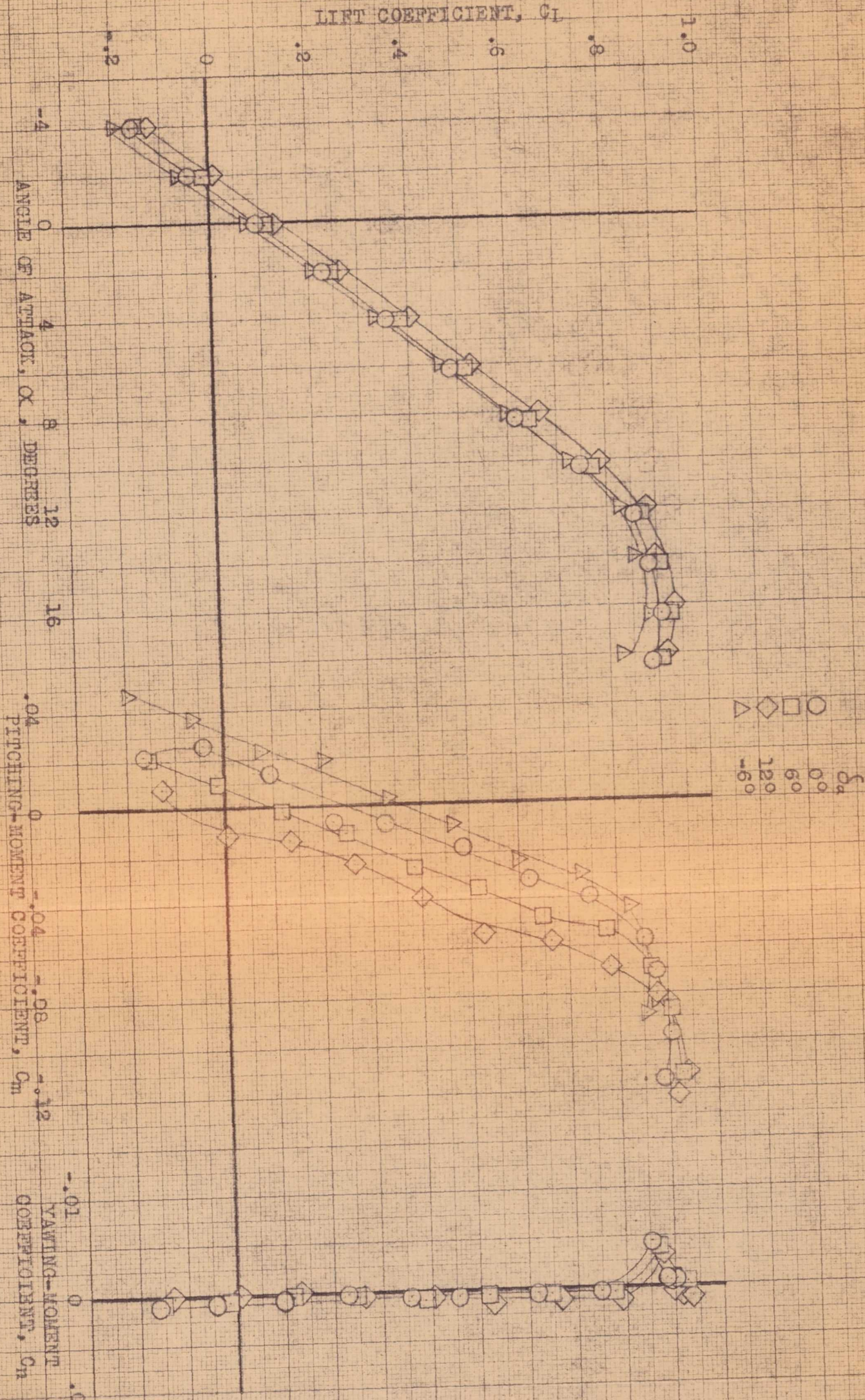

(a) α, C_m, C_n vs C_L.

FIGURE 25.- EFFECT OF FIXED DEFLECTIONS OF THE RIGHT AILERON ON THE AERODYNAMIC CHARACTERISTICS OF THE AIRPLANE IN PITCH. CLEAN CONDITION; ψ, 0°.

(b) C_l, C_{h_a} vs C_L.

FIGURE 25.- CONCLUDED.

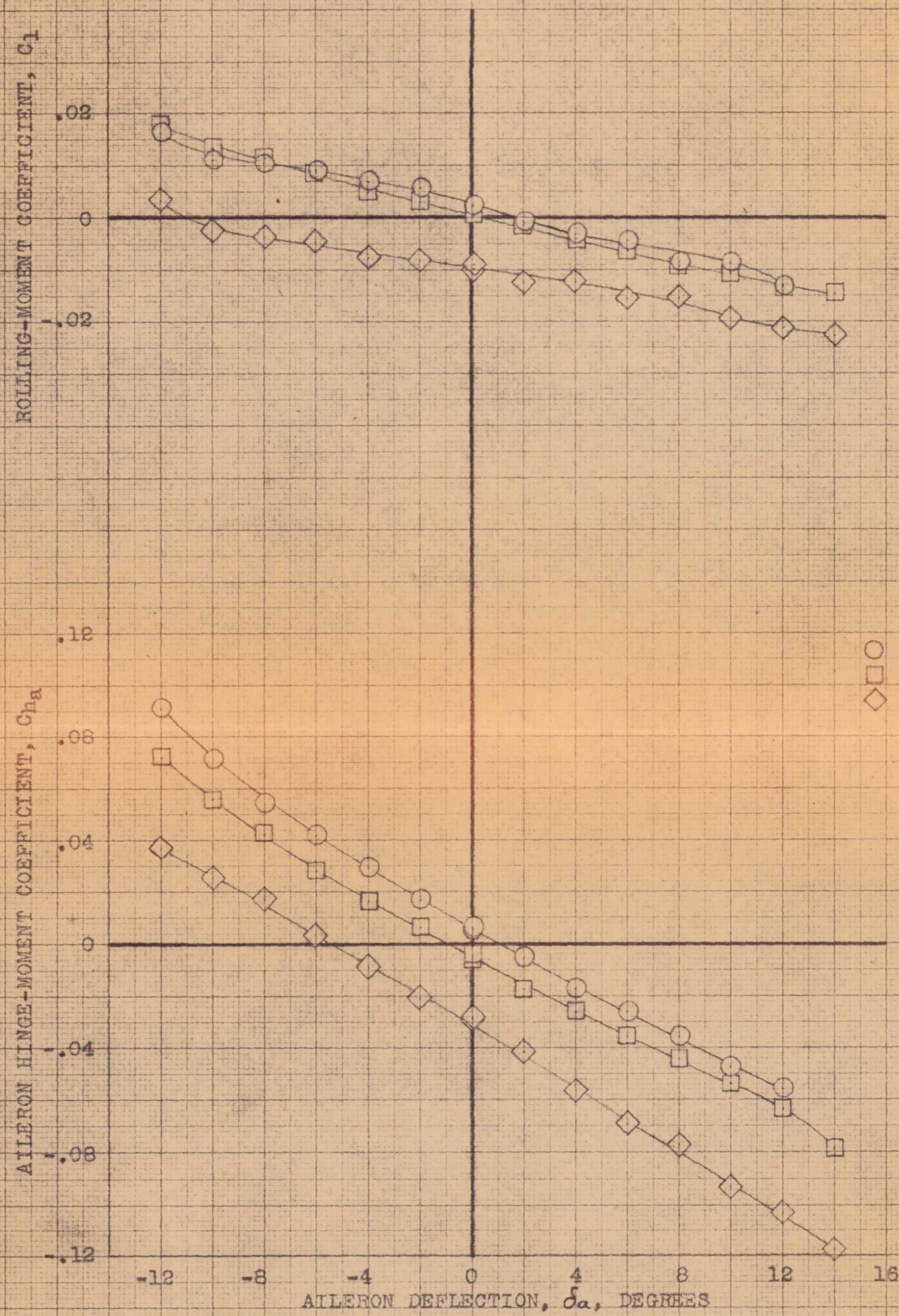

(a) C_l, Ch_a vs δ_a.

FIGURE 26.- VARIATION WITH DEFLECTION OF THE RIGHT AILERON OF THE AERODYNAMIC CHARACTERISTICS OF THE AIRPLANE AT SEVERAL ANGLES OF ATTACK. CLEAN CONDITION; ψ , 0°.

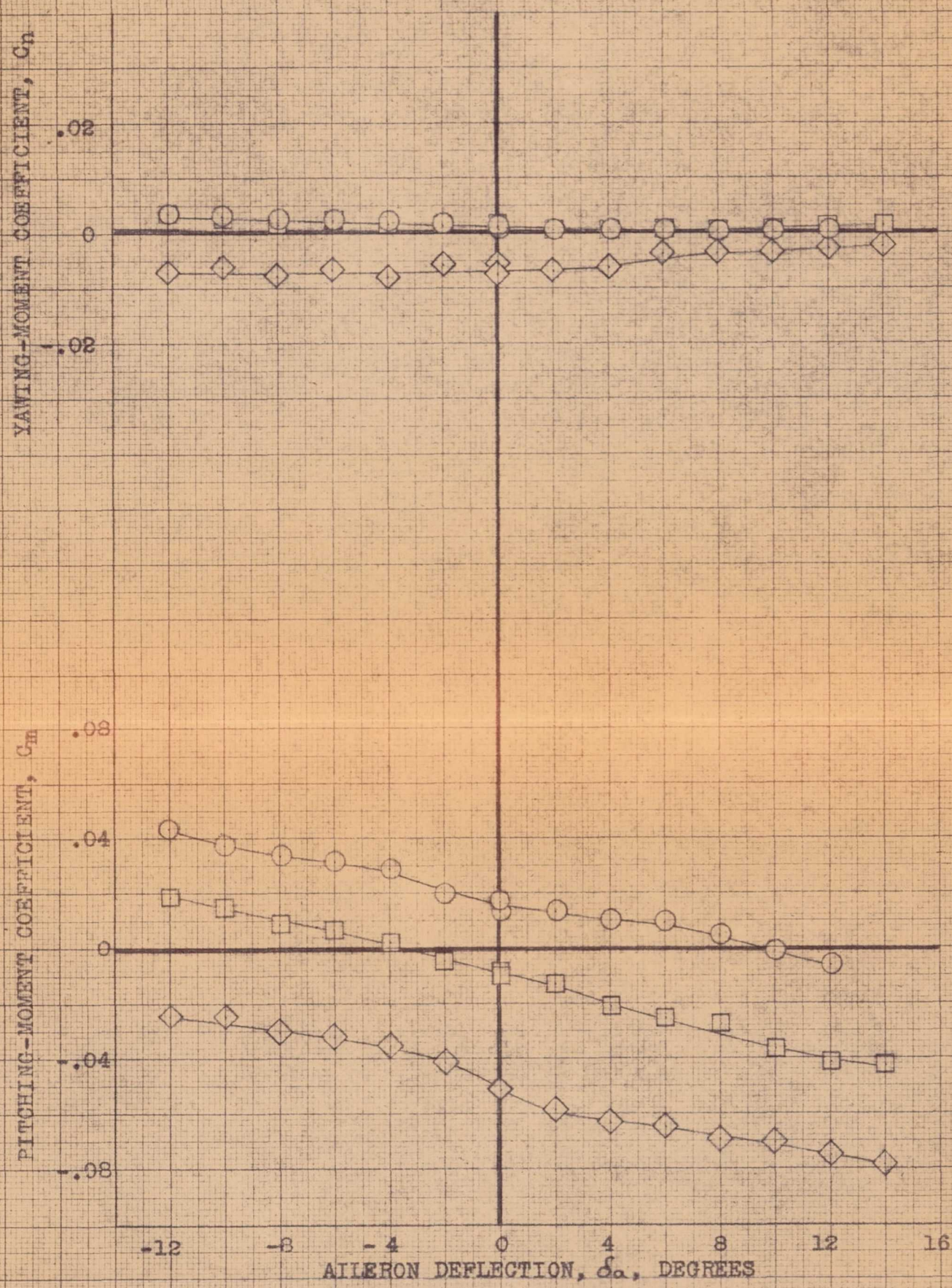

(b) C_n, C_m vs δ_a.

FIGURE 26.- CONCLUDED.

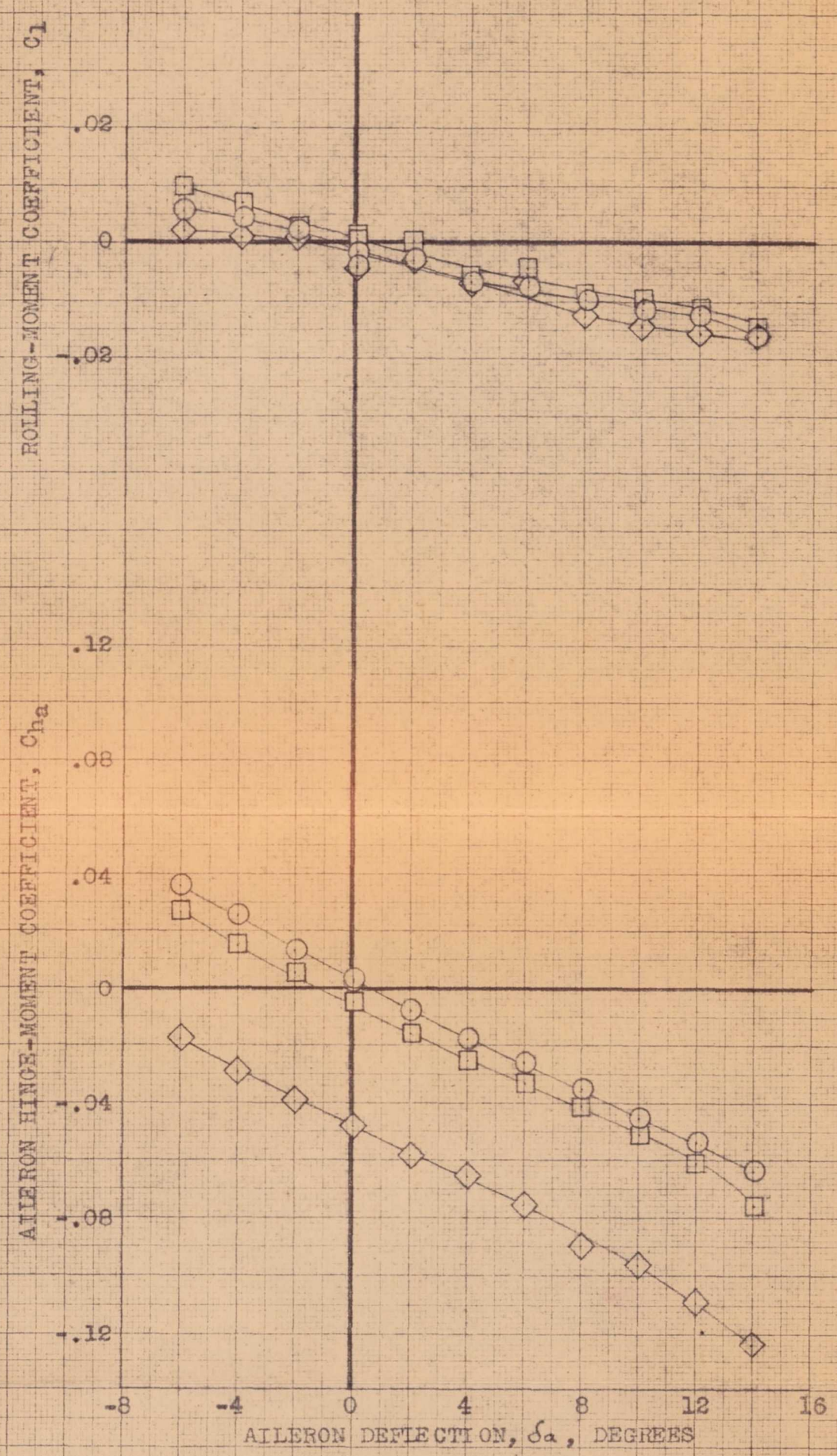

(a) C_l, C_{h_a} vs δ_a.

FIGURE 27.- VARIATION WITH DEFLECTION OF THE RIGHT AILERON OF THE AERODYNAMIC CHARACTERISTICS OF THE AIRPLANE AT SEVERAL ANGLES OF ATTACK. CLEAN CONDITION; ψ, 4°.

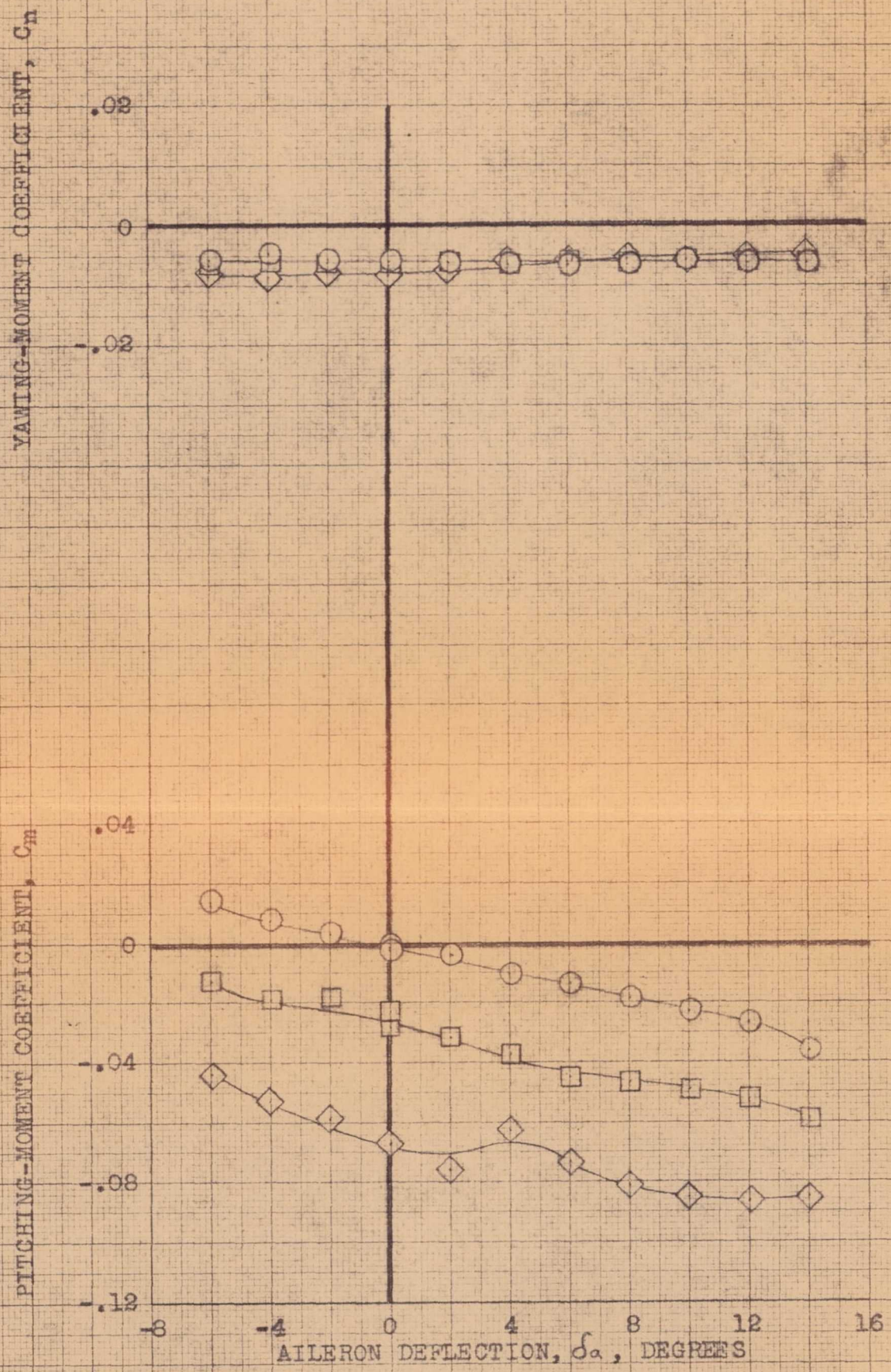

(b) C_n, C_m vs δ_a.

FIGURE 27.- CONCLUDED.

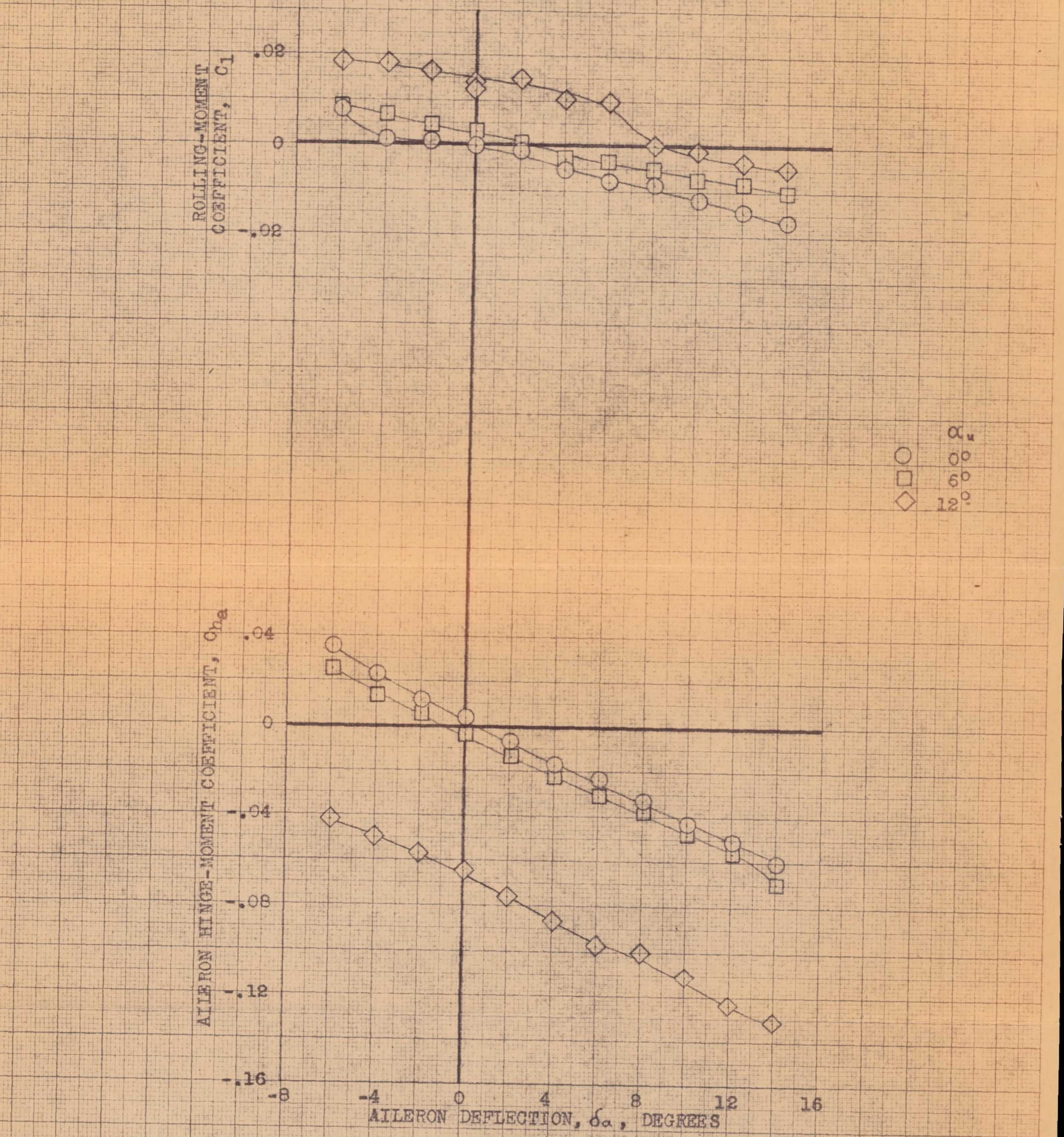

(a) C_l, Ch_a vs δ_a.

FIGURE 28.- VARIATION WITH DEFLECTION OF THE RIGHT AILERON OF THE AERODYNAMIC CHARACTERISTICS OF THE AIRPLANE AT SEVERAL ANGLES OF ATTACK. CLEAN CONDITION; ψ, 8°.

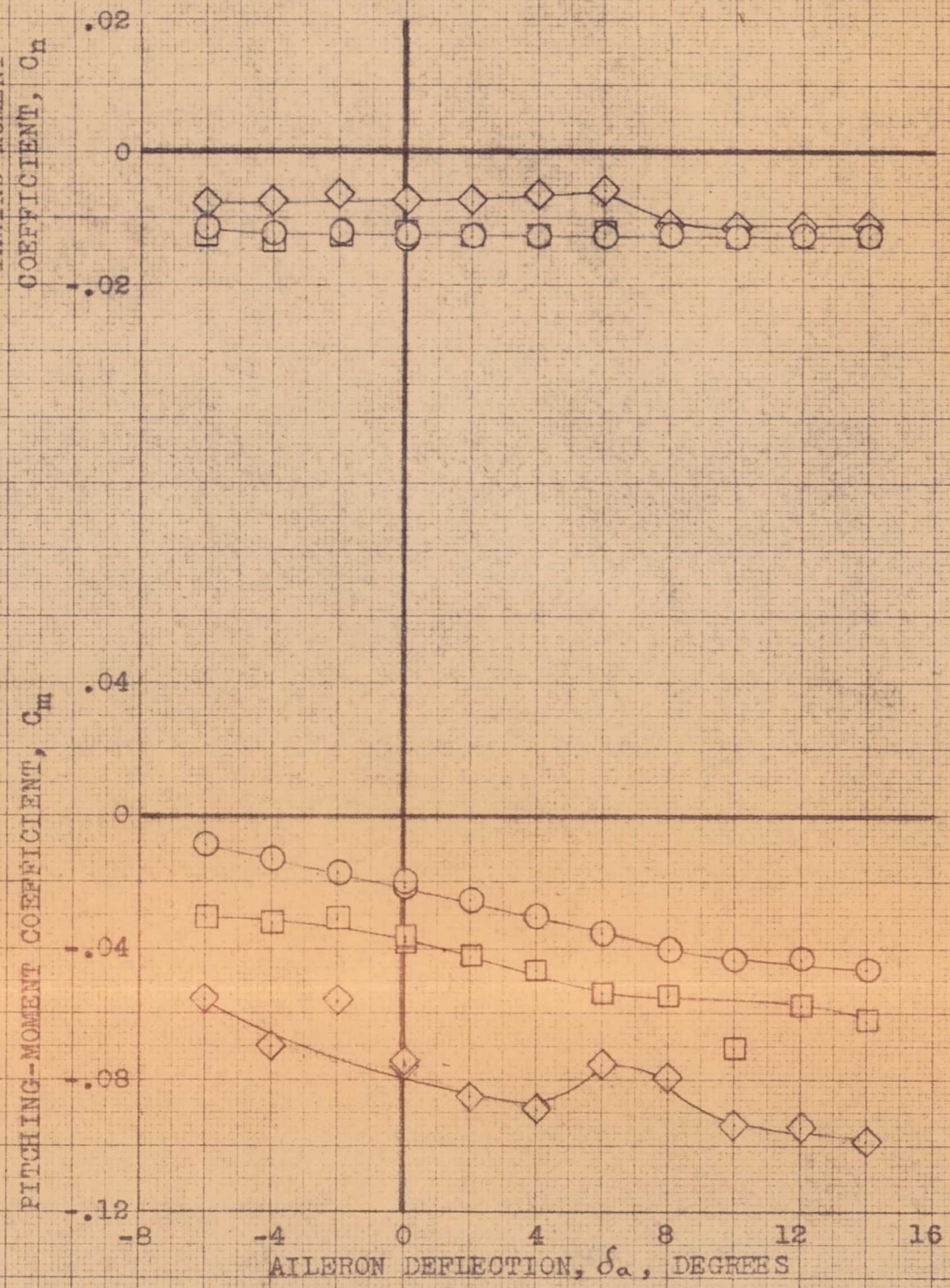

(b) C_n, C_m vs δ_a.

FIGURE 28.- CONCLUDED.

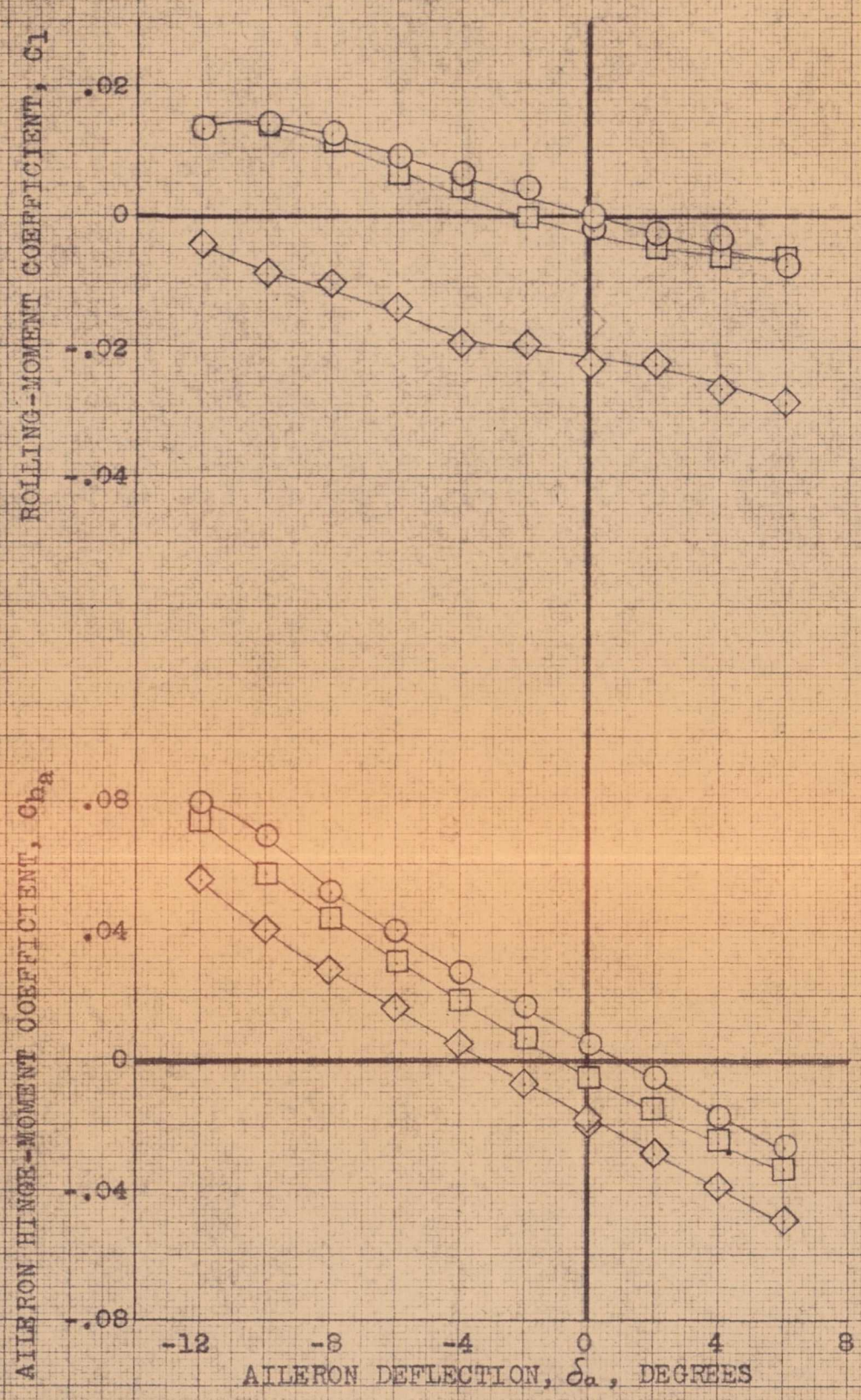

(a) C_l, Ch_a vs δ_a.

FIGURE 29.- VARIATION WITH DEFLECTION OF THE RIGHT AILERON OF THE AERODYNAMIC CHARACTERISTICS OF THE AIRPLANE AT SEVERAL ANGLES OF ATTACK. CLEAN CONDITION; ψ, -4°.

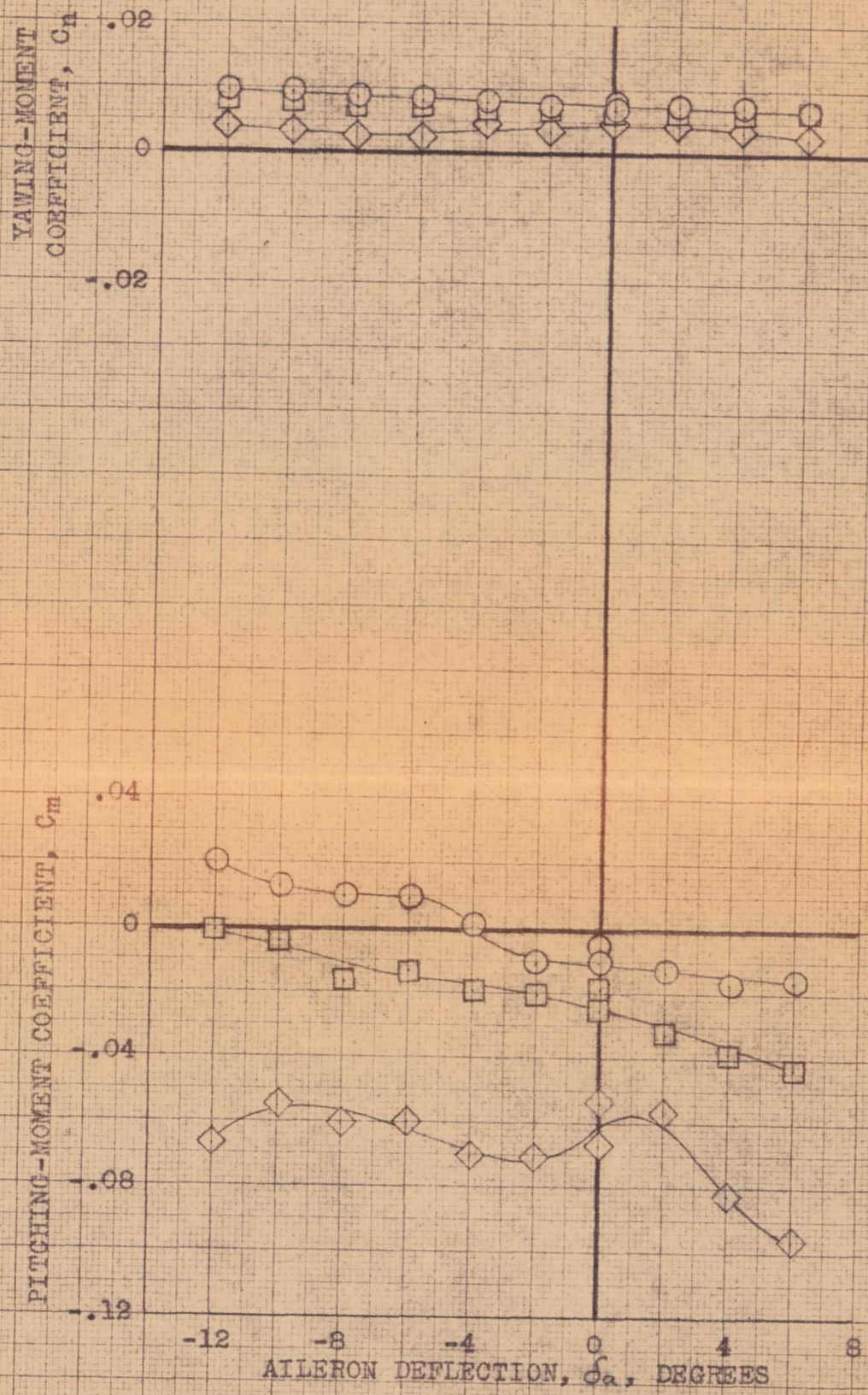

(b) C_n, C_m vs δ_a.

FIGURE 29.- CONCLUDED.

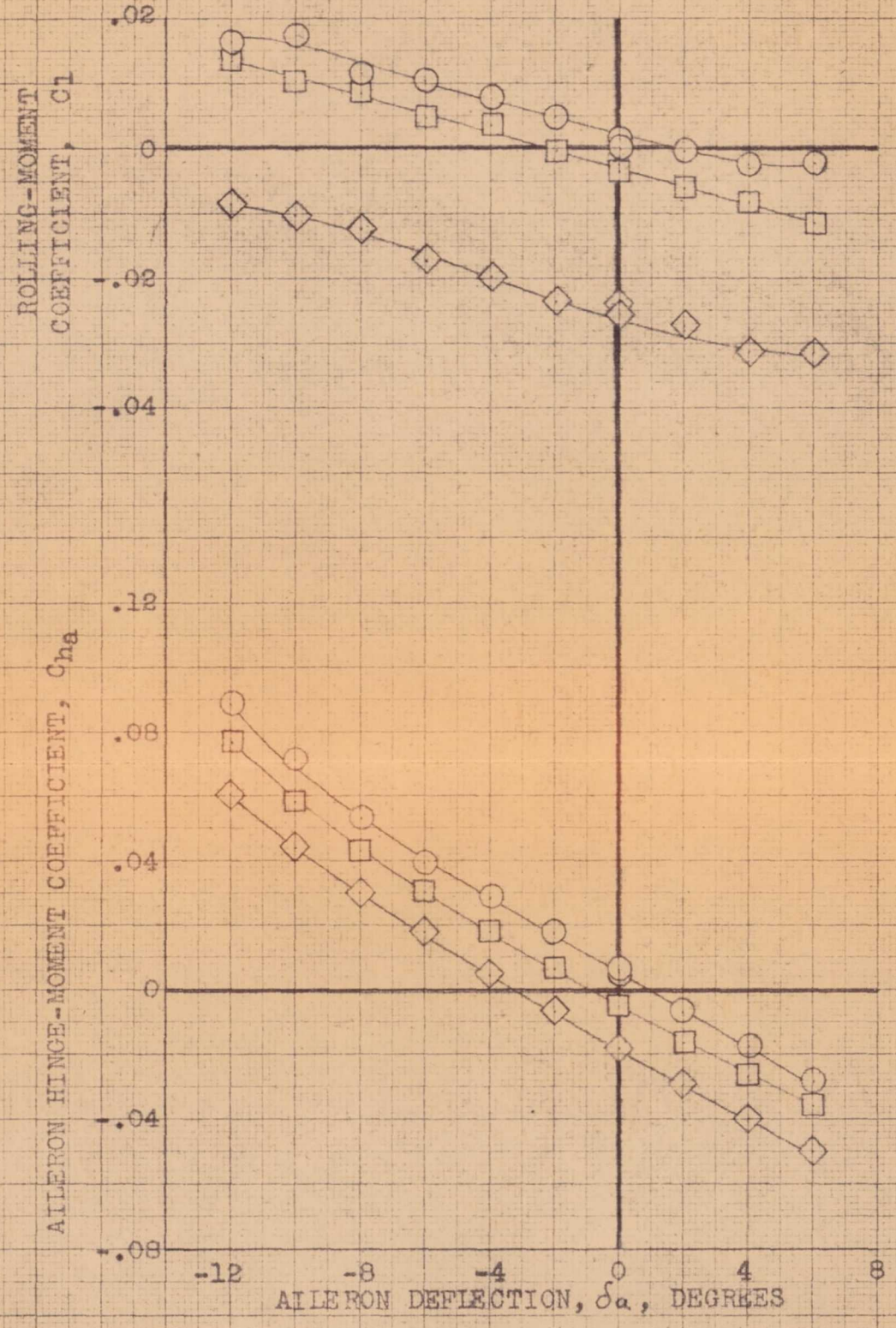

(a) C_l, C_{h_a} vs δ_a.

FIGURE 30.- VARIATION WITH DEFLECTION OF THE RIGHT AILERON OF THE AERODYNAMIC CHARACTERISTICS OF THE AIRPLANE AT SEVERAL ANGLES OF ATTACK. CLEAN CONDITION; ψ, -8°.

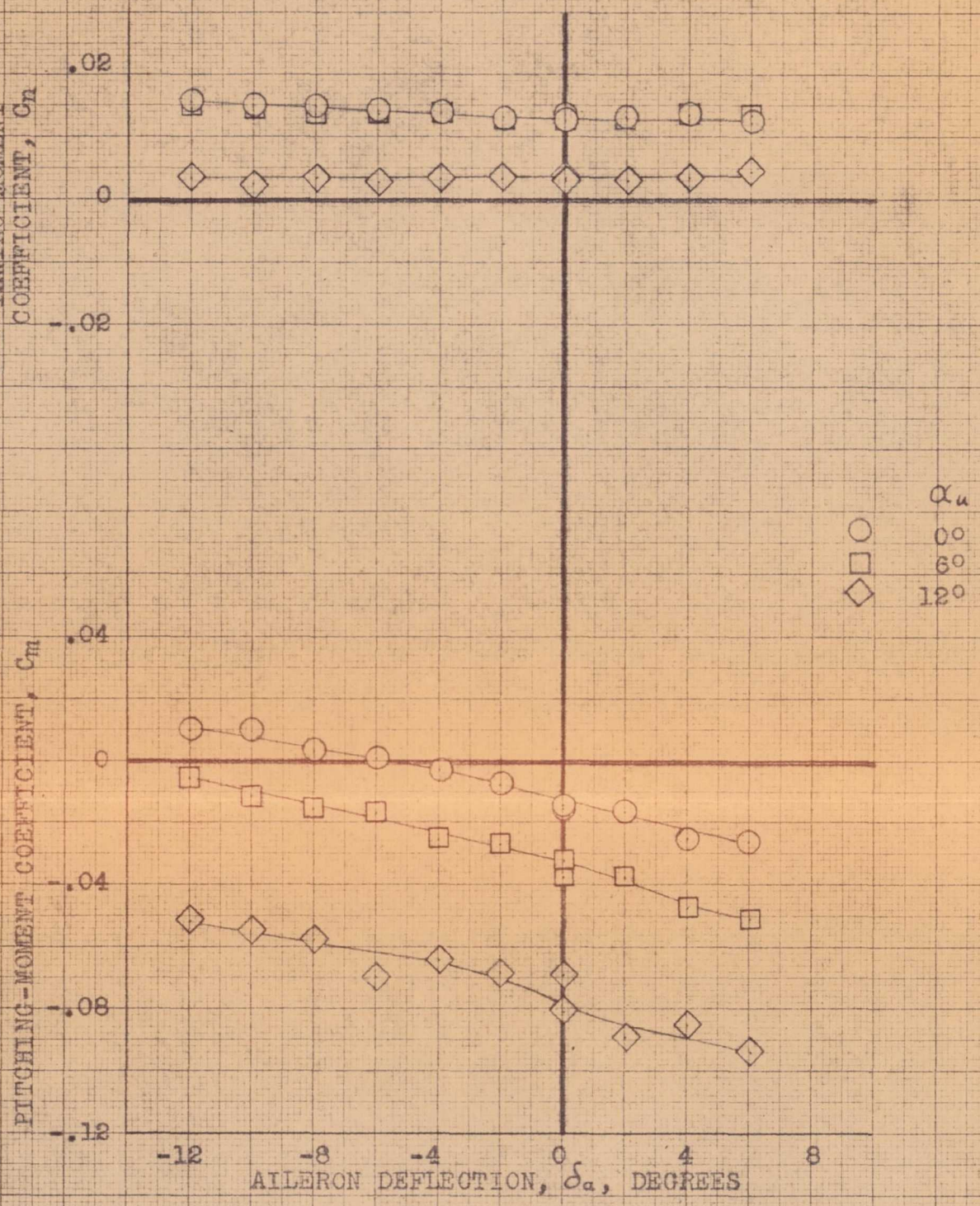

(b) C_n, C_m vs δ_a.

FIGURE 30.- CONCLUDED.

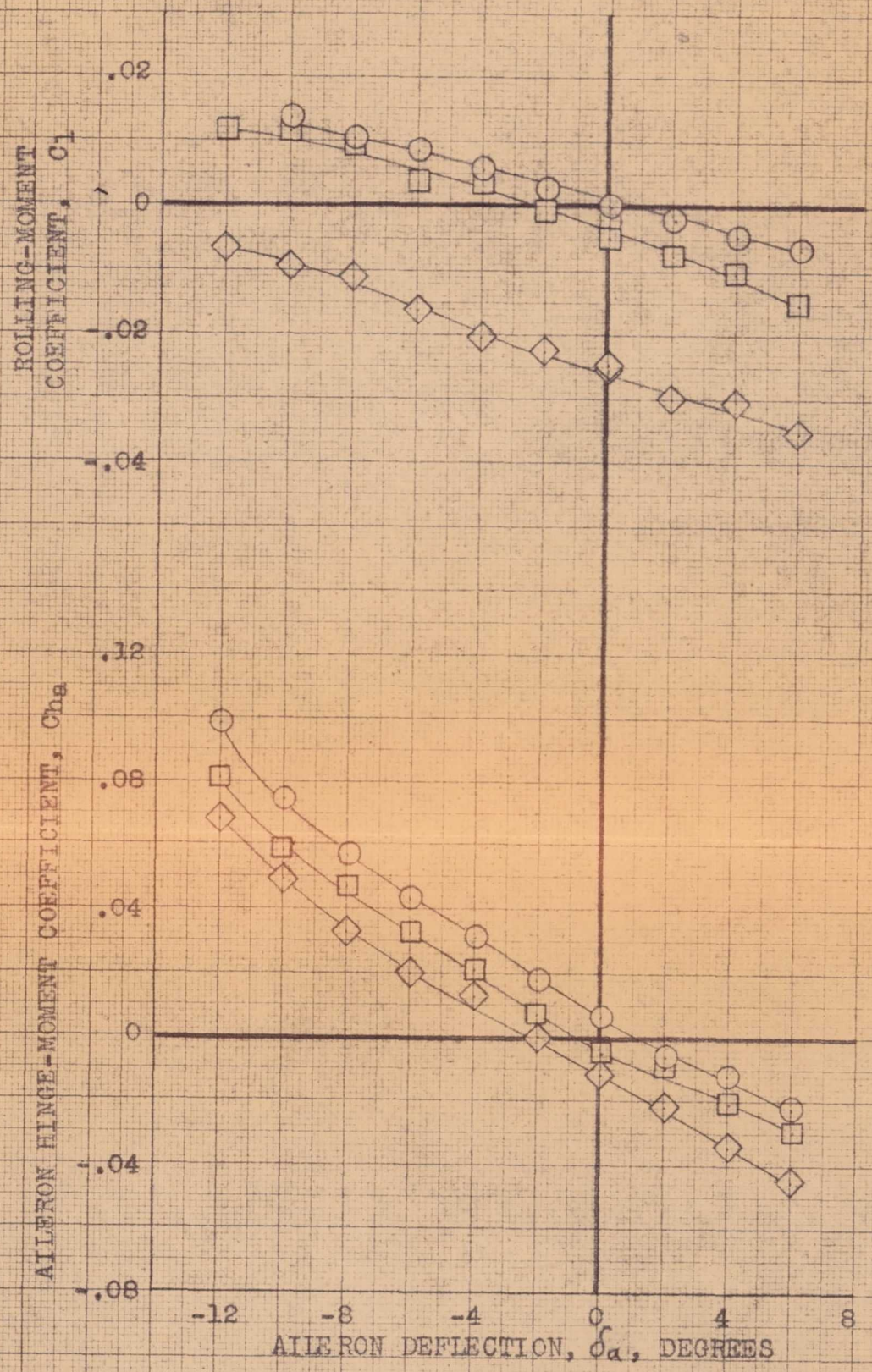

(a) C_l, C_{h_a} vs δ_a.

FIGURE 31.- VARIATION WITH DEFLECTION OF THE RIGHT AILERON OF THE AERODYNAMIC CHARACTERISTICS OF THE AIRPLANE AT SEVERAL ANGLES OF ATTACK. CLEAN CONDITION; ψ , -12°.

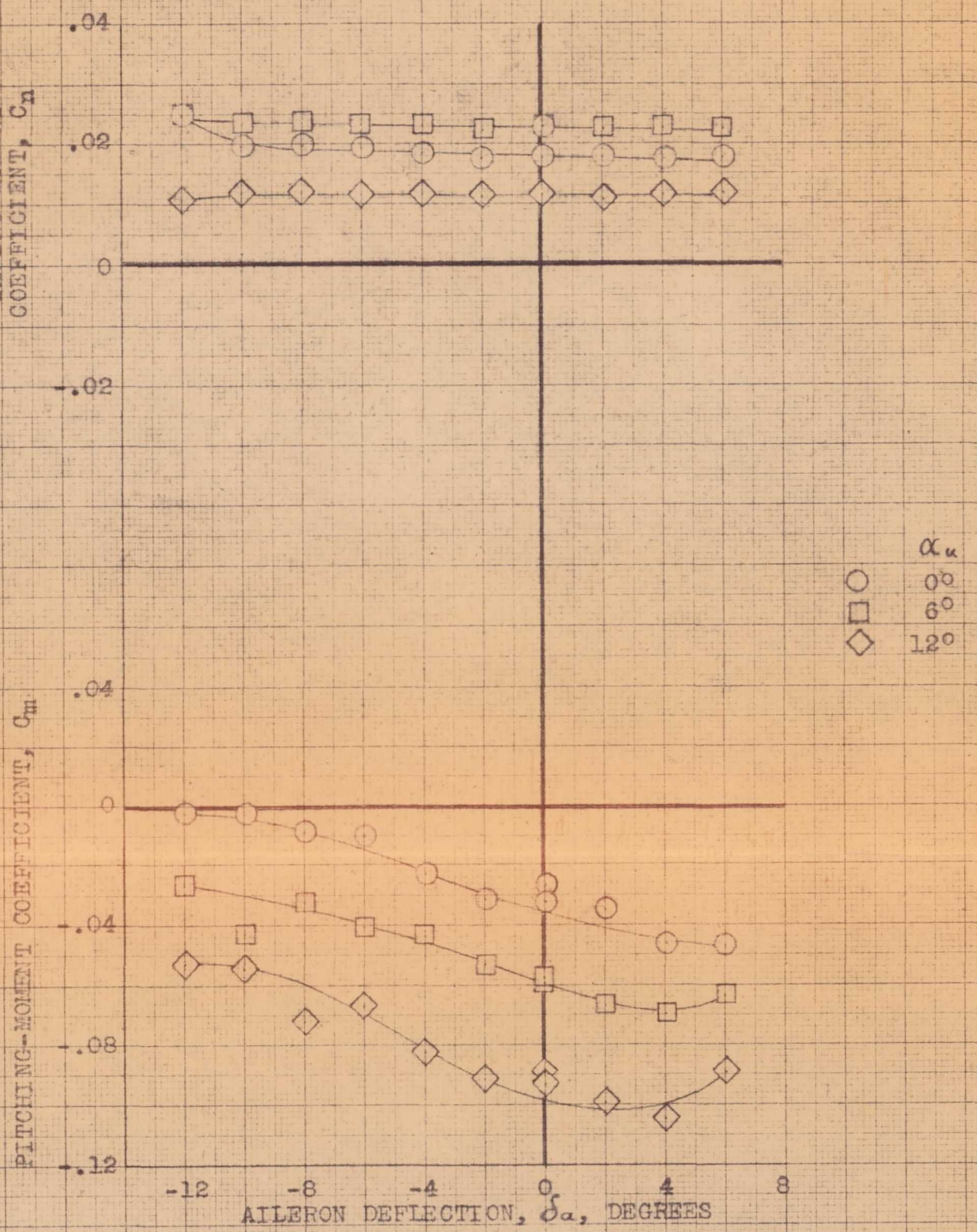

(b) C_n, C_m vs δ_a.

FIGURE 31.- CONCLUDED.

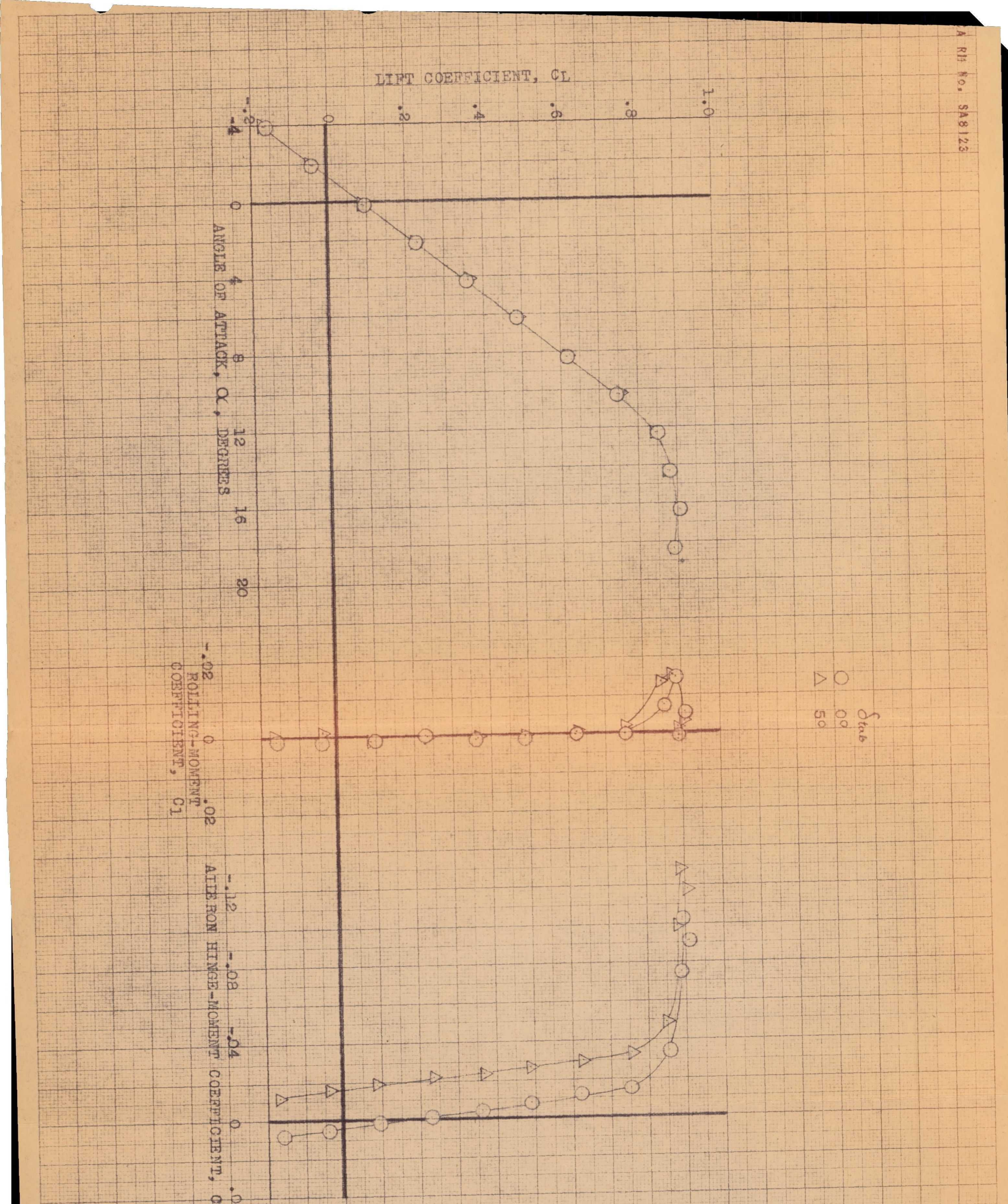

FIGURE 32.- EFFECT OF FIXED DEFLECTIONS OF THE RIGHT AILERON BALANCE TAB ON THE AERODYNAMIC CHARACTERISTICS OF THE AIRPLANE IN PITCH. CLEAN CONDITION; δ_a, 0°; ψ, 0°.

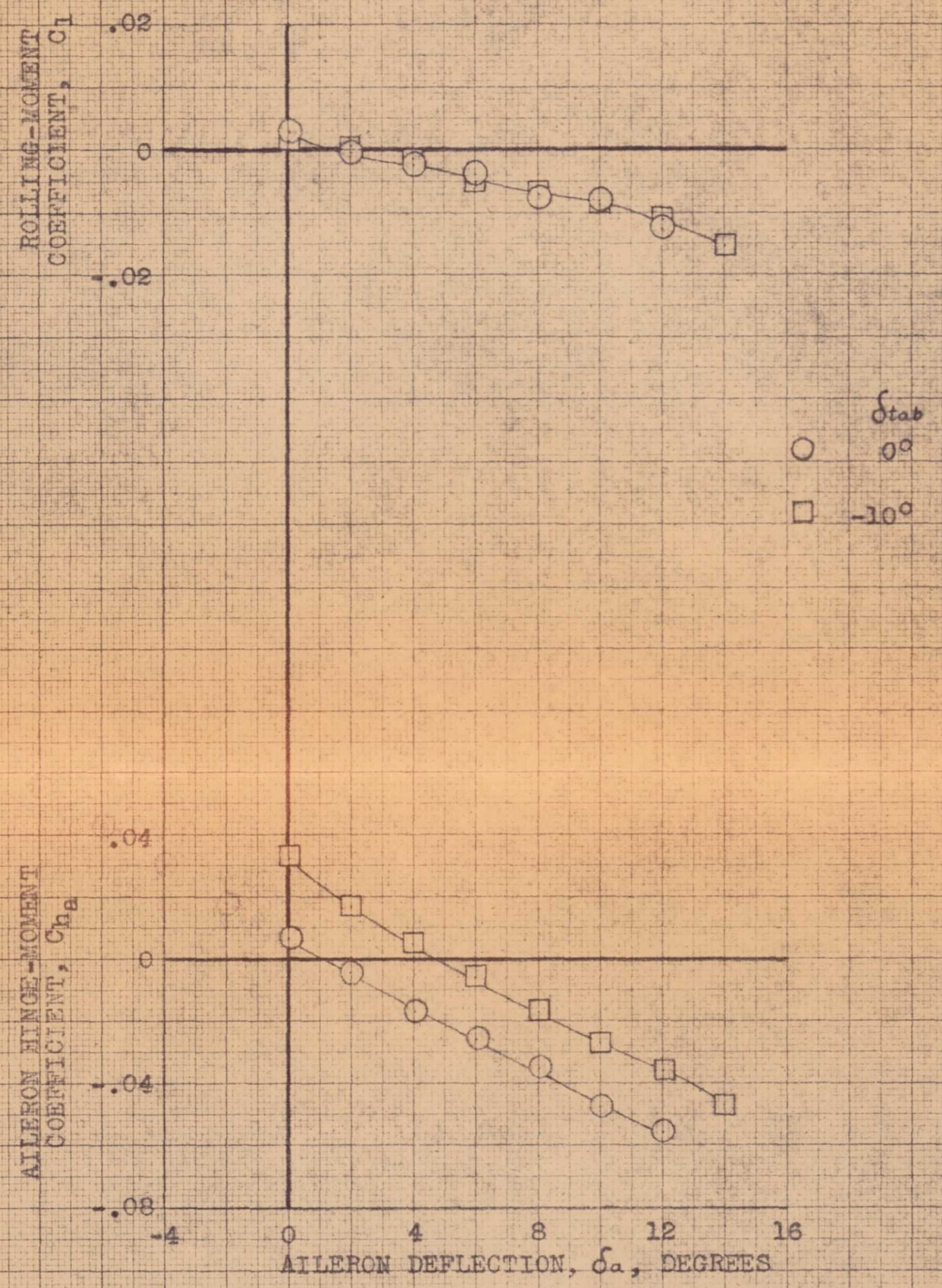

FIGURE 33.- EFFECT OF FIXED DEFLECTIONS OF THE BALANCE TAB ON THE EFFECTIVENESS OF THE RIGHT AILERON. CLEAN CONDITION; α_a, 0°; ψ, 0°.

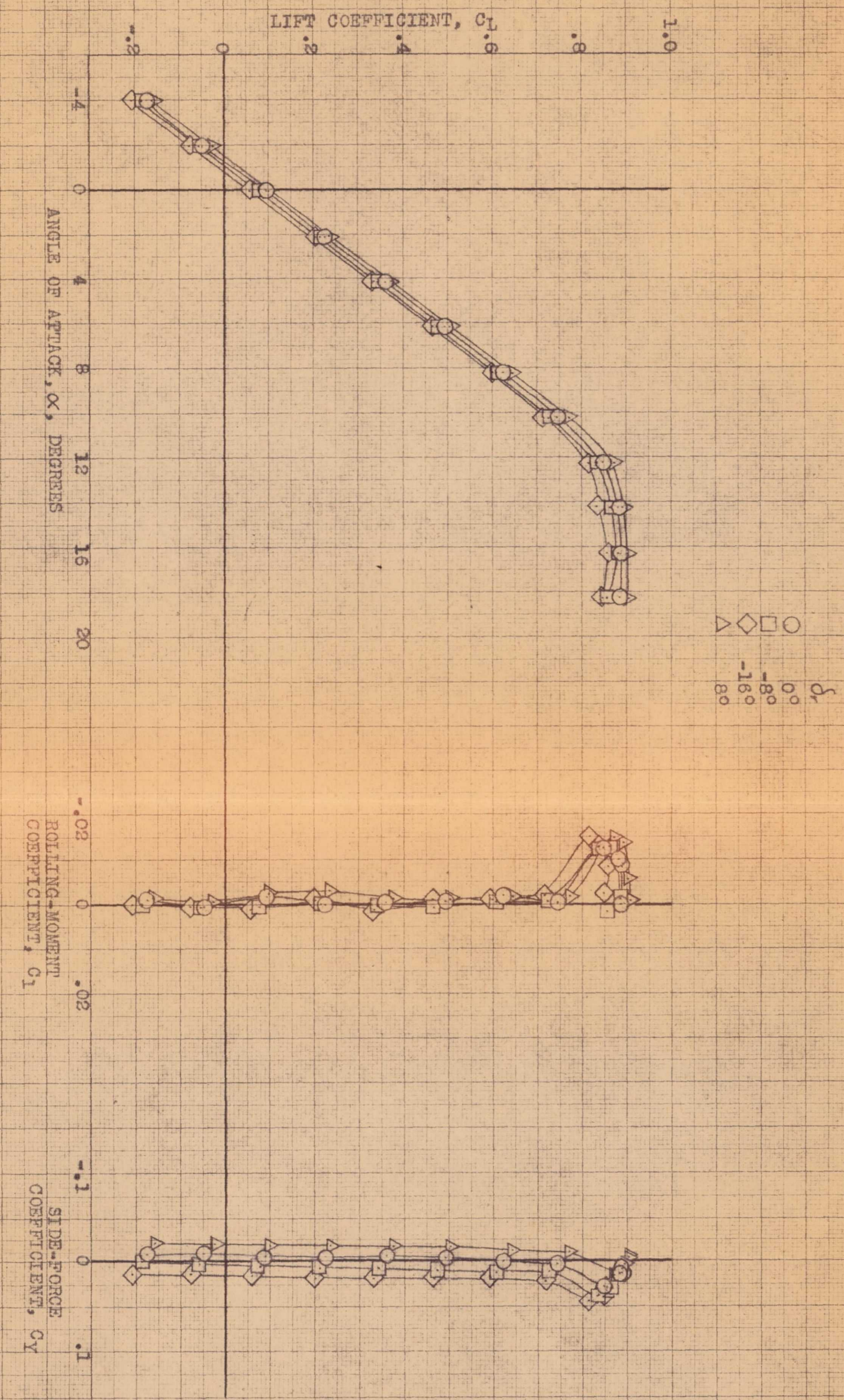

(a) α, C_l, C_Y vs C_L.

FIGURE 34.- EFFECT OF FIXED DEFLECTIONS OF THE UPPER RIGHT AND LOWER LEFT RUDDERVATOR ON THE AERODYNAMIC CHARACTERISTICS OF THE AIRPLANE IN PITCH. CLEAN CONDITION; ψ, 0°.

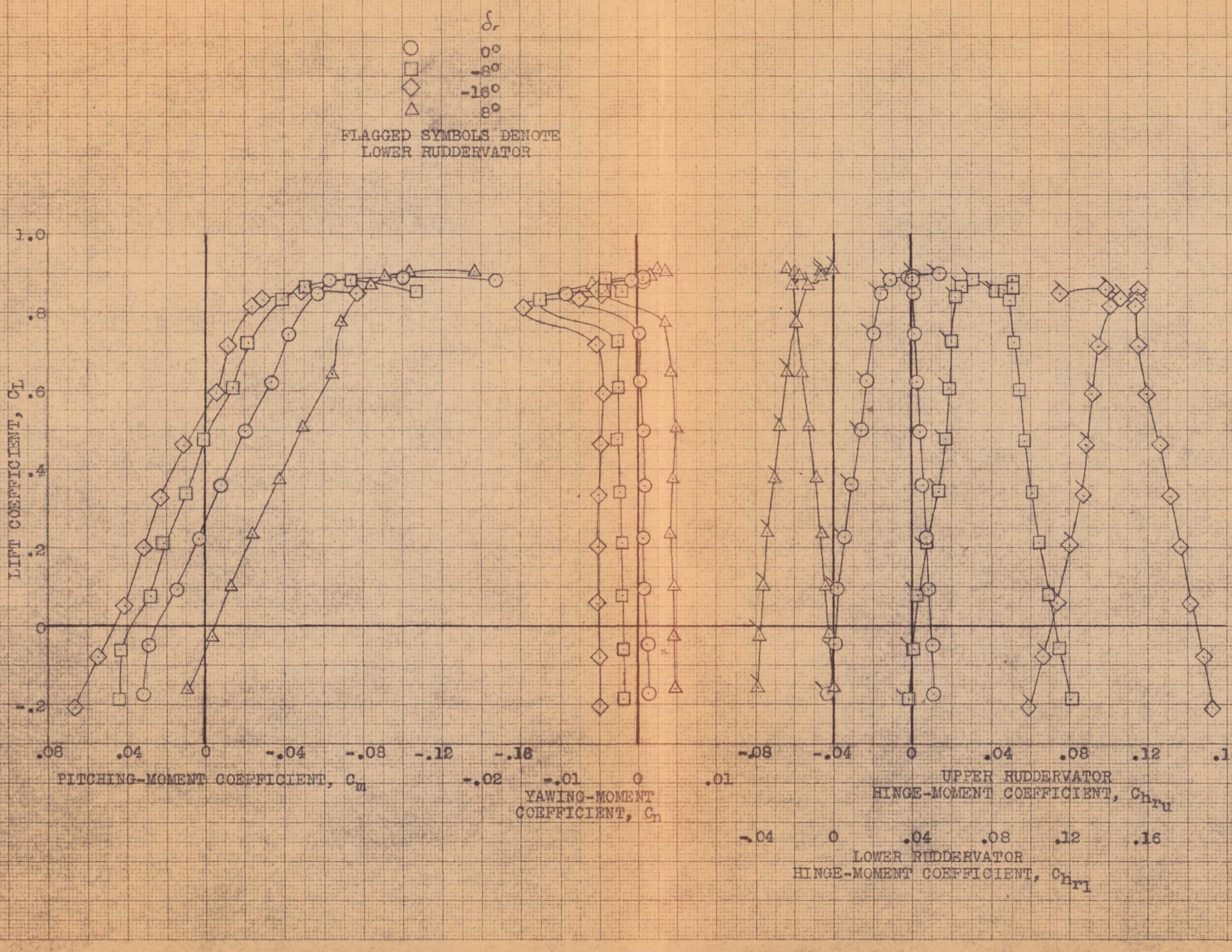

(b) C_m, C_n, C_{h_r} vs C_L.

FIGURE 34.- CONCLUDED.

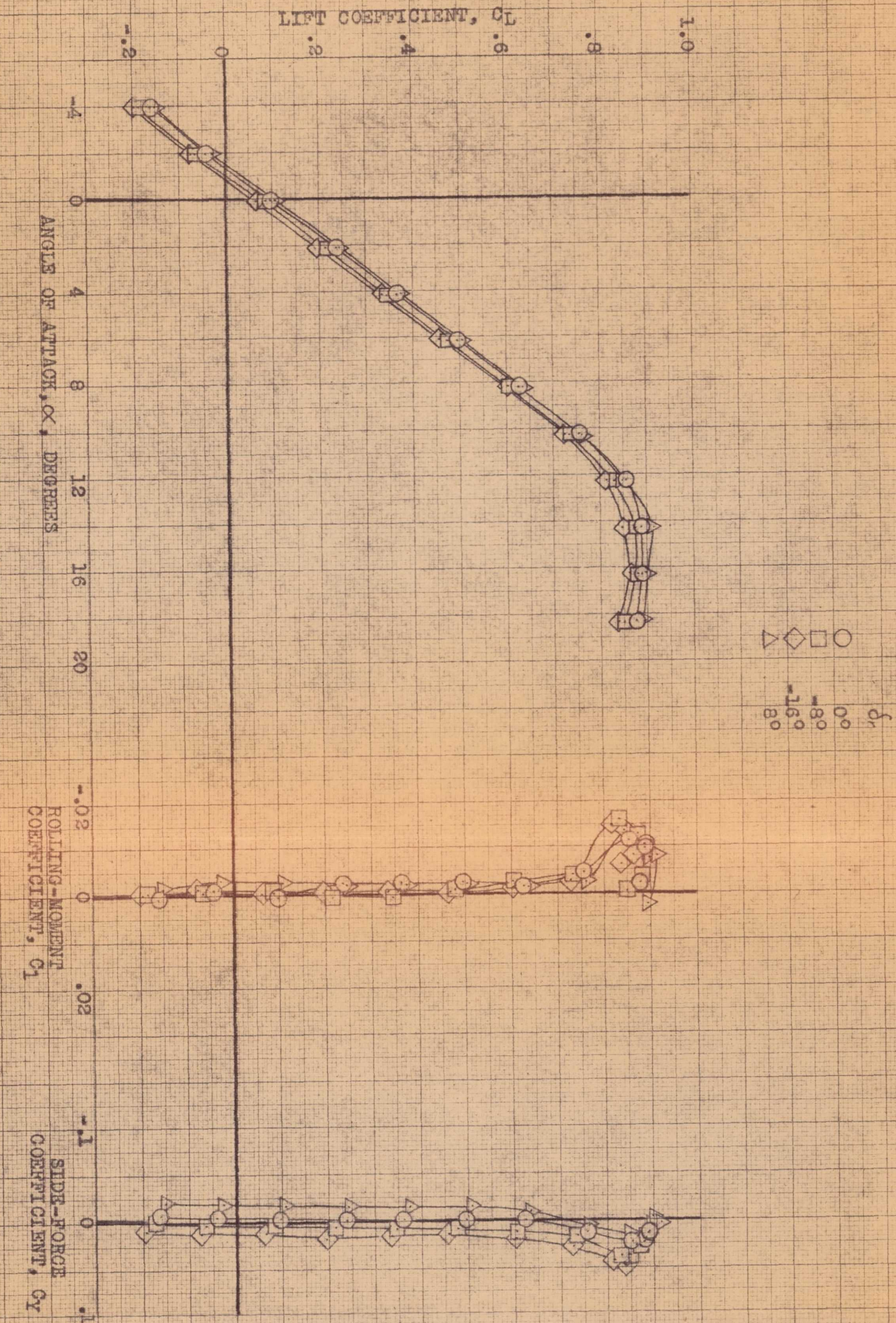

(a) α, C_l, C_Y vs C_L.

FIGURE 35.- EFFECT OF FIXED DEFLECTIONS OF THE UPPER RIGHT AND LOWER LEFT RUDDERVATOR ON THE AERODYNAMIC CHARACTERISTICS OF THE AIRPLANE IN PITCH. SKYHOOK EXTENDED; ψ, 0°.

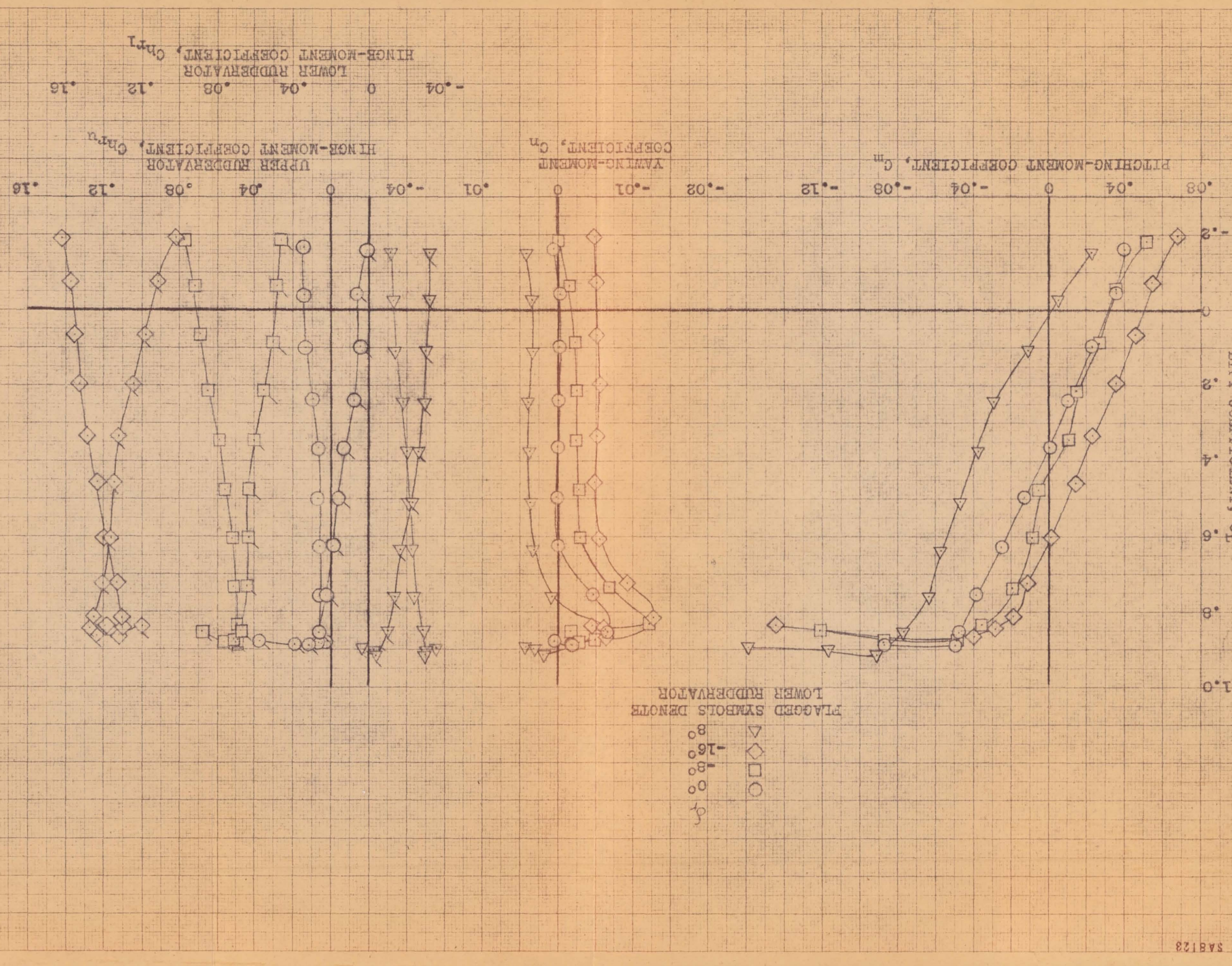

FIGURE 35.- CONCLUDED.

(b) C_m, C_n, C_{hT} vs C_L.

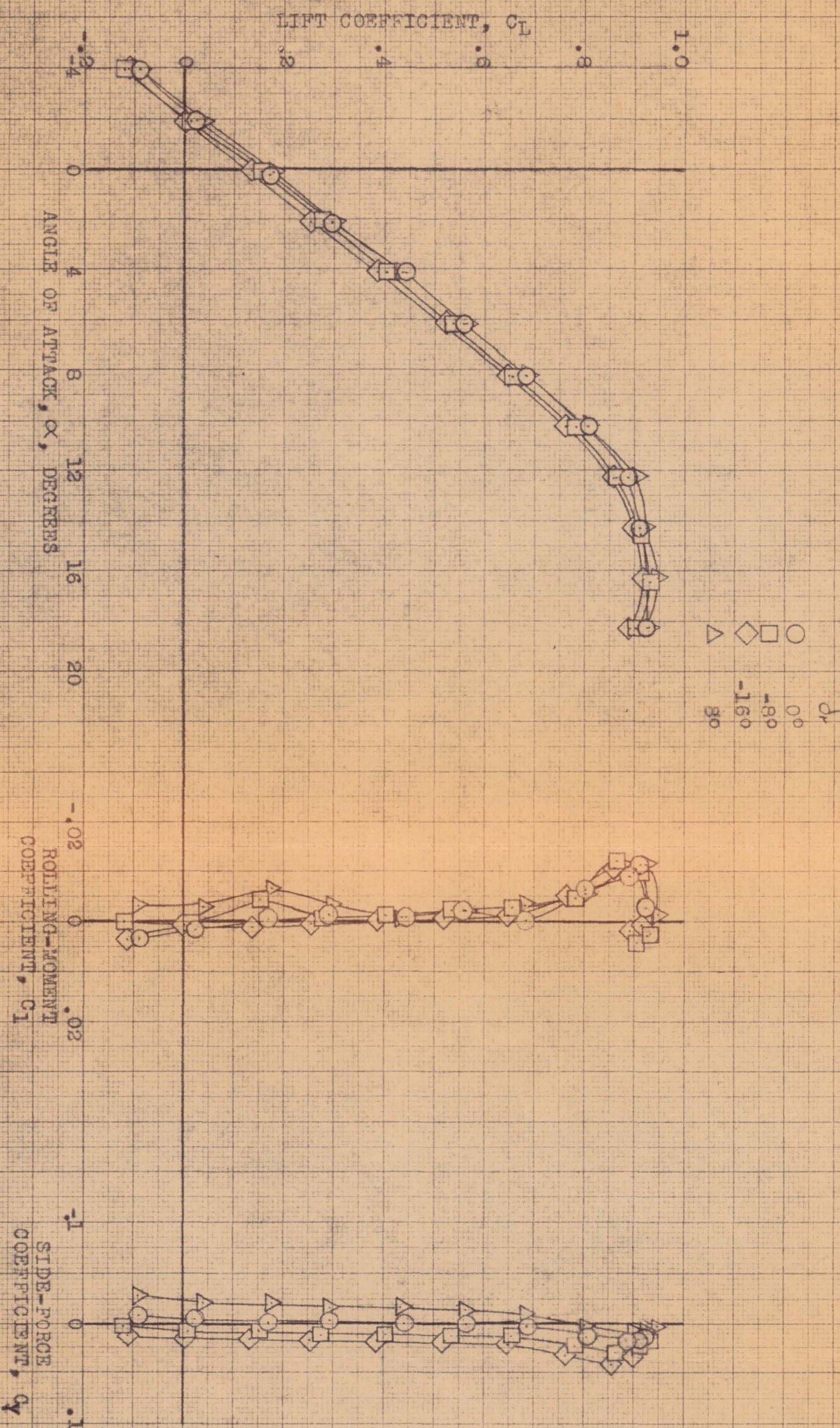

(a) α, C_l, C_Y vs C_L.

FIGURE 36.- EFFECT OF FIXED DEFLECTIONS OF THE UPPER RIGHT AND LOWER LEFT RUDDERVATOR ON THE AERODYNAMIC CHARACTERISTICS OF THE AIRPLANE IN PITCH. DIVE BRAKE EXTENDED; ψ, 0°.

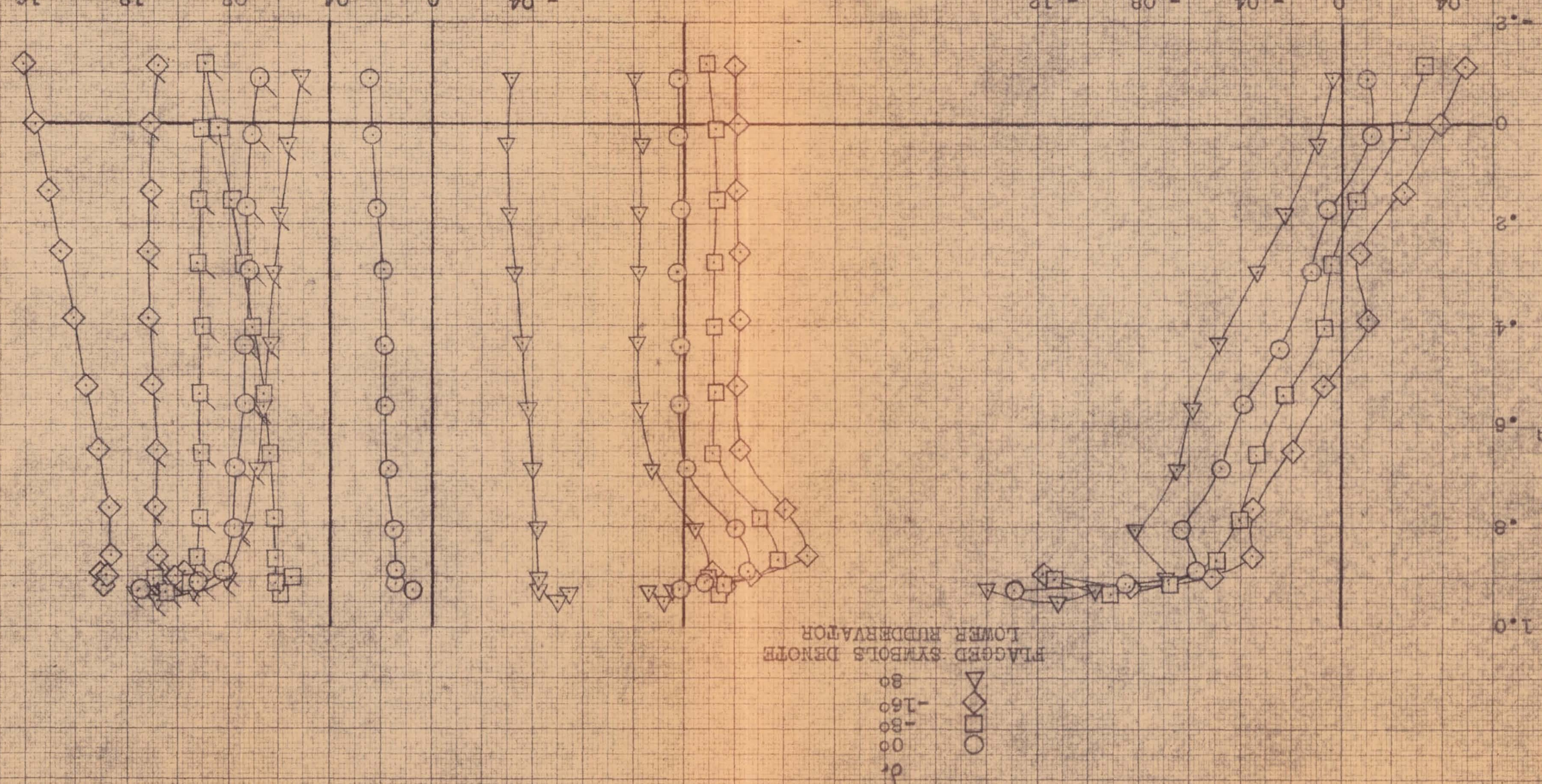

FIGURE 36.- CONCLUDED.

(b) C_m, C_n, Ch_r vs C_L.

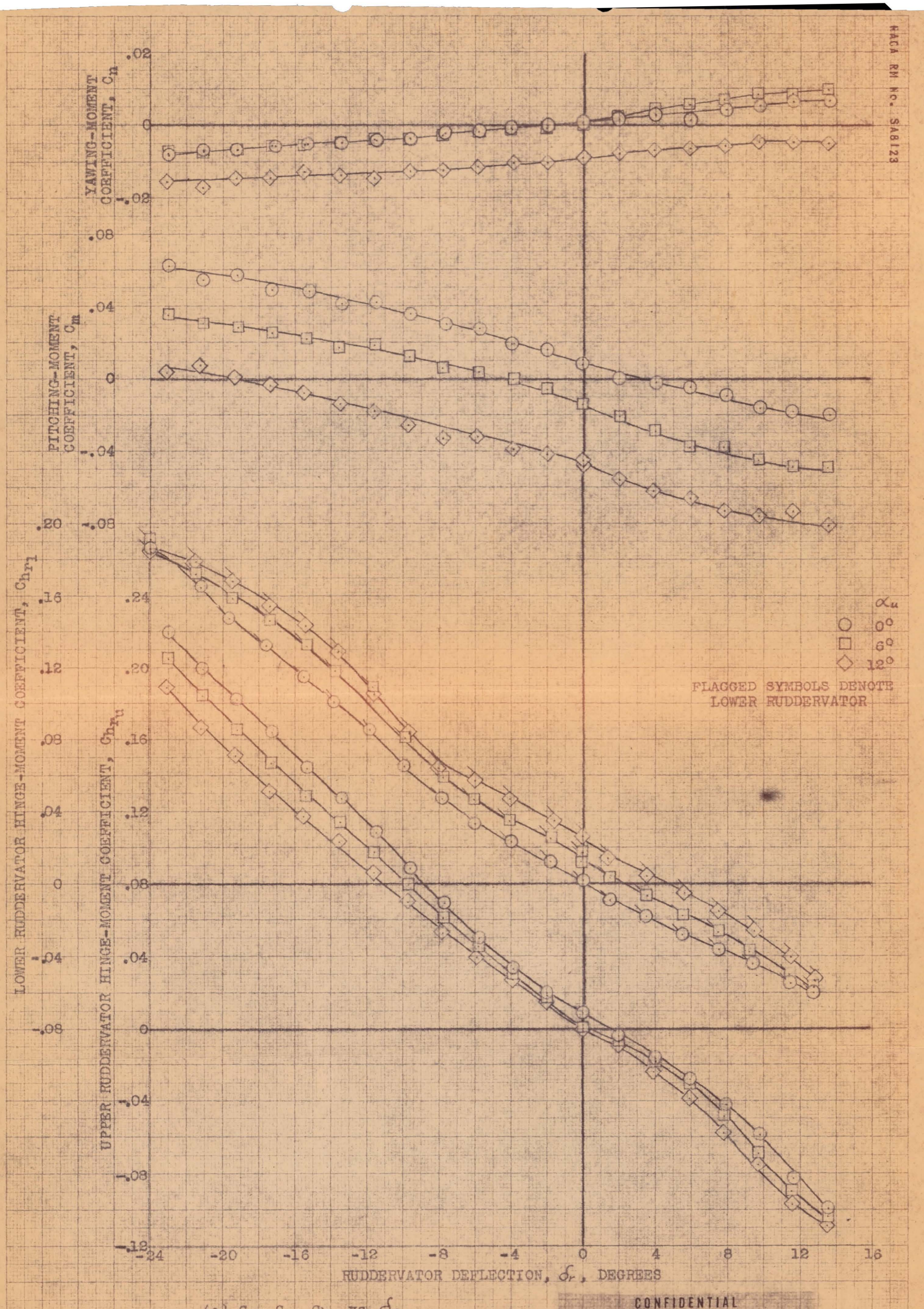

(a) C_n, C_m, C_{h_r} vs δ_r.

CONFIDENTIAL

NATIONAL ADVISORY COMMITTEE FOR AERONAUTICS

FIGURE 37.- VARIATION WITH DEFLECTION OF THE UPPER RIGHT AND LOWER LEFT RUDDERVATOR OF THE AERODYNAMIC CHARACTERISTICS OF THE AIRPLANE AT SEVERAL ANGLES OF ATTACK. CLEAN CONDITION; ψ, 0°.

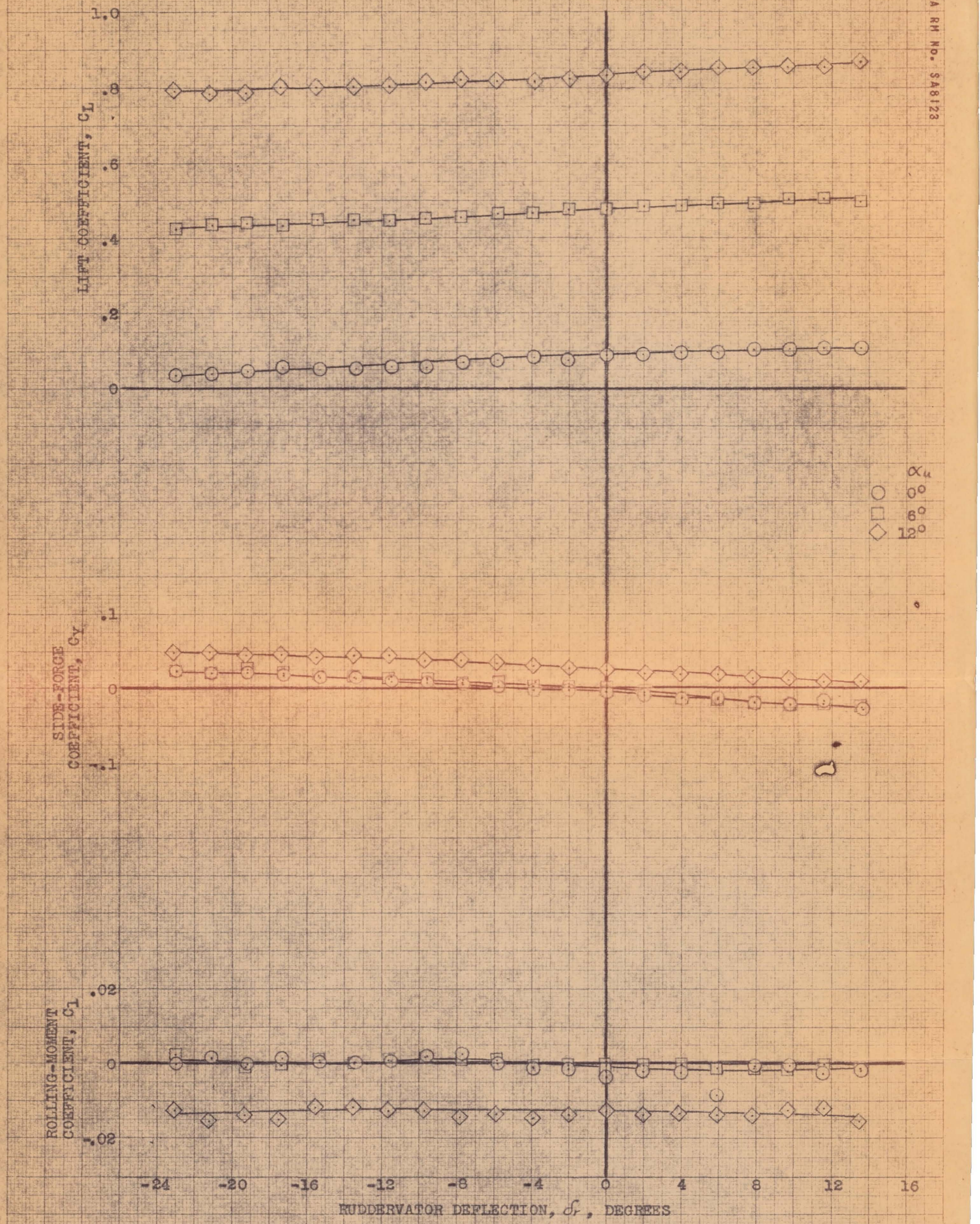

(b) C_L, C_Y, C_l vs δ_r.

FIGURE 37.- CONCLUDED.

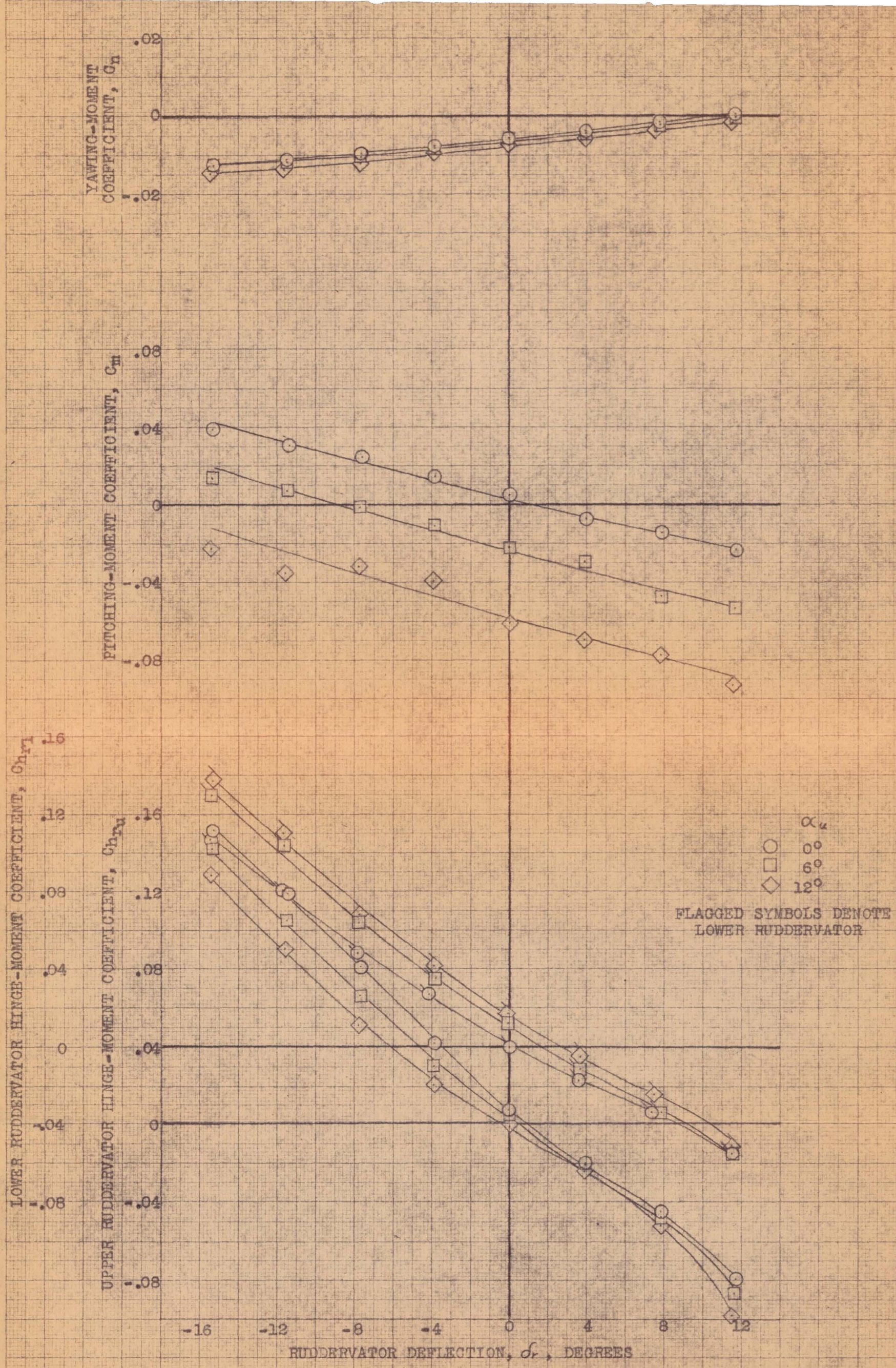

(a) C_n, C_m, C_{h_r} vs δ_r.

FIGURE 38.- VARIATION WITH DEFLECTION OF THE UPPER RIGHT AND LOWER LEFT RUDDERVATOR OF THE AERODYNAMIC CHARACTERISTICS OF THE AIRPLANE AT SEVERAL ANGLES OF ATTACK. CLEAN CONDITION; ψ, 4°.

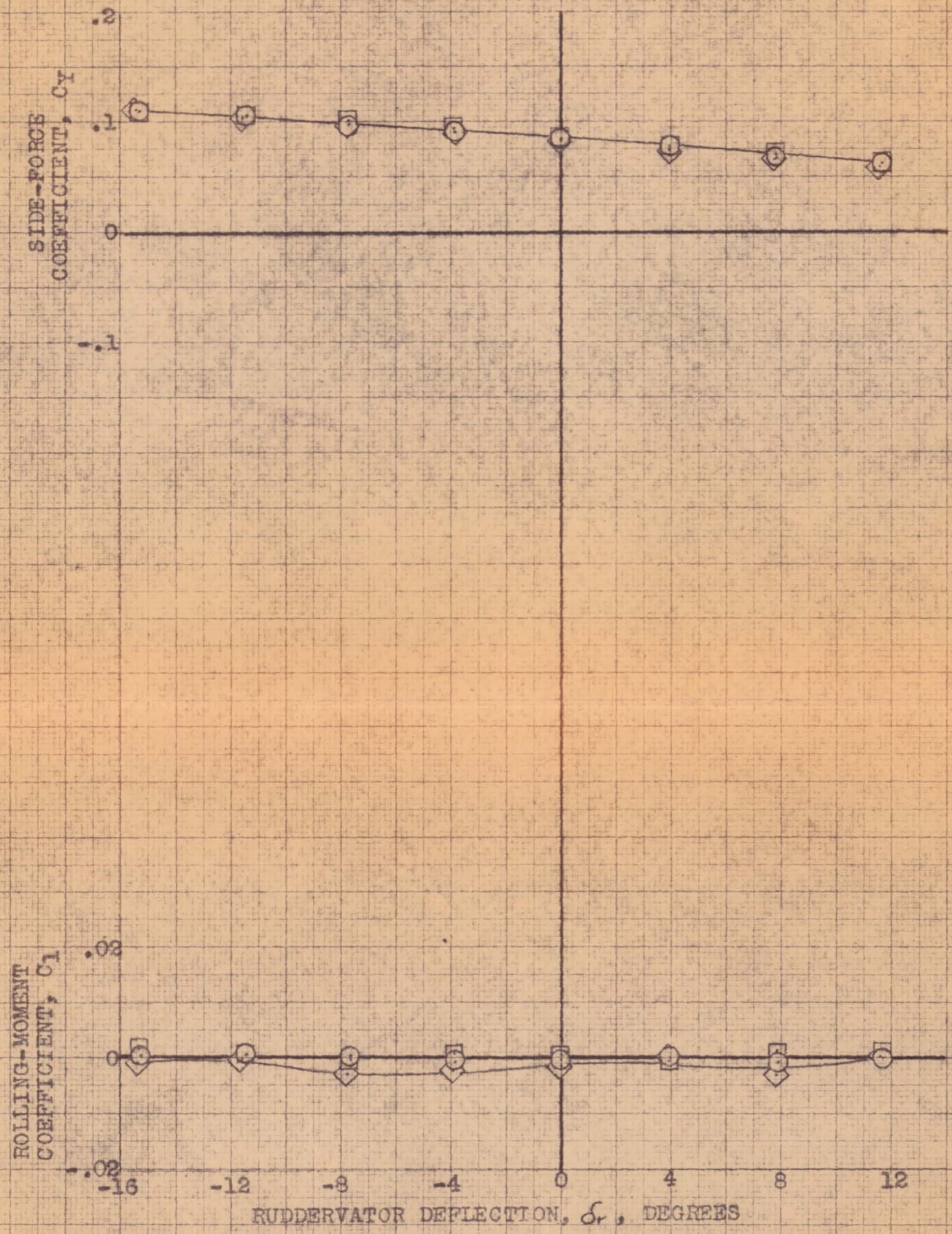

(b) C_Y, C_l vs δ_r.

FIGURE 38.- CONCLUDED.

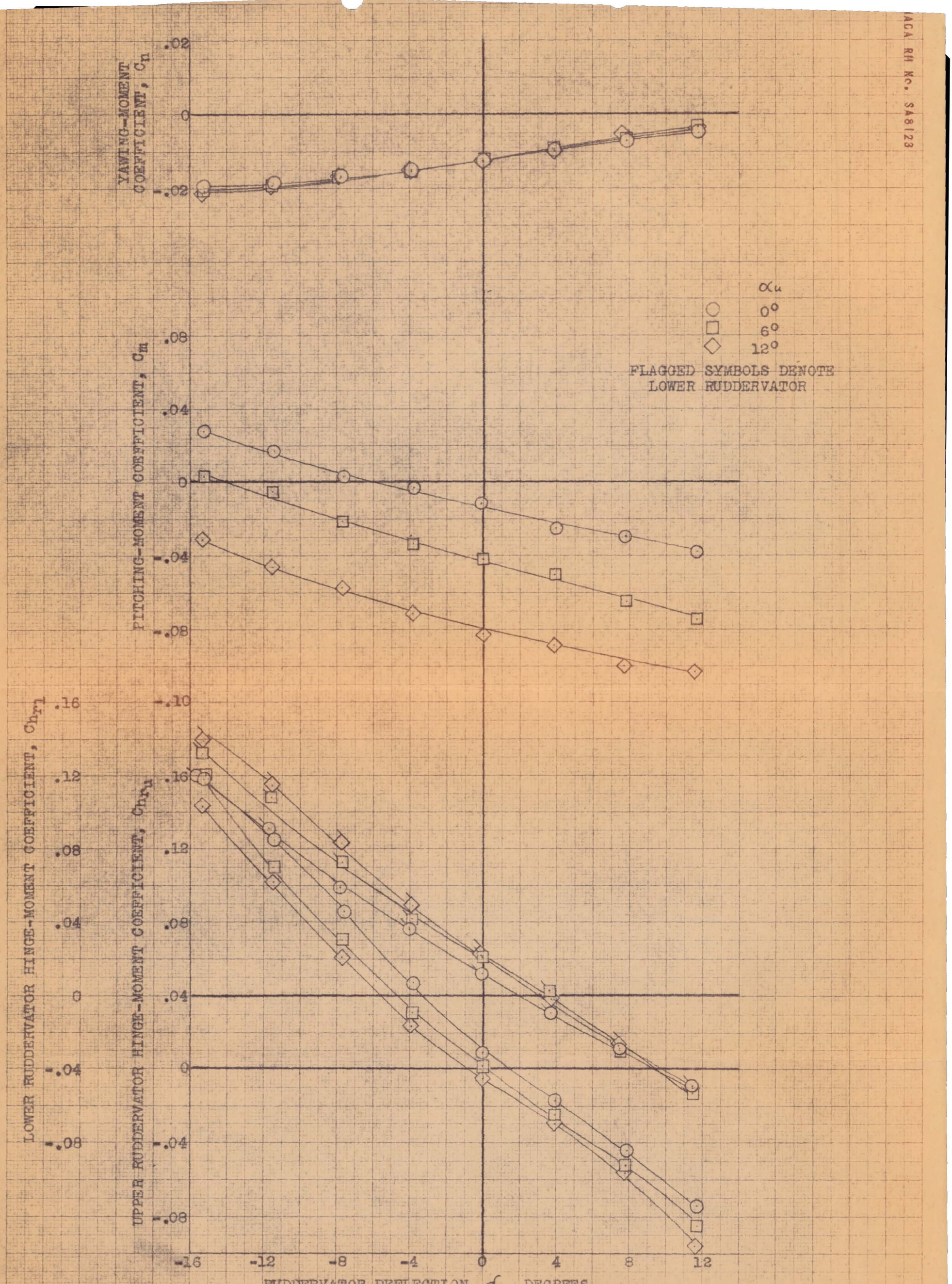

(a) C_n, C_m, C_{h_r} vs δ_r.

FIGURE 39.- VARIATION WITH DEFLECTION OF THE UPPER RIGHT AND LOWER LEFT RUDDERVATOR OF THE AERODYNAMIC CHARACTERISTICS OF THE AIRPLANE AT SEVERAL ANGLES OF ATTACK. CLEAN CONDITION; ψ, 8°.

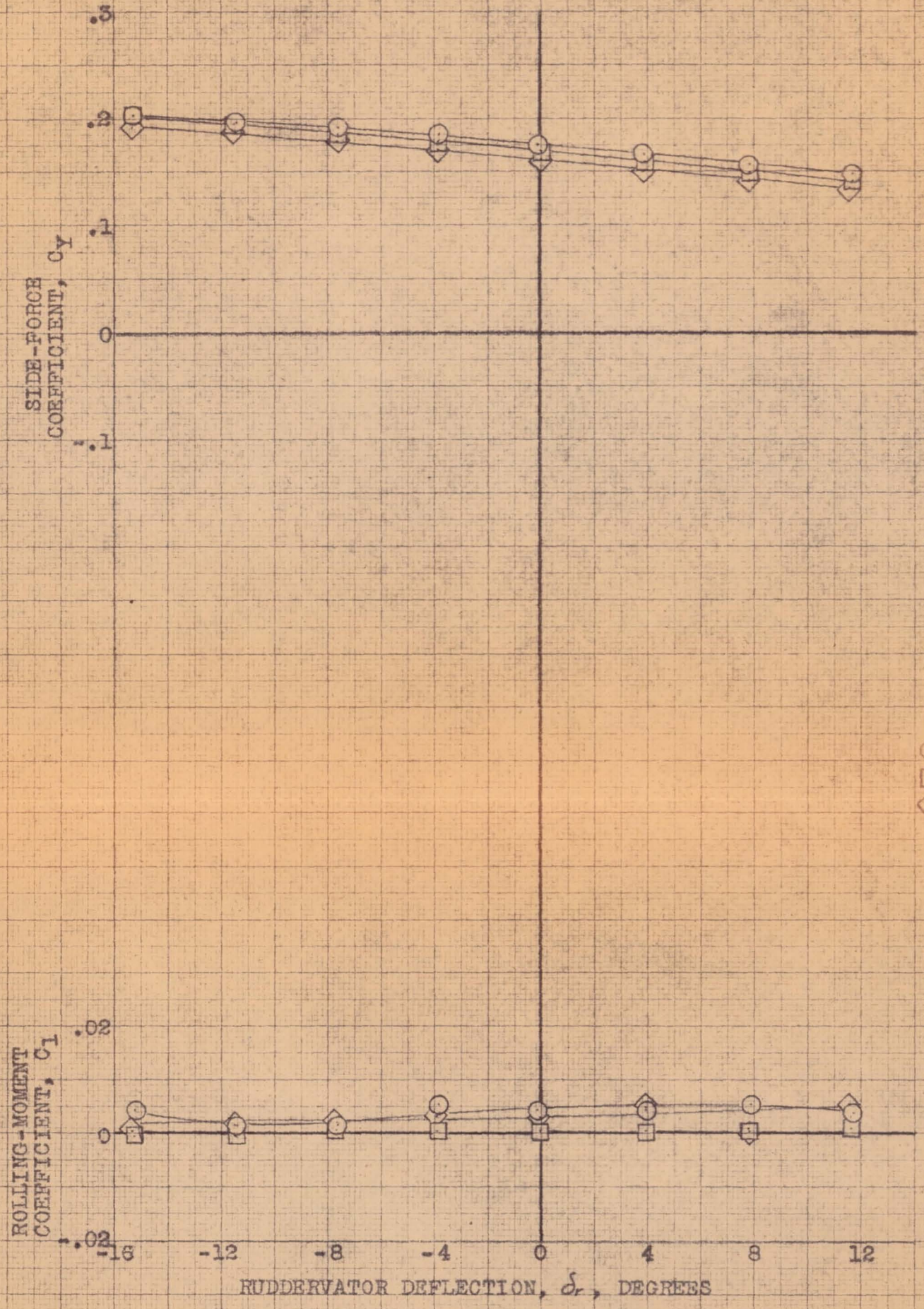

(b) C_Y, C_l vs δ_r.

FIGURE 39.- CONCLUDED.

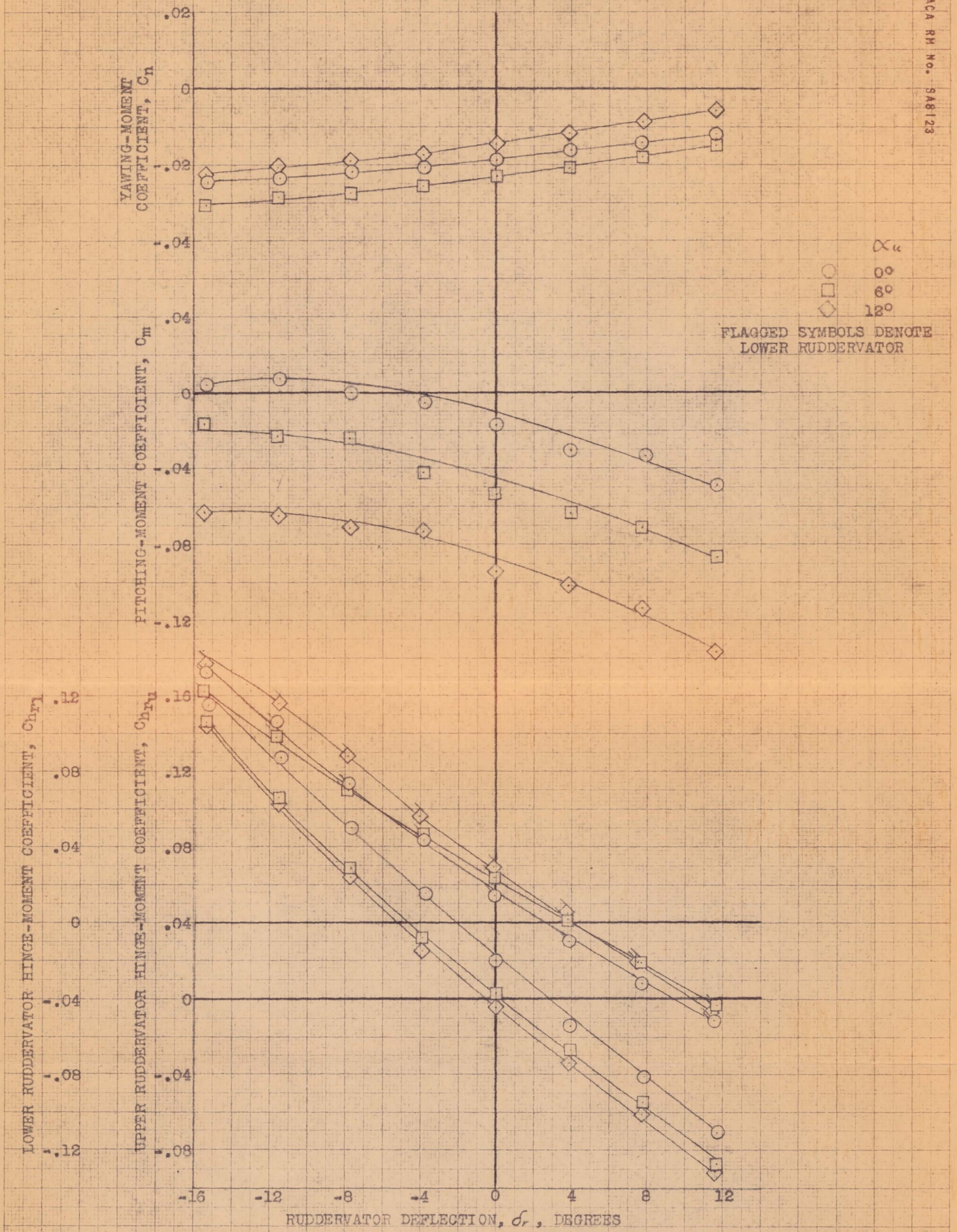

(a) C_n, C_m, C_{h_r} vs δ_r.

CONFIDENTIAL
NATIONAL ADVISORY COMMITTEE FOR AERONAUTICS

FIGURE 40.- VARIATION WITH DEFLECTION OF THE UPPER RIGHT AND LOWER LEFT RUDDERVATOR OF THE AERODYNAMIC CHARACTERISTICS OF THE AIRPLANE AT SEVERAL ANGLES OF ATTACK. CLEAN CONDITION; ψ, 12°

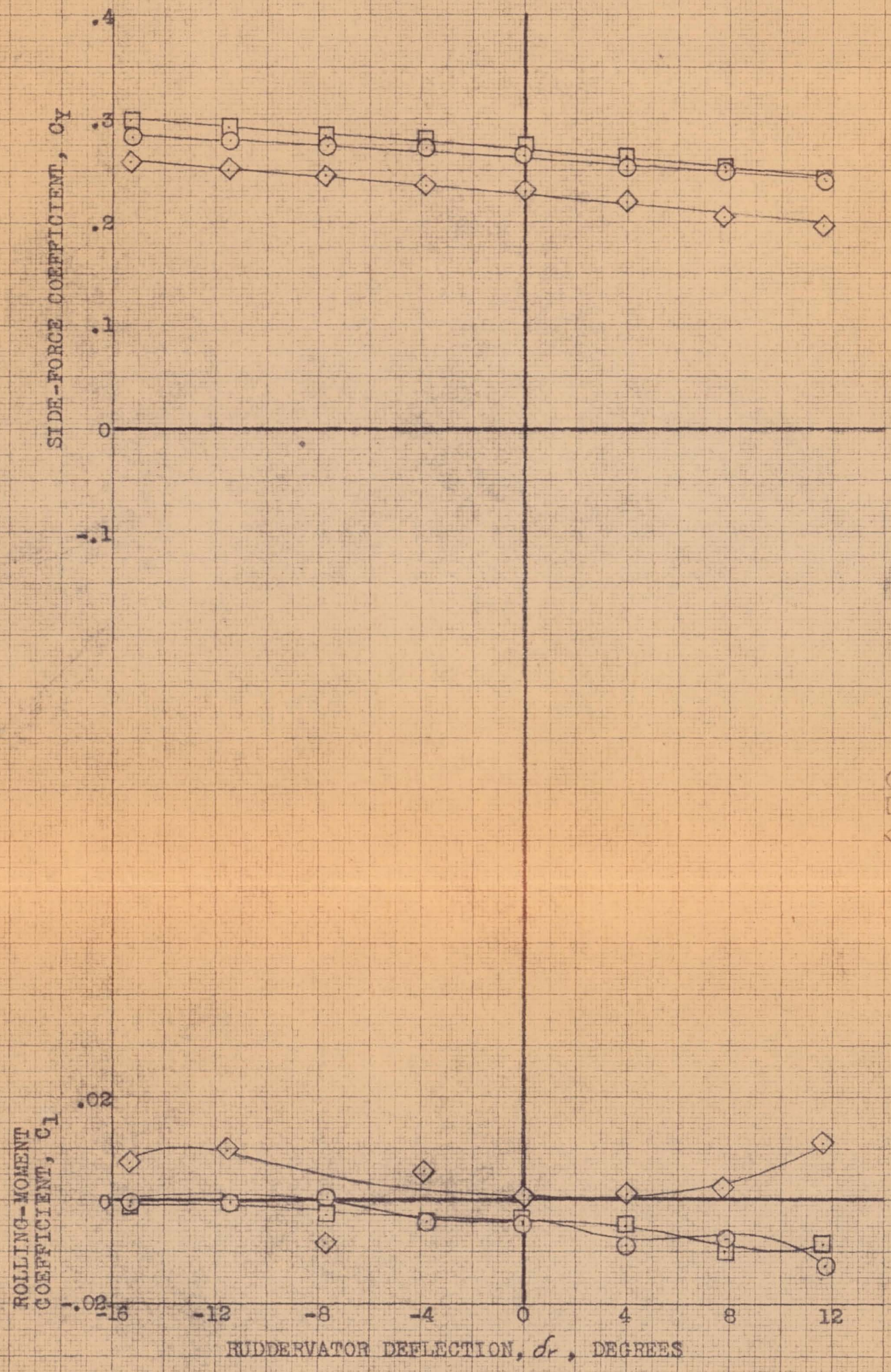

(b) C_Y, C_l vs δ_r.

FIGURE 40.- CONCLUDED.

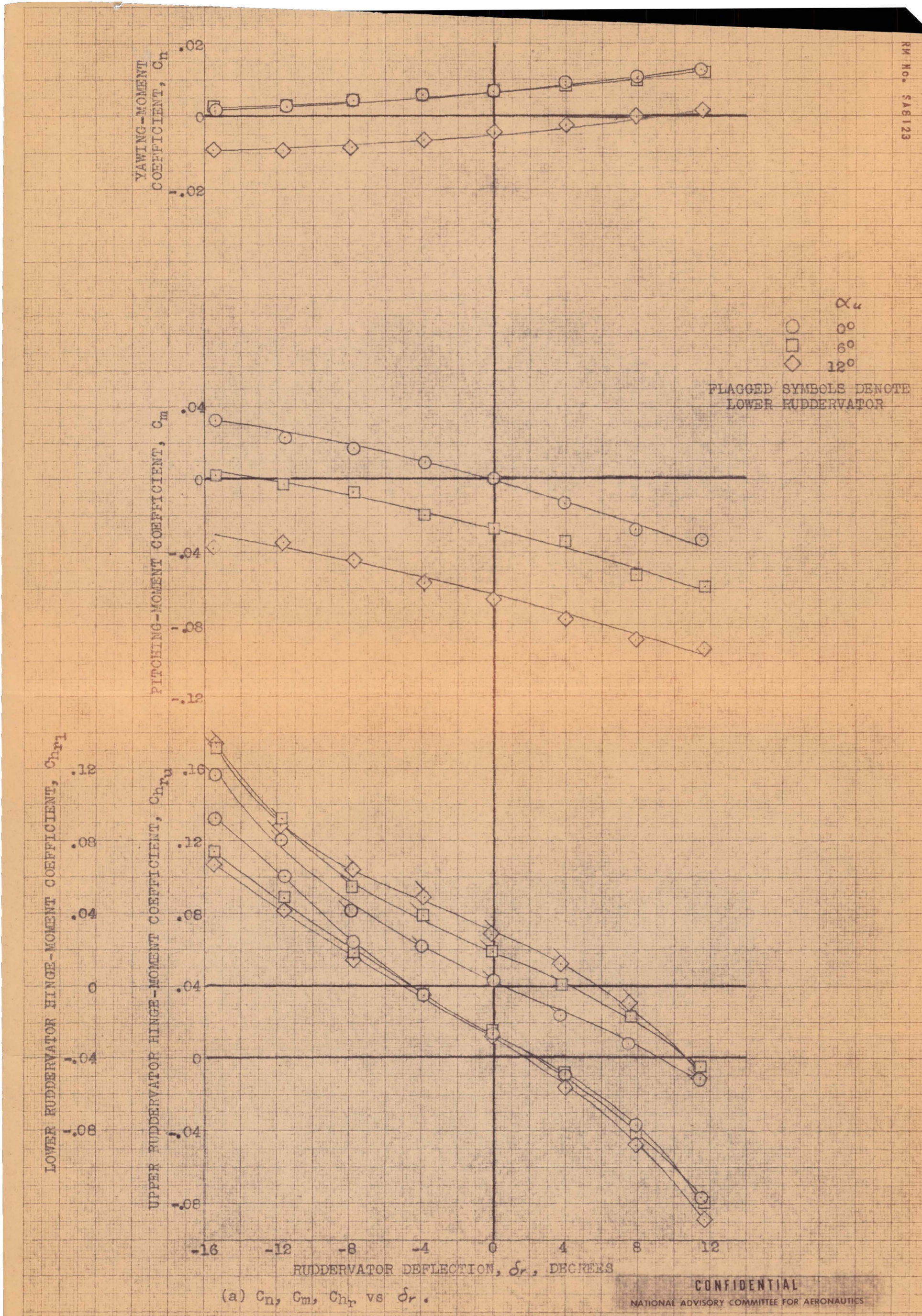

(a) C_n, C_m, C_{h_r} vs δ_r.

FIGURE 41.- VARIATION WITH DEFLECTION OF THE UPPER RIGHT AND LOWER LEFT RUDDERVATOR OF THE AERODYNAMIC CHARACTERISTICS OF THE AIRPLANE AT AT SEVERAL ANGLES OF ATTACK. CLEAN CONDITION; ψ, -4°.

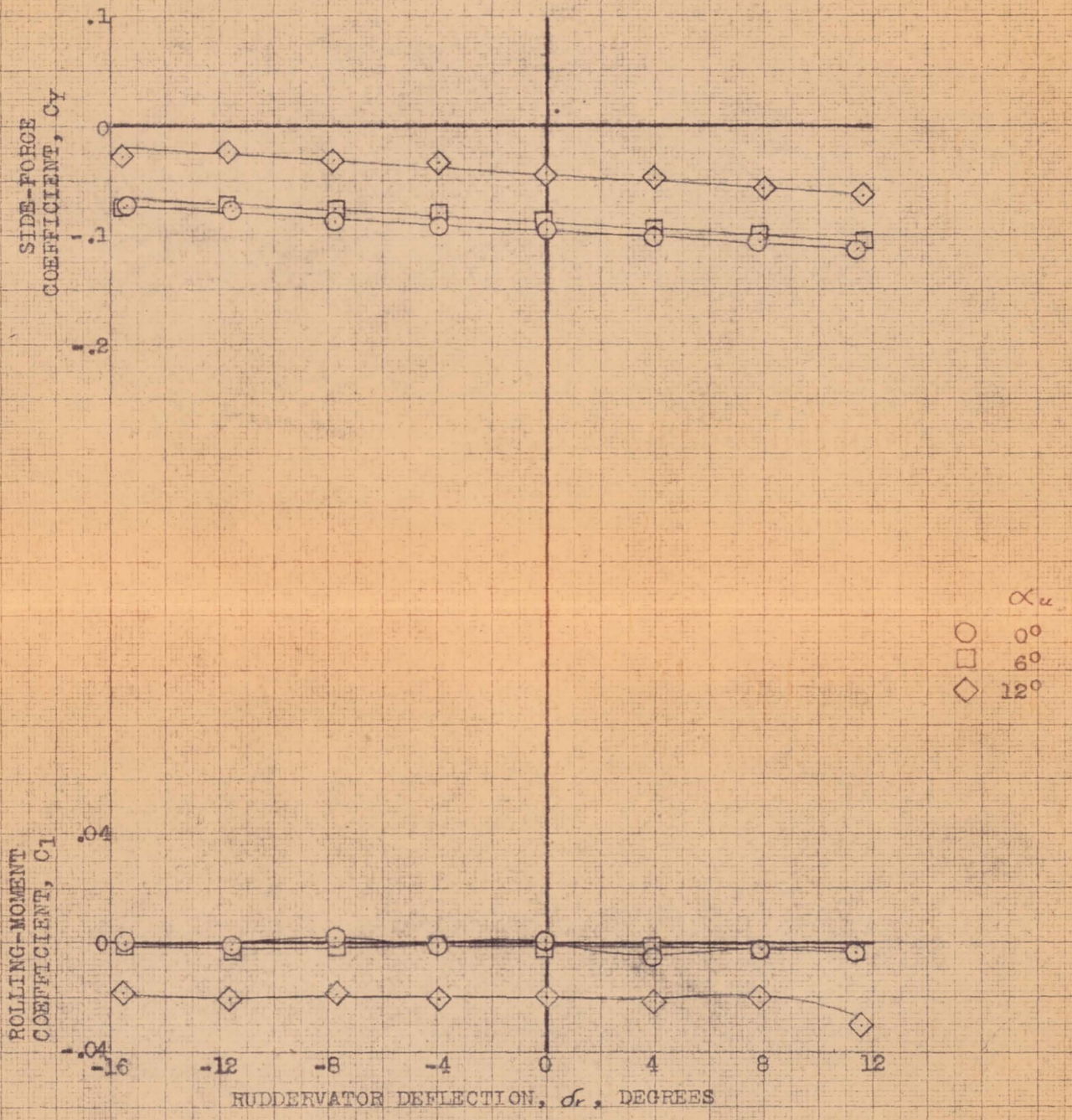

(b) C_Y, C_l vs δ_r.

FIGURE 41.- CONCLUDED.

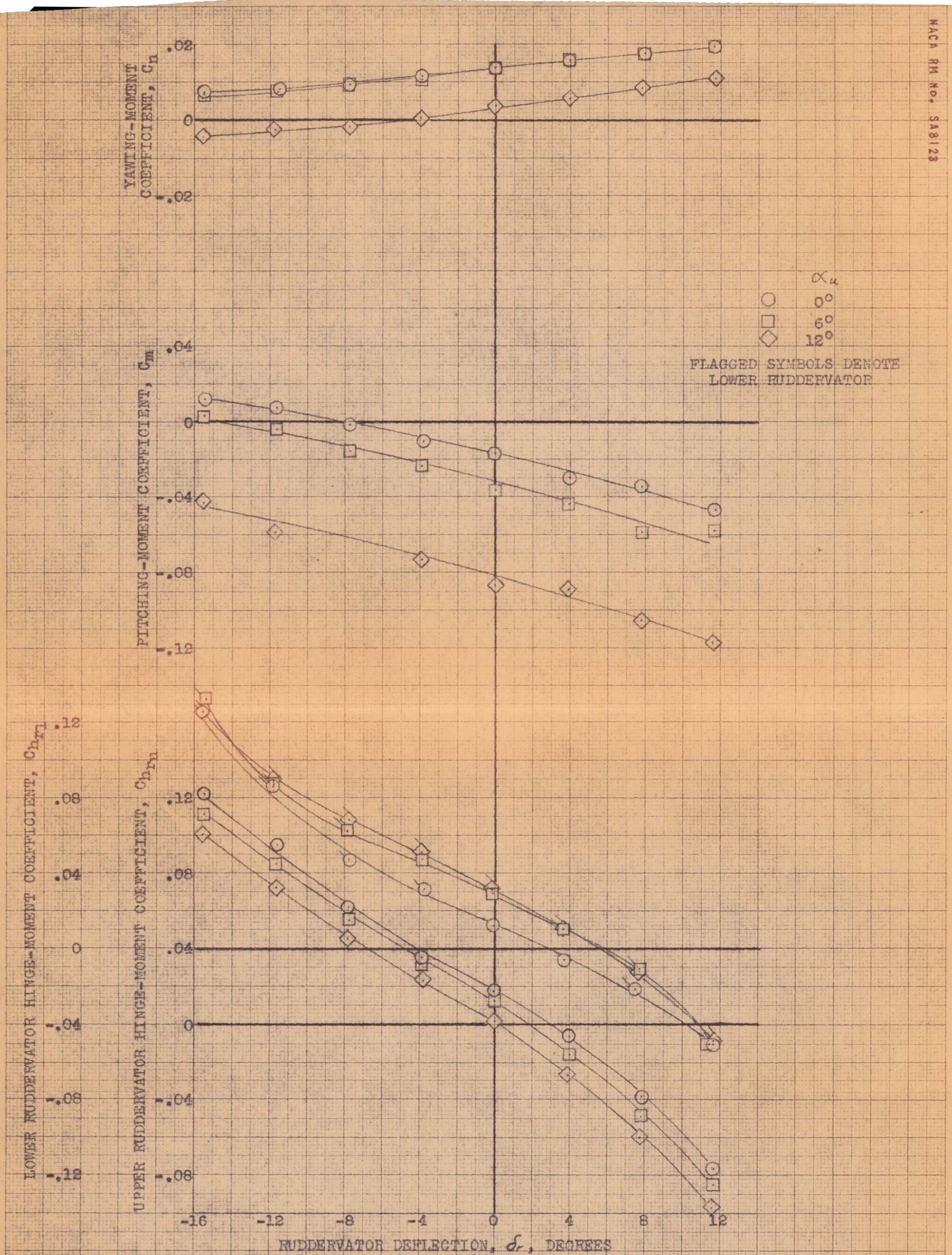

(a) C_n, C_m, C_{h_r} vs δ_r.

FIGURE 42.- VARIATION WITH DEFLECTION OF THE UPPER RIGHT AND LOWER LEFT RUDDERVATOR OF THE AERODYNAMIC CHARACTERISTICS OF THE AIRPLANE AT SEVERAL ANGLES OF ATTACK. CLEAN CONDITION; ψ, -8°.

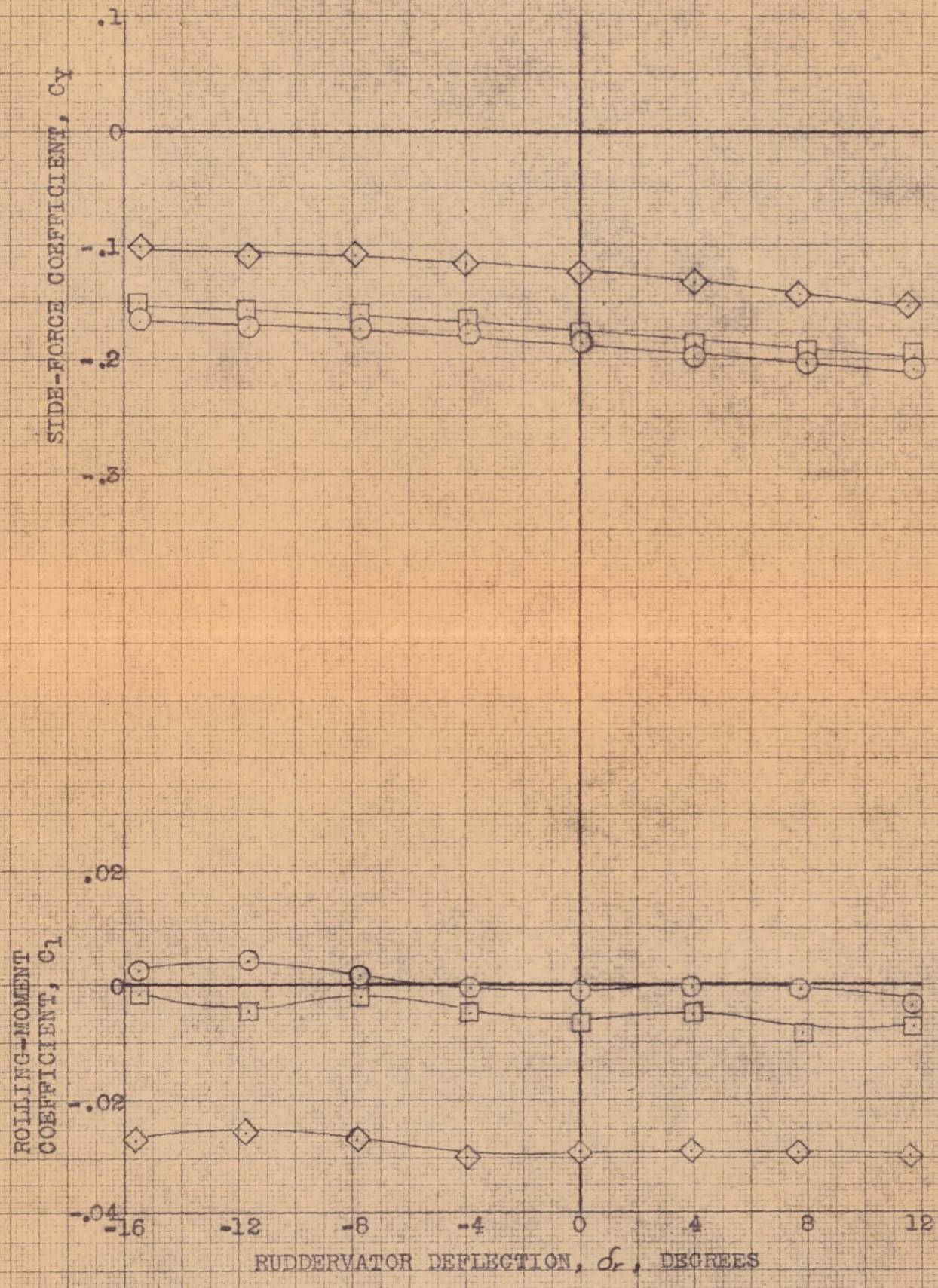

(b) C_Y, C_l vs δ_r.

FIGURE 42.- CONCLUDED.

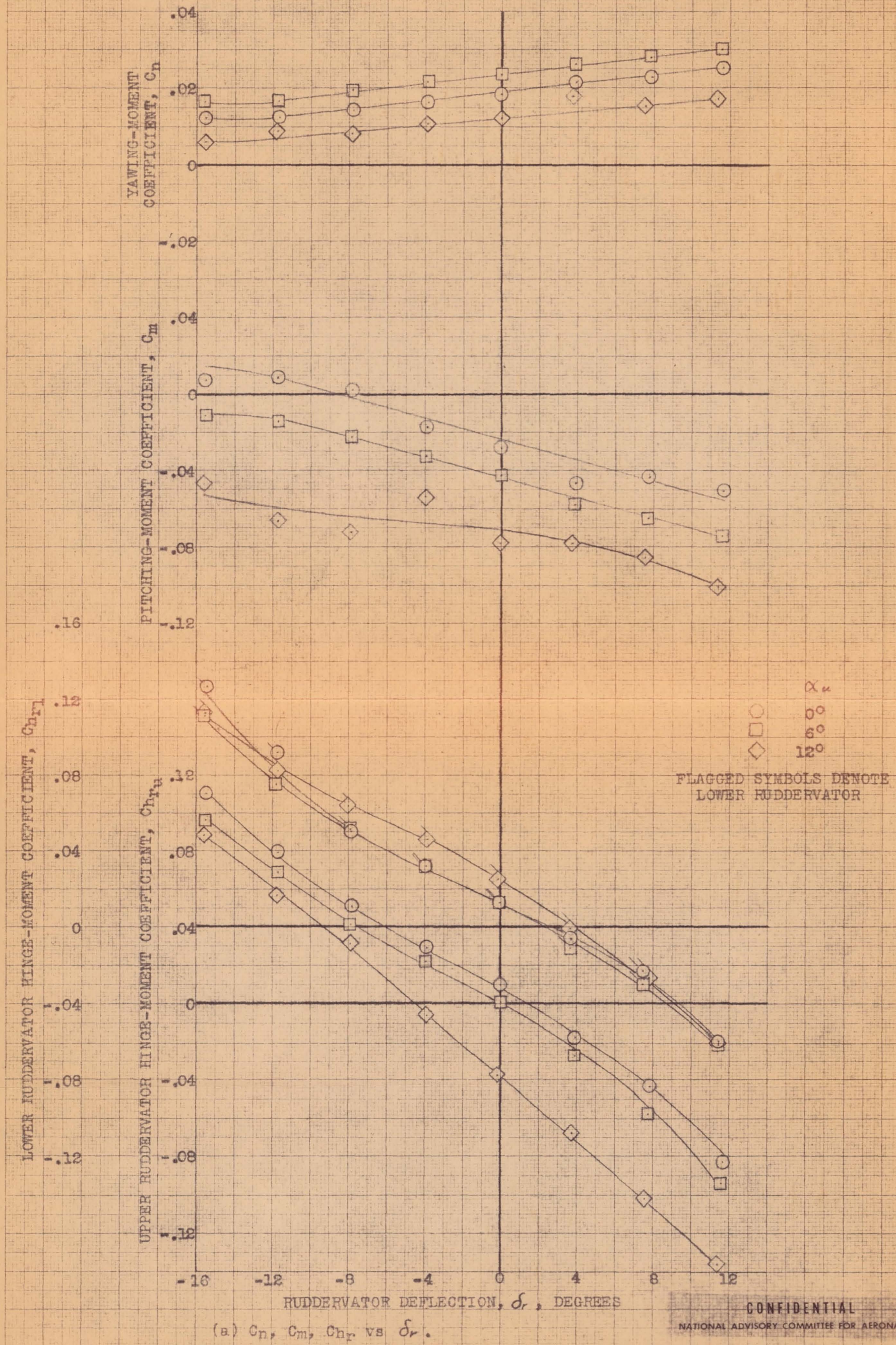

(a) C_n, C_m, C_{h_r} vs δ_r.

FIGURE 43.- VARIATION WITH DEFLECTION OF THE UPPER RIGHT AND LOWER LEFT RUDDERVATOR OF THE AERODYNAMIC CHARACTERISTICS OF THE AIRPLANE AT SEVERAL ANGLES OF ATTACK. CLEAN CONDITION; ψ, -12°.

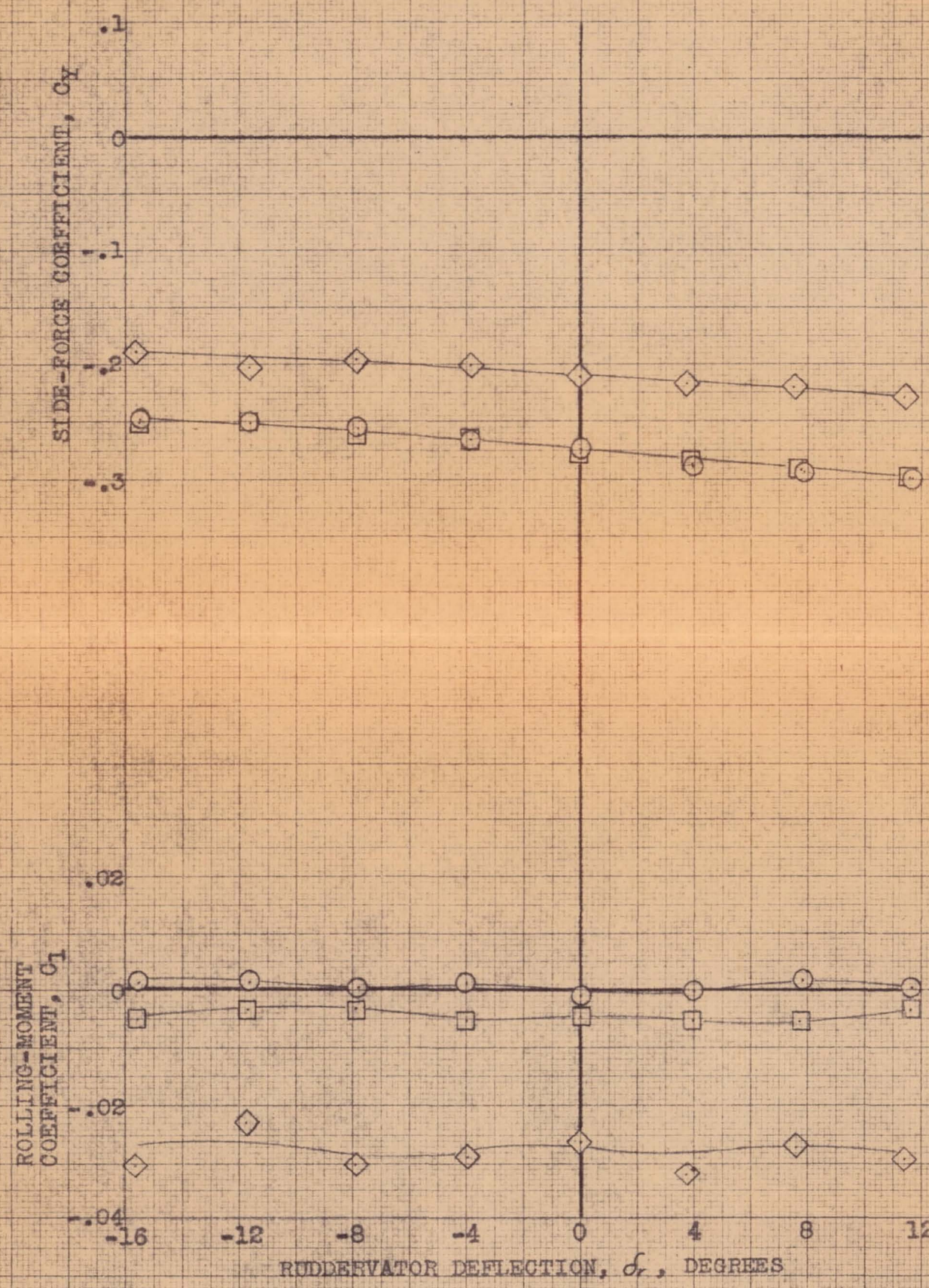

(b) C_Y, C_l vs δ_r.

FIGURE 43.- CONCLUDED.

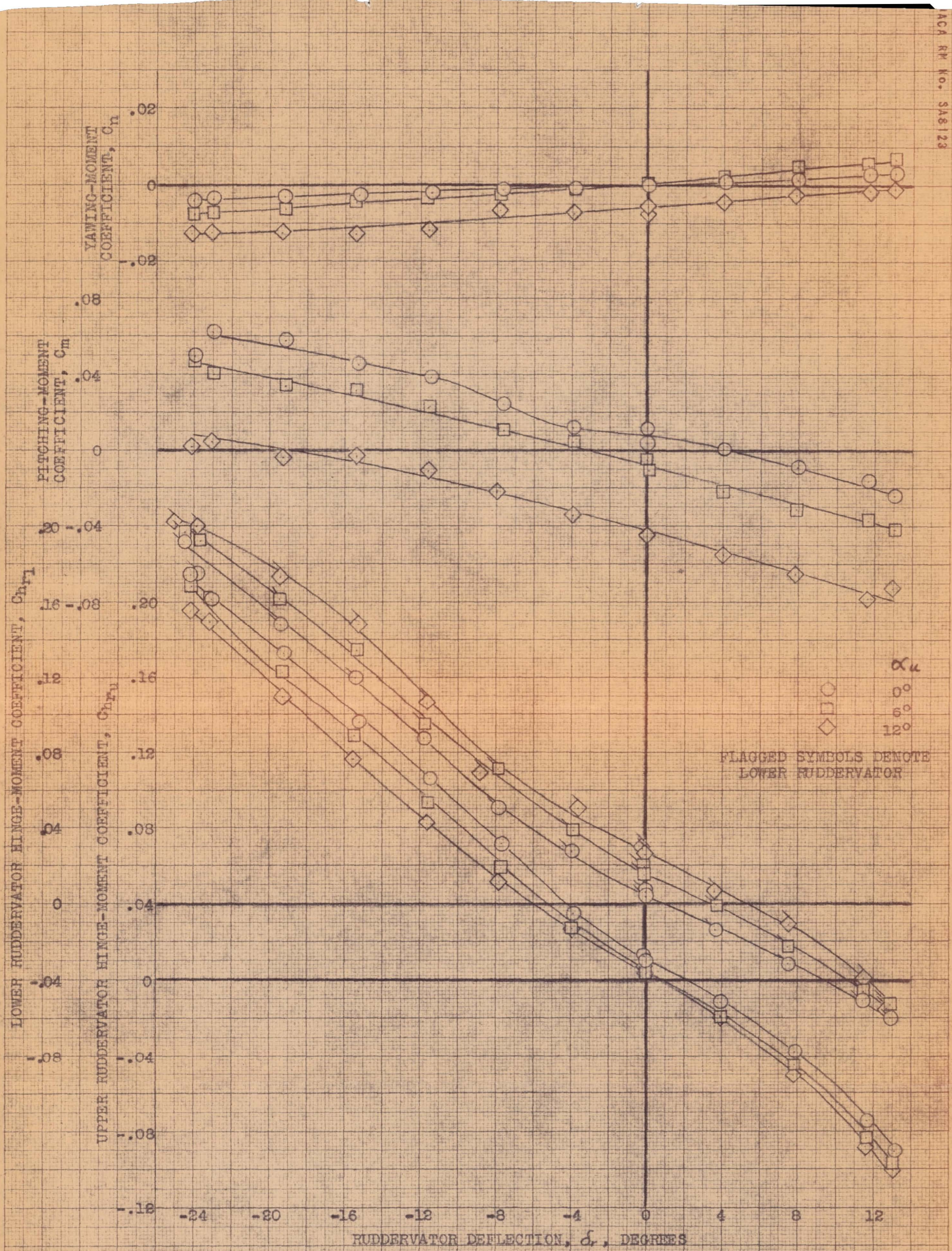

(a) C_n, C_m, C_{h_r} vs δ_r.

FIGURE 44.- VARIATION WITH DEFLECTION OF THE UPPER RIGHT AND LOWER LEFT RUDDERVATOR OF THE AERODYNAMIC CHARACTERISTICS OF THE AIRPLANE AT SEVERAL ANGLES OF ATTACK. SKYHOOK EXTENDED; ψ, 0°.

(b) C_L, C_Y, C_l vs δ_r.

FIGURE 44.- CONCLUDED.

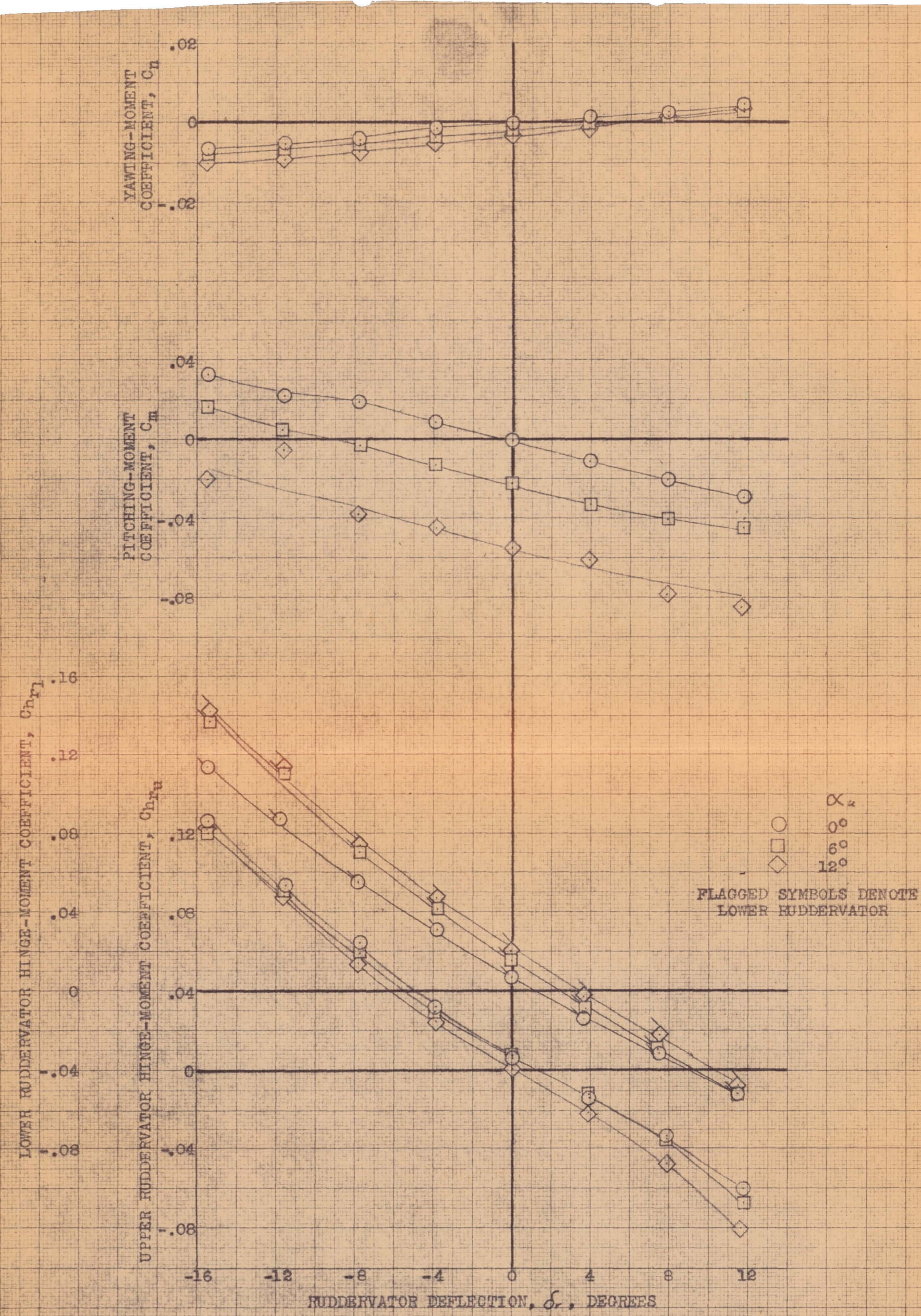

(a) C_n, C_m, C_{h_r} vs δ_r.

FIGURE 45.- VARIATION WITH DEFLECTION OF THE UPPER RIGHT AND LOWER LEFT RUDDERVATOR OF THE AERODYNAMIC CHARACTERISTICS OF THE AIRPLANE AT SEVERAL ANGLES OF ATTACK. SKYHOOK EXTENDED; ψ, 4°.

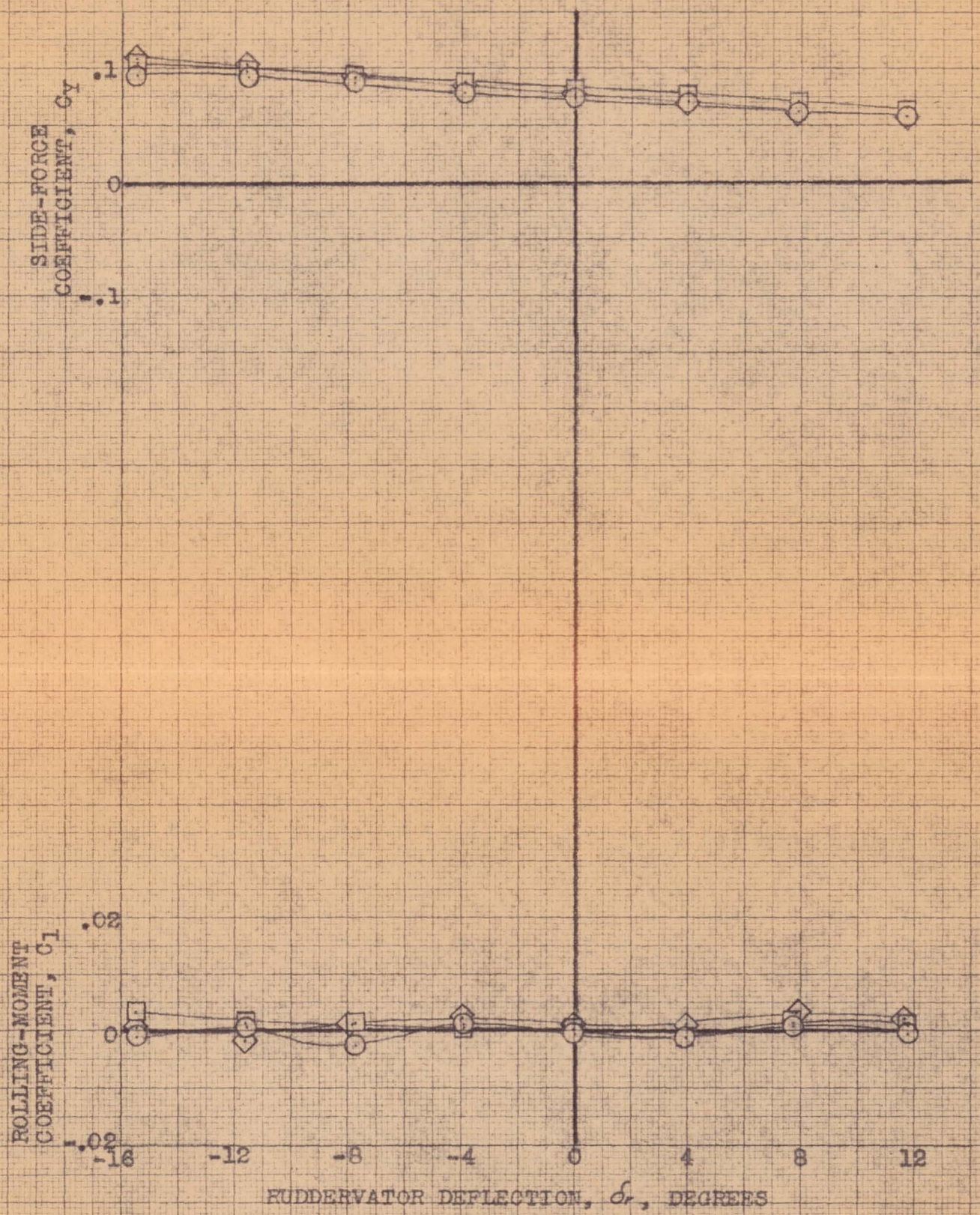

(b) C_Y, C_l vs δ_r.

FIGURE 45.- CONCLUDED.

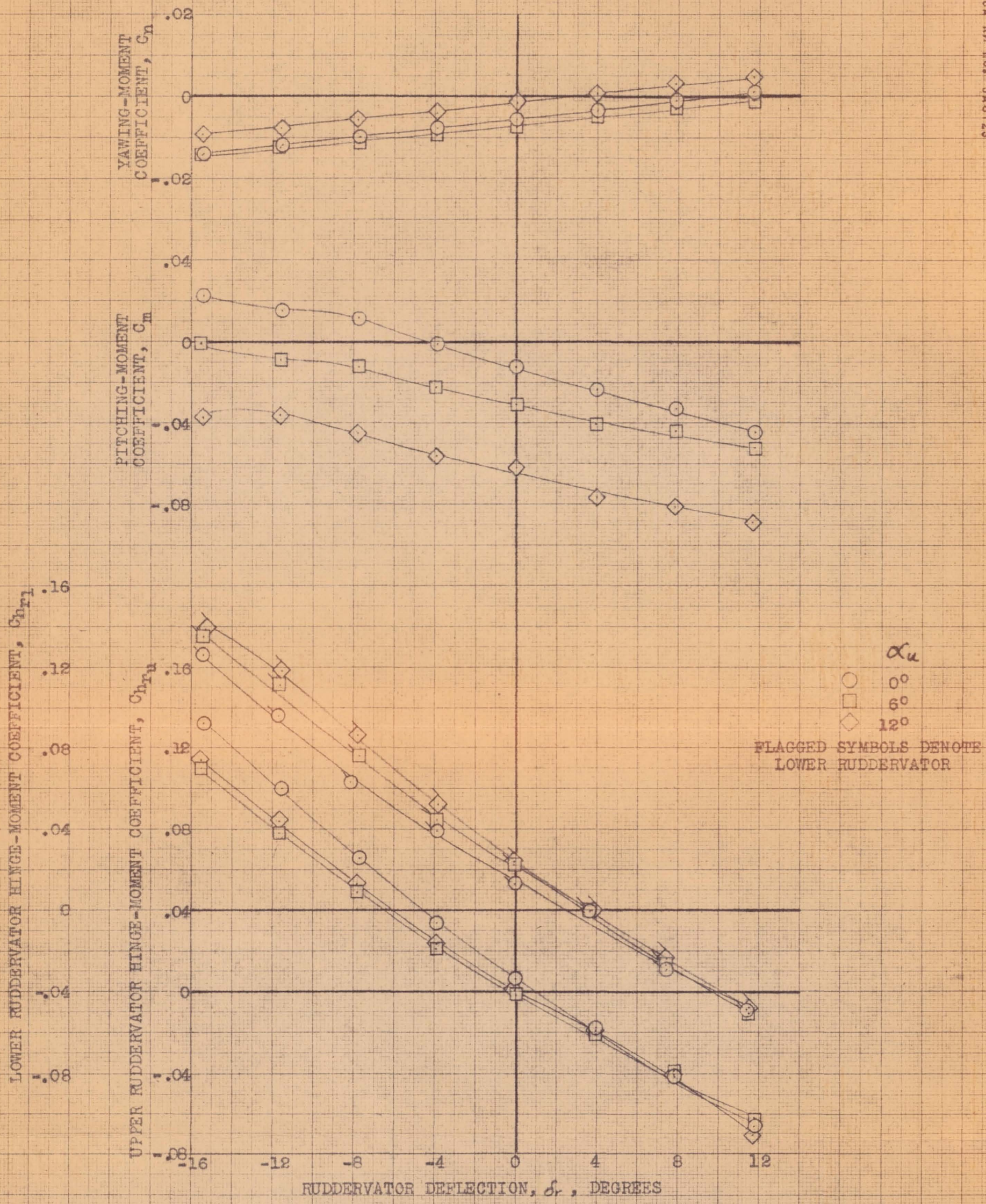

(a) C_n, C_m, C_{h_r} vs δ_r.

FIGURE 46.- VARIATION WITH DEFLECTION OF THE UPPER RIGHT AND LOWER LEFT RUDDERVATOR OF THE AERODYNAMIC CHARACTERISTICS OF THE AIRPLANE AT SEVERAL ANGLES OF ATTACK. SKYHOOK EXTENDED; ψ, 8°.

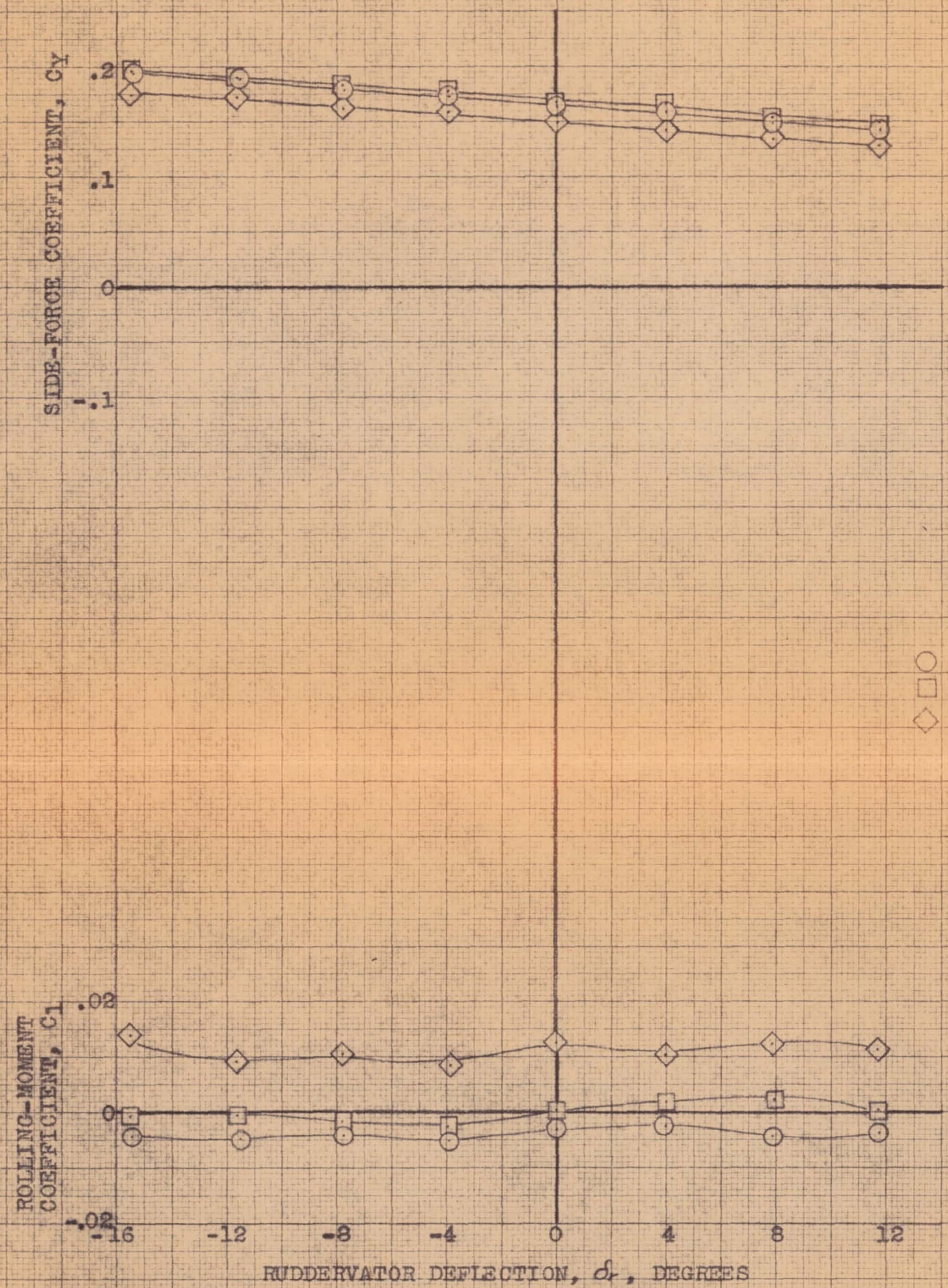

(b) C_Y, C_l vs δ_r.

FIGURE 46.- CONCLUDED.

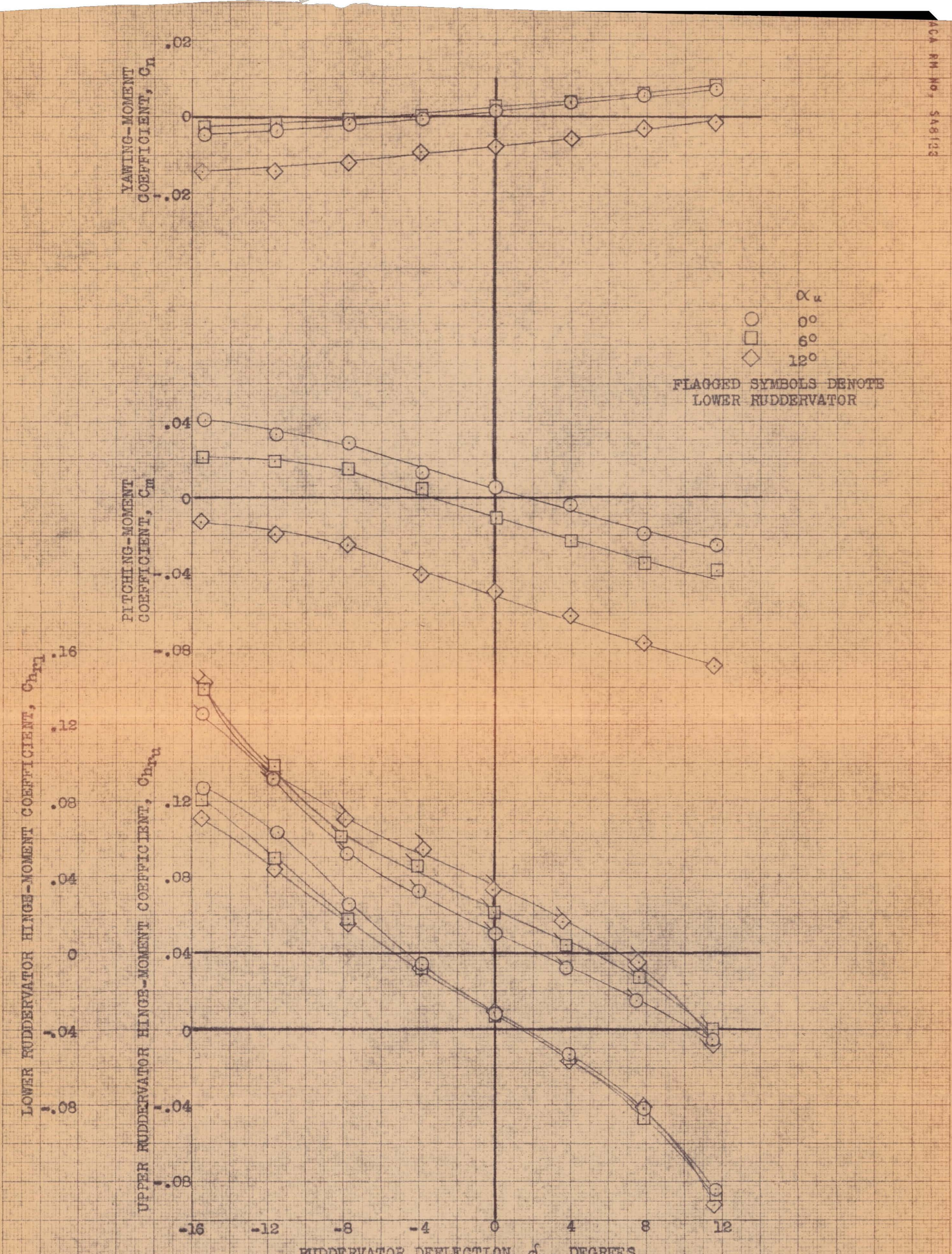

(a) C_n, C_m, C_{h_r} vs δ_r.

FIGURE 47.- VARIATION WITH DEFLECTION OF THE UPPER RIGHT AND LOWER LEFT RUDDERVATOR OF THE AERODYNAMIC CHARACTERISTICS OF THE AIRPLANE AT SEVERAL ANGLES OF ATTACK. SKYHOOK EXTENDED; ψ, -4°.

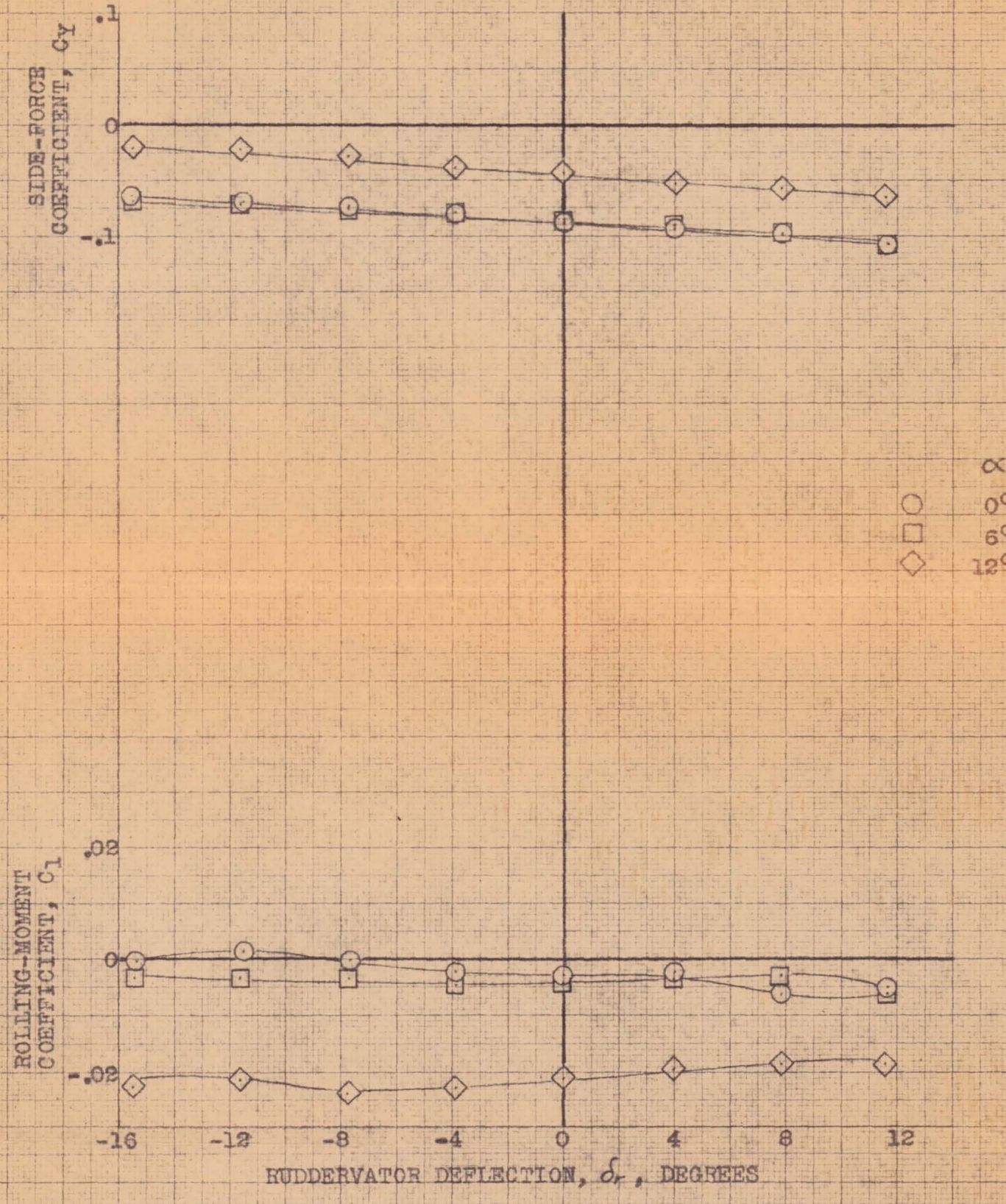

(b) C_Y, C_l vs δ_r.

FIGURE 47.- CONCLUDED.

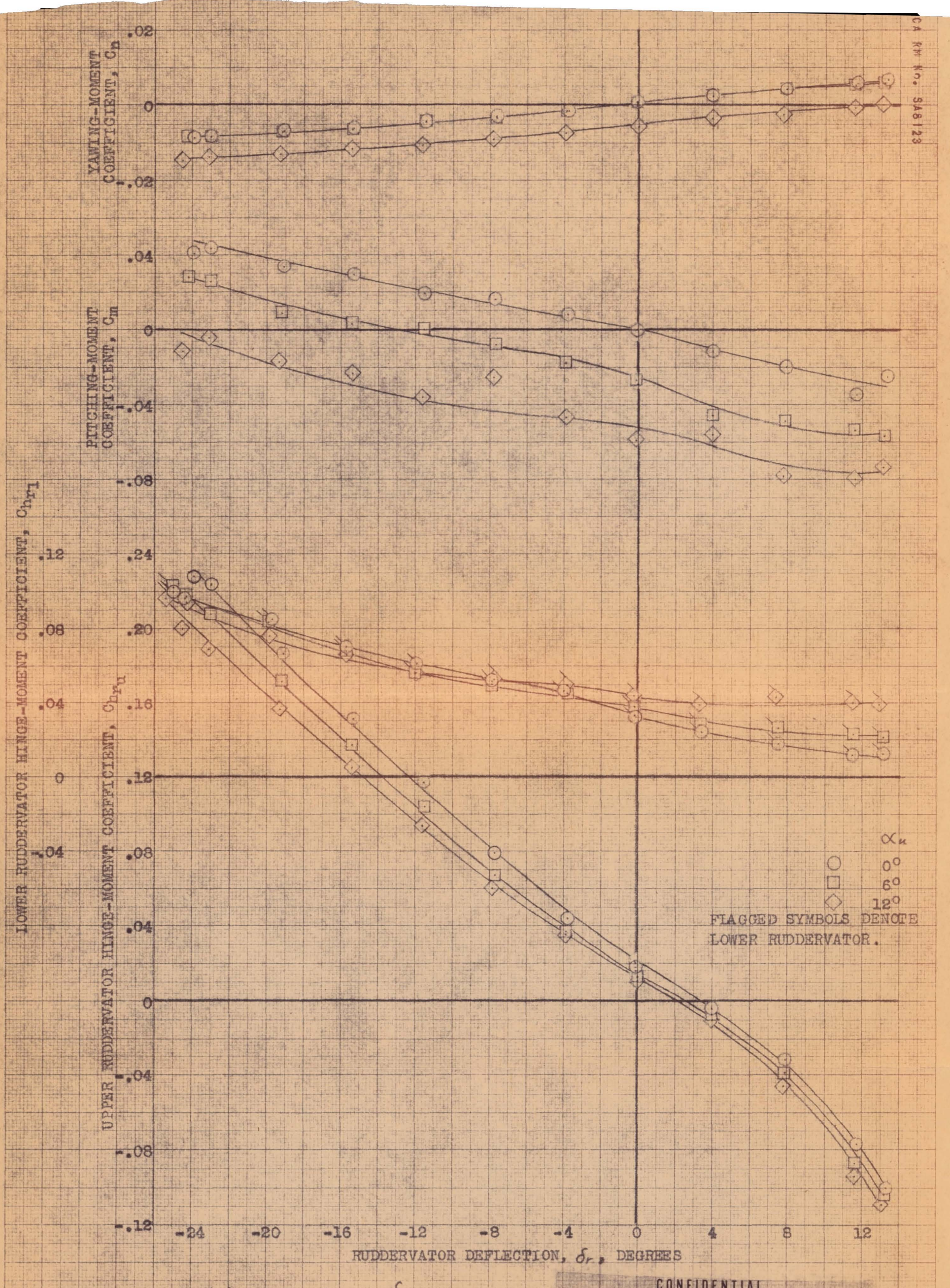

(a) C_n, C_m, Ch_r vs δ_r.

FIGURE 48.- VARIATION WITH DEFLECTION OF THE UPPER RIGHT AND LOWER LEFT RUDDERVATOR OF THE AERODYNAMIC CHARACTERISTICS OF THE AIRPLANE AT SEVERAL ANGLES OF ATTACK. DIVE BRAKE EXTENDED; ψ, 0°.

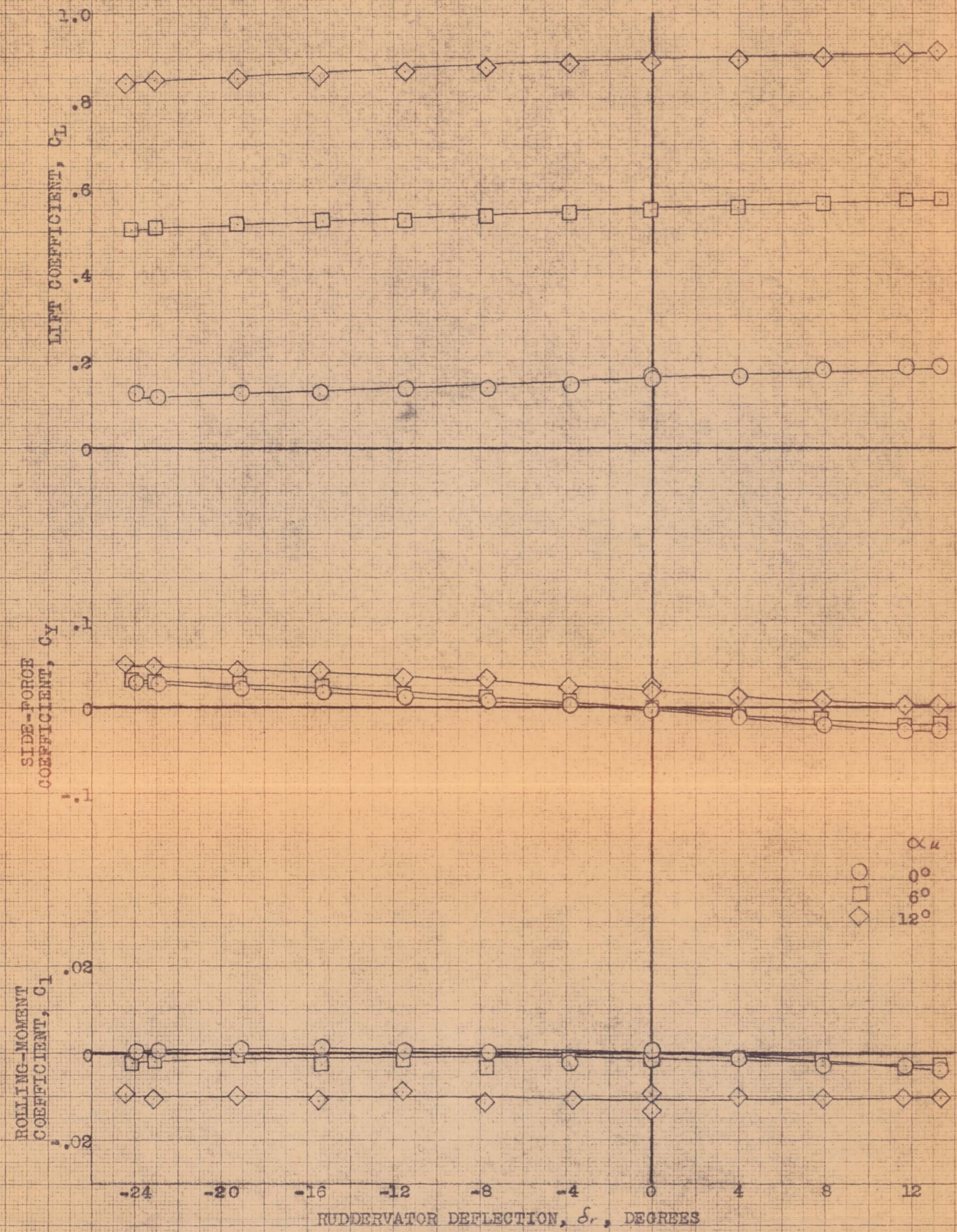

(b) C_L, C_Y, C_l vs δ_r.

FIGURE 48.- CONCLUDED.

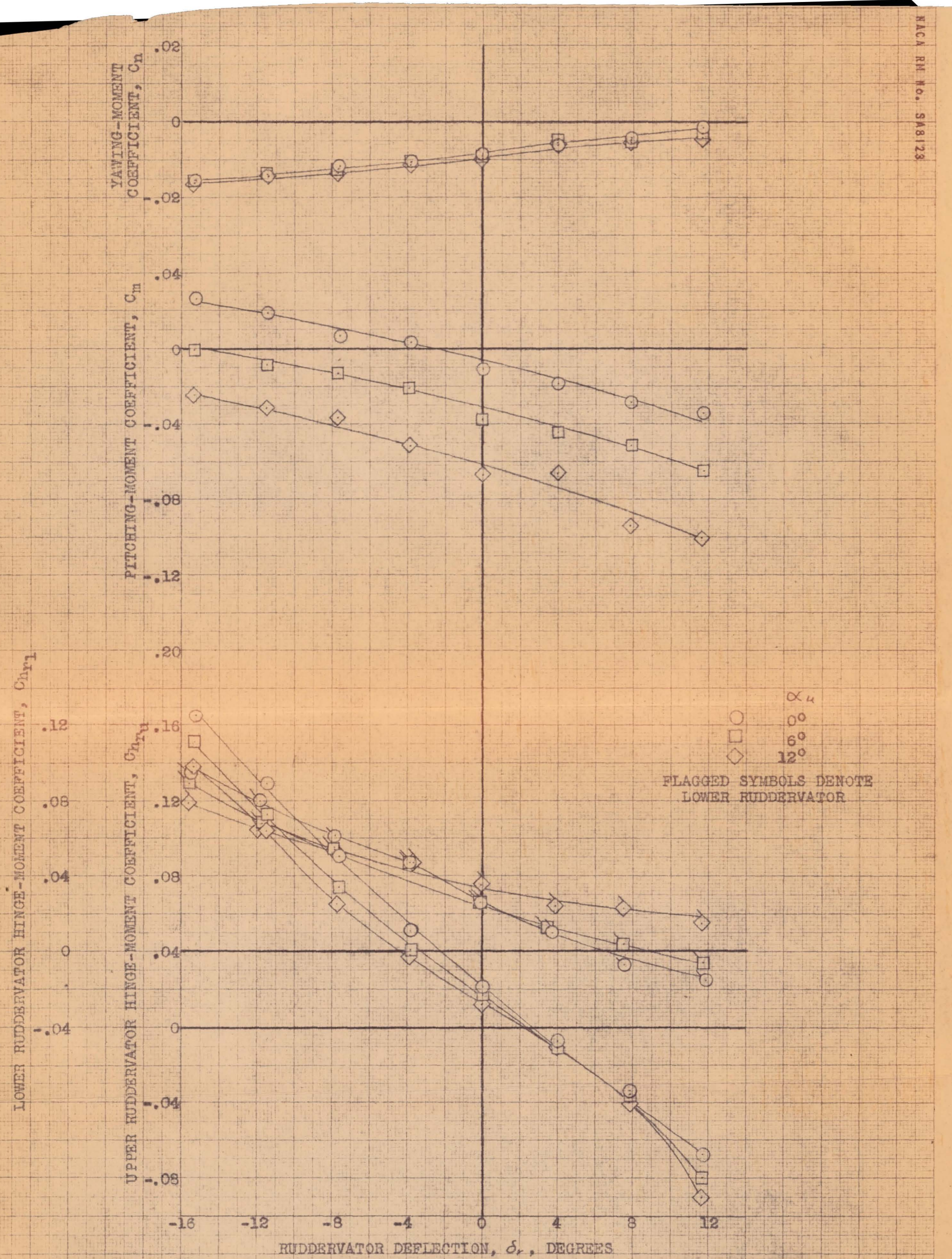

(a) C_n, C_m, C_{h_r} vs δ_r.

FIGURE 49.- VARIATION WITH DEFLECTION OF THE UPPER RIGHT AND LOWER LEFT RUDDERVATOR OF THE AERODYNAMIC CHARACTERISTICS OF THE AIRPLANE AT SEVERAL ANGLES OF ATTACK. DIVE BRAKE EXTENDED; ψ, 4°.

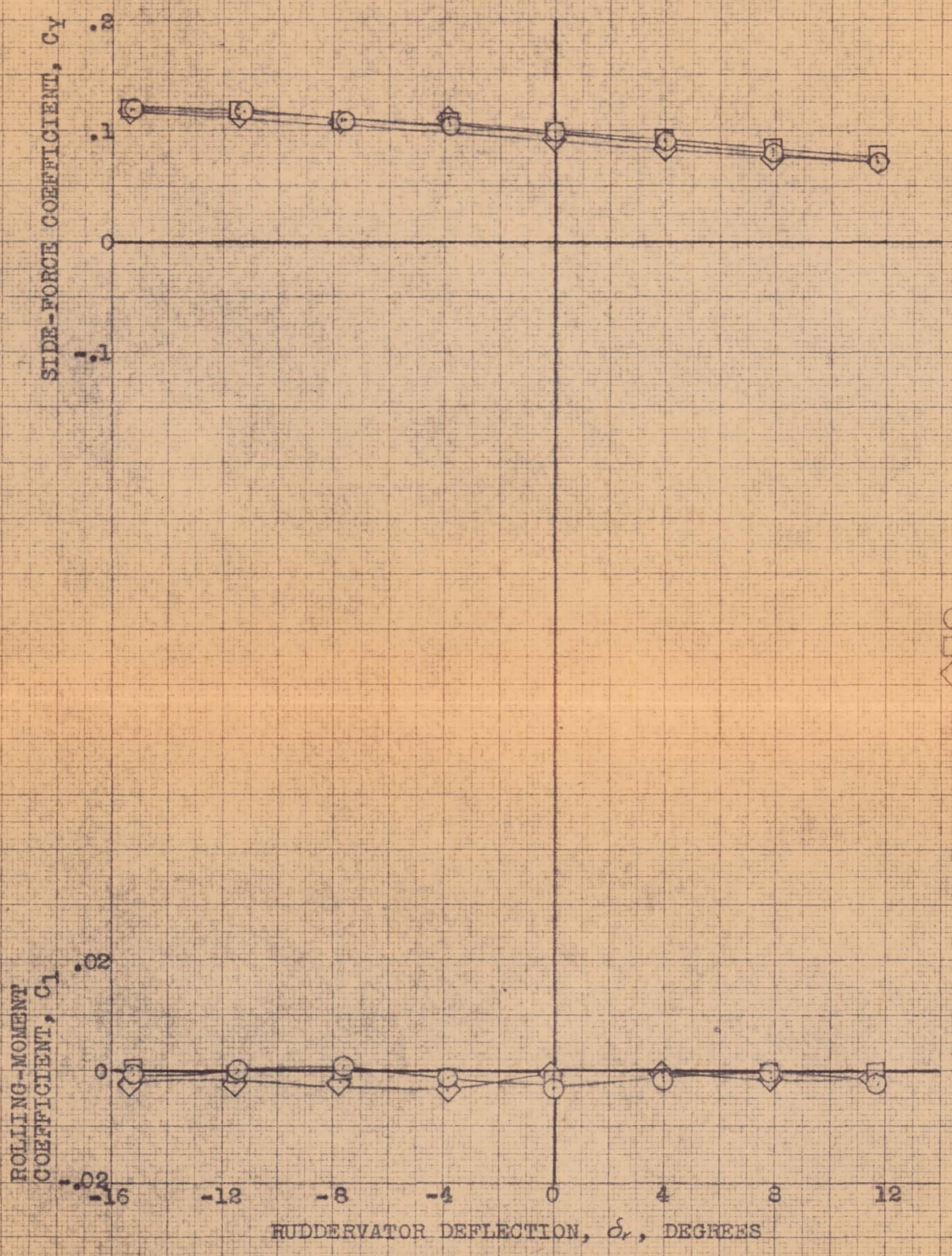

(b) C_Y, C_l vs δ_r.

FIGURE 49.- CONCLUDED.

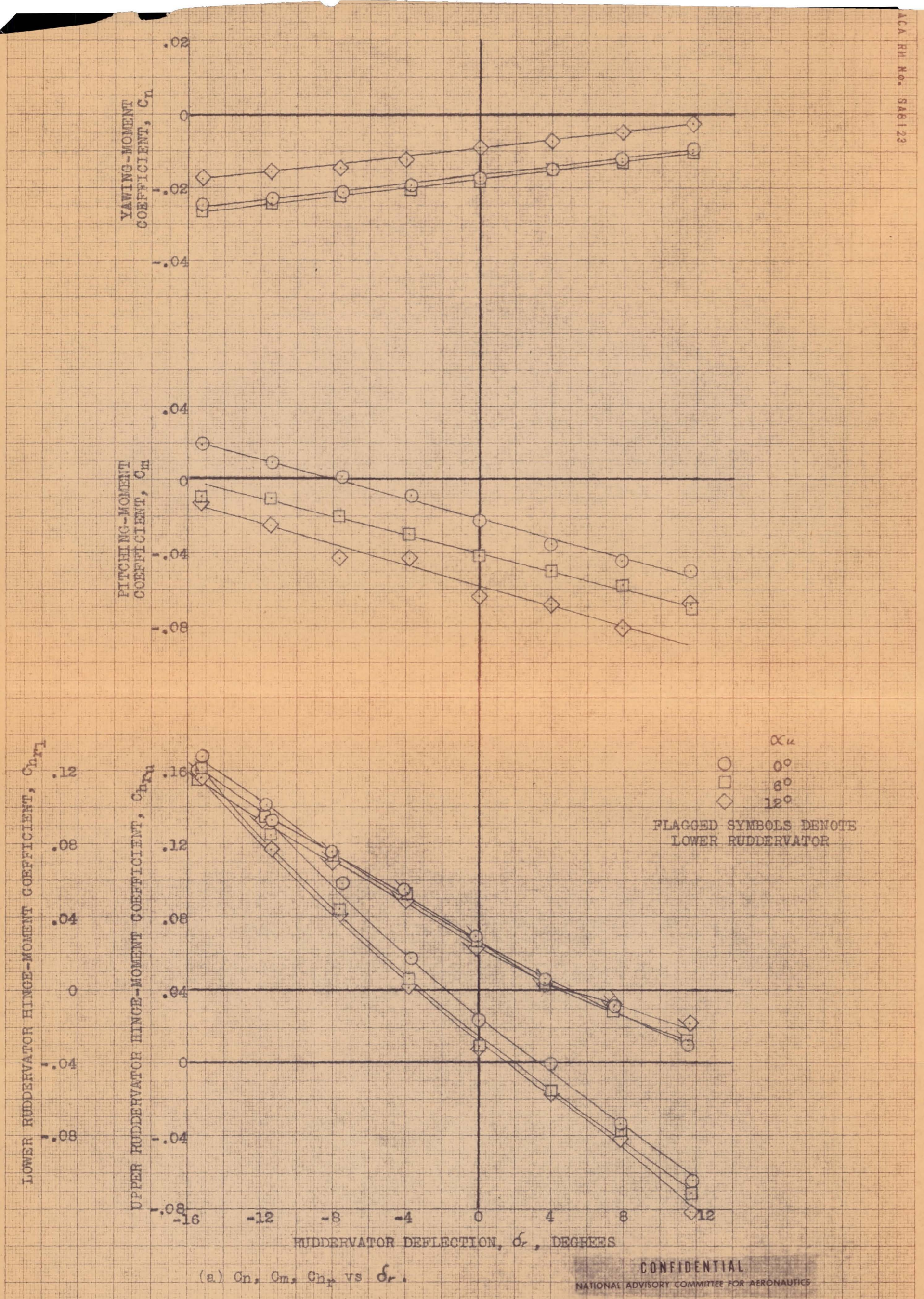

(a) C_n, C_m, C_{h_r} vs δ_r.

FIGURE 50.- VARIATION WITH DEFLECTION OF THE UPPER RIGHT AND LOWER LEFT RUDDERVATOR OF THE AERODYNAMIC CHARACTERISTICS OF THE AIRPLANE AT SEVERAL ANGLES OF ATTACK. DIVE BRAKE EXTENDED; ψ, 8°.

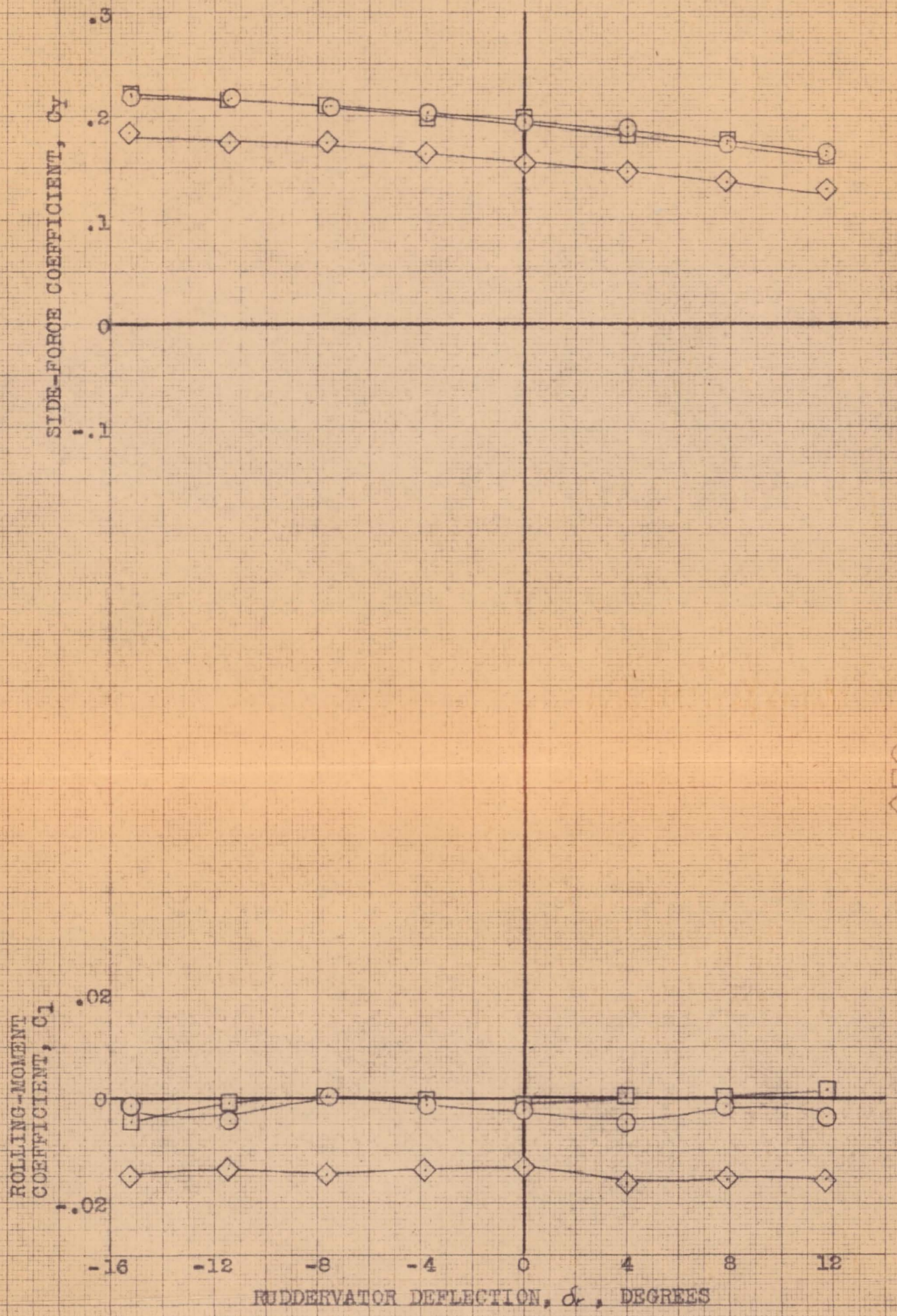

(b) C_Y, C_l vs δ_r.

FIGURE 50.- CONCLUDED.

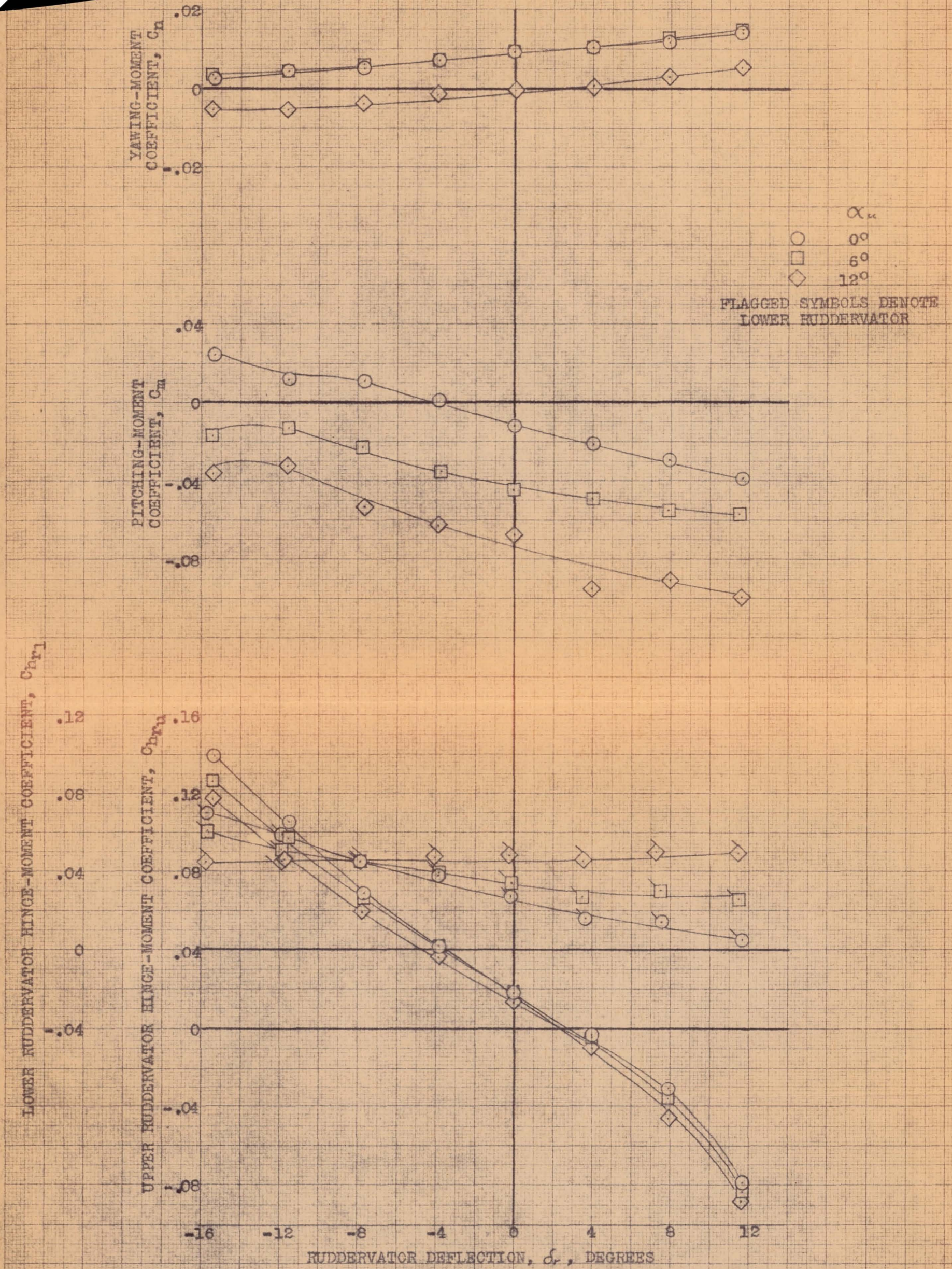

(a) C_n, C_m, C_{h_r} vs δ_r.

FIGURE 51.- VARIATION WITH DEFLECTION OF THE UPPER RIGHT AND LOWER LEFT RUDDERVATOR OF THE AERODYNAMIC CHARACTERISTICS OF THE AIRPLANE AT SEVERAL ANGLES OF ATTACK. DIVE BRAKE EXTENDED; ψ, -4°.

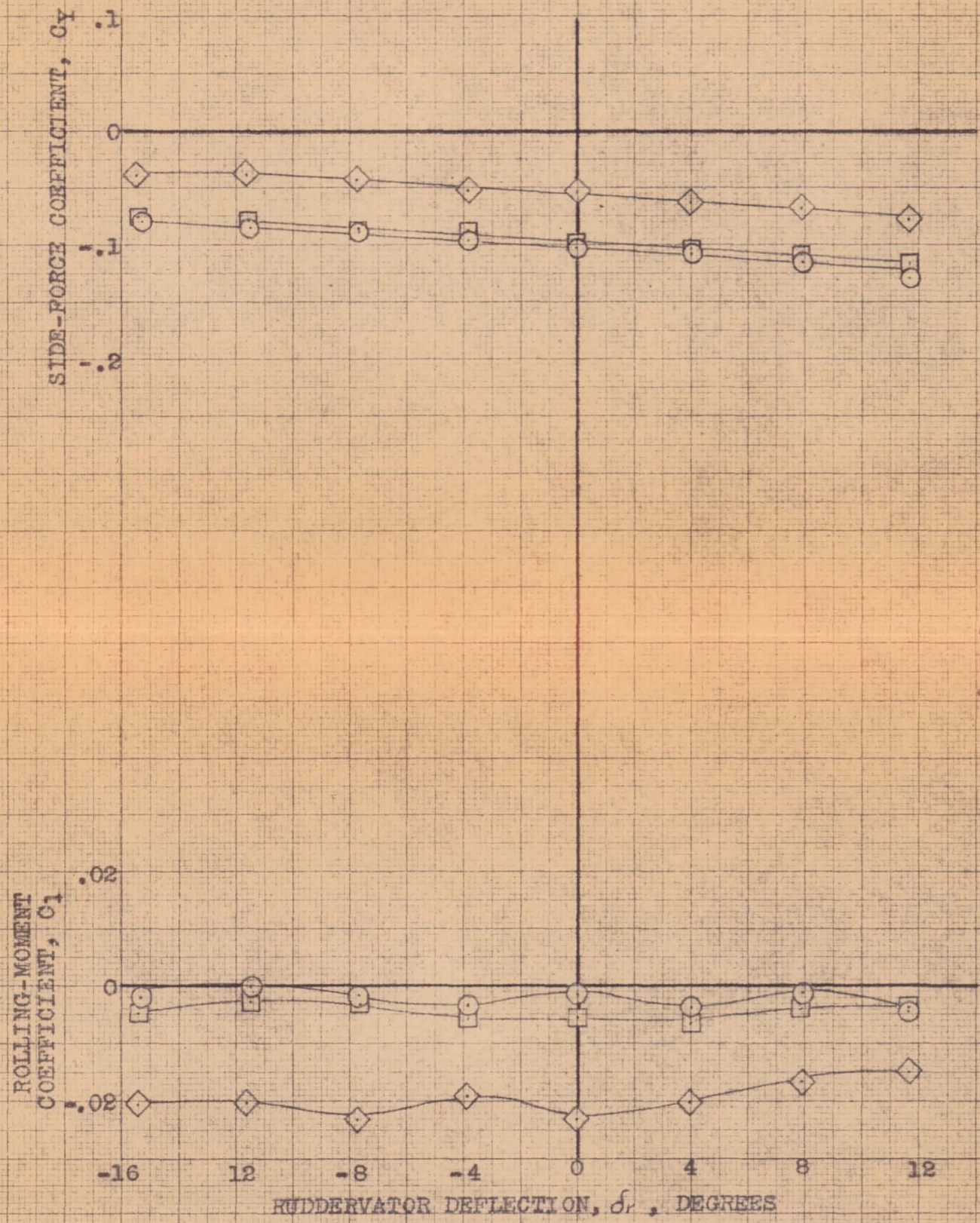

(b) C_Y, C_l vs δ_r.

FIGURE 51.- CONCLUDED.

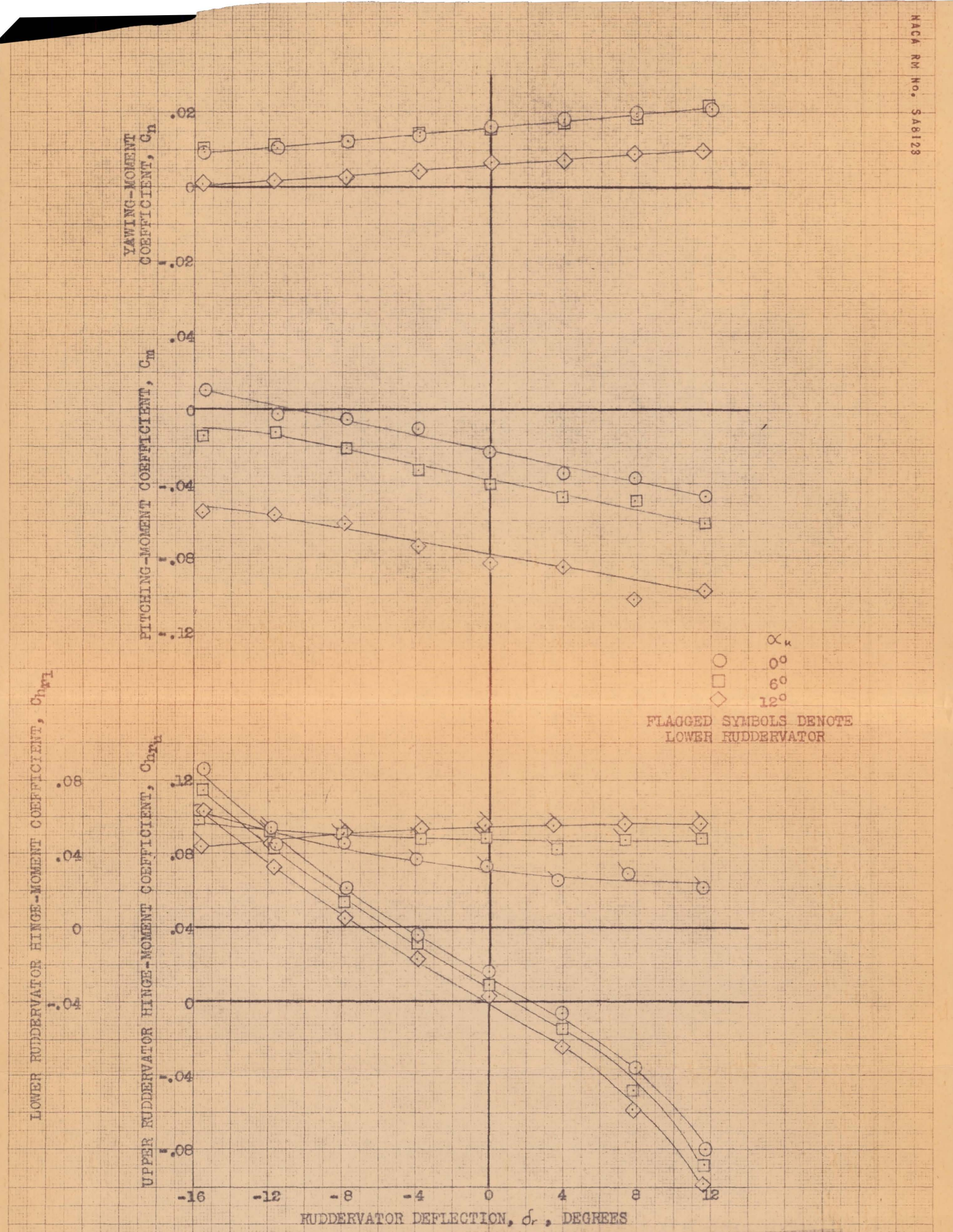

(a) C_n, C_m, C_{h_r} vs δ_r.

FIGURE 52.- VARIATION WITH DEFLECTION OF THE UPPER RIGHT AND LOWER LEFT RUDDERVATOR OF THE AERODYNAMIC CHARACTERISTICS OF THE AIRPLANE AT SEVERAL ANGLES OF ATTACK. DIVE BRAKE EXTENDED; ψ, -8°.

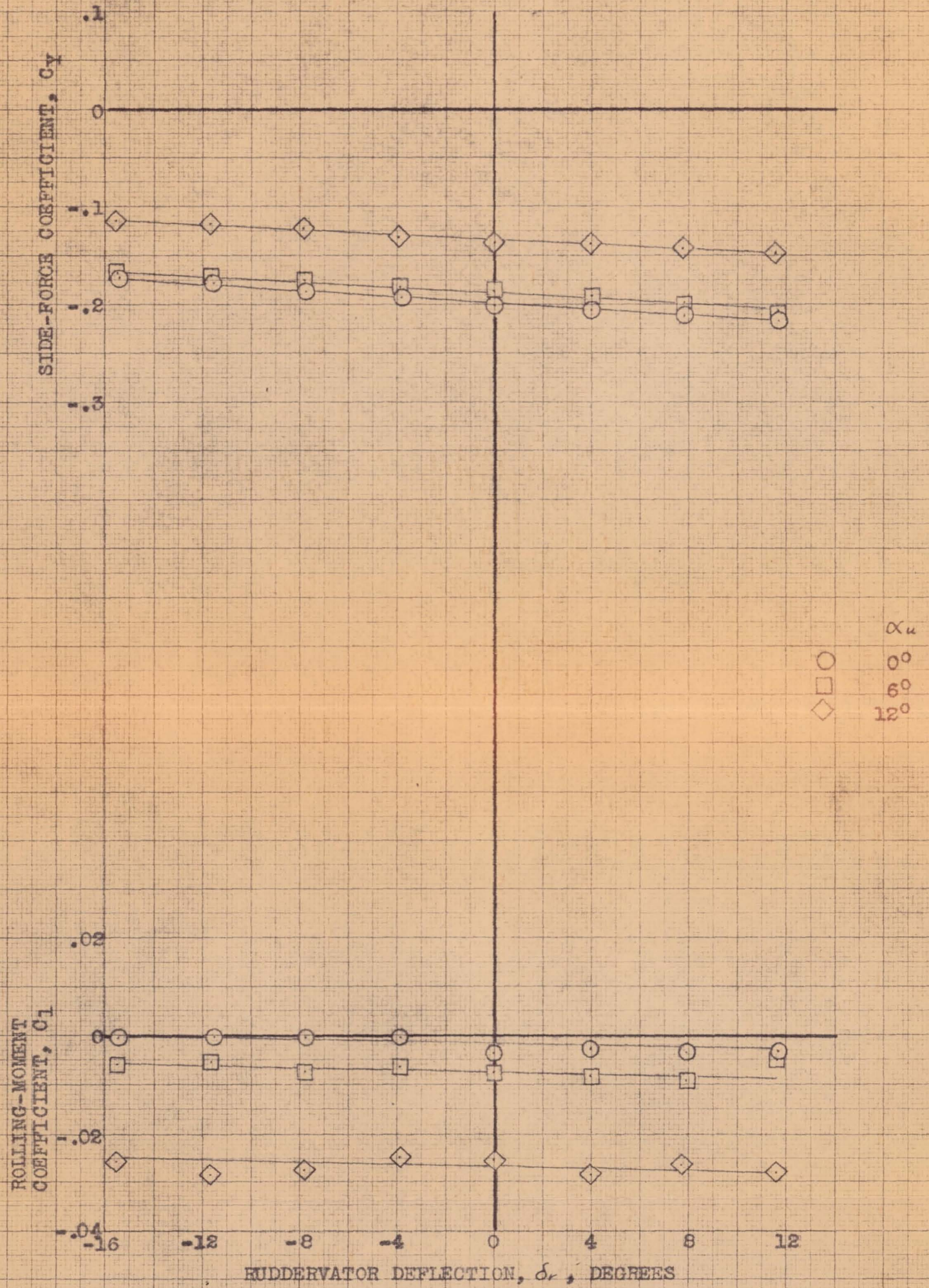

(b) C_Y, C_l vs δ_r.

FIGURE 52.- CONCLUDED.

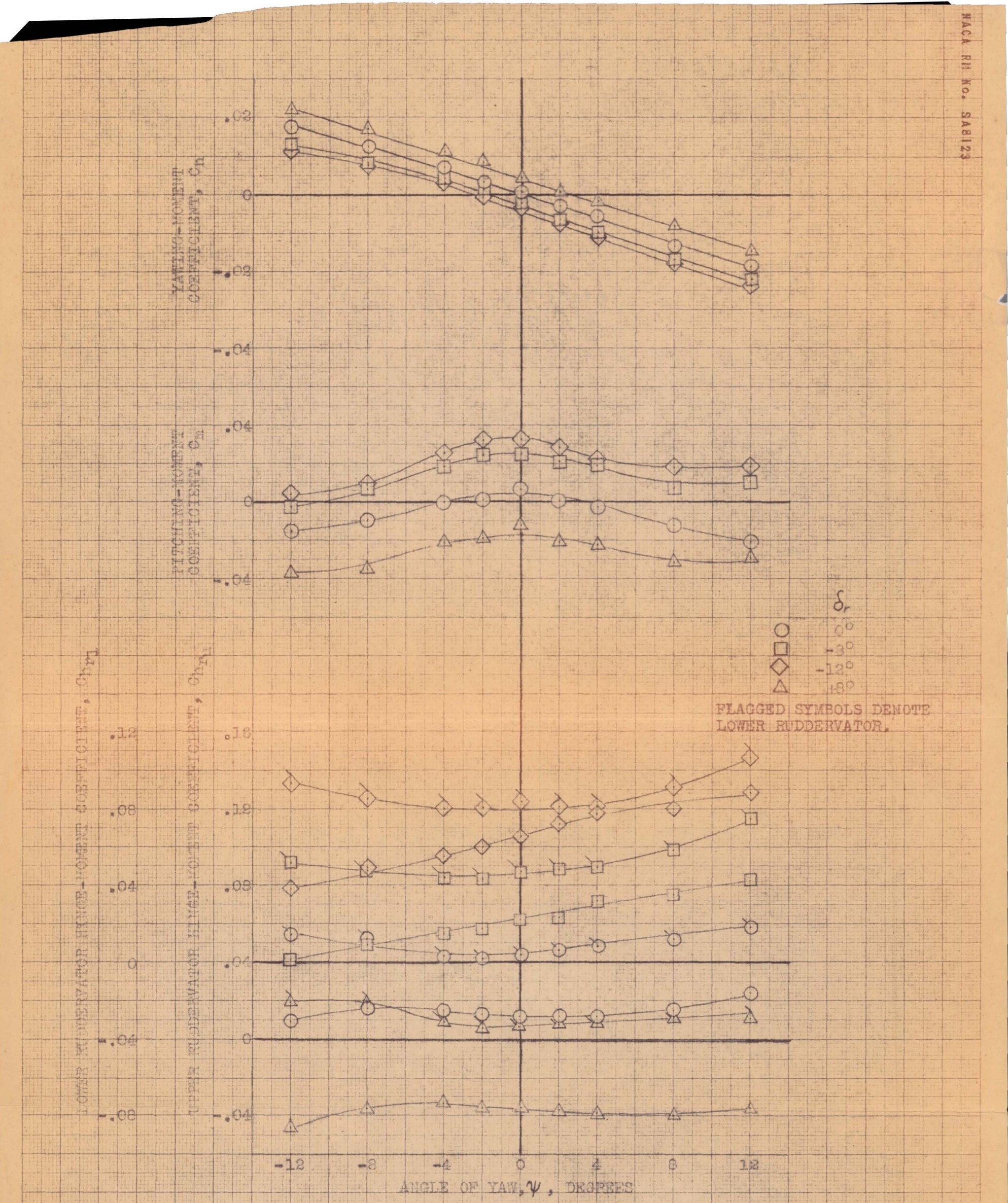

(a) C_n, C_m, C_{h_r} vs ψ.

FIGURE 53.- EFFECT OF FIXED DEFLECTIONS OF THE UPPER RIGHT AND LOWER LEFT RUDDERVATOR ON THE AERODYNAMIC CHARACTERISTICS OF THE AIRPLANE IN YAW. CLEAN CONDITION; α_u, 0°.

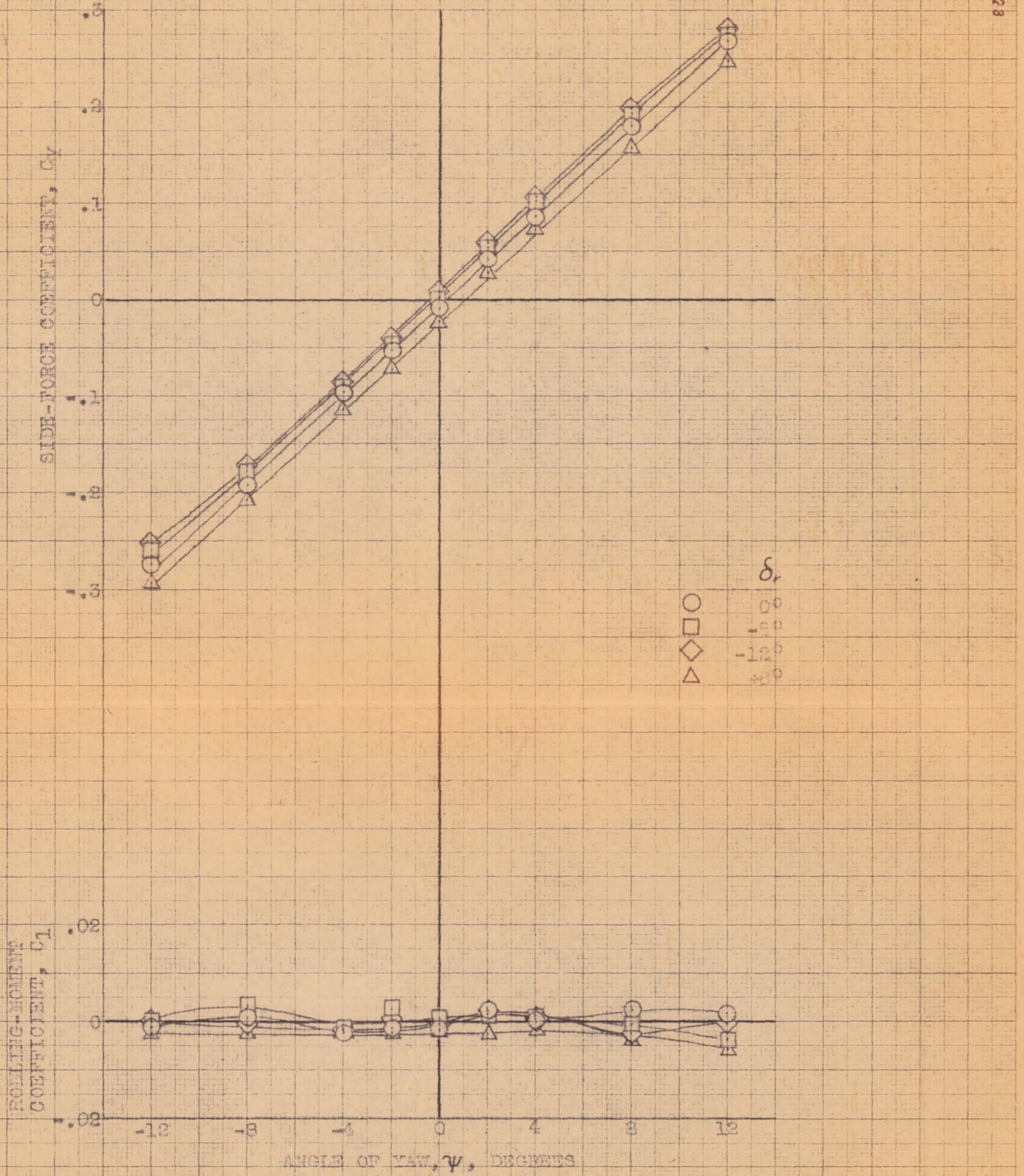

(b) C_Y, C_l vs ψ.

FIGURE 53.- CONCLUDED.

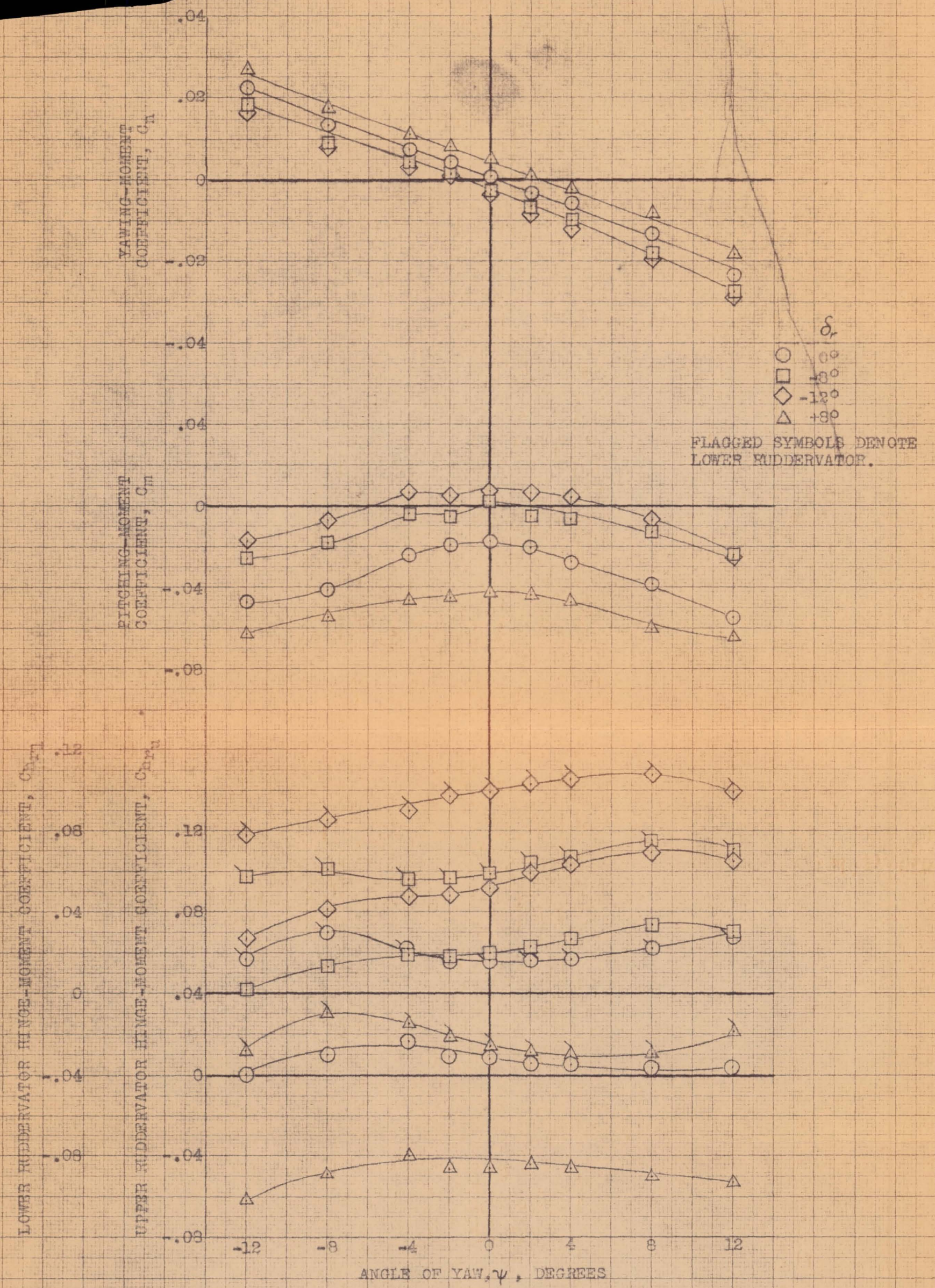

(a) C_n, C_m, C_{h_r} vs ψ.

FIGURE 54.- EFFECT OF FIXED DEFLECTIONS OF THE UPPER RIGHT AND LOWER LEFT RUDDERVATOR ON THE AERODYNAMIC CHARACTERISTICS OF THE AIRPLANE IN YAW. CLEAN CONDITION; α_u, 6°.

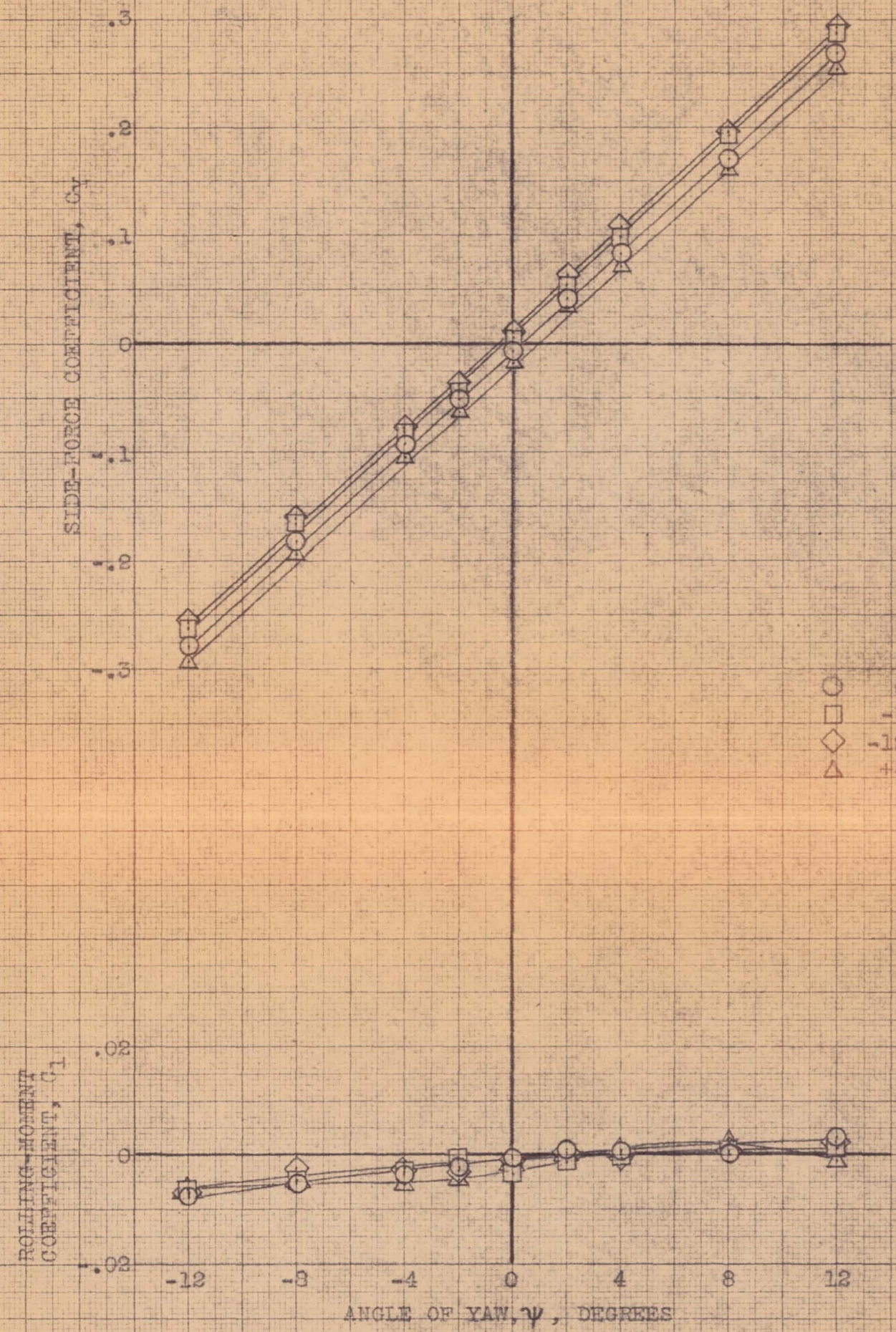

(b) C_Y, C_l vs ψ.

FIGURE 54.- CONCLUDED.

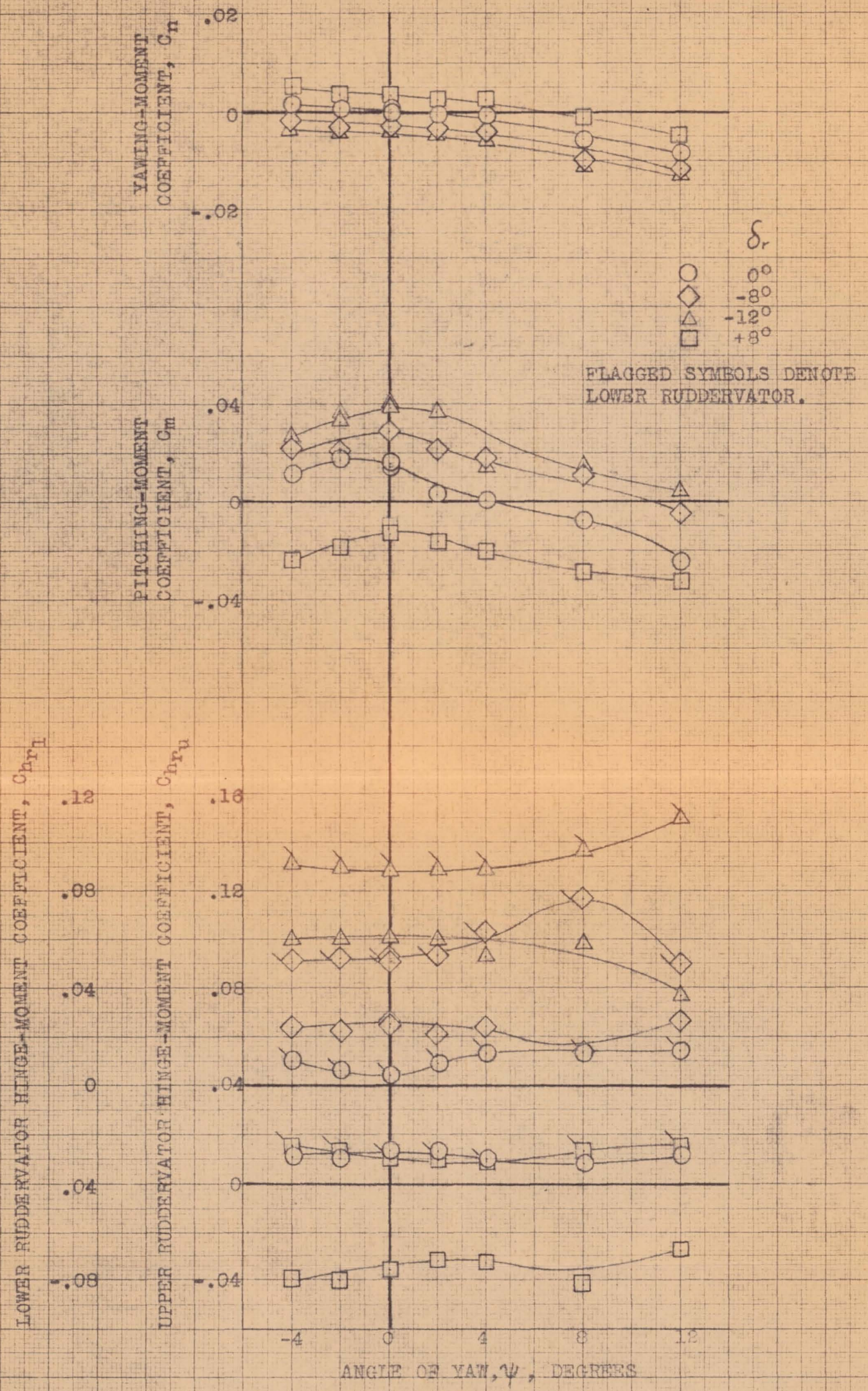

(a) C_n, C_m, C_{h_r} vs ψ.

FIGURE 55.-EFFECT OF FIXED DEFLECTIONS OF THE UPPER RIGHT AND LOWER LEFT RUDDERVATOR ON THE AERODYNAMIC CHARACTERISTICS OF THE AIRPLANE IN YAW. SKYHOOK EXTENDED; α_u, 0°.

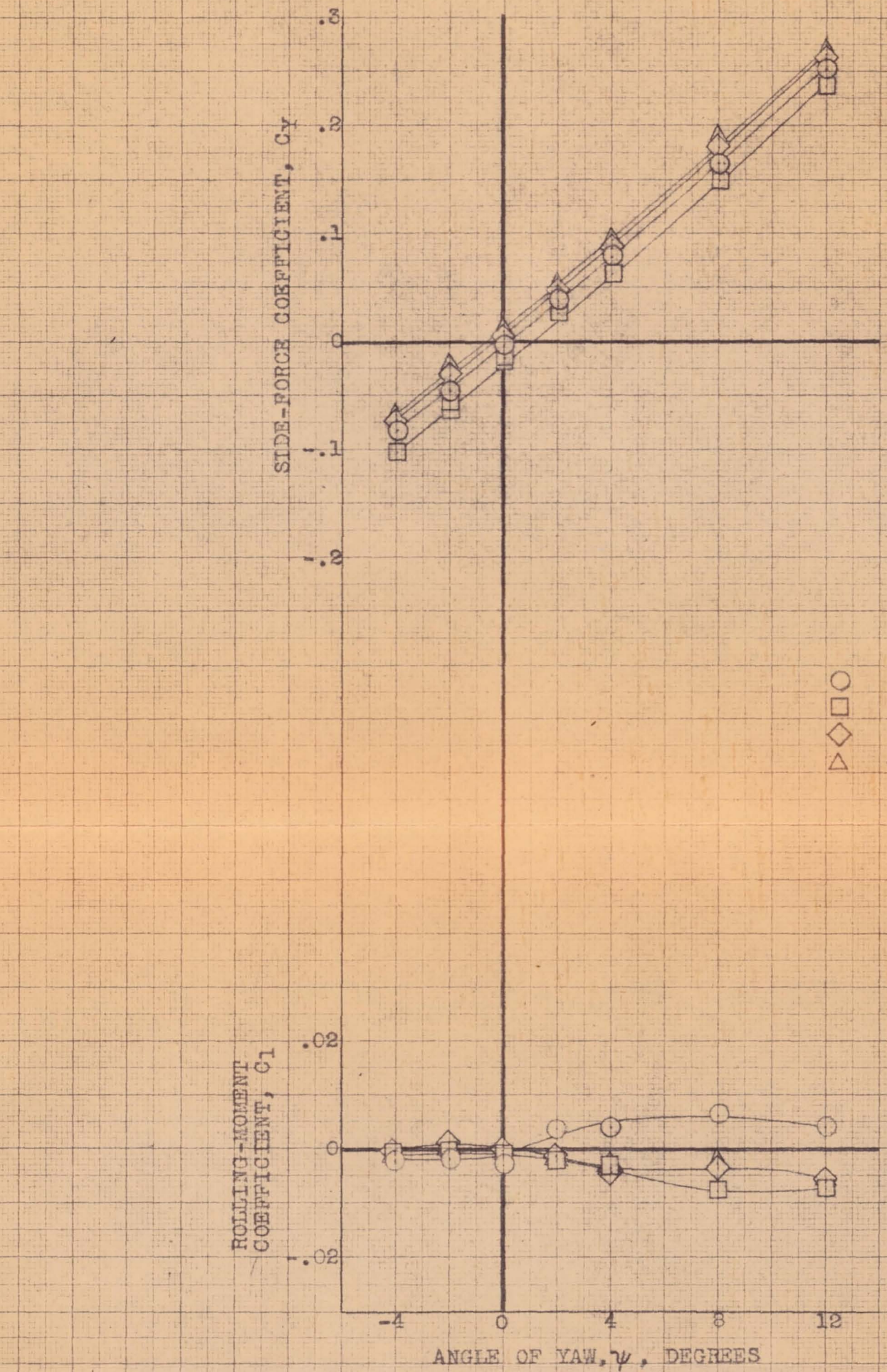

(b) C_Y, C_l vs ψ.

FIGURE 55.- CONCLUDED.

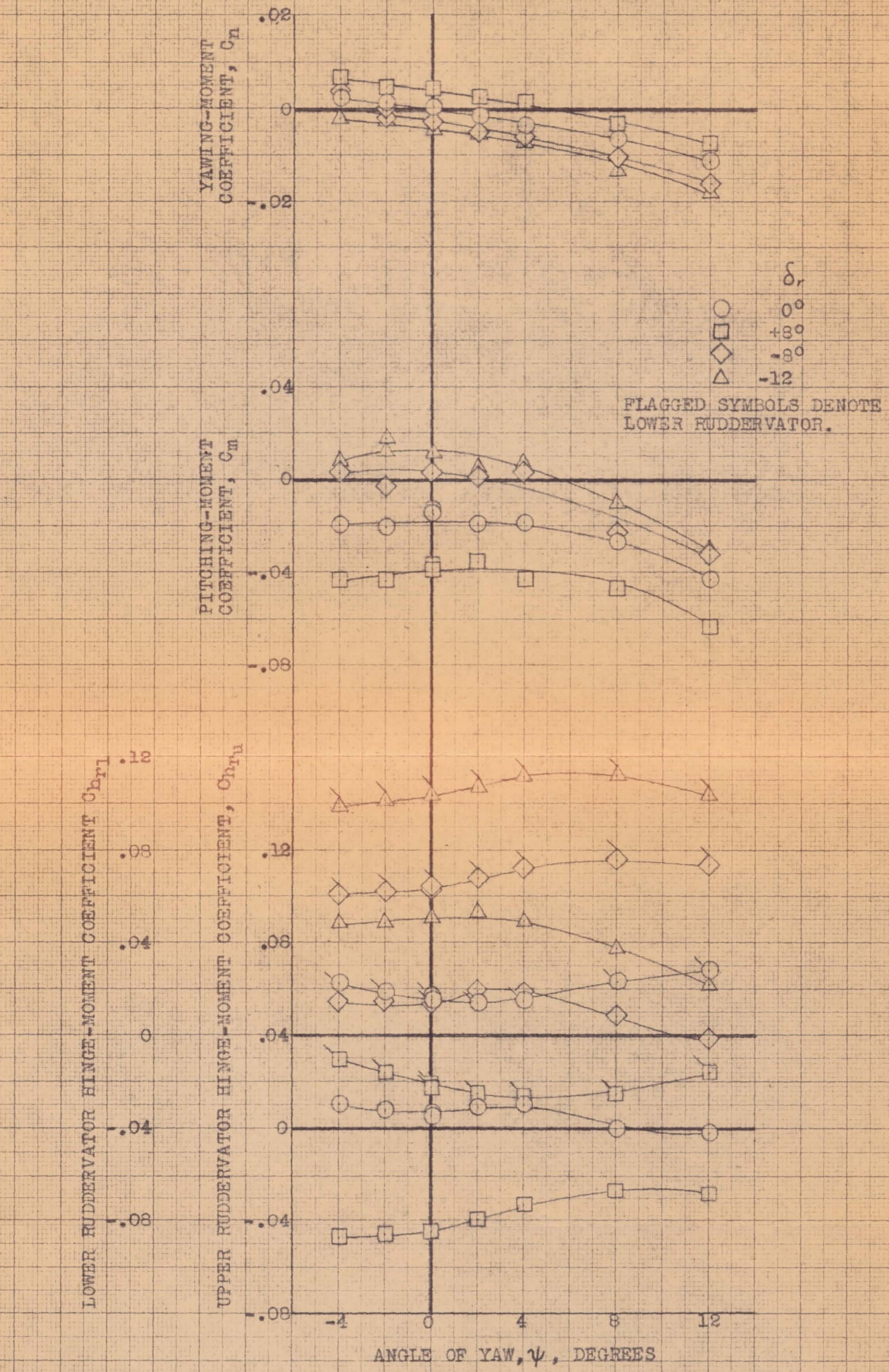

(a) C_n, C_m, Ch_r vs ψ.

FIGURE 56.- EFFECT OF FIXED DEFLECTIONS OF THE UPPER RIGHT AND LOWER LEFT RUDDERVATOR ON THE AERODYNAMIC CHARACTERISTICS OF THE AIRPLANE IN YAW. SKYHOOK EXTENDED; α_u, 6°.

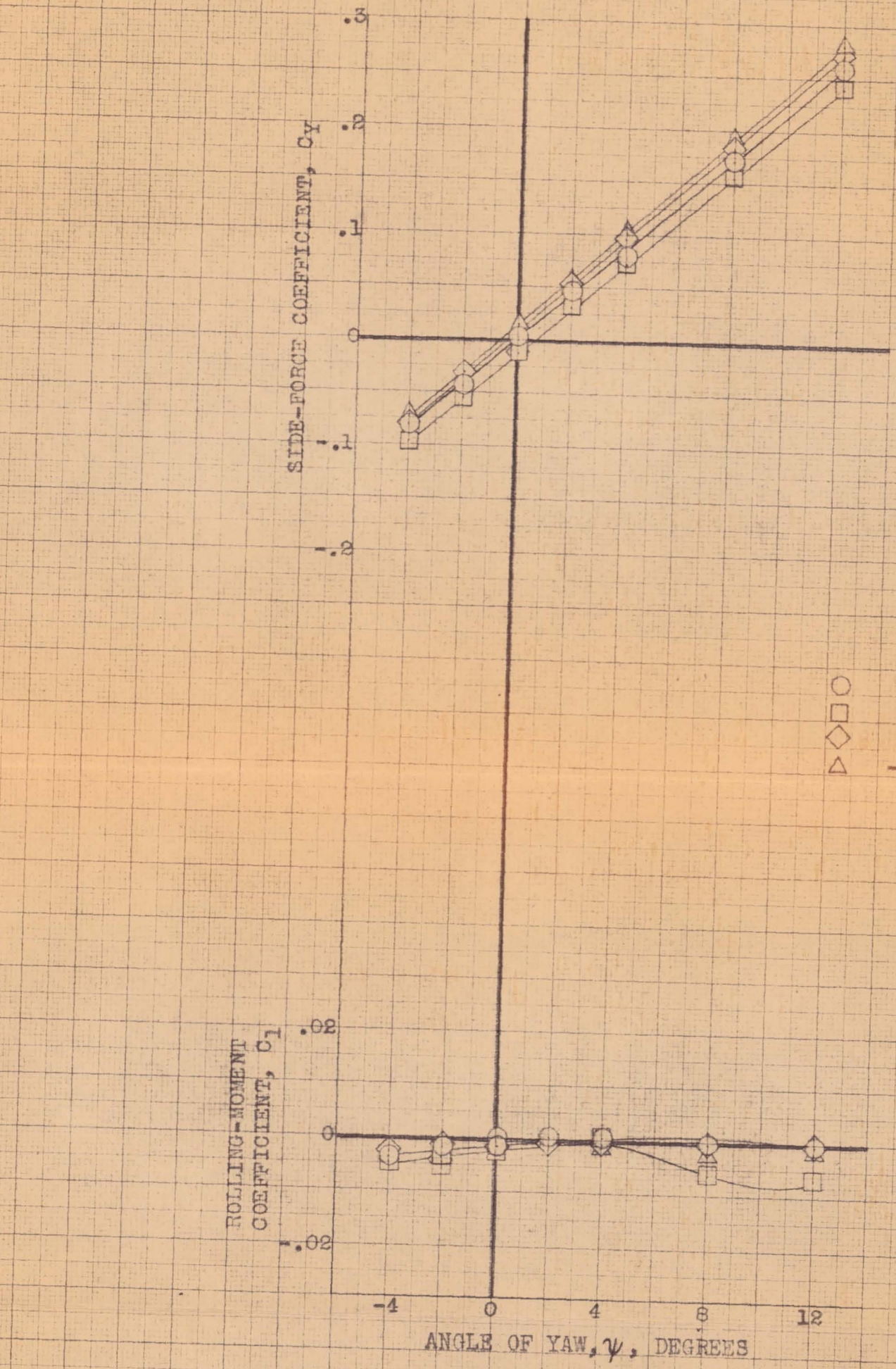

(b) C_Y, C_l vs ψ.

FIGURE 56.- CONCLUDED.

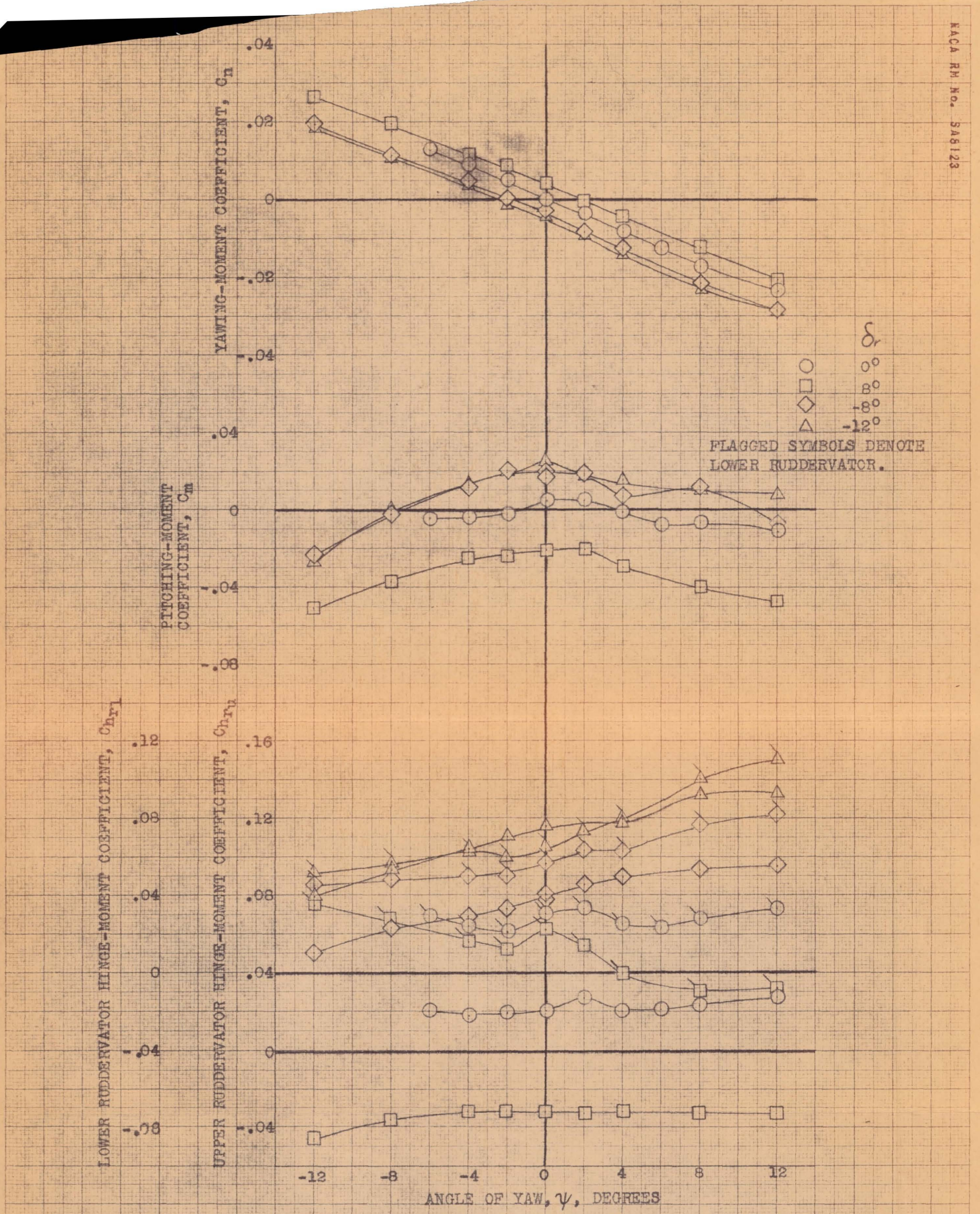

(a) C_n, C_m, C_{h_r} vs ψ.

FIGURE 57.- EFFECT OF FIXED DEFLECTIONS OF THE UPPER RIGHT AND LOWER LEFT RUDDERVATOR ON THE AERODYNAMIC CHARACTERISTICS OF THE AIRPLANE IN YAW. DIVE BRAKE EXTENDED; α_a, 0°.

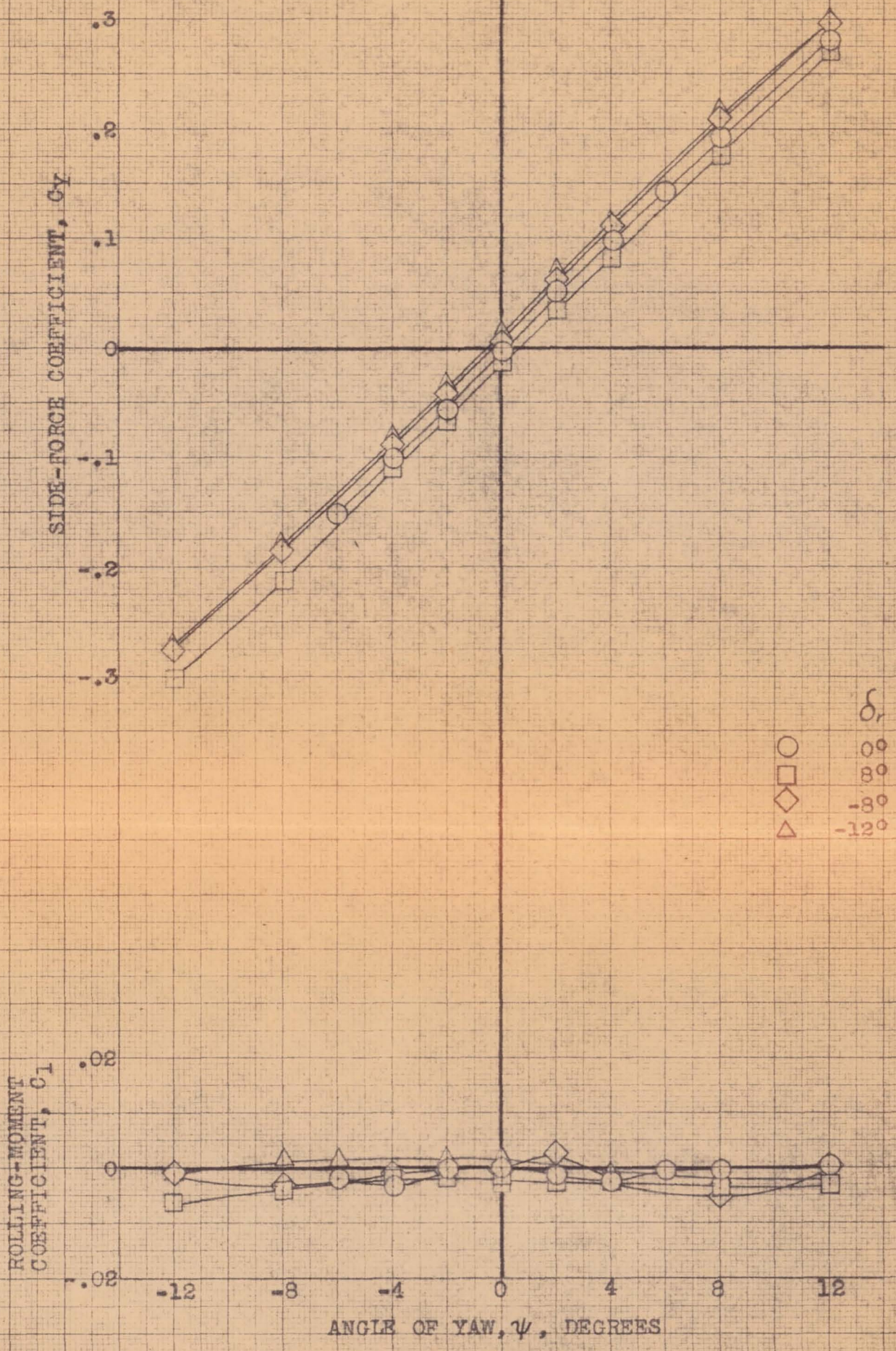

(b) C_Y, C_l vs ψ.

FIGURE 57.- CONCLUDED.

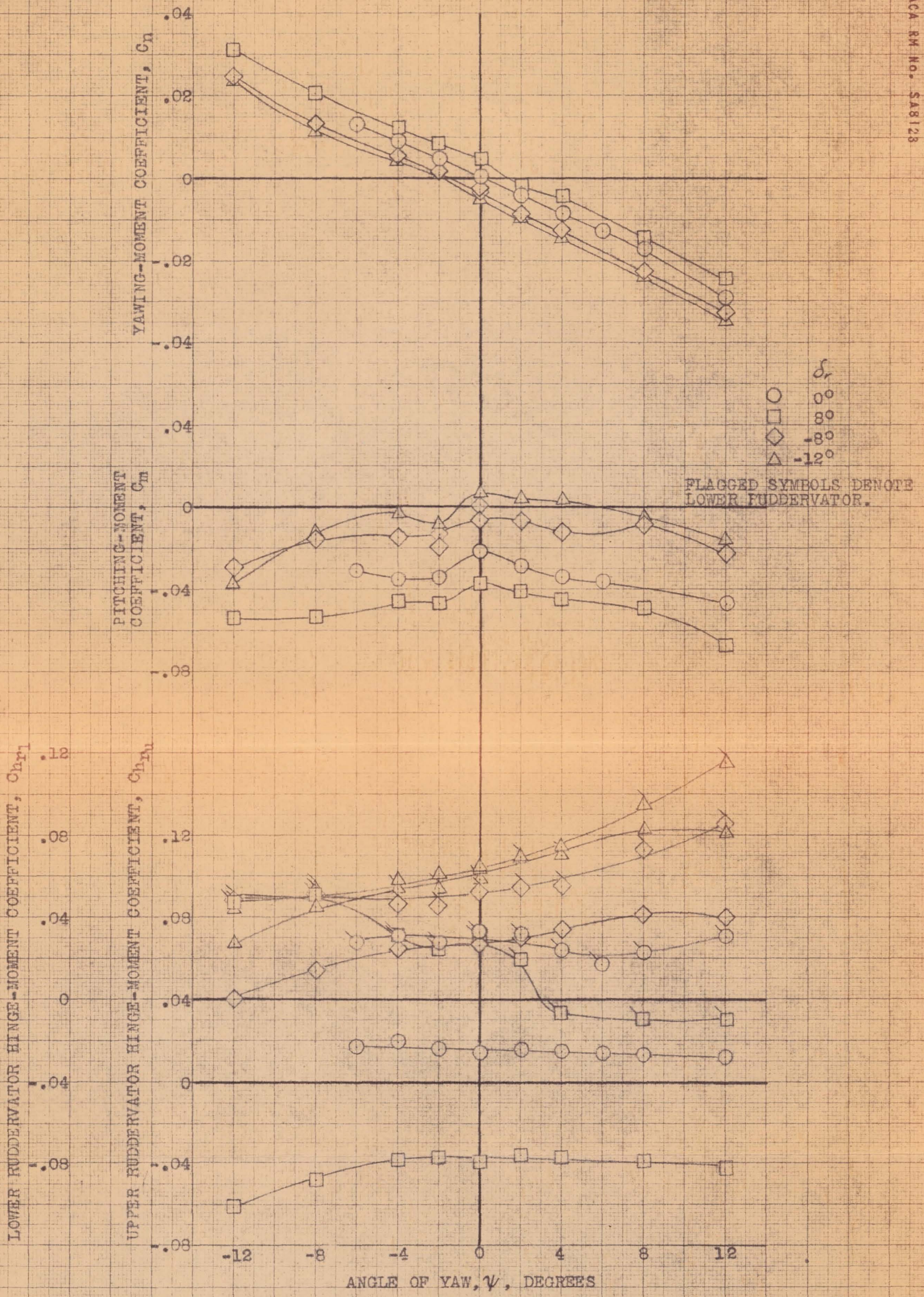

(a) C_n, C_m, C_{h_r} vs ψ.

FIGURE 58.- EFFECT OF FIXED DEFLECTIONS OF THE UPPER RIGHT AND LOWER LEFT RUDDERVATOR ON THE AERODYNAMIC CHARACTERISTICS OF THE AIRPLANE IN YAW. DIVE BRAKE EXTENDED; α_u, 6°.

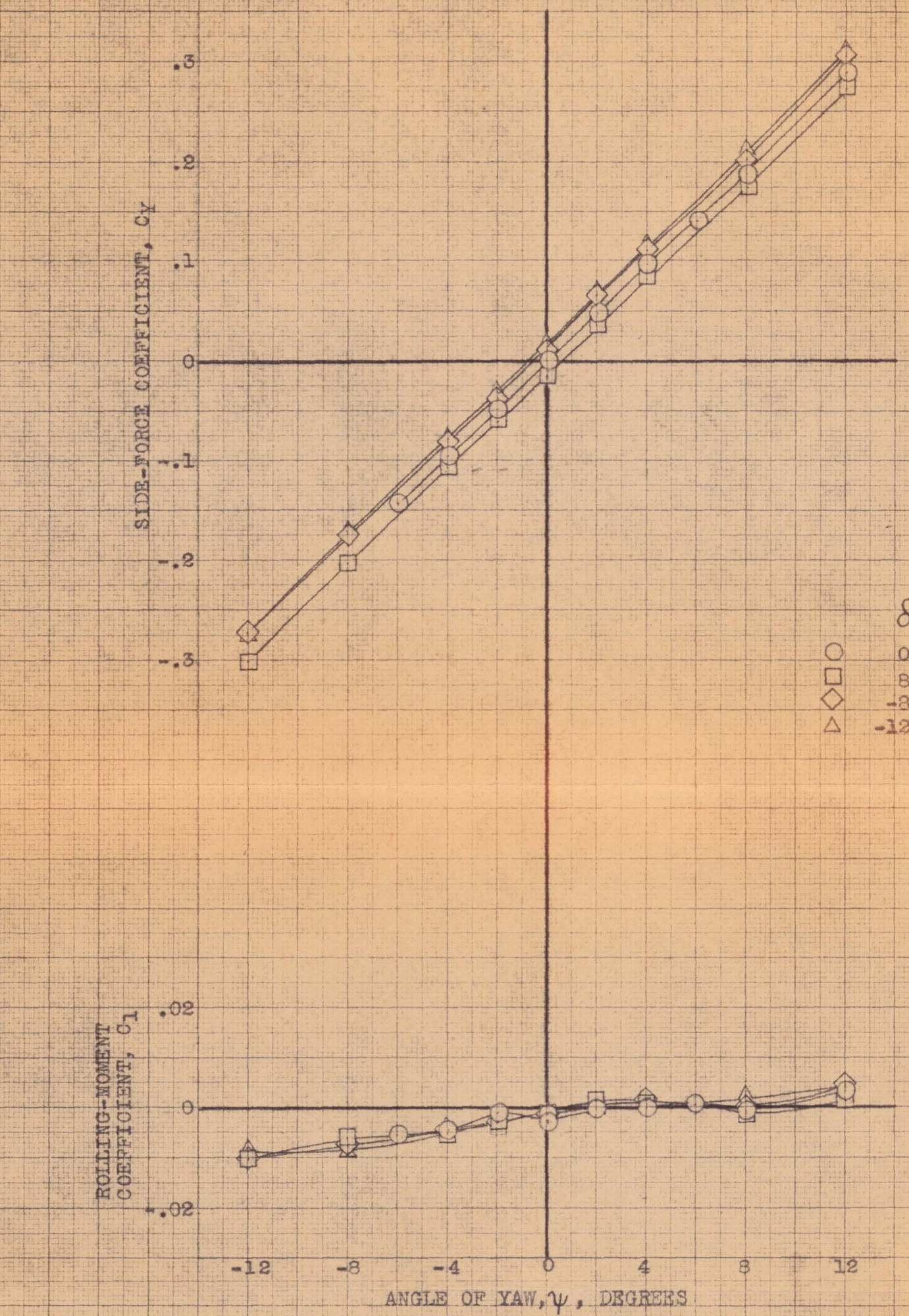

(b) C_Y, C_l vs ψ.

FIGURE 58.- CONCLUDED.

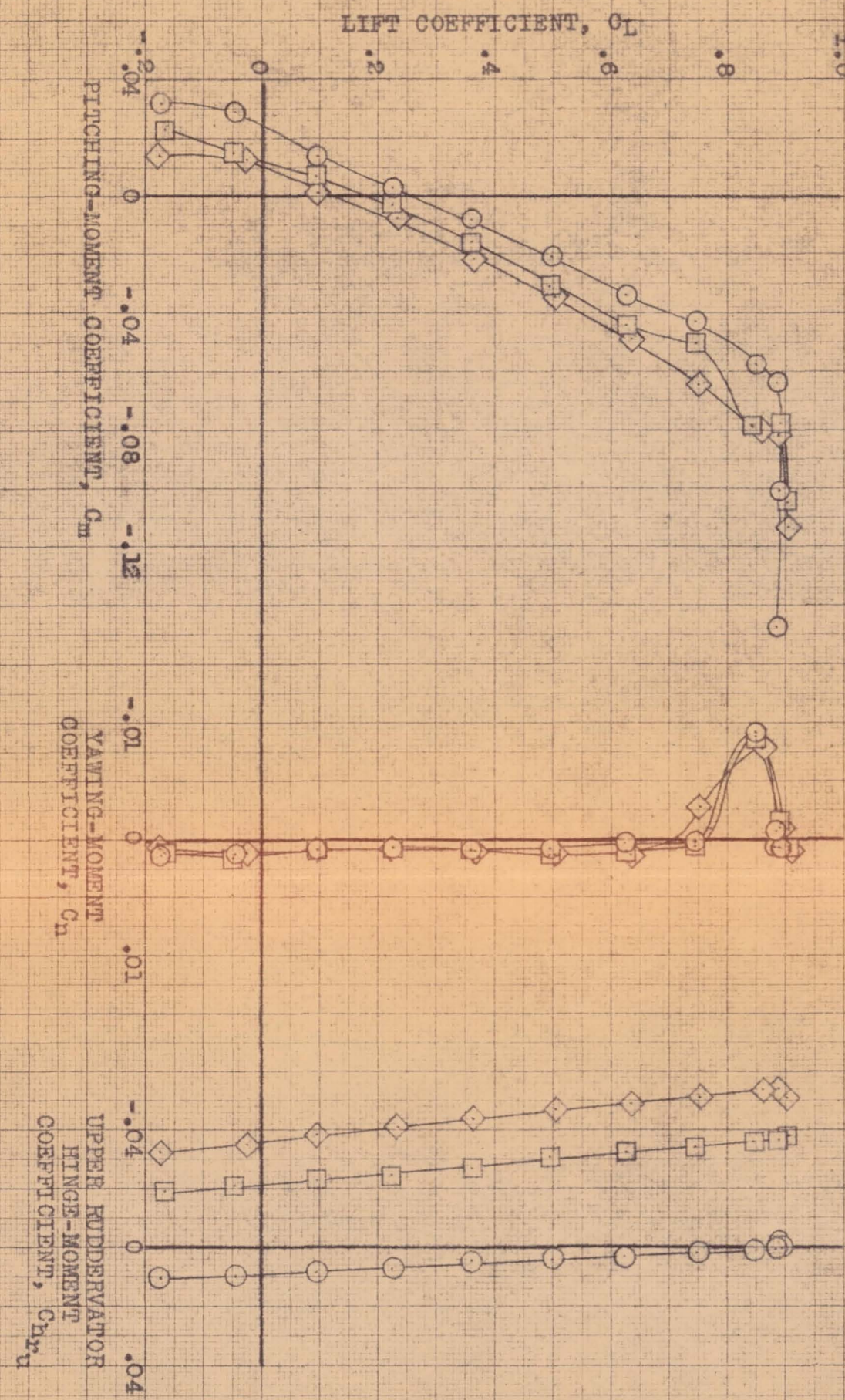

(a) δ_r, 0°.

FIGURE 59.- EFFECT OF FIXED DEFLECTIONS OF THE UPPER RIGHT RUDDERVATOR BALANCE TAB ON THE AERODYNAMIC CHARACTERISTICS OF THE AIRPLANE IN PITCH. CLEAN CONDITION; ψ, 0°.

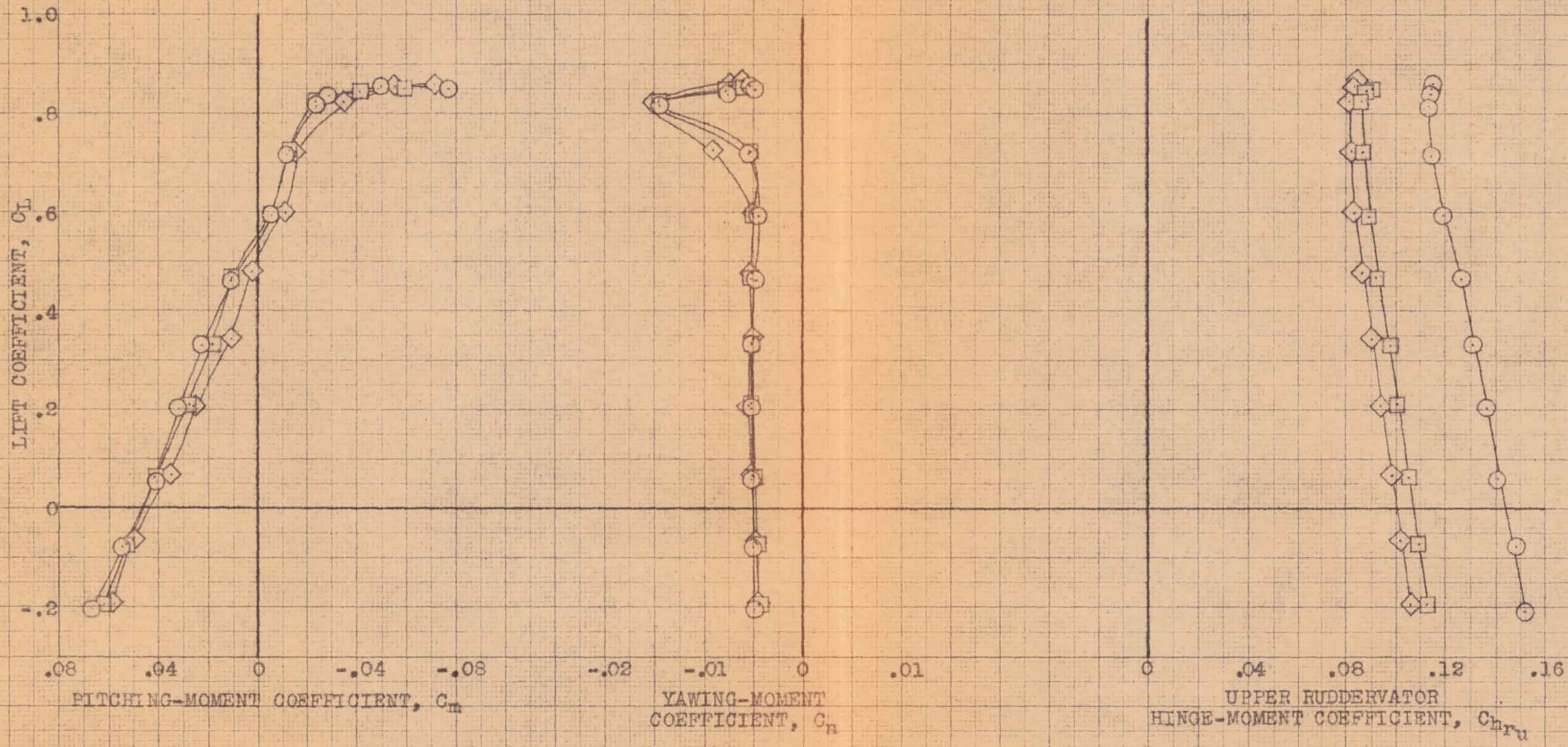

(a) δ_f, -16°.

FIGURE 59.- CONTINUED.

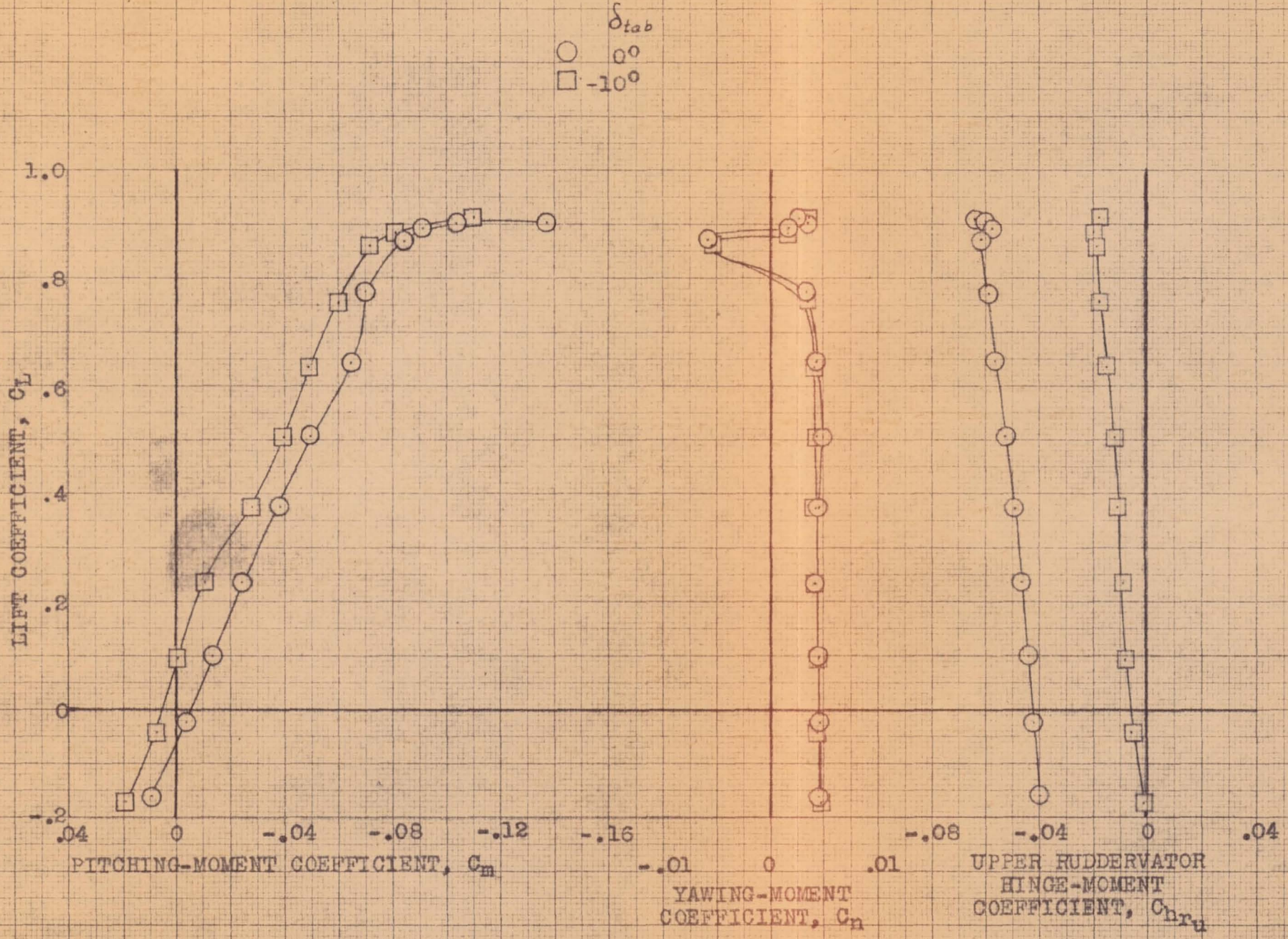

FIGURE 29.- CONCLUDED.

(c) δ_r, 8°.

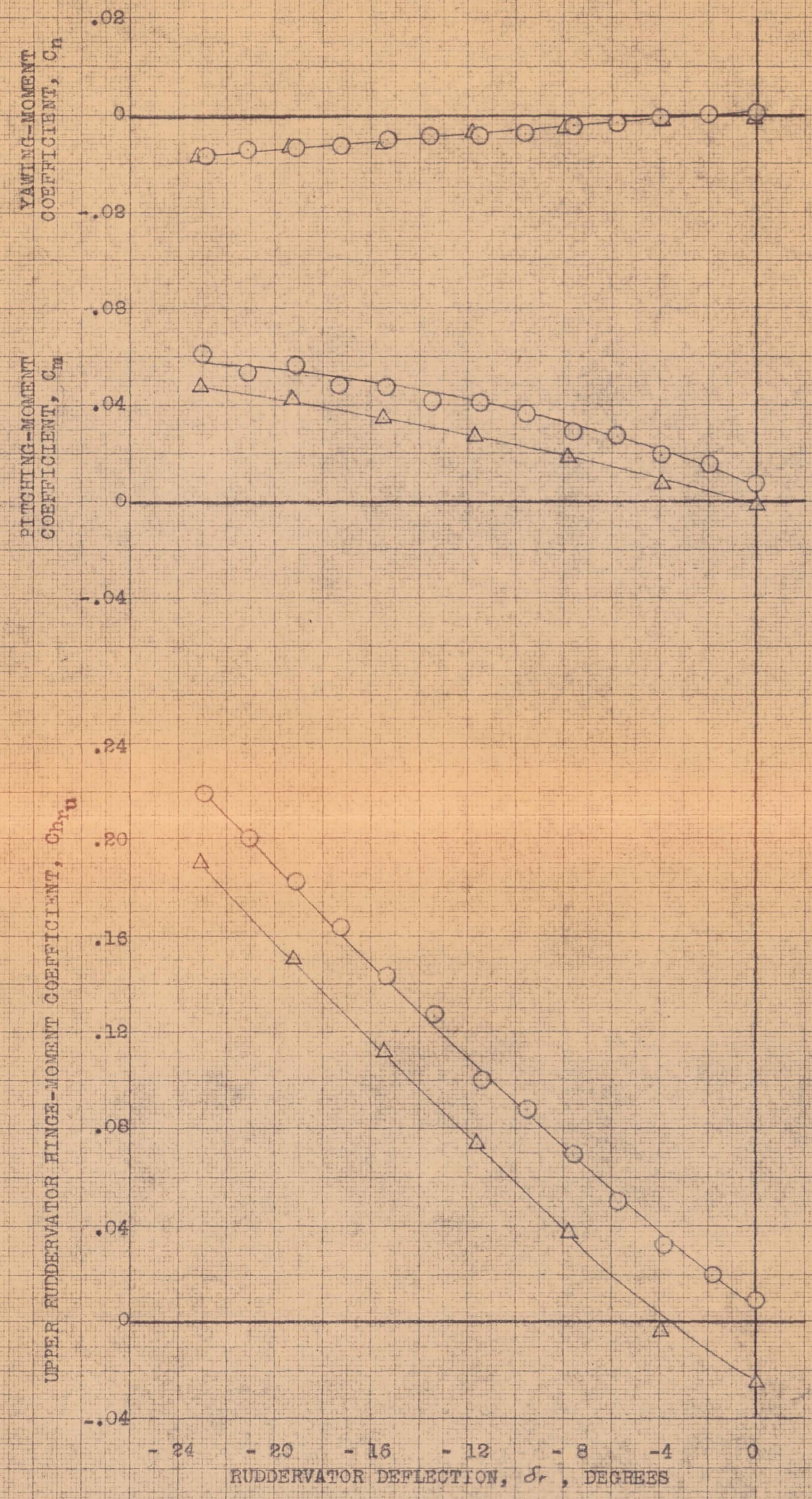

CONFIDENTIAL
NATIONAL ADVISORY COMMITTEE FOR AERONAUTICS

FIGURE 60.- VARIATION WITH DEFLECTION OF THE UPPER RIGHT AND LOWER LEFT RUDDERVATOR OF THE AERODYNAMIC CHARACTERISTICS OF THE AIRPLANE WITH VARIOUS FIXED DEFLECTIONS OF THE UPPER RIGHT RUDDERVATOR BALANCE TAB. CLEAN CONDITION; α_u, 0°, ψ, 0°.

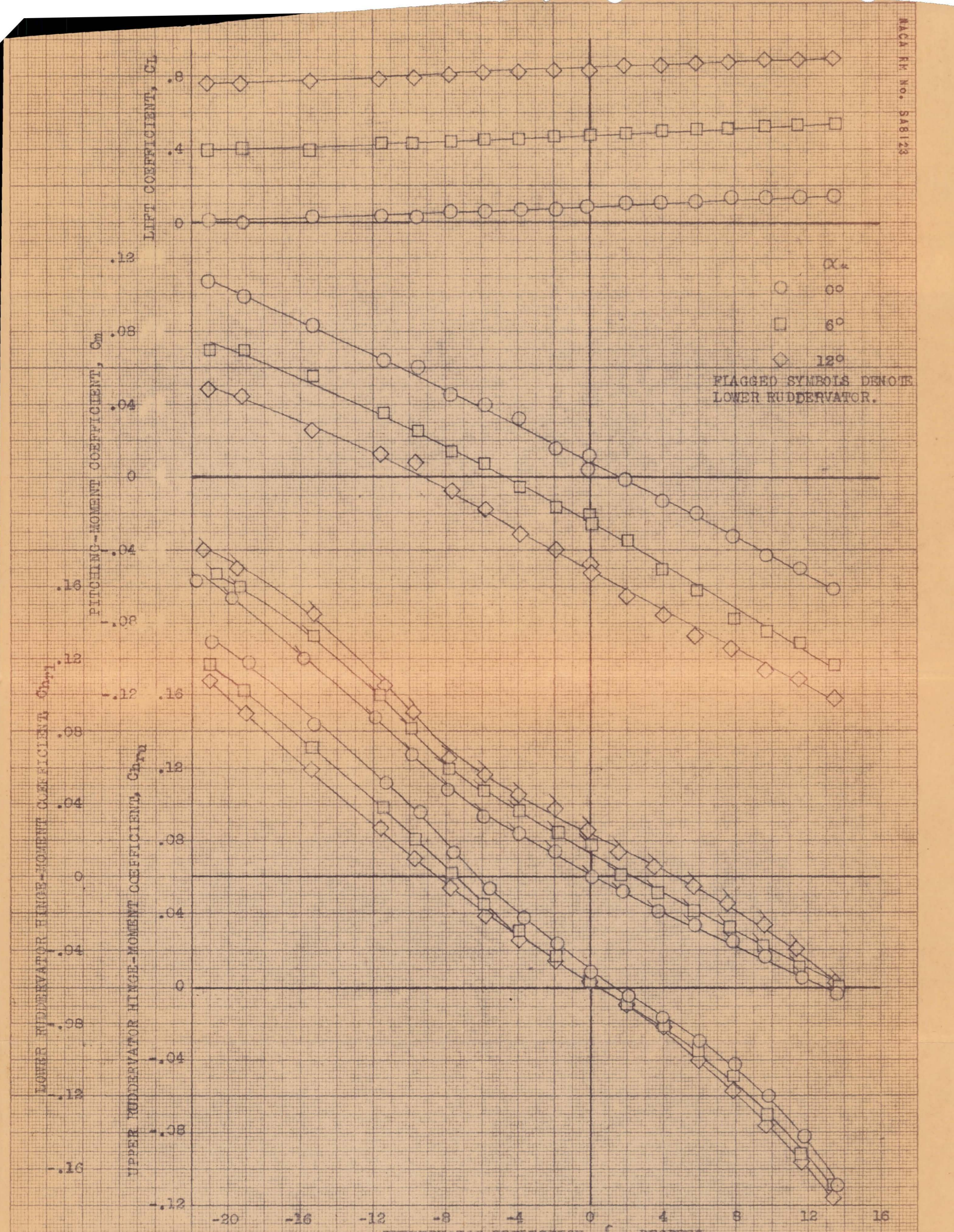

CONFIDENTIAL
NATIONAL ADVISORY COMMITTEE FOR AERONAUTICS

FIGURE 61.- VARIATION OF THE AERODYNAMIC CHARACTERISTICS OF THE AIRPLANE AT SEVERAL ANGLES OF ATTACK WITH DEFLECTION OF THE COMPLETE RUDDERVATOR SYSTEM OPERATED FOR PURE ELEVATOR ACTION. CLEAN CONFIGURATION; ψ, 0°.

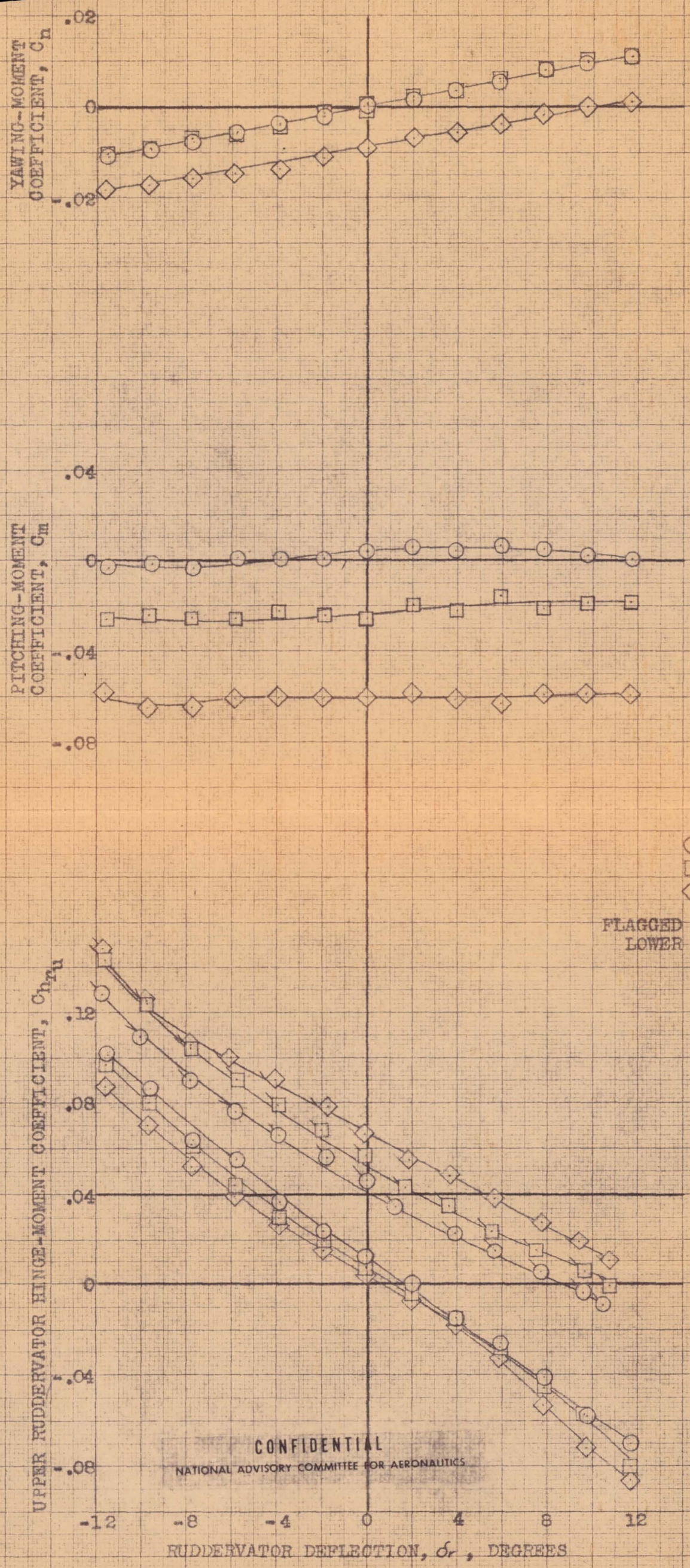

(a) C_n, C_m, C_{h_r} vs δ_r.

FIGURE 62.- VARIATION OF THE AERODYNAMIC CHARACTERISTICS OF THE AIRPLANE AT SEVERAL ANGLES OF ATTACK WITH DEFLECTION OF THE COMPLETE RUDDERVATOR SYSTEM OPERATED FOR PURE RUDDER ACTION. CLEAN CONFIGURATION; ψ, 0°.

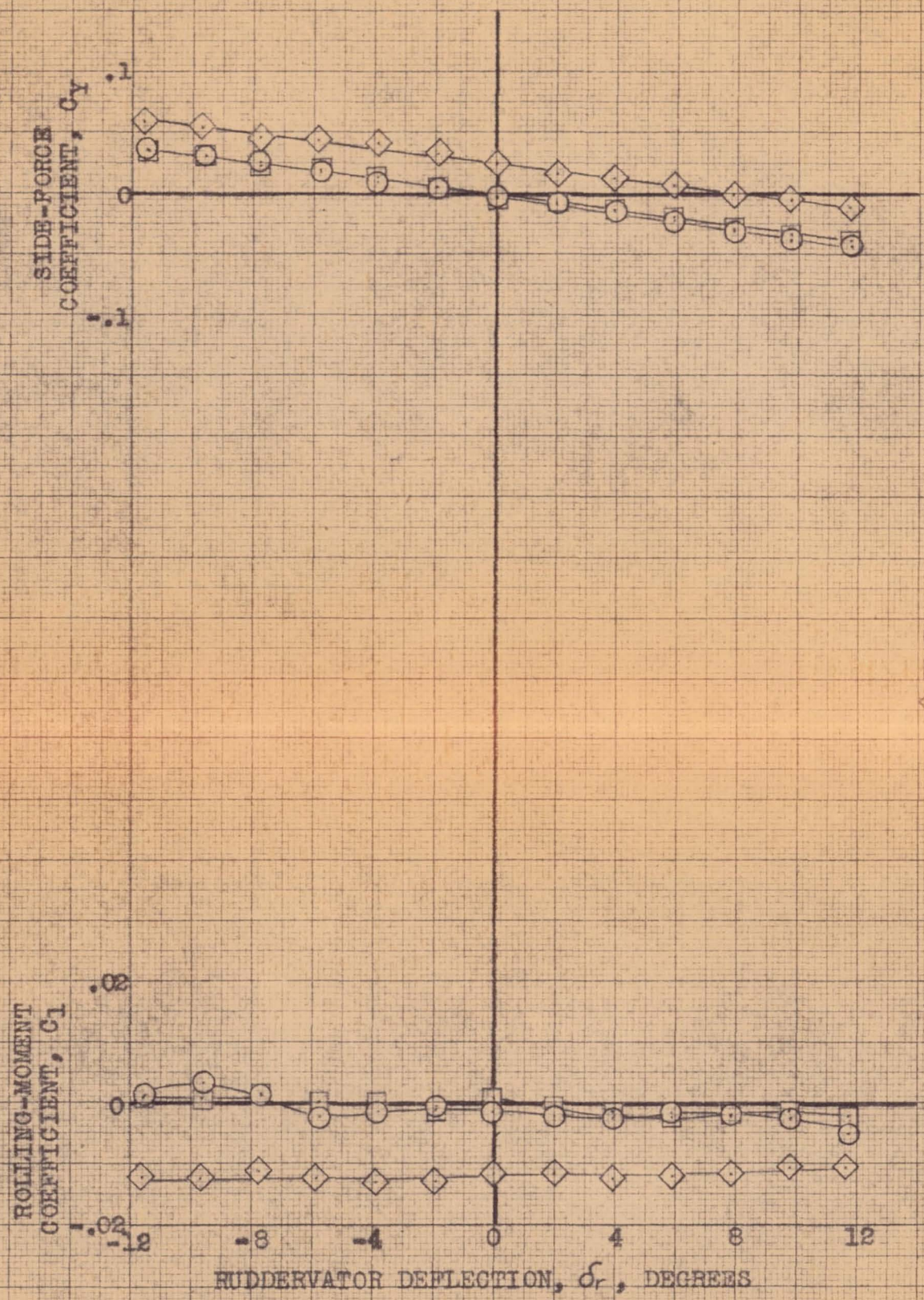

(b) C_Y, C_l vs δ_r.

FIGURE 62.- CONCLUDED.

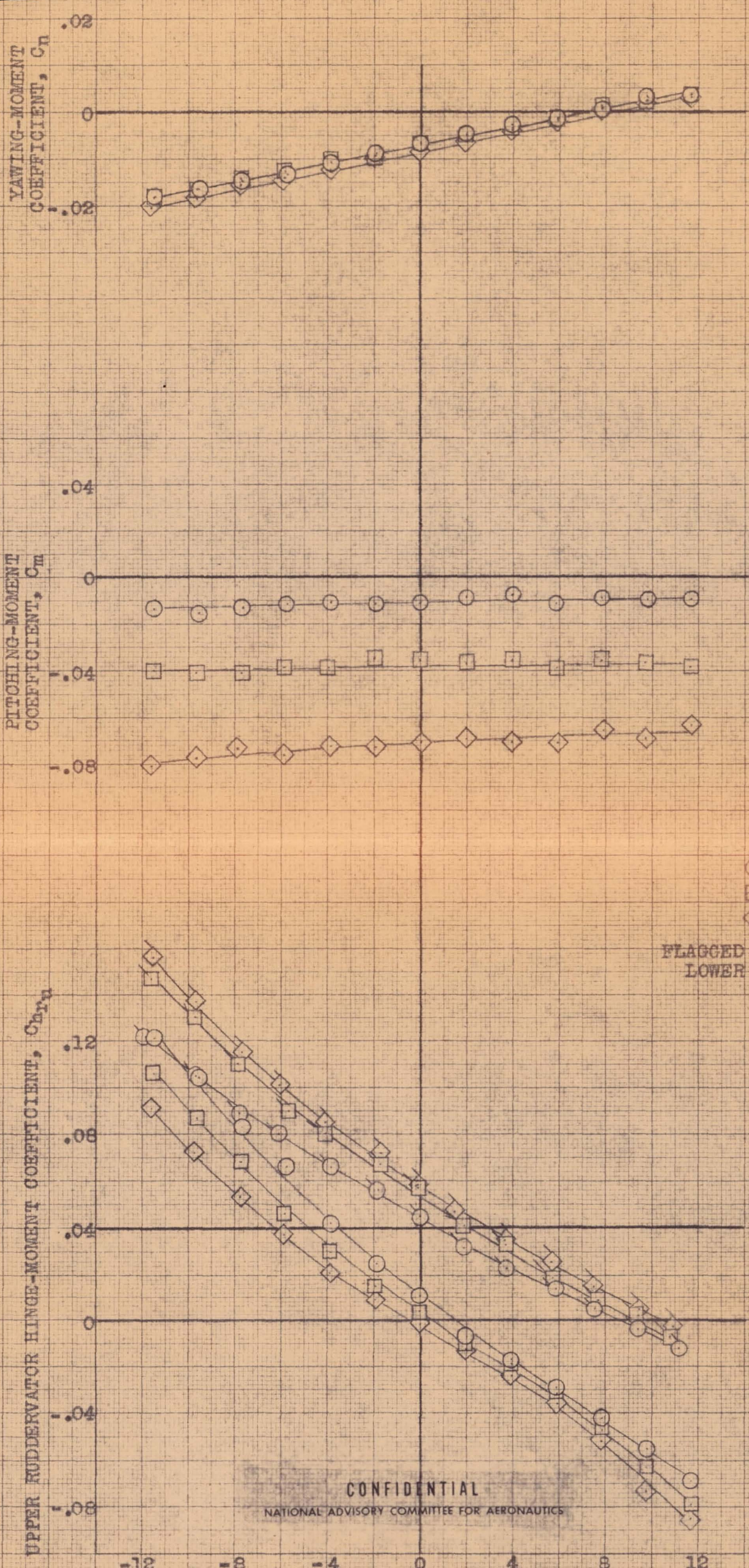

(a) C_n, C_m, C_{h_r} vs δ_r.

FIGURE 63.- VARIATION OF THE AERODYNAMIC CHARACTERISTICS OF THE AIRPLANE AT SEVERAL ANGLES OF ATTACK WITH DEFLECTION OF THE COMPLETE RUDDERVATOR SYSTEM OPERATED FOR PURE RUDDER ACTION. CLEAN CONFIGURATION; ψ, 4°.

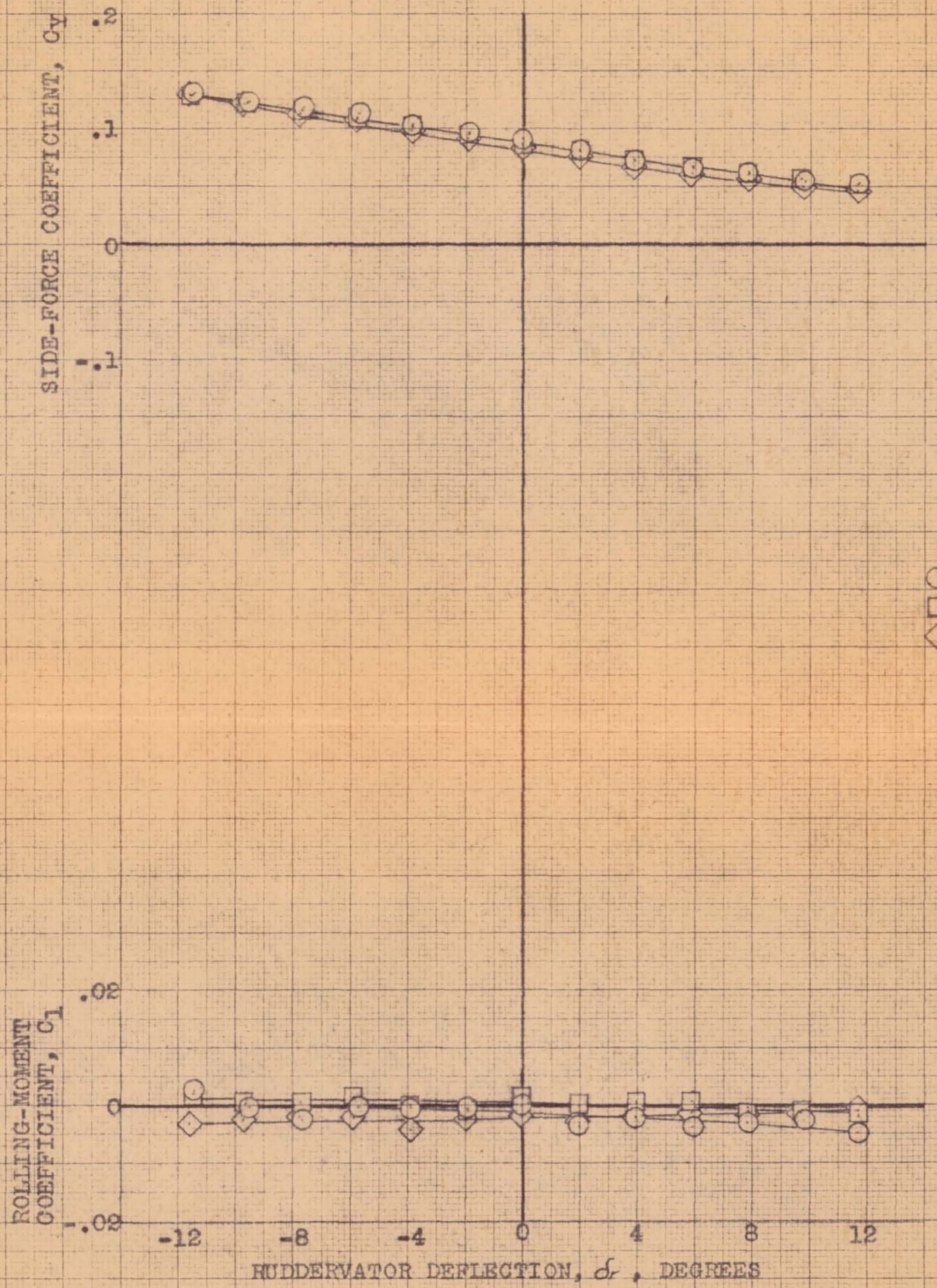

(b) C_Y, C_l vs δ_r.

FIGURE 63.- CONCLUDED.

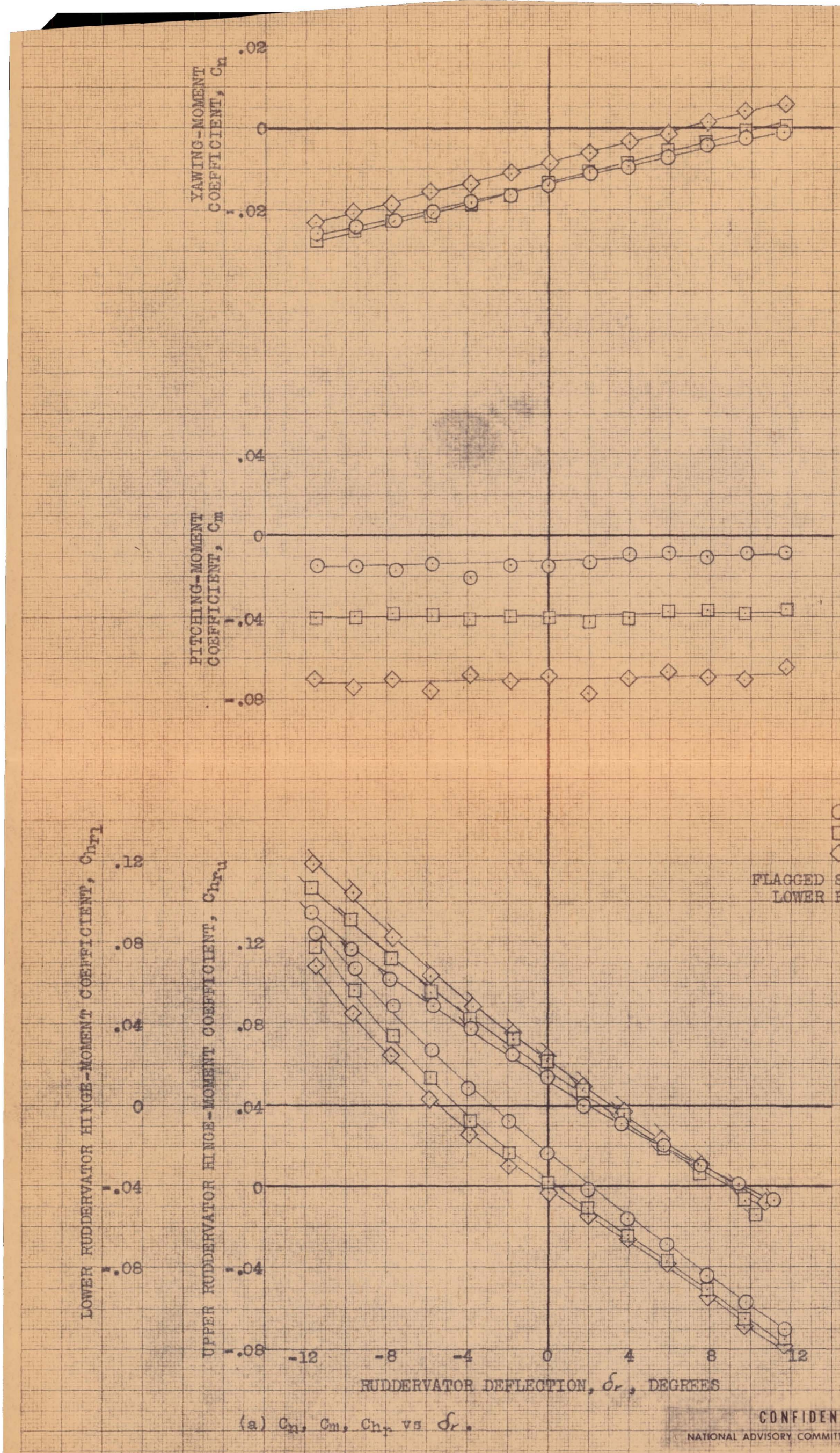

(a) C_n, C_m, C_{h_r} vs δ_r.

CONFIDENTIAL

NATIONAL ADVISORY COMMITTEE FOR AERONAUTICS

FIGURE 64.- VARIATION OF THE AERODYNAMIC CHARACTERISTICS OF THE AIRPLANE AT SEVERAL ANGLES OF ATTACK WITH DEFLECTION OF THE COMPLETE RUDDERVATOR SYSTEM OPERATED FOR PURE RUDDER ACTION. CLEAN CONFIGURATION; ψ, 8°.

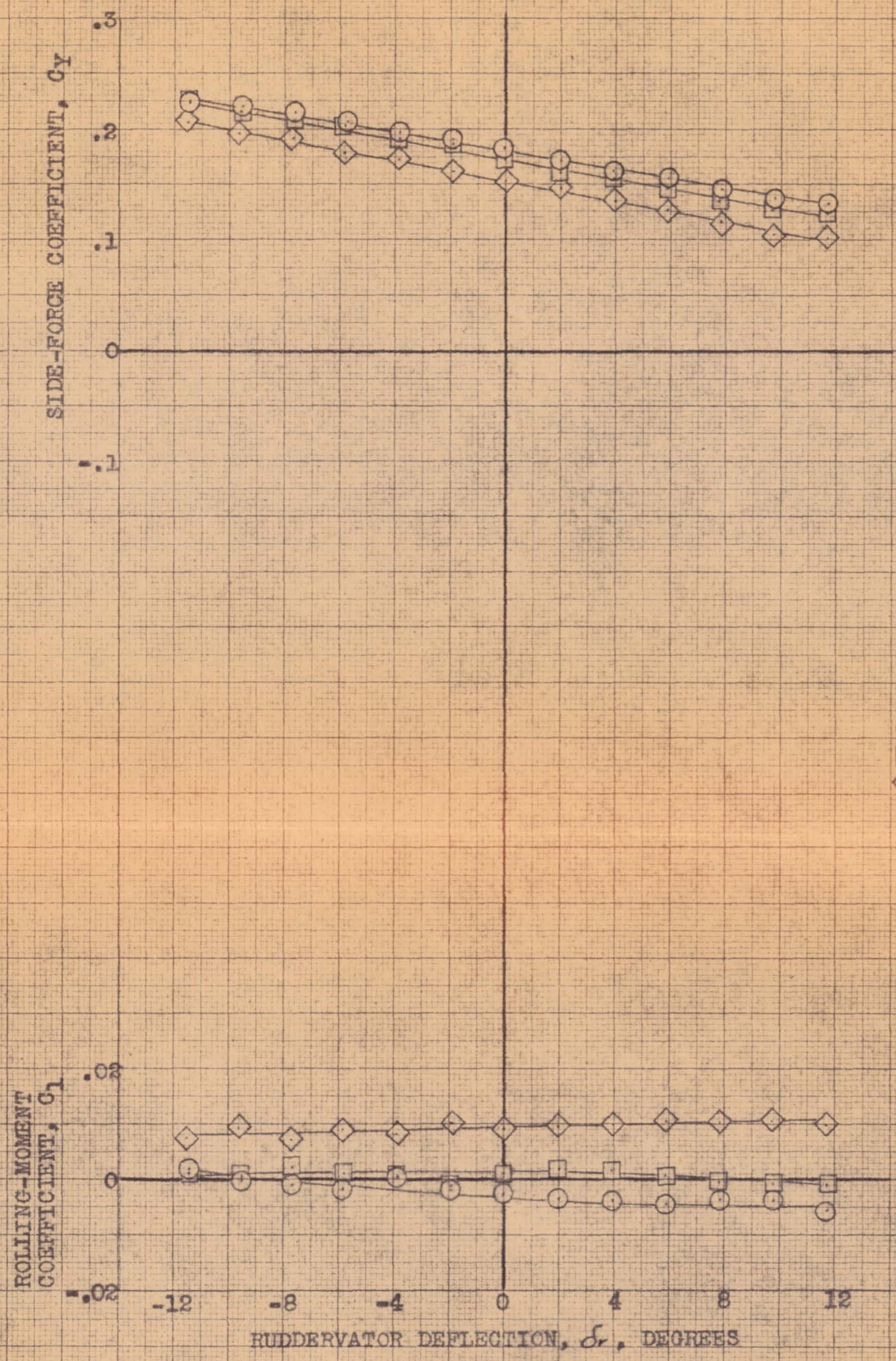

(b) C_Y, C_l vs δ_r.

FIGURE 64.- CONCLUDED.

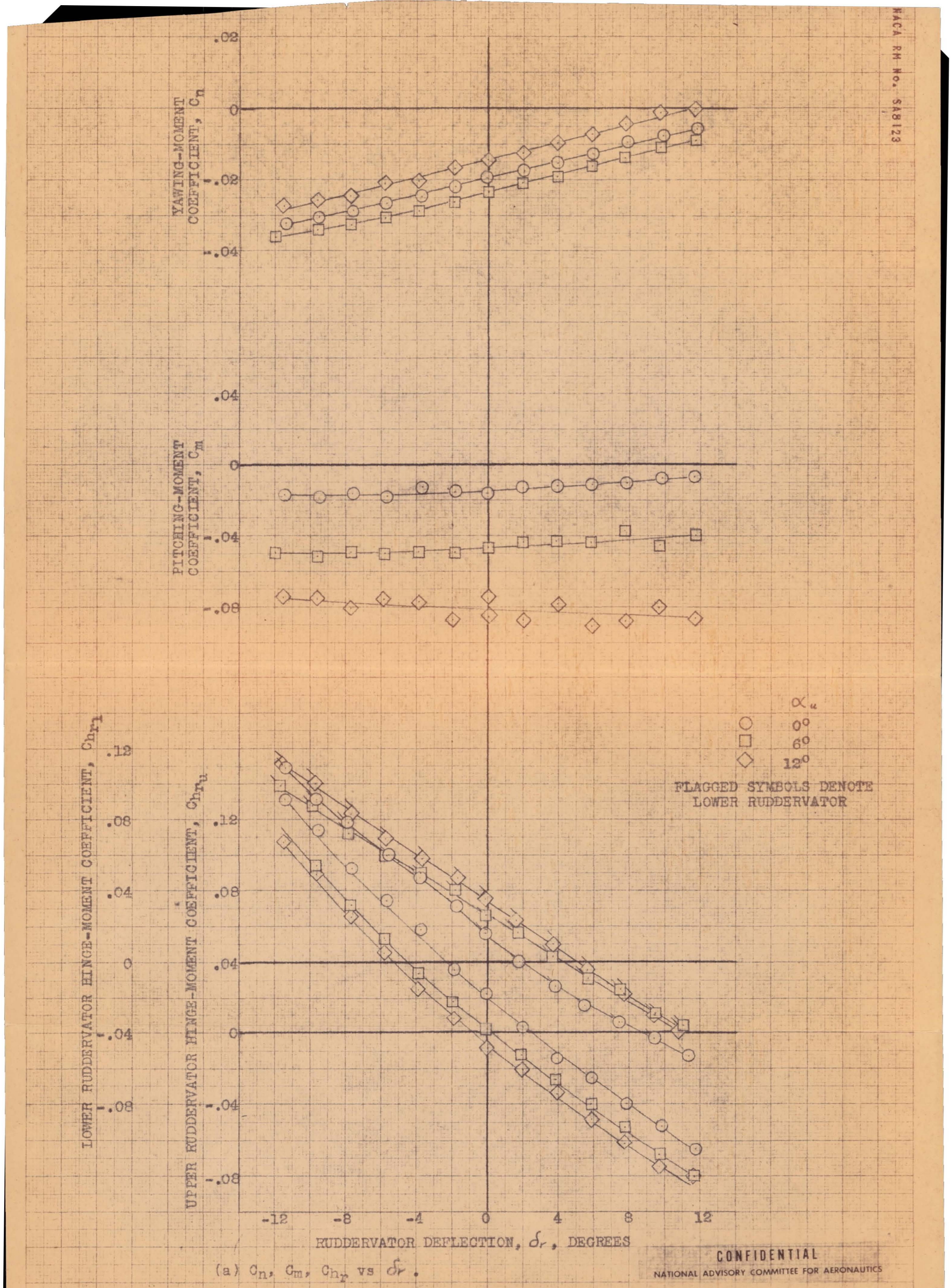

(a) C_n, C_m, C_{h_r} vs δ_r.

CONFIDENTIAL

NATIONAL ADVISORY COMMITTEE FOR AERONAUTICS

FIGURE 65.- VARIATION OF THE AERODYNAMIC CHARACTERISTICS OF THE AIRPLANE AT SEVERAL ANGLES OF ATTACK WITH DEFLECTION OF THE COMPLETE RUDDERVATOR SYSTEM OPERATED FOR PURE RUDDER ACTION. CLEAN CONFIGURATION; ψ, 12°.

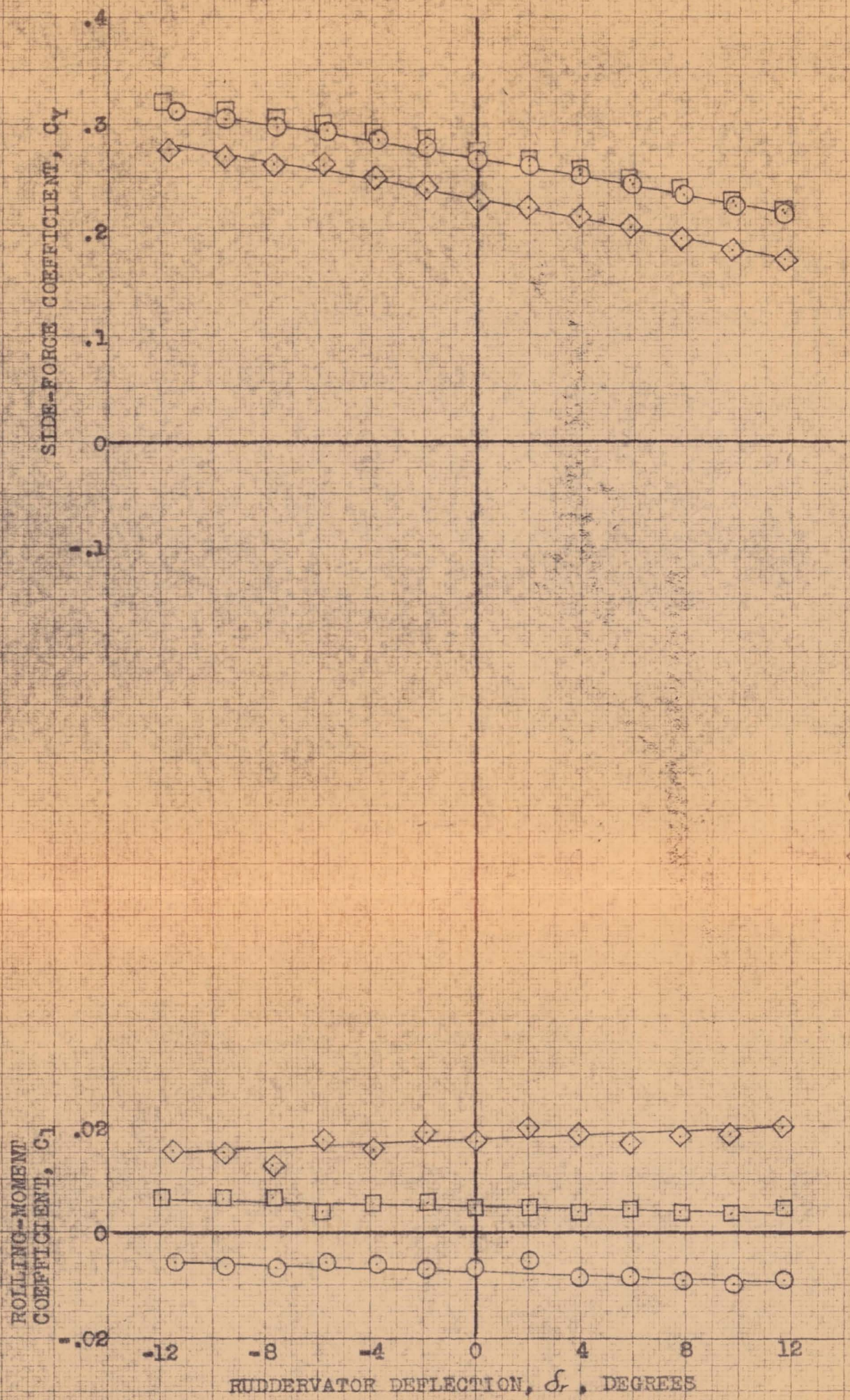

(b) C_Y, C_l vs δ_r.

FIGURE 65.- CONCLUDED.

CONFIGURATION

DATA

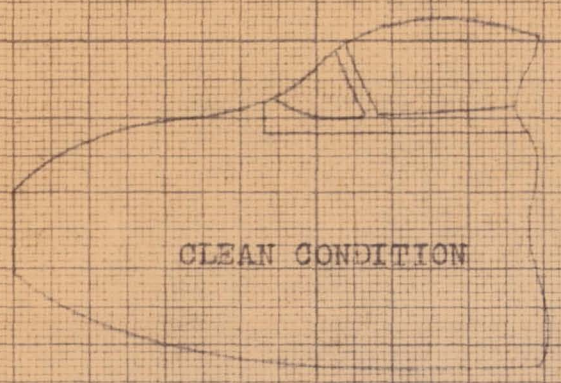

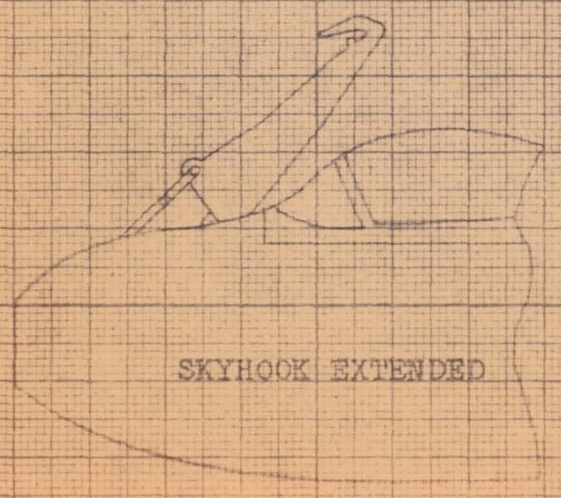

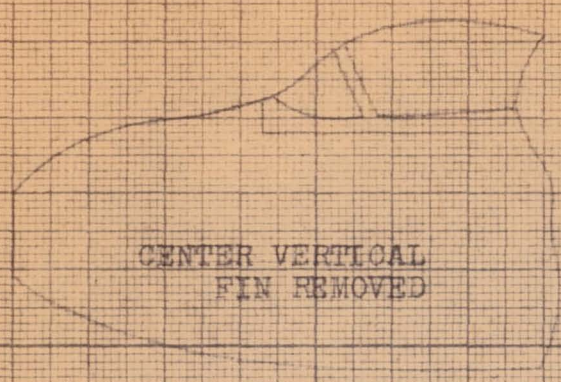

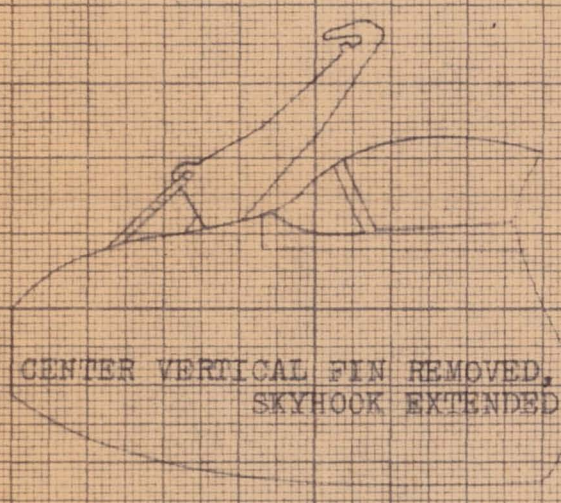

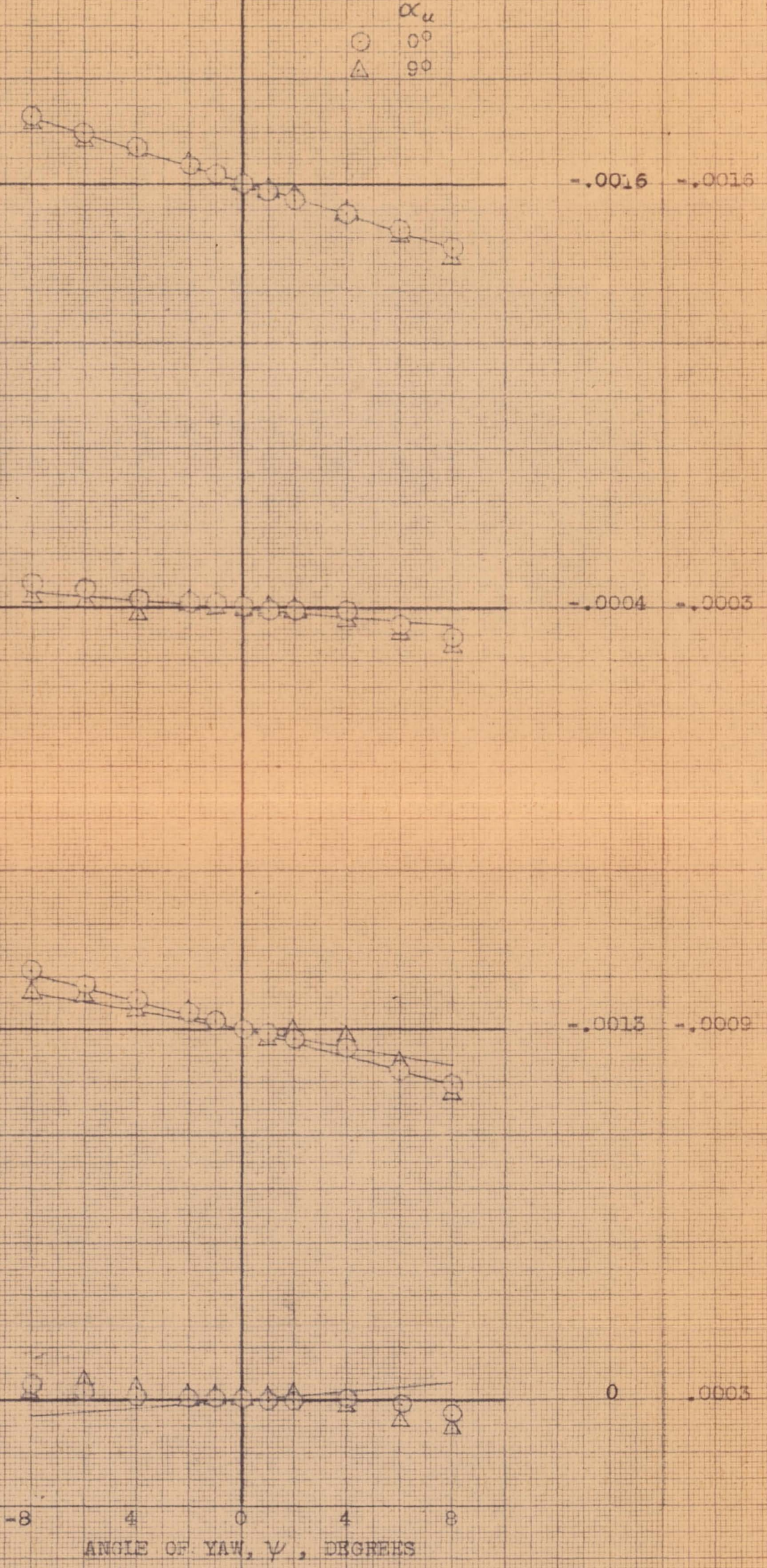

(a) MODIFICATIONS 1 to 4.

FIGURE 66.- SUMMARY OF THE DIRECTIONAL STABILITY CHARACTERISTICS OF THE AIRPLANE FROM TESTS OF 20 MODIFICATIONS MADE IN THE INVESTIGATION OF THE SKYHOOK DIRECTIONAL STABILITY PROBLEM.

CONFIGURATION

DATA

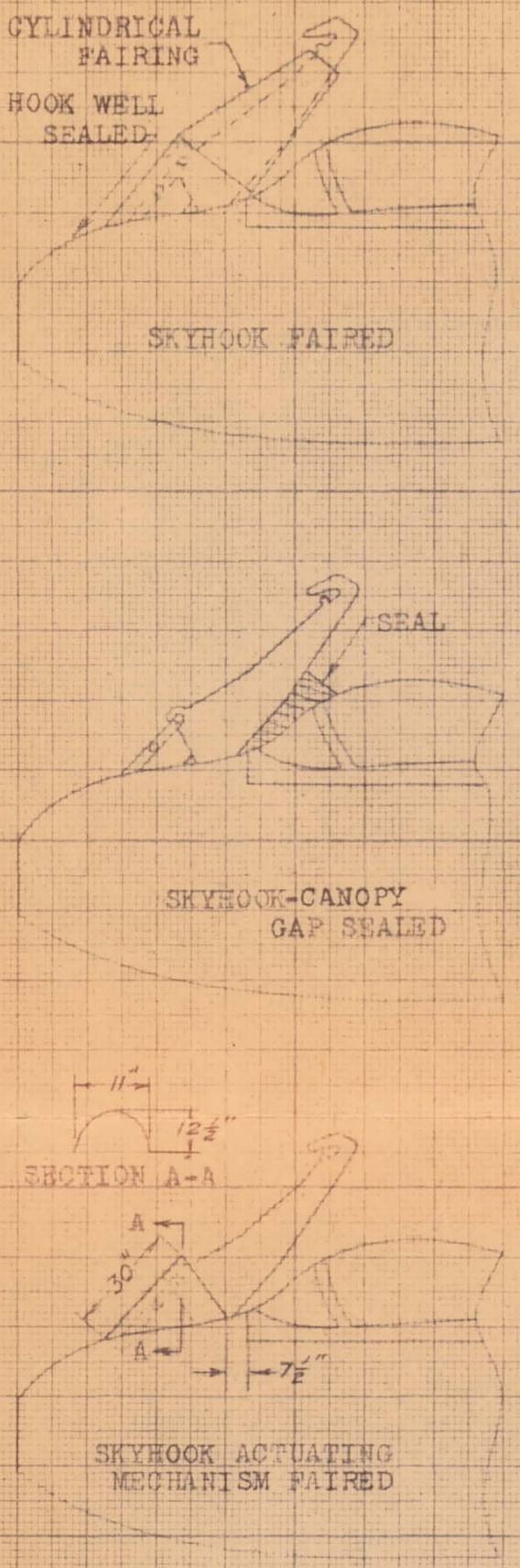

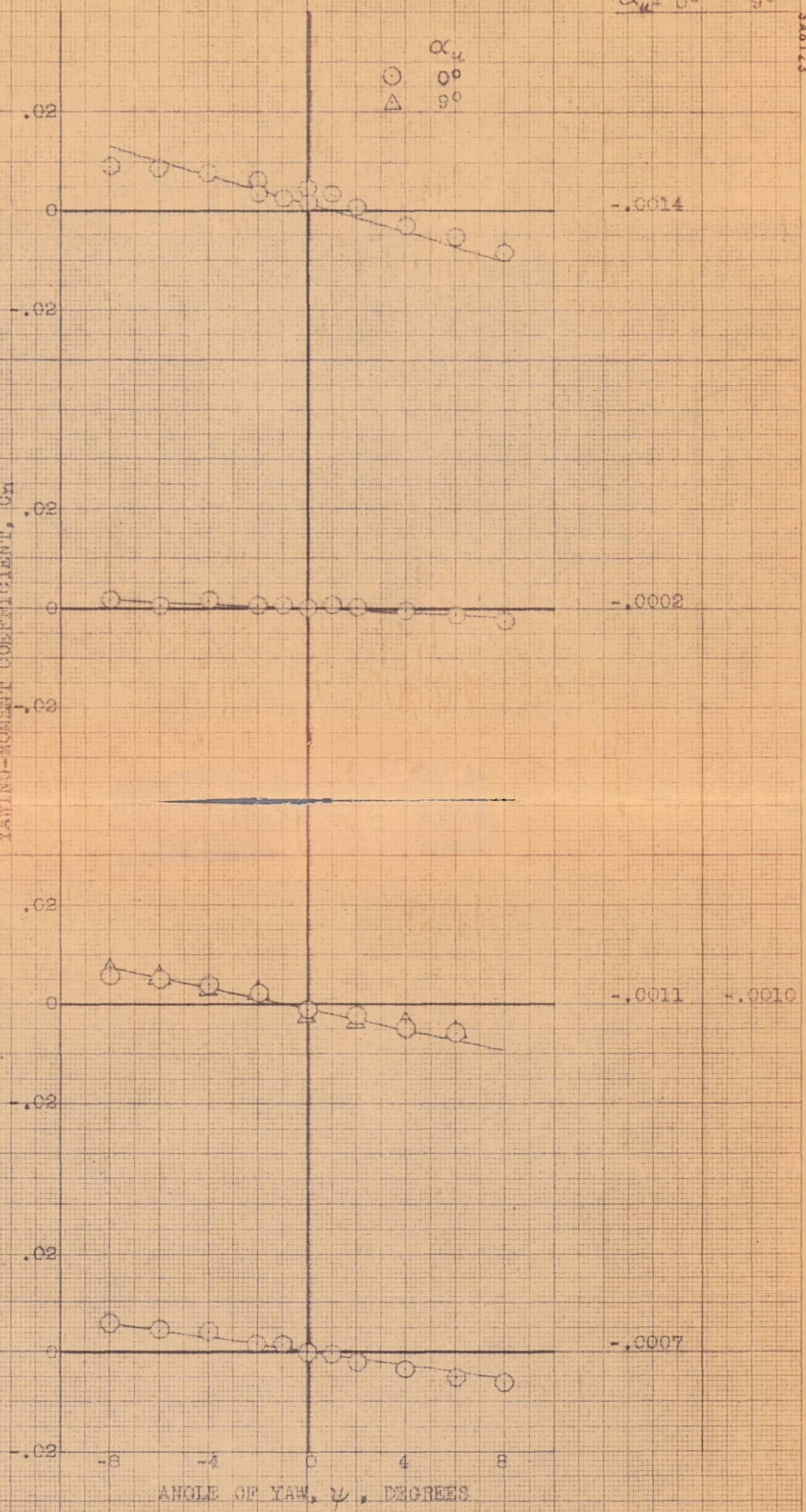

(b) MODIFICATIONS 5 to 8.

FIGURE 66.- CONTINUED.

CONFIGURATION

1" ROUND MOULDING — BACK FLANGE OFF

WEB AREAS CUT OUT

HOOK WELL SEALED

SKYHOOK COMPLETELY VENTED

40"

10"

1"

SKYHOOK, SIMULATED HATCH DOORS #1

2"

21"

18"

1"

SKYHOOK, SIMULATED HATCH DOORS #2

2"

F.S. 87.0

A

A

SECT. A-A

SKYHOOK, CANOPY SPOILER

DATA

C_{n_ψ}

α_μ 0° 9°

α_μ
○ 0°
△ 9°

.02
0
-.02

-.0007 -.0009

-.0006

-.0005 -.0006

.0006

YAWING-MOMENT COEFFICIENT, C_n

-8 -4 0 4 8

ANGLE OF YAW, ψ, DEGREES

(c) MODIFICATIONS 9 to 12.

FIGURE 66.- CONTINUED.

CONFIGURATION

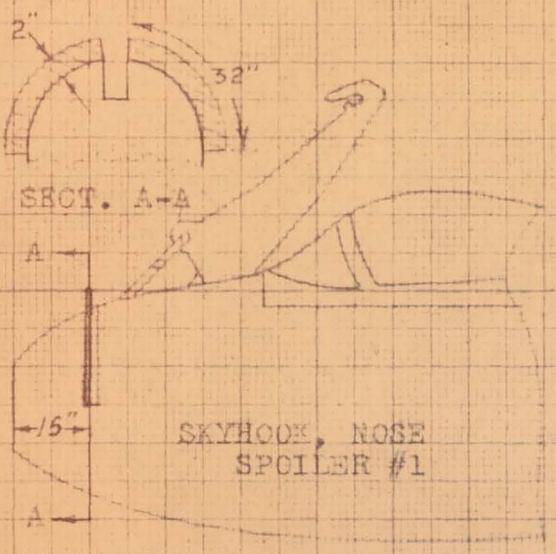

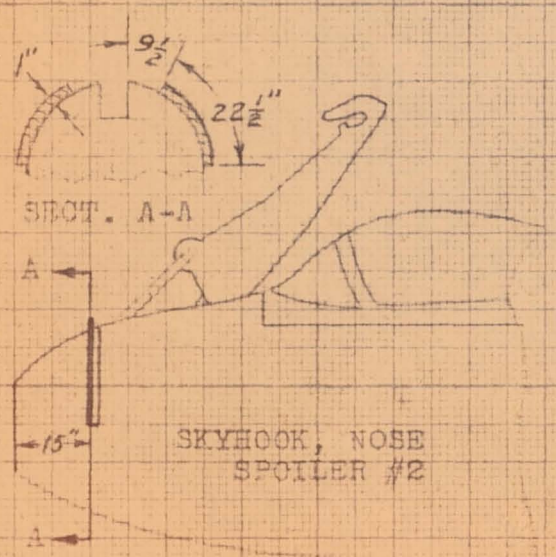

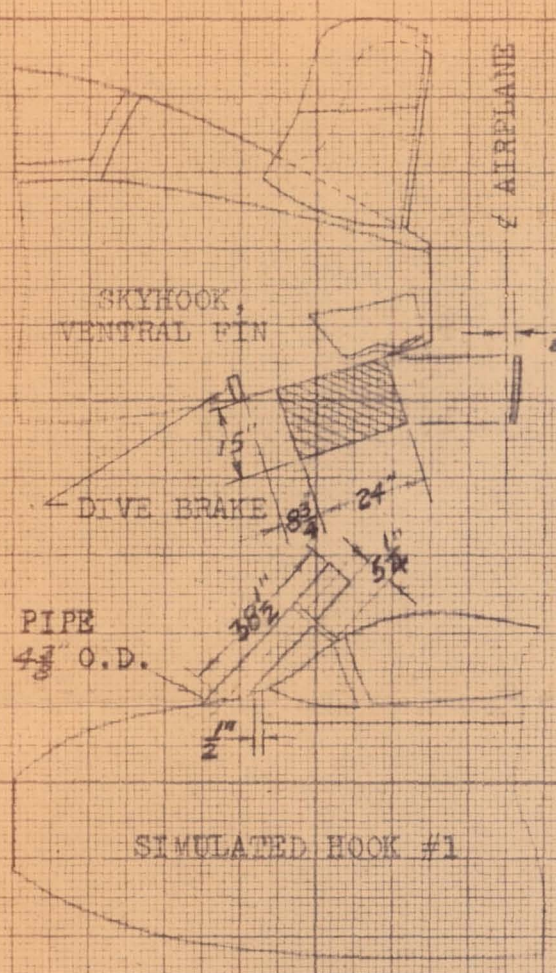

DATA

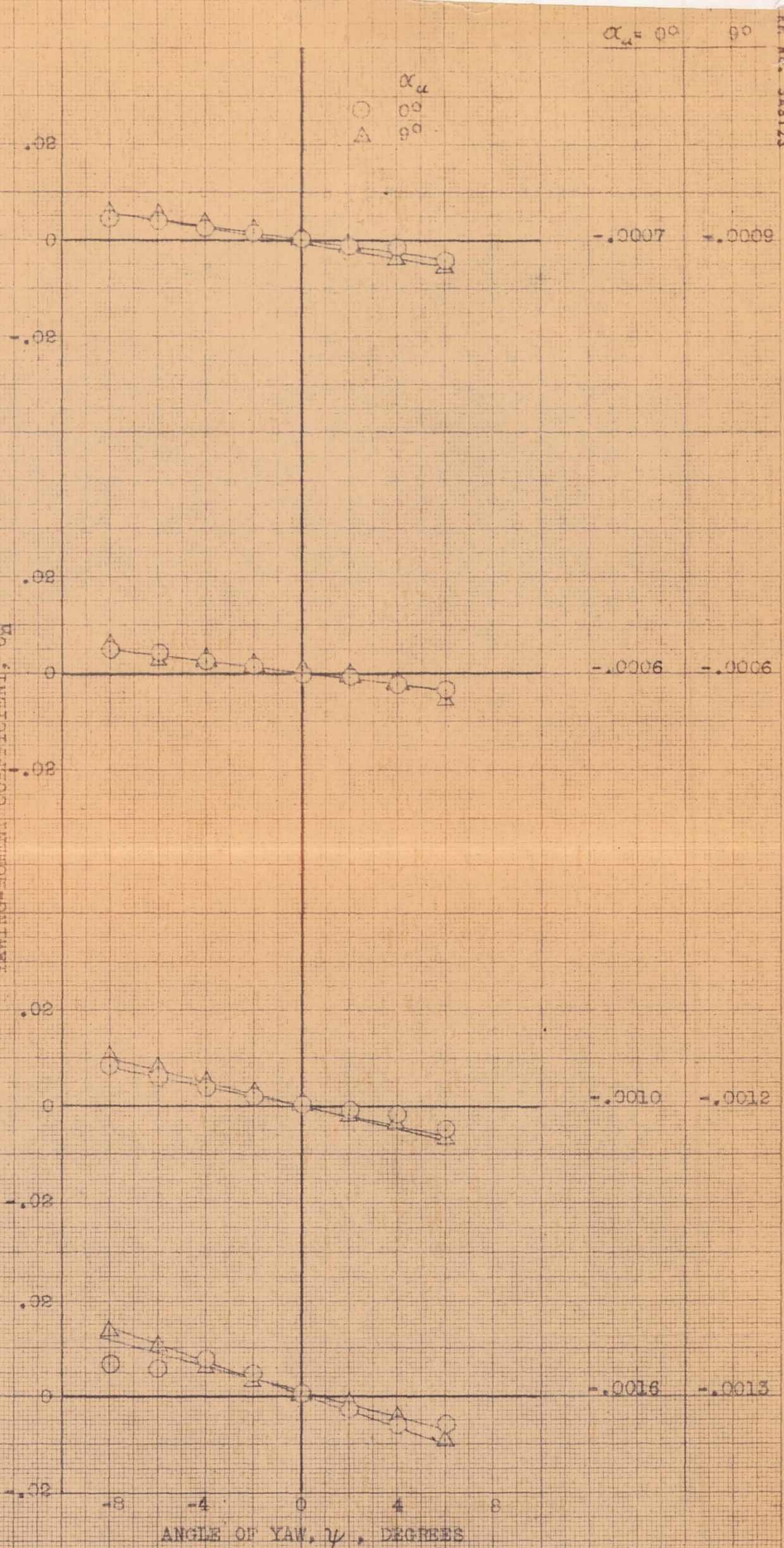

(a) MODIFICATIONS 13 to 16.

FIGURE 66.- CONTINUED.

CONFIDENTIAL

NATIONAL ADVISORY COMMITTEE FOR AERONAUTICS

NACA RM No. SA8123

CONFIGURATION

TWO SIDE PLATES 4 3/8" APART

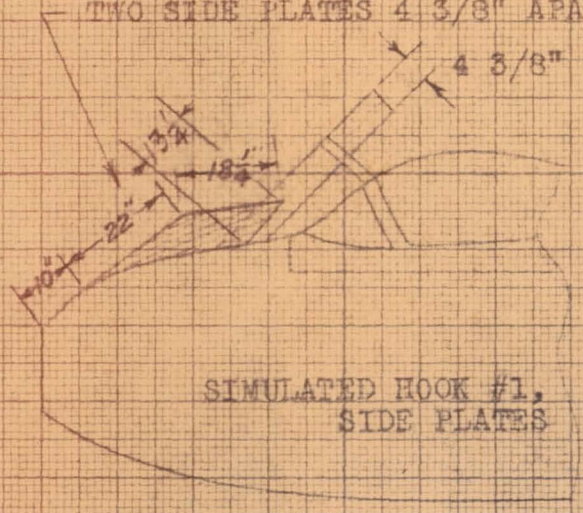

SIMULATED HOOK #1, SIDE PLATES

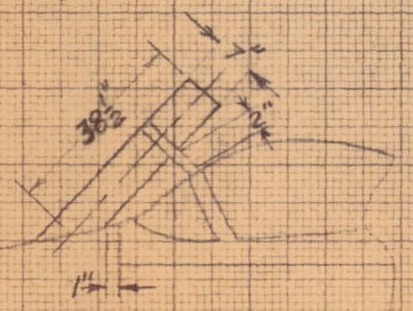

SIMULATED HOOK #2

TUBING 7/8" O.D.

5" WIDE

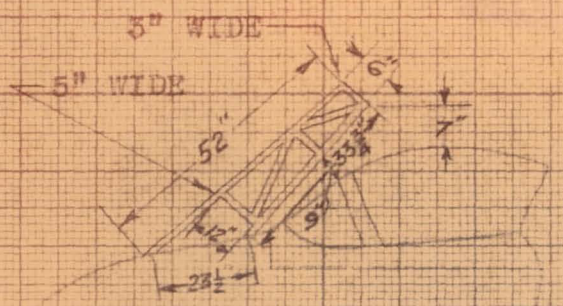

SIMULATED HOOK #3

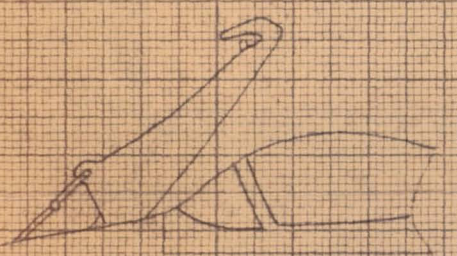

SKYHOOK, DIVE BRAKE, DROOP NOSE FLAP, STALL VANES P_2

DATA

C_{n_ψ}

α_u =	0°	9°
	-.0010	-.0007
	-.0014	-.0011
	-.0014	-.0014
	-.0011	-.0015

○ α_u = 0°
△ 9°

YAWING-MOMENT COEFFICIENT, C_n

.02
0
-.02

-8 -4 0 4 8

ANGLE OF YAW, ψ, DEGREES

(e) MODIFICATIONS 17 to 20.

FIGURE 66.- CONCLUDED.